Effects of endogenous cannabinoids and related substances on electrical activity and contraction in cardiac ventricular muscle

A thesis presented for the degree of Doctor of Philosophy

Michaelmas Term 2013

By

Emma Louise Bolton

Lincoln College, Oxford

University Department of Pharmacology, Oxford

Effects of endogenous cannabinoids and related substances on electrical activity and contraction in cardiac ventricular muscle

Emma Louise Bolton, Lincoln College, Oxford.

Submitted for the degree of Doctor of Philosophy, Michaelmas Term, 2013

Stimulation of cardiac β-adrenoceptors is the primary mechanism by which cardiac output is increased to meet metabolic demands of the body. Recently, nicotinic acid adenine dinucleotide phosphate (NAADP), has been implicated as a novel component of the β-adrenoceptor signalling pathway. NAADP is thought to mobilise Ca^{2+} from acidic endolysosomal stores which then supplements sarcoplasmic reticulum Ca^{2+} load, leading to a positive inotropic effect. Recent progress in the field has been made with the identification of two-pore channel 2 (TPC2) as a candidate NAADP receptor. Isolated ventricular myocytes from mice lacking TPC2 proteins (*Tpcn2*$^{-/-}$) displayed blunted maximal responses to the β-adrenoceptor agonist isoprenaline. This blunted response was also evident in Langendorff-perfused *Tpcn2*$^{-/-}$ hearts. Furthermore, a blunted response was observed in guinea pig ventricular myocytes which had been treated with bafilomycin A1, which disrupts the integrity of acidic endolysosomal stores. These data add to the body of evidence that NAADP signalling forms an important additional component of the β-adrenoceptor signalling pathway.

Chronic activation of the β-adrenoceptor pathway is associated with certain disease states including heart failure and arrhythmias. Anandamide is an endogenous cannabinoid, ('endocannabinoid'), with similar properties to Δ^9-tetrahydrocannabinol (Δ^9-THC), the primary active constituent of *Cannabis sativa.* These compounds have widespread physiological effects through actions at cannabinoid CB_1 and CB_2 receptors, which are negatively coupled to adenylyl cyclases and are expressed in cardiac muscle. Exposure of guinea pig ventricular myocytes to anandamide resulted in a reduction in the amplitude of contractions and Ca^{2+} transients. This was associated with a reduction in action potential duration and amplitude of I_{CaL}. These effects of anandamide could not be prevented by cannabinoid receptor antagonists, and could not be mimicked by cannabinoid receptor agonists. An inhibition of I_{Ks} was also observed.

Given the reported G_i-protein coupling of cannabinoid receptors, it may be expected that additional negative inotropic actions of anandamide might be observed when adenylyl cyclases are stimulated. However, the effects of anandamide to reduce amplitude of contraction and I_{CaL} were no greater in the presence of isoprenaline. Furthermore, the effects of anandamide were not prevented by pre-treatment of myocytes with pertussis toxin (PTX). This is in contrast to the actions of adenosine, which displayed clear PTX sensitive actions in the presence of isoprenaline. These data suggest that cannabinoid receptors are not involved in mediating the negative inotropic actions of anandamide. Another endocannabinoid, 2-arachidonoylglycerol, was without significant effect on action potentials or contractions in the absence or presence of isoprenaline. Δ^9-THC shared many of the actions of anandamide. It appears that anandamide and Δ^9-THC exert significant effects on cardiac muscle through direct modulation of ion channel function, although additional actions, for example, on the sarcoplasmic reticulum or myofilaments, cannot be ruled out.

Acknowledgements

Firstly, I would like to thank my supervisor Prof Derek Terrar, not only for giving me the opportunity to carry out my work in his lab, but also for his endless support, encouragement and kindness. It has been a privilege to have worked with a leading cardiac electrophysiologist who has such resolute enthusiasm and vast scientific knowledge.

Thanks must also go to Dr Laura Elson and Dr Steve Raković for their guidance in the early days, and Dr Rebecca Capel for being there with a cup of tea and a sympathetic ear when things felt particularly tough during the 'second year blues'. Thank you also to the other members of the lab who helped me make the final year of my DPhil one of the most productive. Sam Lin Wee Khang, Bobojon 'Professor' Nazarov, Dr Cynthia Sam, (who will forever be known as 'Dr Sam'), and Dr Daniel Aston; I will be eternally grateful for all the support, friendship and laughter you brought to the lab. Special additional mention must go to Sam: thank you for all your help with so many mouse cell isolations and for your enthusiastic approach to experimental troubleshooting and research in general – I found this inspirational!

Some of the work presented here would not have been possible without the donation of *TPCN2*$^{-/-}$ mice from Prof Antony Galione's lab. Special thanks to Dr Margarida Ruas da Silva for assisting in co-ordinating the use of these mice.

During my time in Oxford I have been lucky enough to meet some of my closest friends. Particular thanks must go to Dr Ruth Faram. After bonding over our mutual love of ale and northern roots during day one of our MSc in Pharmacology, we went through the highs and lows of the DPhil process together. Thank you for all your support and understanding, I can count on you for anything. I must also thank my lifelong friend Emma Wallis. I can laugh with you like no one else; you helped take my mind off things when I just needed a break.

Finally, I must thank my parents and family for their love, support and unwavering faith in me.

Table of Contents

Chapter 1 Introduction 1

1.1 General introduction 2

1.2 Cardiac muscle 7

1.3 Electrical activity 8

1.3.1 Resting membrane potentials 9

1.3.2 Action potentials 10

1.3.2.1 Phase 0: rapid depolarisation. 11

1.3.2.2 Phase 1: early repolarisation. 11

1.3.2.3 Phase 2: the plateau. 12

1.3.2.4 Phase 3: late repolarisation. 13

1.3.2.5 Phase 4: resting membrane potential. 13

1.3.3 Modulation of cardiac ionic currents 14

1.3.3.1 L-Type Ca^{2+} Currents (I_{CaL}) 14

1.3.3.2 The delayed rectifier K^+ current, I_K 18

1.4 Initiation of contraction: Ca^{2+} entry across the sarcolemma ... 20

1.4.1 L-Type Ca^{2+} Channels 20

1.4.2 Other mechanisms 21

1.5 Initiation of contraction: release of Ca^{2+} from intracellular stores 22

1.5.1 Ca^{2+}-induced Ca^{2+} release 22

1.5.2 Ryanodine receptors 23

1.5.3 Local control of Ca^{2+} release from the SR: Ca^{2+}sparks, quarks and blinks 24

1.5.4 Local control of Ca^{2+} release: termination 27

1.5.5 Modulation of ryanodine receptor function 28

1.5.5.1 Calsequestrin, triadin and junctin 30

1.5.5.2 FK506 binding proteins (FKBPs) 30

1.5.5.3 PKA 31

1.5.5.4 Calmodulin-dependent protein kinase (CaMK) II 32

1.6 Mechanism of contraction 34

1.7 Mechanism of relaxation 35

1.7.1 Ca^{2+} uptake 36

1.7.2 Extrusion of Ca^{2+} across the sarcolemma 37
1.7.3 Competition between uptake and extrusion mechanisms..... 37
1.8 Physiological regulation of cardiac function..... 38
1.8.1 The sympathetic nervous system and β-adrenoceptor stimulation..... 39
1.8.2 The parasympathetic nervous system..... 41
1.9 Novel modulators of cardiac function: Ca^{2+} mobilising second messengers..... 42
1.9.1 Inositol Trisphosphate (IP_3)..... 42
1.9.2 Cyclic Adenosine Diphosphate Ribose (cADPR)..... 44
1.9.3 Nicotinic Acid Adenine Dinucleotide Phosphate (NAADP) 44
1.9.3.1 NAADP synthesis..... 45
1.9.3.2 Properties of NAADP-mediated Ca^{2+} release..... 46
1.9.3.3 NAADP-sensitive Ca^{2+} stores..... 47
1.9.3.4 Store interaction: the 'two-pool' hypothesis..... 50
1.9.3.5 Molecular targets of NAADP..... 50
1.9.3.6 Antagonists of NAADP signalling..... 54
1.9.3.7 Role of NAADP in the heart..... 55
1.10 Novel modulators of cardiac function: the endocannabinoid system 59
1.10.1 Discovery..... 60
1.10.2 Cannabinoid receptor signalling..... 62
1.10.2.1 Regulation of cAMP..... 63
1.10.2.2 Regulation of ion channels..... 65
1.10.2.3 Other signalling pathways..... 66
1.10.3 Synthesis of endocannabinoids..... 66
1.10.3.1 Anandamide..... 66
1.10.3.2 2-AG..... 68
1.10.4 Metabolism of endocannabinoids..... 69
1.10.4.1 Anandamide..... 69
1.10.4.2 2-AG..... 71
1.10.5 Cannabinoid receptor-independent actions of endocannabinoids..... 72
1.10.6 Effects on the cardiovascular system..... 74
1.10.6.1 In vivo studies..... 74
1.10.6.2 In vitro studies: the vascular system..... 76

1.10.6.3 In vitro studies: the heart 78
1.10.7 Role in cardiac pathologies 81
1.10.7.1 Ischaemia reperfusion 81
1.10.7.2 Hypertension and heart failure 83
1.11 Aims 84

Chapter 2 Methods 85

2.1 Cell Isolation 86
2.1.1 Guinea Pig 87
2.1.2 Mouse 89
2.2 Cell superfusion 90
2.3 Electrical field stimulation 90
2.4 Electrophysiology 91
2.4.1 Sharp microelectrodes 91
2.4.2 Patch electrodes 92
2.4.3 Setup for electrophysiological recording 93
2.4.4 Impalement of cells using a sharp microelectrode 95
2.4.5 Patching of cells in whole-cell or 'permeabilised' configuration 97
2.4.6 Protocol for the recording of action potentials 97
2.4.7 Protocols for the recording of L-type Ca^{2+} currents 98
2.4.8 Protocol for the recording of delayed rectifier K^{+} currents 99
2.4.9 Data acquisition and analysis 99
2.5 Measurement of cell contractions 100
2.6 Fluorescent indicators for ions 101
2.6.1 Choice of Ca^{2+} sensitive fluorescent probe 102
2.6.2 Loading of cells with fluorescent probes 105
2.6.3 Measurements of whole-cell Ca^{2+} transients 106
2.7 Measurement of coronary perfusion pressure, force and rate of contraction in Langendorff-perfused mouse hearts 107
2.8 Drugs 109
2.9 Statistics 110

Chapter 3 Novel pathways in the positive inotropic response to isoprenaline in ventricular muscle 111

3.1 Introduction 112

3.2 Methods 114

3.3 Results.....115

3.3.1 The contractile response to β-adrenoceptor stimulation was blunted in ventricular myocytes from Tpcn2$^{-/-}$ mice.....115

3.3.2 The contractile response to β-adrenoceptor stimulation was blunted in Langendorff-perfused hearts from Tpcn2$^{-/-}$ mice 120

3.3.3 The contractile response to β-adrenoceptor stimulation was blunted in guinea pig ventricular myocytes pre-treated with bafilomycin 124

3.3.4 There was a trend towards a blunting of the contractile response to β-adrenoceptor stimulation in guinea pig ventricular myocytes pre-treated with Ned-19 125

3.3.5 Bafilomycin exerted an anti-arrhythmic action in the presence of high-dose isoprenaline.....130

3.4 Discussion 130

Chapter 4 Effects of endocannabinoids on excitation-contraction coupling in guinea pig ventricular myocytes 137

4.1 Introduction 138

4.2 Methods 140

4.3 Results.....143

4.3.1 Anandamide markedly reduced ventricular myocyte contractility 143

4.3.2 Anandamide reduced amplitude of whole-cell Ca^{2+} transients ……146

4.3.3 Anandamide reduced action potential duration 149

4.3.4 The effects of anandamide on action potential duration and contraction were not due to breakdown to metabolic products.....155

4.3.5 Anandamide inhibited L-type Ca^{2+} currents (I_{CaL}) 157

4.3.6 Anandamide accelerated inactivation of the L-type Ca^{2+} channel 163

4.3.7 Anandamide inhibited the slowly activating (I_{Ks}) but not the rapidly activating component (I_{Kr}) of the delayed rectifier K^+ current (I_K). 170

4.3.8 The effects of anandamide did not appear to be mediated by conventional cannabinoid receptors 171

4.3.9 Selective cannabinoid receptor agonists failed to mimic the effects of anandamide 178

4.3.10 2-arachidonoylglycerol was without significant effect on ventricular myocyte action potential parameters or contractions 188

4.4 Discussion 188

Chapter 5 Effects of endocannabinoids on excitation-contraction coupling in the presence of β-adrenoceptor stimulation 196

5.1 Introduction 197

5.2 Methods 199

5.3 Results 201

5.3.1 Adenosine attenuated the increases in contraction and I_{CaL} amplitude evoked by isoprenaline 201

5.3.2 The effects of adenosine were pertussis toxin sensitive 203

5.3.3 The effects of anandamide to reduce myocyte contractility and action potential duration were smaller in magnitude in the presence of isoprenaline 210

5.3.4 Anandamide inhibited L-type Ca^{2+} currents in the presence of isoprenaline 217

5.3.5 The effects of anandamide in the presence of isoprenaline were not prevented by pre-treatment of myocytes with pertussis toxin 218

5.3.6 The negative inotropic effect of nifedipine was reduced in the presence of isoprenaline 227

5.3.7 Anandamide exerted an anti-arrhythmic action in the presence of high dose isoprenaline 229

5.3.8 ACEA, a selective CB_1 receptor agonist was without significant effect on I_{CaL} amplitude in the presence of isoprenaline 231

5.3.9 Effect of 2-arachidonoylglycerol on action potentials and contractions in the presence of isoprenaline 232

5.4 Discussion 235

Chapter 6 Effects of Δ^9-tetrahydrocannabinol on excitation-contraction coupling in guinea pig ventricular myocytes 240

6.1 Introduction 241

6.2 Methods 242

6.3 Results 243

6.3.1 Δ^9-THC markedly reduced myocyte contractility 243

6.3.2 Δ^9-THC inhibited the L-type Ca^{2+} current (I_{CaL}) 244

6.3.3 Δ^9-THC inhibited the slowly activating (I_{Ks}) but not the rapidly activating component (I_{Kr}) of the delayed rectifier K^+ current (I_K) ... 255

6.3.4 Δ^9-THC reduced myocyte contractility in the presence of isoprenaline 259

6.4 Discussion 262

Chapter 7 General discussion 265

7.1 Novel pathways in cardiac β-adrenoceptor signalling: NAADP 266

7.2 Effects of anandamide and Δ^9-THC on cardiac EC coupling 270

7.2.1 Evidence against a receptor-mediated negative inotropic action of cannabinoids in cardiac ventricular muscle 271

7.2.2 Possible mechanisms of action of anandamide and Δ^9-THC in ventricular muscle 274

List of figures

Chapter 3

Figure 3.1 Mean data showing the blunted contractile response to isoprenaline in ventricular myocytes from *Tpcn2-/-* mice.....116

Figure 3.2 Representative contraction traces showing the response to 3 nM isoprenaline a cells from *Tpcn2*$^{-/-}$ and wild-type mice. 117

Figure 3.3 Mean data showing lack of difference in basal force of contraction between wild-type and *Tpcn2*$^{-/-}$ myocytes.....118

Figure 3.4 Representative action potential traces showing the effects of 3 nM isoprenaline in wild-type and *Tpcn2*$^{-/-}$ cells. 119

Figure 3.5 Mean data showing the similarities between wild-type and *Tpcn2*$^{-/-}$ Langendorff-perfused hearts in the absence of isoprenaline. 121

Figure 3.6 Mean data showing the blunted contractile response to isoprenaline in Langendorff-perfused *Tpcn2*$^{-/-}$ hearts. 122

Figure 3.7 Mean data showing the effects of isoprenaline on coronary perfusion pressure and spontaneous rate in wild-type and *Tpcn2*$^{-/-}$ hearts. 123

Figure 3.8 Mean data showing the effects of bafilomycin on contractile responses to isoprenaline in guinea pig ventricular myocytes. 126

Figure 3.9 Mean data showing the effect of Ned-19 pre-incubation on contractile responses to isoprenaline in guinea pig ventricular myocytes.....128

Figure 3.10 Mean data showing the effect of Ned-19 on contractile responses to isoprenaline with the application of exclusion criteria. 129

Figure 3.11 Bar graph showing the cumulative proportion of bafilomycin- and DMSO-treated cells showing arrhythmias after application of 50 nM isoprenaline. 131

Chapter 4

Figure 4.1 Representative contraction after superfusion with anandamide.....144

Figure 4.2 Time course of effect of anandamide or ethanol on amplitude of sarcomere shortening.....145

Figure 4.3 Effect of anandamide on Ca^{2+} transient amplitude.....147

Figure 4.4 Effects of anandamide on Ca^{2+} transient amplitude measured using the pentapotassium salt of Fluo-5F.....148

Figure 4.5 Action potential parameters in the absence of drugs.....151

Figure 4.6 Time course of effect of anandamide or ethanol on action potential parameters 152

Figure 4.7 Representative action potential and contraction trace from a cell superfused with anandamide for 10 minutes 153

Figure 4.8 Concentration-dependent effects of anandamide on action potential duration 154

Figure 4.9 Representative action potential and contraction trace from a cell superfused with (R)-(+)-methanandamide 156

Figure 4.10 Effects of anandamide on I_{CaL} parameters over time 159

Figure 4.11 Effects of anandamide on current voltage relationship for I_{CaL} 160

Figure 4.12 Effect of 0.07 % ethanol on current voltage relationship for I_{CaL} 161

Figure 4.13 Effects of anandamide on I_{CaL} properties 162

Figure 4.14 Effects of ethanol on I_{CaL} current voltage relationship in the presence of Cs^+ 164

Figure 4.15 Effects of ethanol on voltage-dependence of inactivation of I_{CaL} in the presence of Cs^+. 165

Figure 4.16 Representative traces showing the effects of ethanol on inactivation of I_{CaL} assessed by a double-pulse protocol delivered via a patch electrode containing Cs^+ ... 166

Figure 4.17 Effect of anandamide on I_{CaL} current voltage relationship in the presence of Cs^+ 167

Figure 4.18 Effects of anandamide on voltage-dependence of inactivation of I_{CaL} in the presence of Cs^+ 168

Figure 4.19 Representative traces showing the effects of ethanol on inactivation of I_{CaL} assessed by a double-pulse protocol delivered via a patch electrode containing Cs^+ ... 169

Figure 4.20 Representative traces showing the effects of anandamide on I_K. 172

Figure 4.21 Effects of anandamide on I_K. 173

Figure 4.22 Representative traces showing the effects of ethanol on I_K. 174

Figure 4.23 Effects of ethanol vehicle on I_K. 175

Figure 4.24 Effects of anandamide on I_{Ks}. 176

Figure 4.25 Effects of the CB_1 receptor antagonist AM281 on contractile response to anandamide. 179

Figure 4.26 Time course of the effects of 10 μM anandamide in the presence of AM 281 (or equivalent concentrations of vehicle) on action potential parameters. 180

Figure 4.27 Concentration-dependent effects of anandamide on action potential duration in the absence and presence of AM281. 181

Figure 4.28 Effects of the CB_2 receptor antagonist AM630 on contractile response to anandamide. 182

Figure 4.29 Time course of the effects of 10 μM anandamide in the presence of AM 630 (or equivalent concentrations of vehicle) on action potential parameters. 183

Figure 4.30 Concentration-dependent effects of anandamide on action potential duration in the absence and presence of AM630. 184

Figure 4.31 Representative action potential traces from cells superfused with cannabinoid receptor agonists 185

Figure 4.32 Effects of the CB_1 receptor agonist ACEA (10 μM) on current voltage relationship for I_{CaL}. 186

Figure 4.33 Effects of the CB_2 receptor agonist HU308 (10 μM) on current voltage relationship for I_{CaL}. 187

Figure 4.34 Representative traces to show lack of effect of 2-AG on action potentials and contractions. 189

Chapter 5

Figure 5.1 Lack of effect of adenosine on I_{CaL} current voltage relationship in the absence of isoprenaline 204

Figure 5.2 Effects of adenosine on sarcomere shortening in the presence of isoprenaline 205

Figure 5.3 Effects of adenosine on isoprenaline-stimulated I_{CaL} 206

Figure 5.4 Lack of effect of DMSO vehicle on isoprenaline-stimulated I_{CaL}. 207

Figure 5.5 Lack of effect of adenosine on isoprenaline-stimulated I_{CaL} in cells pre-treated with pertussis toxin 208

Figure 5.6 Mean effects of adenosine on isoprenaline-stimulated I_{CaL} amplitude in the absence and presence of pertussis toxin 209

Figure 5.7 Effects of anandamide on amplitude of contraction in the presence of isoprenaline 212

Figure 5.8 Representative action potential trace from a cell superfused with isoprenaline and anandamide 213

Figure 5.9 Effects of anandamide or ethanol on action potential parameters in the presence of isoprenaline 214

Figure 5.10 Concentration-dependent effects of anandamide in the absence and presence of isoprenaline on amplitude of cell contractions 215

Figure 5.11 Concentration-dependent effects of anandamide on action potential duration in the absence and presence of isoprenaline 216

Figure 5.12 Effects of ethanol vehicle on isoprenaline-stimulated I_{CaL} 220

Figure 5.13 Effects of anandamide on isoprenaline-stimulated I_{CaL} 221

Figure 5.14 Mean data showing comparisons of the effects of anandamide and ethanol to reduce isoprenaline-stimulated I_{CaL} 222

Figure 5.15 Mean reduction in I_{CaL} amplitude in cells superfused with anandamide in the absence and presence of isoprenaline 223

Figure 5.16 Lack of effect of pertussis toxin pre-treatment on the negative inotropic response to anandamide (AEA) in the presence of isoprenaline 224

Figure 5.17 Lack of effect of PTX pre-treatment on the effect of anandamide to reduce amplitude of isoprenaline-stimulated I_{CaL}.....225

Figure 5.18 Mean data summarising the lack of effect of pertussis toxin in preventing the effect of anandamide (AEA) to reduce amplitude of isoprenaline-stimulated I_{CaL} 226

Figure 5.19 Effects of nifedipine on sarcomere shortening in the absence and presence of isoprenaline.....228

Figure 5.20 Example of spontaneous electrical activity induced by 50 nM isoprenaline and suppressed by anandamide.....230

Figure 5.21 Lack of effect of the CB_1 receptor agonist ACEA on isoprenaline-stimulated I_{CaL}.....233

Figure 5.22 Lack of effect of ACEA on isoprenaline-stimulated contractions 234

Chapter 6

Figure 6.1 Concentration-dependent effects of Δ^9-THC on ventricular myocyte contractility 246

Figure 6.2 Lack of effect of 10 µM Δ^9-THC on action potential parameters.....247

Figure 6.3 Representative traces to show the effect of 10 µM Δ^9-THC on action potentials and contractions in guinea pig ventricular myocytes.....248

Figure 6.4 Effects of ethanol vehicle on current voltage relationship for I_{CaL} measured using the perforated patch technique 249

Figure 6.5 Effects of ethanol on voltage-dependence of I_{CaL} inactivation measured using the perforated patch technique.....250

Figure 6.6 Current voltage relationship for I_{CaL} in the presence of 10 µM Δ^9-THC 251

Figure 6.7 Acceleration of the voltage-dependence of inactivation of I_{CaL} in the presence of 10 µM Δ^9-THC.....252

Figure 6.8 Effect of Δ^9-THC on I_{CaL} current voltage relationship in the presence of Cs^+ 253

Figure 6.9 Acceleration of the voltage-dependence of inactivation of I_{CaL} in the presence of Δ^9-THC with Cs^+ in the patch electrode.....254

Figure 6.10 Effects of 10 µM Δ^9-THC on amplitude of I_K.....256

Figure 6.11 Lack of effect of ethanol vehicle on I_K measured using amphotericin-permeabilised patch 257

Figure 6.12 Effect of 10 µM Δ^9-THC on amplitude of I_K in the presence of 1 µM E4031 258

Figure 6.13 Effect of Δ^9-THC on amplitude of contraction in the presence of isoprenaline.....260

Figure 6.14 Representative trace illustrating the effects of Δ^9-THC in the presence of isoprenaline on action potentials and contractions in guinea pig ventricular myocytes. 261

Chapter 7

Figure 7.1 Schematic diagram illustrating the putative interaction between the β-adrenoceptor signalling pathway, NAADP and TPC2. 269

List of Abbreviations

2-AG	2-arachidonoylglycerol
2-APB	2-aminoethoxydiphenylborane
4-AP	4-aminopyridine
AC	Adenylyl cyclase
AEA	N-arachidonoylethanolamine
AKAP	A-kinase anchoring protein
-AM	Acetoxymethyl ester
AMP	Adenosine monophosphate
AP	Action potential
APD_{90}	Time to 90% action potential repolarisation
APD_{50}	Time to 50% action potential repolarisation
APD_{20}	Time to 20% action potential repolarisation
ARC	ADP-ribosyl cyclase
ATP	Adenosine triphosphate
AVN	Atrio-ventricular node
BAPTA	1,2-bis(o-aminophenoxy)ethane-N,N,N',N'-tetraacetic acid
BZ194	3-carboxy-1-octylcarbamoylmethyl-pyridinium
$[Ca^{2+}]_i$	Intracellular calcium concentration
cADPR	Cyclic adenosine diphopsphate ribose
cADPR-P	Cyclic adenosine diphopsphate ribose phosphate
CaMKII	Calmodulin dependent protein kinase II
cAMP	3'-5'-cyclic adenosine monophosphate
cDNA	Complementary deoxyribonucleic acid
CB	Cannabinoid
CGRP	Calcitonin gene related peptide
CHO	Chinese hamster ovary
CICR	Calcium-induced calcium release
CNS	Central nervous system
COX	Cyclooxygenase
CPA	Cyclopiazonic acid
CPVT	Catecholaminergic polymorphic ventricular tachycardia
DAG	Diacylglycerol
DCC	Discontinuous current clamp
DHP	Dihydropyridine
dSEVC	Discontinuous single electrode voltage clamp
DMEM	Dulbecco's modified Eagle's medium
DMSO	Dimethyl sulphoxide
EC_{50}	Half maximal effective concentration
EGTA	Ethylene glycol tetraacetic acid
ER	Endoplasmic reticulum
EtOH	Ethanol
FAAH	Fatty acid amide hydrolase
FKBP	FK506 binding protein
GDE	Glycerophosphodiesterase
GIRK channel	G-protein-coupled inwardly rectifying potassium channel
GPCR	G-protein-coupled receptor
GPN	Glycyl-L-phenylalanine 2-naphthylamide
GP-NAE	Glycerophospho-*N*-acylethanolamine
GTP	Guanosine triphosphate
GTPγS	Guanosine 5'-O-(3-thiotriphosphate)
HEPES	4-(2-hydroxyethyl)-1-piperazineethanesulphonic acid
HERG	Human ether-a-go-go related gene
HPLC	High performance liquid chromatography
IC_{50}	Half maximal inhibitory concentration

I_{CaL}	L-type calcium current
I_K	Potassium current
I_{KACh}	Inward-rectifying potassium channel activated by acetylcholine
I_{Kr}	Rapidly activating component of the delayed rectifier potassium current
I_{Ks}	Slowly activating component of the delayed rectifier potassium current
I_{Na}	Sodium current
IP_3	Inositol 1,4,5-trisphosphate
I_{si}	Second inward current
I_{to}	Transient outward current
K_d	Dissociation constant
LAMP	Lysosomal associated membrane protein
L-NAME	Nω-Ntiro-L-arginine methyl ester
LQT3	Long QT syndrome type 3
LTCC	L-type calcium channel
MAGL	Monoacylglycerol lipase
mAKAP	Muscle A kinase anchoring protein
MAP kinase	Mitogen activated protein kinase
MS	Mass spectrometry
mRNA	Messenger ribonucleic acid
NAAA	*N*-acylethanolamine-hydrolysing acid amidase
NAADP	Nicotinic acid adenine dinucleotide phosphate
NAD^+	Nicotinamide adenine dinucleotide
$NADP^+$	Nicotinamide adenine dinucleotide phosphate
NAPE	*N*-arachidonoylphosphatidyl ethanolamine
NAT	*N*-acyl transferase
NCX	Sodium calcium exchanger
Ned	NAADP EON discovered
NKA	Sodium potassium ATPase
NMR	Nuclear magnetic resonance
PIP_2	Phosphatidylinositol 4,5-bisphosphate
PKA	Protein kinase A
PLB	Phospholamban
PLC	Phospholipase C
PMCA	Plasma membrane calcium ATP-ase
PP	Protein phosphatase
PTX	Pertussis toxin
PSS	Physiological salt solution
QCD	Quarky calcium depletion
QCR	Quarky calcium release
RMP	Resting membrane potential
ROCS	Rapid overlay of chemical structures
RyR	Ryanodine receptor
SAN	Sino-atrial node
SERCA	Sarco/endoplasmic reticulum calcium ATPase
SR	Sarcoplasmic reticulum
Δ^9-THC	Δ^9-tetrahydrocannabinol
TnC	Troponin C
TnI	Troponin I
TnT	Troponin T
TPC	Two-pore channel
TRP-ML1	Transient receptor potential mucolipin 1
TRPV1	Transient receptor potential vanilloid 1
UV	Ultraviolet
ZINC	Zinc is not commercial

Chapter 1
Introduction

1.1 General introduction

The heart is a four-chambered muscular organ that serves to pump blood around the body such that all organs and tissues are supplied with sufficient oxygen and nutrients to maintain function, and toxic waste products are removed. In mammals, the heart operates as part of a double circulatory system, with the right side collecting deoxygenated blood from the body and circulating it to the lungs (pulmonary circulation) and the left side supplying oxygenated blood to the body (systemic circulation). The two upper chambers of the heart (atria) collect blood and contract to supply it to the two lower chambers, the ventricles. The majority of the heart's contractile force arises from the ventricles, and the thick muscular wall of the left ventricle enables blood to be expelled at sufficient pressure to supply the entire systemic circulation.

Cardiac muscle is made up of contractile muscle cells, termed myocytes, which contract in a co-ordinated manner in response to electrical stimuli termed action potentials (APs). Key to maintaining co-ordinated contraction of individual cells are gap junctions, specialised connecting regions which provide a pathway of low resistance for the passage of APs between cells, permitting the heart to function as an electrical syncytium.

The essential requirement of Ca^{2+} for the generation of cardiac contractile force was first recognised over a century ago by Sydney Ringer, who famously observed that when hearts were perfused with hard London tap water they would continue to beat for hours, but when perfused with distilled water, would cease beating within minutes unless Ca^{2+} salts were added (Ringer, 1883). Since Ringer's discovery, the role of Ca^{2+}

in regulation of cardiac contractile force has been the subject of detailed investigation in a vast array of research studies.

A general scheme of the mechanism underlying cardiac contraction is now widely accepted, and Ca^{2+} is a key player (Bers, 2002; Bers, 2008). In this scheme, Ca^{2+} enters cardiac myocytes upon arrival of an AP, flowing down its concentration gradient via specialised protein channels, known as L-type Ca^{2+} channels (LTCCs) located at the cell surface of cardiac myocytes (the sarcolemma). An increase in sarcoplasmic Ca^{2+} concentration triggers the opening of ryanodine receptors (RyR; RyR2 in the heart), which are specialised intracellular Ca^{2+} gated channels located to the sarcoplasmic reticulum (SR, the primary intracellular Ca^{2+} store in muscle cells). Upon RyR opening, a much larger quantity of Ca^{2+} is released from the SR taking the sarcoplasmic Ca^{2+} concentration from around 100 nM to in excess of 1 μM, and as high as 10 μM in localised regions (Cannell *et al.*, 2012). This amplification process, known as Ca^{2+}-induced Ca^{2+} release (CICR) is the fundamental mechanism underlying initiation of contraction in cardiac muscle. This transient elevation in $[Ca^{2+}]_i$ (referred to as the Ca^{2+} transient) increases Ca^{2+} binding to the protein troponin C, which regulates the function of the cellular contractile machinery (myofilaments). Relaxation ensues when the Ca^{2+} transient decays as a result of transportation of Ca^{2+} out of the sarcoplasm. This transportation occurs via several pathways including uptake of Ca^{2+} back into the SR store via a Ca^{2+} ATPase located to the SR (called the sarco/endoplasmic reticulum ATPase or SERCA; SERCA2 isoform in the heart) and to a lesser extent into mitochondria, or by extrusion to the extracellular space via a sarcolemmal Na^+ Ca^{2+} exchanger protein (NCX; NCX1 in the heart) and to a lesser extent by a Ca^{2+} ATPase located at the sarcolemmal membrane (Bers, 2008).

Despite the crucial nature of Ca^{2+} to the contractile mechanism in cardiac myocytes, Ca^{2+} is inherently toxic to all cells. In fact, Ca^{2+} is a ubiquitous and multifunctional second messenger which transduces extracellular signals to intracellular messages (a 'second messenger') in virtually all cell types (Berridge *et al.*, 2000). The shape of the Ca^{2+} signal varies depending on the message to be conveyed; for example longer lasting increases in $[Ca^{2+}]_i$ activate metabolic processes and are associated with gene transcription, while the Ca^{2+} transients which trigger contraction are shorter, lasting (50 – 200 ms) (Berridge *et al.*, 2000; Bers, 2008).

In the heart, modulation of $[Ca^{2+}]_i$ is the key mechanism by which force of contraction may be regulated. In the well-known 'fight or flight' response to stress, activation of the sympathetic nervous system leads to release of neurotransmitters (in particular the catecholamines adrenaline and noradrenaline, acting at specific cardiac cell surface receptors, in particular β_1-adrenoceptors), which potently increase the rate and force of cardiac contraction so that blood flow to muscles will be adequate to meet increased metabolic demand (Levick, 1999). Activation of enzymes called adenylyl cyclases by stimulatory G-proteins (G_s; linked to β_1-adrenoceptors) leads to increased synthesis of cyclic adenosine monophosphate (cAMP; a second messenger first described by Sutherland (Sutherland, 1972)), which then activates a protein kinase enzyme, cAMP-dependent protein kinase (PKA). PKA phosphorylates various proteins involved in the CICR process, culminating in increased Ca^{2+} entry into cells, increased release of Ca^{2+} from the SR and increased contractility. Aberrations in this, and other intracellular signal transduction pathways can lead to impaired cardiac Ca^{2+} handling, and are associated with various cardiac pathologies including congestive heart failure, cardiac hypertrophy and arrhythmias (Marks, 2003). Tight spatial and temporal control of intracellular Ca^{2+} homeostasis is therefore critical to normal cardiac function.

Understanding the mechanisms by which Ca^{2+} dynamics are regulated in the heart is therefore of clinical interest and scientific importance.

Recently the Ca^{2+}mobilising messenger nicotinic acid adenine dinucleotide phosphate (NAADP) has been implicated not only as a novel modulator of cardiac EC coupling under normal conditions, but as a potential player in mediating the positive inotropic response to cardiac β-adrenoceptor stimulation (Higashida *et al.*, 1999; Macgregor *et al.*, 2007a; Lewis *et al.*, 2012). However, there is some debate in the literature regarding the nature of the molecular target for NAADP. One potential player is the two-pore channel 2 (TPC2) (Calcraft *et al.*, 2009), but investigations regarding its role in the cardiac myocytes are limited (Elson *et al.*, 2010). The aims of chapter 4 in this thesis were to further investigate the role of TPC2 in the positive inotropic response to β-adrenoceptor stimulation in cardiac ventricular muscle.

It is well known that administration of Δ^9-tetrahydrocannabinol (Δ^9-THC), the principal psychoactive constituent in *Cannabis sativa* preparations, has depressant effects on heart rate and contractility in addition to numerous other pharmacological effects, not least its well-known psychotropic action. Interest in the actions of cannabinoids on the heart has grown in recent years following the discovery that many of the effects of Δ^9-THC are mediated through specific receptors, (the most studied of which are cannabinoid CB_1 and CB_2 receptors (Howlett *et al.*, 2002)), and that a lipid signalling molecule named 'anandamide' (the first endogenous ligand of cannabinoid receptors to be discovered, (Devane *et al.*, 1992b)) also has effects on cardiac contractility and rate when administered to animals *in vivo* (Malinowska *et al.*, 2012). It has been argued that at least some of these effects may be mediated by direct actions on cardiac muscle cells (Ford *et al.*, 2002; Li *et al.*, 2009).

Yet further interest has arisen following suggestions that targeting cannabinoid receptors may prove a promising therapeutic strategy in a number of disease states (Pacher *et al.*, 2006; Montecucco *et al.*, 2012). Since many new chemical entities fail as a result of cardiotoxicity, an understanding of the actions of endogenous cannabinoids and the function of cardiac cannabinoid receptors is crucial if therapies targeting cannabinoid receptors are to succeed. However, the picture has been complicated by findings that many of the effects of cannabinoids and their endogenous counterparts are mediated through mechanisms which are independent of conventional cannabinoid receptors. In particular, the highly lipophilic nature of both Δ^9-THC and endocannabinoids means they have also been found to have direct actions on ion channels and on the cell membrane itself (Oz, 2006). Recent evidence has confirmed that cannabinoid receptors are present in the myocardium (Weis *et al.*, 2010). Despite this, very few studies have addressed the actions of cannabinoids and endogenous cannabinoids in the heart, and even fewer in single cardiac myocytes. Of the studies which have been performed, findings are conflicting, and underlying mechanisms controversial (Andrag *et al.*, 2013).

In light of this controversy, the aim of this thesis is to provide further insight into the effects of anandamide, Δ^9-THC and related cannabinoids in isolated cardiac ventricular myocytes in the absence and presence of β-adrenoceptor stimulation. This chapter includes a review of the mechanisms underlying cardiac excitation-contraction coupling, an overview of the endocannabinoid system concentrating particularly on its role in the cardiovascular system, and an overview of Ca^{2+} mobilising second messengers, in particular NAADP.

1.2 Cardiac muscle

Healthy ventricular myocytes are rod-shaped, with average dimensions 140 µm x 30 µm x 13 µm (Bers, 2001). Cells from the atria or nodal regions are generally smaller and more spindle-shaped, but cell morphology is highly variable.

Myocytes are packed with myofibrils which account for 45 – 60 % of the total cell volume and stretch the length of the cell with an anchoring point at each end: the fascia adherens junction (Bers, 2001). Each myofibril is composed of several repeating contractile units termed sarcomeres (resting length 1.8 – 2.4 µm) (Walker *et al.*, 1999), consisting of an overlapping arrangement of thick (myosin) and thin (actin) filaments, which give cells their characteristic striated appearance when viewed under a light microscope. Actin filaments, together with associated regulatory proteins troponin and tropomyosin, are anchored to the protein α-actinin at the Z line (Z for 'zwischen', which marks the edge of the sarcomere), and form the isotropic I band. Myosin filaments (anisotropic A-bands) are located centrally within the sarcomere, around the M line, and are anchored by titin filaments which act as molecular springs, spanning the length of the sarcomere and providing structural support (Bers, 2001).

Ventricular myocytes contain a large number of transverse tubules (T-tubules), invaginations of the sarcolemma that run along the Z-lines (Bers, 2001). Soeller and Cannell have used two-photon microscopy to demonstrate that T-tubules actually form a complex network deep within myocytes which contains many transverse and longitudinal elements (Soeller *et al.*, 1999). This arrangement places the electrically excitable sarcolemma in very close proximity with the SR. T-tubule membrane fractions contain a higher density of LTCCs than the surface sarcolemma (Scriven *et al.*, 2000), and these are separated from RyRs by a distance of just 12 nm (Brochet *et*

al., 2005). This close apposition at the so-called 'dyadic cleft' allows for highly efficient delivery of extracellular Ca^{2+} to the RyR, while the extensive T-tubular network allows for a homogenous release of SR Ca^{2+} in close proximity to each sarcomere (Bers, 2001). T-tubule regulation is therefore highly critical in efficient EC coupling; dysregulation has been associated with heart failure and diabetic cardiomyopathy (Ibrahim *et al.*, 2011).

Cardiac muscle is rich in mitochondria, which synthesise ATP by oxidative phosphorylation in order to supply energy for repeated contraction (Bers, 2001).

1.3 Electrical activity

All cardiac myocytes are linked electrically by specialised connections known as intercalated discs. These connections contain gap junctions, composed of the protein connexin, which forms a hollow tube such that the cytoplasm of adjacent cells is connected, permitting the low resistance transfer of electrical signals between cells allowing the heart to function as an electrical syncitium (Bers, 2001).

EC coupling in the heart is triggered by an electrical waveform known as an AP, which originates in a specialised region known as the sino-atrial node (SAN) located in the right atrium (Levick, 1999). Excitatory signals pass first through the atria, which contract to force blood into the ventricles and coronary circulation. In order to allow for adequate ventricular filling, the electrical impulse is delayed by a non-conducting barrier between atria and ventricles (the annulus fibrosus cordis), and must instead pass through a specialised conducting region, the atrioventricular node (AVN) which delays the transmission of the impulse to the ventricles by around 100 ms (Levick, 1999). It is then transmitted via the bundle of His to the apex of the heart, and up through the

ventricular tissue via Purkinje fibres, so that the ventricular contraction commences at the apex. The AP waveform is generated by the activities of various ion channels and exchangers present at the sarcolemmal membrane of cardiac myocytes (Levick, 1999).

1.3.1 Resting membrane potentials

In the absence of electrical stimulation, atrial and ventricular myocytes are quiescent and maintain a stable electrical potential difference across their cell membranes of -70 to -90 mV (i.e. the intracellular side of the cell membrane is more negative with respect to the extracellular side). In a resting myocyte, the permeability of the sarcolemmal membrane to K^+ is far greater than to Na^+, Ca^{2+} and Cl^- ions, due largely to the existence of inwardly rectifying I_{K1} channels, through which K^+ ions diffuse down their concentration gradient, leaving an excess negative charge intracellularly. Inwardly rectifying channels pass current at potentials more negative to E_K far more readily than they pass current at potentials positive to E_K (where the electrochemical gradient for K^+ under physiological conditions would favour outward flow of K^+ and repolarisation) (Whalley *et al.*, 1995). This is due to block of the channel at positive potentials by intracellular Mg^{2+} and polyamines which essentially 'plug' the channel, preventing efflux of K^+ and reducing repolarising influences at positive potentials (Matsuda *et al.*, 1987).

As a result, the resting membrane potential is close to the Nernst equilibrium or 'reversal' potential for K^+ (E_K), which would be -91 mV assuming the following effective concentrations of K^+: $[K]_o$ 4.5 mM, $[K]_i$ 135 mM at 37ºC (Whalley *et al.*, 1995). In reality the resting membrane potential is usually slightly more positive than E_K (-80 to -85 mV in a ventricular cell) due to a small inward leak of Na^+ ions. The resting membrane potential of a cell can be predicted by the Goldman-Hodgkin-Katz

equation, which takes into account the permeability of the cell membrane to various ions and their concentration gradients (Goldman, 1943). Given the far greater permeability of the membrane to K^+ than other ions, it is unsurprising that in hyperkalaemic patients, the membrane would become depolarised, as a result of reduced driving force for K^+ efflux. The chemical gradients for K^+ and Na^+ ions are maintained by the Na^+-K^+ ATPase (NKA) (Levick, 1999).

In contrast to atrial and ventricular myocytes, cells from the SAN or AVN display unstable diastolic potentials which contribute to the spontaneous generation of APs. Cells from these regions therefore contract in the absence of electrical stimulation. SAN cells have the fastest intrinsic rate of firing, and under physiological conditions would act as the cardiac 'pacemaker', setting the rate of contraction. In some pathological conditions where these cells are damaged, those from the AVN can take over as the chief pacemaker region, albeit at a lower rate. In these patients artificial pacemakers are considered (Levick, 1999).

1.3.2 Action potentials

The application of a depolarising stimulus to an atrial or ventricular myocyte results in the generation of an AP. The AP waveform is determined by the flux of various inward and outward ionic currents, as well as transporter activity (Whalley *et al.*, 1995). The ventricular AP may be described as consisting of five phases:

1.3.2.1 Phase 0: rapid depolarisation.

Depolarisation of the membrane results in the activation of voltage-gated Na^+ channels and results in a brief increase in the permeability of the membrane to Na^+ ions, which flow into the cell along their electrochemical gradient. The critical firing threshold is the potential at which enough voltage-gated Na^+ channels are activated to overcome the strong repolarising influence of inwardly rectifying I_{K1} channels (around -60 mV). Influx of Na^+ forces the membrane potential to a peak of around +40 mV, so that there is an excess of positive charge intracellularly. The peak of the AP never reaches the reversal potential for Na^+ (around +70 mV), because there is always some small outward flow of K^+ ions, despite the inward rectification properties of I_{K1} channels (Whalley *et al.*, 1995). More than 200 mutations have been identified in the gene encoding the cardiac Na^+ channel α subunit, *SCN5A*, which are associated with conditions such as long QT syndrome type 3 (LQT3) and Brugada syndrome (Ruan *et al.*, 2009).

Depolarisation of the cell membrane then triggers the activation of numerous time-dependent outward K^+ conductances, which along with LTCCs, are key players in mediating the subsequent stages of the AP, which will now be described. The nature of these K^+ conductances leads to considerable heterogeneity in AP configuration within individual hearts and between species.

1.3.2.2 Phase 1: early repolarisation.

Voltage-dependent inactivation of Na^+ channels occurs 1-2 ms after they open (Whalley *et al.*, 1995). As a result, further influx of Na^+ is prevented and another current, the transient outward current (I_{to}) is activated. I_{to} is thought to consist of 2

components (Tseng *et al.*, 1989): I_{to1} is sensitive to 4-AP and therefore carried by K^+ ions; I_{to2} or $I_{Ca.Cl}$ is a Ca^{2+} activated transient Cl^- current (inward flow of Cl^- ions). Atrial myocytes, and ventricular myocytes from mouse and rat exhibit prominent I_{to} currents, and therefore have a prominent early repolarisation phase. This leads to a shorter ventricular AP in these species, which lacks the prolonged plateau phase characteristic of guinea pig, rabbit and human ventricular APs. Guinea pig ventricular myocytes in contrast do not have any I_{to} current (Sipido *et al.*, 1995b), and therefore do not exhibit the 'notch' characteristic of early repolarisation. Expression of I_{to} currents also appears to vary within the ventricular wall of many species (reviewed in Lukas, 1997). LTCCs are activated at potentials positive to around -40 mV, and so are also active during the early repolarisation phase (Whalley *et al.*, 1995).

1.3.2.3 Phase 2: the plateau.

At the beginning of the plateau phase, I_{to} inactivates, and the depolarising influence of Ca^{2+} influx through LTCCs (which are slow to inactivate, ~ 100 ms) is dominant. The primary role of this inward Ca^{2+} current is to trigger Ca^{2+} release from the sarcoplasmic reticulum (a process termed Ca^{2+}-induced Ca^{2+} release; CICR), which then activates the myofilaments and initiates cell contraction, which will be discussed later. As LTCCs begin to inactivate as a function of time, voltage and intracellular Ca^{2+} concentration, NCX (operating in Ca^{2+} extrusion mode; efflux of 1 Ca^{2+} ion in exchange for entry of 3 Na^+ ions) becomes dominant in maintaining depolarisation (Bers, 2002). During the plateau, inward currents are finely balanced with outward K^+ currents which occur predominantly through the delayed outward rectifier K^+ current (I_K), which activates slowly during the plateau phase. The inward rectification property

of I_{K1} channels is also important in enabling the plateau to remain stable at positive potentials (Whalley *et al.*, 1995).

1.3.2.4 Phase 3: late repolarisation.

The stable plateau comes to an end as I_{CaL} inactivates, and I_K becomes fully activated. In several species, including guinea pig, I_K consists of 2 components: I_{Kr}, the rapidly activating component which is sensitive to the class III antiarrhythmic agents E-4031 and d-sotalol, and I_{Ks}, the slowly activating component (Sanguinetti *et al.*, 1990). I_{Kr} exhibits strong inward rectification at depolarised membrane potentials due to C-type inactivation, while I_{Ks} does not rectify and has an almost linear current voltage relationship. It is not sensitive to methanesulphonanilide class III antiarrhythmic agents (Sanguinetti *et al.*, 1990). As the depolarising influence of K^+ efflux dominates, I_{K1} channels begin to contribute again to a steady outward conductance which brings the membrane back to resting potential. In atrial cells, another K^+ current, I_{KACh}, contributes to the maintenance of resting potential when there is some vagal tone, and plays a dominant role in repolarisation during phase 3 (Whalley *et al.*, 1995). I_{KACh} is present in ventricular cells of some species, for example ferret (Ito *et al.*, 1995) and rat (Song *et al.*, 1996) but not guinea pig (Song *et al.*, 1996).

1.3.2.5 Phase 4: resting membrane potential.

As the repolarisation phase is completed, cells return to their original resting potential, as outlined previously.

1.3.3 Modulation of cardiac ionic currents

The various ionic currents contributing to the shape of the AP varies according to species, region of the heart being studied, and position of cells within the myocardial wall (endocardial, epicardial or mid-myocardial). The large degree of AP heterogeneity observed in cells from one heart, and indeed from different species is therefore unsurprising. In addition, many, if not all, of the ion channels carrying these currents can be modulated by intracellular signal transduction pathways leading to altered function. The channels which have most relevance to this thesis will now be discussed, with particular reference to their modulation during β-adrenoceptor stimulation.

1.3.3.1 L-Type Ca^{2+} Currents (I_{CaL})

Depolarisation of cardiac ventricular or atrial myocytes after the AP upstroke opens LTCCs leading to Ca^{2+} influx, which generates the AP plateau and is also the major trigger for CICR (which will be discussed in section 1.5.1). The first evidence for an inward current carried by Ca^{2+} ions in the heart was obtained from voltage-clamp experiments in Purkinje fibres (Reuter, 1967). Because the recorded current took several tens of milliseconds to reach a peak (in contrast to the rapid peak of the TTX-sensitive Na^{+} current), it was reported in the literature as 'slow' or sometimes 'second' inward current, I_{si}. It was appreciated that initial recordings of I_{si} in multicellular preparations were inaccurate due to problems with series resistance and poor voltage control. The development of methods for the isolation of single ventricular myocytes and the use of a two-electrode voltage-clamp technique, enabled investigators to record a whole-cell Ca^{2+} current with a larger amplitude than I_{si} and which reached a peak in 2 ms (Mitchell *et al.*, 1983). Following this, work by Nowycky and colleagues revealed

the existence of three types of Ca^{2+} current in dorsal root ganglion cells, which they named L-, T- and N-type according to their properties (Nowycky *et al.*, 1985). These names were subsequently adopted in the literature.

LTCCs are composed of 4 subunits, α_1, which is the main functional component of the channel complex, and the auxiliary subunits β and α_2-δ. The functional subunit of the cardiac LTCC (CaV1.2) was cloned in 1989 (Mikami *et al.*, 1989). There are at least 10 different genes encoding α_1 subunits expressed in different tissues, for example skeletal muscle (CaV1.1). The α_1 subunit comprises 4 homologous domains, each of which has six transmembrane α-helices, designated S1 to S6. The S5 and S6 segments of each domain form the inner walls of the hydrophobic channel pore and positively charged arginine and lysine residues in the S4 segments confer voltage sensitivity; depolarisation of the sarcolemma towards the threshold for activation (~-40 mV) leads to an outward rotation of the S4 segments leading to opening of the channel pore and Ca^{2+} influx (Catterall, 2000). The β subunit is located intracellularly, and is thought to play a role in trafficking of the α_1 subunit to the sarcolemma, as well as in modulating its gating properties (Kamp *et al.*, 2000). The δ subunit has a single transmembrane domain, and is linked to the extracellular α_2 subunit via a disulphide bridge. It may play a role in modulating the biophysical properties of the channel and trafficking to the membrane (Davies *et al.*, 2007).

Inactivation of I_{CaL} occurs through both voltage and Ca^{2+}-dependent mechanisms (Cens *et al.*, 2006). Voltage-dependent inactivation has a much slower time course than Ca^{2+}-dependent inactivation as illustrated in classical experiments where Ca^{2+} is substituted by Ba^{2+} as the charge carrier, or in patch clamp experiments with Ca^{2+} in the presence of EGTA to abolish cellular Ca^{2+} transients (Bers *et al.*, 1999). Under physiological conditions, Ca^{2+} dependent inactivation plays a more

prominent role than voltage-dependent inactivation of I_{CaL} and is influenced both by Ca^{2+} entering through the channel itself, and by Ca^{2+} released from the SR via RyRs (Sham *et al.*, 1995); increasing SR load accelerates inactivation (Sipido *et al.*, 1995a). The process is mediated by Ca^{2+} binding to calmodulin tethered to the C-terminus of the α_1 subunit (Peterson *et al.*, 1999). The use of engineered Ca^{2+}-insensitive calmodulins has been shown to prolong APs, demonstrating the importance of Ca^{2+} dependent inactivation in determining APD (Alseikhan *et al.*, 2002). During prolonged depolarisation, I_{CaL} can become largely inactivated during the Ca^{2+} transient but can recover as $[Ca^{2+}]_i$ declines (Sipido *et al.*, 1995a), a mechanism which could underlie the development of early afterdepolarisations and arrhythmias. Ca^{2+} dependent inactivation therefore results in a local negative feedback mechanism, presumably to prevent harmful cellular Ca^{2+} overload, which is facilitated by the close apposition of LTCCs and RyRs at the dyadic cleft.

Modulation of LTCC properties by various signalling pathways and drugs can influence the inotropic state of the heart. Noradrenaline, and other agonists acting at cardiac β_1-adrenoceptors cause a positive inotropic effect by increasing the amplitude of I_{CaL} through stimulation of adenylyl cyclases leading to activation of cAMP-dependent protein kinase A (PKA). Phosphorylation sites for PKA exist on the α_1-subunit of the LTCC at Ser-1928 (De Jongh *et al.*, 1996) and at Ser-459, Ser-478 and Ser-479 of the β subunit (Gerhardstein *et al.*, 1999). PKA-induced phosphorylation of the channel results in augmentation of whole-cell I_{CaL} through an increase in open probability of the channels (Tsien *et al.*, 1986) rather than through an increase in conductance or increase in the number of channels in the membrane (Brum *et al.*, 1984). It is therefore frequently observed that the voltage dependence of activation of I_{CaL} is shifted to more negative potentials under conditions of β-adrenoceptor stimulation, such that peak I_{CaL}

occurs at more negative potentials (Bers *et al.*, 1999). PKA signalling is highly compartmentalised, and PKA itself is anchored to the LTCC at the C-terminus of the α_1 subunit by A-kinase anchoring protein 15 (AKAP15) (Hulme *et al.*, 2003).

A key pharmacological characteristic of LTCCs is their sensitivity to dihydropyridines (DHPs); indeed, this was crucial in the initial molecular characterisation of the pore forming α_1 subunit from skeletal muscle (Tanabe *et al.*, 1987). Most DHPs inhibit I_{CaL} (e.g. nifedipine, amlodipine), exhibiting voltage dependent block such that they bind preferentially to the channel in its inactivated state (i.e. binding with greater affinity at more positive potentials) (Hockerman *et al.*, 1997). For example, the K_d for I_{CaL} block by nitrendipine is 700 nM at -80 mV and 0.36 nM at -10 mV (Bean *et al.*, 1984). Other DHPs such as (-)-Bay K 8644 enhance I_{CaL} by greatly prolonging open times of the channel (Hess *et al.*, 1984), binding preferentially to and stabilising the open/inactivated state (Hockerman *et al.*, 1997). Specific amino acids within IIIS5, IIIS6 and IVS6 transmembrane domains of the α_1 subunit have been implicated in DHP binding, which can only occur from the external face of the channel (Hockerman *et al.*, 1997). DHP Ca^{2+} channel blockers are commonly used clinically to reduce blood pressure: vascular LTCCs tend to exhibit far more prolonged depolarisations than skeletal muscle, hence favouring the voltage dependent block of DHPs. Other Ca^{2+} channel blockers such as verapamil (a charged compound) block LTCCs preferentially in their open state and therefore display 'use dependent' block (i.e. requiring depolarising pulses) (Sanguinetti *et al.*, 1984). As a result, verapamil is more cardioselective than DHP Ca^{2+} channel blockers, and is used clinically for the treatment of supraventricular tachycardia, but is contraindicated in heart failure due to its marked negative inotropic action in ventricular muscle.

Other substances including anaesthetics (Hanley *et al.*, 2004) and endogenous lipids such as arachidonic acid (Boland *et al.*, 2008; Roberts-Crowley *et al.*, 2009) can inhibit LTCC activity, and therefore cardiac contraction.

1.3.3.2 The delayed rectifier K^+ current, I_K

The delayed rectifier K^+ current, I_K, is the predominant outward current involved in guinea pig ventricular myocyte repolarisation, and as previously discussed in section 1.3.2.4, comprises two components (I_{Kr} and I_{Ks}) (Sanguinetti *et al.*, 1990).

Voltage-gated K^+ channels are tetramers of α subunits (MacKinnon, 1991). Each α-subunit has six transmembrane domains: S1-S4 form the voltage sensing domain and S5 and S6 form the pore. Pore domains from each of the four α-subunits associate to form a single pore in the middle of the channel (reviewed in Jonsson *et al.*, 2012). In addition to the α-subunits, it is likely that an array of accessory β subunits modulate K^+ channel function and can influence the properties of the ventricular AP and repolarisation, although the precise nature of these is under debate (Abbott *et al.*, 2007).

The channel carrying I_{Ks} is formed by a tetramer of α-subunits encoded by the KCNQ1 (Kv7.1) gene and an accessory subunit minK (encoded by the gene KCNE1, the first discovered member of a family of at least 5 'MinK-related Proteins', designated KCNE1-5 (Abbott *et al.*, 2007)). I_{Ks} activates slowly during depolarisation but does not show appreciable inactivation, and as a result is responsible for the well-known rate-dependent shortening of the AP which is seen, for example, under conditions of β-adrenoceptor stimulation where heart rate is increased. As heart rate rises, the number of open I_{Ks} channels accumulates, leading to a faster rate of repolarisation (Terrenoire *et al.*, 2005). I_{Ks} has been shown to be enhanced by β-adrenoceptor stimulation (Walsh *et al.*, 1988), as a consequence of elevated levels of

intracellular cAMP, which is associated with a shift in the voltage dependence of activation to more negative potentials (Sanguinetti *et al.*, 1991; Han *et al.*, 2001). The molecular mechanisms underlying β-adrenoceptor-mediated phosphorylation of I_{Ks} are under current investigation. Marx and colleagues demonstrated that a targeting protein, 'yotiao' is necessary for PKA-mediated modulation of human KCNQ1 channels (Marx *et al.*, 2002). It has recently been demonstrated using an *in vivo* phosphoproteomic approach that phosphorylation occurs at at least two sites on KCNQ1 channels, with phosphorylation at a site at Ser92 specifically resulting in an increase in current amplitude (Lundby *et al.*, 2013).

The rapidly activating component of I_K, I_{Kr}, activates more quickly than I_{Ks} during depolarisation, and in contrast to I_{Ks}, exhibits rapid inactivation, as a result of a fast form of C-type inactivation. I_{Kr} α-subunits are encoded by human *ether-a-gogo-related-gene* (HERG). Although artificially expressed HERG1 channels exhibit some biophysical characteristics of native $I_{Kr,}$ for example strong inward rectification, activation by extracellular K^+ and block by lanthanum (Sanguinetti *et al.*, 1995), there is evidence that additional subunits are present in native I_{Kr} which mediate sensitivity to anti-arrhythmic drugs such as E4031 (Sanguinetti *et al.*, 1995).

Conflicting information has been generated regarding the effects of β-adrenoceptor stimulation on I_{Kr} (Heath *et al.*, 2000; Karle *et al.*, 2002). Karle and colleagues reported an inhibition of I_{Kr} in response to isoprenaline, but their experimental conditions included the use of nifedipine to block I_{CaL} and chromanol to block I_{Ks} (Karle *et al.*, 2002). However, under conditions where I_{CaL} was not blocked, cytosolic Ca^{2+} was not buffered and the cell interior was not dialysed, Heath and Terrar were able to observe an stimulation of I_{Kr} in response to β-adrenoceptor stimulation

which was mediated by a cross-talk between the β-adrenoceptor signalling pathway and activation of protein kinase C (Heath *et al.*, 2000).

1.4 Initiation of contraction: Ca^{2+} entry across the sarcolemma

1.4.1 L-Type Ca^{2+} Channels

Following the classical studies of Fabiato (Fabiato, 1983), it is now well accepted that Ca^{2+} influx into cardiac myocytes via LTCCs provides the majority of trigger Ca^{2+} to initiate CICR from the SR. Both L- and T-type Ca^{2+} currents have been reported in guinea pig ventricular myocytes in single channel experiments (Nilius *et al.*, 1985) and in patch clamp studies, where they could be separated by clamping the membrane at -40 mV to inactivate T-type currents or at -100 mV, whereby both T- and L-type Ca^{2+} currents could be recorded (Mitra *et al.*, 1986). The T-type current is so small it probably contributes very little to Ca^{2+} influx in guinea pig ventricular myocytes (Nilius *et al.*, 1985), and indeed is absent in ventricular myocytes of many other species (reviewed in Bean, 1989).

In contrast, LTCCs are found in all cardiac myocytes. Their importance in EC coupling is demonstrated by observations that the voltage dependences of Ca^{2+} transients and contraction are very similar to the bell-shaped current/voltage relationship of I_{CaL} (Cannell *et al.*, 1987; Beuckelmann *et al.*, 1988). In addition, Näbauer and colleagues showed that rapid removal of extracellular Ca^{2+} resulted in the immediate inhibition of cardiac myocyte contraction (Näbauer *et al.*, 1989). Furthermore, with Ba^{2+} or Na^{+} as the charge carrier, current flow through LTCCs was not sufficient to trigger Ca^{2+} release from the SR (Näbauer *et al.*, 1989). Pharmacological inhibition of LTCCs (e.g. with Cd^{2+} or Ca^{2+} channel blockers) results

in a significant reduction or even complete abolition of cardiac cell contractions and Ca^{2+} transients (Bers *et al.*, 1988; Isenberg *et al.*, 1994; Trafford *et al.*, 2003), further illustrating their critical importance in cardiac EC coupling.

1.4.2 Other mechanisms

It is generally accepted that NCX, with its 3 Na^+:1 Ca^{2+} stoichiometry (Reeves *et al.*, 1984), is the primary mechanism by which Ca^{2+} is extruded from cardiac myocytes (Bers, 2002). However, it has been proposed that Ca^{2+} can enter cells via 'reverse mode' NCX to provide trigger Ca^{2+} for CICR (Leblanc *et al.*, 1990). Since the direction of NCX transport is influenced both by concentration gradients for Na^+ and Ca^{2+}, as well as by cell membrane potential (which all change throughout the AP), when $[Na^+]_i$ is high and membrane potential more positive than the reversal potential for NCX (around -50 mV at resting $[Ca^{2+}]_i$,) Ca^{2+} influx can be favoured at the time of AP upstroke. However, the rapid increase in $[Ca^{2+}]_i$ which follows as a result of activation of LTCCs and SR Ca^{2+} release is likely to limit Ca^{2+} influx in this manner under physiological conditions (Bers, 2008). However, influx of Ca^{2+} on NCX can be favoured if the AP duration is prolonged, the Ca^{2+} transient is reduced or $[Na^+]_i$ is high, such as in heart failure (Grantham *et al.*, 1996; Bers, 2008).

An alternative Ca^{2+} entry mechanism which has been proposed is that of 'slip mode conductance', whereby Na^+ channels become permeable to Ca^{2+} (Santana *et al.*, 1998). However this only occurs under certain conditions, for example in the presence of β-adrenoceptor agonists, and is controversial (Piacentino *et al.*, 2002).

1.5 Initiation of contraction: release of Ca^{2+} from intracellular stores

The SR is an intracellular, membrane-bounded organelle capable of efficiently sequestering and storing Ca^{2+}. Ca^{2+} released from the SR contributes significantly to the magnitude of the Ca^{2+} transient and cell contraction (as will be described later). Key to this process are RyRs: specialised ligand-gated ion channels, selective for Ca^{2+}, which are critical in the regulation and fine-tuning of SR Ca^{2+} release during cardiac EC coupling.

1.5.1 Ca^{2+}-induced Ca^{2+} release

The SR is highly specialised for the sequestration and storage of Ca^{2+}, and has at least two continuous but distinct components. The longitudinal SR, which courses around the myofilaments is a site of Ca^{2+} uptake, while the terminal cisternae, specialised enlarged regions located at the Z lines, are sites of uptake and release (Inui *et al.*, 1988).

The concept of CICR was first proposed by Fabiato (Fabiato, 1983), and is now generally accepted. Fabiato carried out meticulous experiments measuring contractile force and aequorin fluorescence (as a measure of $[Ca^{2+}]_i$) in mechanically skinned canine purkinje fibres, and demonstrated that these parameters could be graded with both the amplitude and speed of application of known concentrations of Ca^{2+} (Fabiato, 1985a; Fabiato, 1985b). At higher Ca^{2+} concentrations, CICR was inactivated (pCa < 5.4). CICR was also found to exhibit a refractory period, during which no further Ca^{2+} release could be initiated by application of Ca^{2+}, but could be initiated by application of caffeine. This refractory period is crucial since it prevents dangerous self-perpetuation of the CICR mechanism and allows refilling of the SR ready for the next contraction.

Subsequently, the regulation of this process, such that tight control of the CICR mechanism can be achieved, has received much attention.

1.5.2 Ryanodine receptors

The discovery that the neutral plant alkaloid ryanodine bound with high affinity to a protein at the terminal cisternae, and inhibited Ca^{2+} release from heavy SR fractions (containing terminal cisternae) led to the isolation and purification of the RyR in 1987 (reviewed in Fill *et al.*, 2002). RyR2, the predominant RyR isoform expressed in cardiac muscle, is a tetrameric protein with a molecular mass of 565 kDa per subunit (Otsu *et al.*, 1990).

Morphological evidence supports the CICR theory proposed by Fabiato, and the tight coupling of RyR activation to Ca^{2+} entering cardiac myocytes via LTCCs. RyRs are readily observed in electron micrographs as the 'junctional foot protein' between SR (terminal cisternae) and T-tubular membranes (Radermacher *et al.*, 1992), and the majority of RyRs are located in discrete clusters, close to the Z-line (Chen-Izu *et al.*, 2006). It is estimated that 10-25 LTCCs and 100-200 RyRs are clustered at junctions between T-tubule membrane and SR in a local Ca^{2+} signalling unit called a couplon (Bers, 2008), where the distance between the terminal cisternae (or 'junctional' SR) is just 12 nm (Brochet *et al.*, 2005).

Investigations using pharmacological agents which interfere with RyR function (notably ryanodine and caffeine) have been used to assess the critical importance of SR Ca^{2+} release in EC coupling. At low concentrations (< 10 μM), ryanodine activates the RyR and appears to lock it into a sub-conductance state, causing a depletion of intracellular Ca^{2+} stores (Rousseau *et al.*, 1987). At high millimolar concentrations,

ryanodine causes complete block of the channel (Lai *et al.*, 1989). Application of 10 μM ryanodine to isolated guinea pig ventricular myocytes has been reported to cause a marked reduction in amplitude of Ca^{2+} transients and contractions (up to 89%) (Isenberg *et al.*, 1994). However, also using guinea pig ventricular myocytes, Chiesi and colleagues reported a 23% and 20% reduction in amplitude of Ca^{2+} transients and contractions respectively, in the presence of 10 μM ryanodine (Chiesi *et al.*, 1994). The discrepancy in these results is likely to be due to different experimental conditions. Chiesi and colleagues performed their study at room temperature, and at a simulation frequency of 0.5 Hz, which is substantially lower than under physiological conditions for guinea pig. These conditions would be likely to reduce the degree of SR Ca^{2+} loading, and hence lead to an underestimation in the contribution of SR Ca^{2+} release to generation of Ca^{2+} transients and contractions. In contrast, caffeine (at micromolar concentrations, e.g. ~250 μM) increases open probability of RyR leading to increased amplitude of Ca^{2+} transients and contractions in cardiac ventricular myocytes (O'Neill *et al.*, 1990; Diaz *et al.*, 2005). At high millimolar concentrations, caffeine activates both skeletal and cardiac RyR, causing depletion of the SR (Rousseau *et al.*, 1989); indeed, rapid application of caffeine (e.g. 10 mM) to cardiac myocytes (in the absence of electrical stimulation to cause Ca^{2+} influx via LTCCs) is a tool commonly used to assess the SR Ca^{2+} load under different experimental conditions (for example, seeMacgregor *et al.*, 2007a).

1.5.3 Local control of Ca^{2+} release from the SR: Ca^{2+}sparks, quarks and blinks

Because the trigger for Ca^{2+} release from the SR is Ca^{2+} itself, ‘common pool’ mathematical models of SR Ca^{2+} release led to a regenerative all-or-nothing release of

Ca^{2+}, which would not explain how contractility of the heart could be modulated. In 1992, Stern therefore proposed a mathematical 'local control' model of cardiac muscle CICR (Stern, 1992). In this model, Stern postulated the existence of Ca^{2+} 'release units', in which entry of Ca^{2+} via a single LTCC would trigger the opening of a cluster of adjacent RyRs in an all-or-nothing fashion. Recruitment of individual clusters as a result of Ca^{2+} entry via LTCCs, would lead to graded Ca^{2+} release, and therefore graded contractile responses. The gain of the system would be dependent on SR Ca^{2+} load, and under 'normal' conditions would be low, such that activation of a single Ca^{2+} release unit would not be sufficient to activate an adjacent unit. Under conditions of increased SR Ca^{2+} load, the gain of the system would increase meaning that activation of a local release unit could trigger the activation of an adjacent unit (independently of Ca^{2+}influx via LTCCs) and lead to the generation of spontaneous Ca^{2+} releases and arrhythmogenic Ca^{2+} oscillations (Stern, 1992). This theory also supported the finding that RyRs preferentially respond to Ca^{2+} signals in the dyadic cleft and are relatively insensitive to other sources of Ca^{2+} as a trigger (Niggli *et al.*, 1990); numerous subsequent investigations also provide support for the 'local control' theory.

The advent of confocal Ca^{2+} imaging techniques, and use of the Ca^{2+}-sensitive fluorescent probe fluo-3, enabled Cheng and colleagues to make the first observations of localised, spontaneous increases in $[Ca^{2+}]_i$ in quiescent rat cardiac myocytes, which they termed 'Ca^{2+} sparks' (Cheng *et al.*, 1993). The frequency of Ca^{2+} sparks was found to increase in the presence of low concentrations of ryanodine, consistent with the hypothesis that they occur as a result of spontaneous openings of RyRs (Cheng *et al.*, 1993). Later, using a combination of measurements of fluo-3 and di-8-ANEPPs fluorescence (to locate Ca^{2+} sparks and t-tubular membranes respectively), Shacklock and colleagues reported that 85% of Ca^{2+} sparks in electrically-stimulated rat

ventricular myocytes occurred within 0.5 μm of a T-tubule (Shacklock *et al.*, 1995) lending support to the idea that RyRs are regulated by their close apposition to LTCCs in the dyadic cleft. It was initially thought that a Ca^{2+} spark may represent the opening of a single RyR, but studies concerning the flux of Ca^{2+} through RyR (in lipid bilayer experiments, where the concentrations of important regulatory factors such as Mg^{2+} and ATP were close to those of physiological conditions) have estimated that Ca^{2+} flux through RyR could be as little as < 0.6 pA (Mejia-Alvarez *et al.*, 1999). Lukyanenko and colleagues therefore proposed that sparks were more likely to represent the opening of a cluster of RyR (~20) (Lukyanenko *et al.*, 2007), lending support to the earlier suggestion of Lipp and Niggli that the fundamental Ca^{2+} signalling event in cardiac myocytes (which they termed a Ca^{2+} 'quark') is smaller in amplitude than a Ca^{2+} spark, possibly arising through the opening of a single RyR (Lipp *et al.*, 1996). The observation by Brochet and colleagues that Ca^{2+} sparks are associated with a corresponding depletion of SR Ca^{2+} content, termed a Ca^{2+} 'blink' (Brochet *et al.*, 2005), has been taken forward to improve techniques for the resolution of localised Ca^{2+} signals (Brochet *et al.*, 2011). Using line-scan confocal microscopy and the Ca^{2+} indicators rhod-2 AM and fluo-5N AM, these investigators studied Ca^{2+} spark-blink pairs in rabbit ventricular myocytes. Only Ca^{2+} sparks which could be visualised in focus with corresponding Ca^{2+} blinks were studied, enabling the investigators to observe Ca^{2+} release/depletion events which were one-tenth to one-third of the amplitude of Ca^{2+} sparks: these were termed 'quarky Ca^{2+} release (QCR)-quarky Ca^{2+} depletion (QCD)' events (Brochet *et al.*, 2011). QCR was found to occur more frequently than spontaneous Ca^{2+} sparks (Brochet *et al.*, 2011).

1.5.4 Local control of Ca^{2+} release: termination

In his classical studies, Fabiato observed a refractory period in the CICR mechanism (Fabiato, 1985a; Fabiato, 1985b). This refractory period is crucial since it prevents dangerous self-perpetuation of the CICR mechanism and allows refilling of the SR ready for the next contraction. The process by which local Ca^{2+} release events are terminated has received much attention in the literature but there is no consensus on the mechanisms.

Stochastic attrition, whereby the spontaneous decay of Ca^{2+} release from active clusters of RyRs occurs due to random channel closure (Stern *et al.*, 2004) is thought to contribute to an extent. However, theoretical calculations of the mean time for stochastic attrition to terminate a spark have produced results that are not reflected by experimental recordings of spark kinetics, and so although stochastic attrition is an inherent property of RyRs, it is unlikely to fully account for spark termination (Stern *et al.*, 2004).

Gyorke and Fill observed that RyR open probabilities are reduced (but the channels themselves are not inactivated) in the presence of increased $[Ca^{2+}]$ at the cytoplasmic face of the channel, and suggested that adaptation, rather than inactivation of the RyR underlies the responses observed by Fabiato (Gyorke *et al.*, 1993). Valdivia and colleagues subsequently demonstrated that RyR adaptation occurs over a millisecond timescale in response to photorelease of Ca^{2+} from a caged analogue (Valdivia *et al.*, 1995), raising the possibility that this mechanism could occur under physiological conditions. However, interpretation of these results could be confounded by differences in the methods used for reconstitution of RyR proteins in lipid bilayers. It remains possible that RyRs are inactivated by mechanisms involving regulatory

proteins which form complexes with them *in vivo*, but that these mechanisms cannot be recreated *in vitro* due to the loss of accessory proteins during the purification and reconstitution procedure. Further discrepancies with *in vivo* data and single channel recordings in lipid bilayers may arise if RyRs located in clusters are able to influence openings of adjacent RyRs to produce a highly localised negative feedback mechanism. It has been observed that multiple RyRs in a lipid bilayer can synchronise their openings such that they function as a single channel with multiple conductance states (Marx *et al.*, 1998). This 'coupled gating' has been most frequently observed with RyR1, but isolated reports suggest it can also occur with the RyR2, and is thought to involve physical coupling of the receptors by the accessory protein FK506 binding protein 12.6 (FKBP12.6) (Marx *et al.*, 2001). However, coupled gating cannot be the sole mechanism for Ca^{2+} spark termination, since sparks are observed to terminate, even in the absence of FKBP12.6, which presumably would prevent coupled gating from occurring.

More recent mathematical modelling studies by Cannell and colleagues suggest that an intrinsic inactivation or Ca^{2+} sensing mechanism is not necessary for spark termination. Rather, when SR Ca^{2+} is depleted during CICR, Ca^{2+} flux through RyRs is decreased, which means that in turn, additional RyRs cannot be recruited because their closed time is extended. This process has been termed 'induction decay' (Cannell *et al.*, 2013; Laver *et al.*, 2013).

1.5.5 Modulation of ryanodine receptor function

The functional properties of RyRs have been assessed in lipid bilayer experiments. Micromolar concentrations of *cis* free Ca^{2+} (i.e. applied to the face of the channel expected to reside in the cardiac myocyte cytoplasm) increase the open

probability of the RyR2, providing direct support for the CICR mechanism (Rousseau *et al.*, 1989). Observations in lipid bilayer studies have also led to suggestions that RyR function is regulated by SR luminal [Ca^{2+}] (Sitsapesan *et al.*, 1994). Reducing *trans* [Ca^{2+}] (i.e. at the face of the channel expected to reside within the SR) was associated with a reduced probability of RyR opening (Gyorke *et al.*, 1998), while increasing *trans* Ca^{2+} from 10 μM to 1 mM resulted in increased probability of opening (Ching *et al.*, 2000), a mechanism which may underlie the increased gain of CICR observed when SR Ca^{2+} content is high. Support for this suggestion has been obtained by Cheng and colleagues, who observed an increase in the frequency, amplitude and spatial spread of spontaneous Ca^{2+} sparks in rat ventricular myocytes when SR Ca^{2+} content was elevated (by raising extracellular Ca^{2+} to 10 mM) (Cheng *et al.*, 1996). In addition, the use of tetracaine, to reduce RyR open probability, reduces frequency of Ca^{2+} sparks before resulting in an increase in the SR Ca^{2+} content and a recovery of Ca^{2+} spark frequency (Gyorke *et al.*, 1998; Zima *et al.*, 2008). This has been taken to (indirectly) indicate that higher levels of SR Ca^{2+} produce a greater RyR open probability.

However, not all investigators have observed an increase in RyR open probability with increased SR luminal [Ca^{2+}]. It has been suggested that the increase in RyR sensitivity with increased luminal [Ca^{2+}] may occur as a result of the binding of Ca^{2+} to the protein calsequestrin, which may regulate RyR sensitivity to SR luminal Ca^{2+} (Gyorke *et al.*, 2004); calsequestrin is physically coupled to RyRs by the proteins junctin and triadin (Zhang *et al.*, 1997), especially in the junctional SR. Thus, it is possible that conflicting observations (regarding regulation of RyR function by luminal Ca^{2+}) in lipid bilayer studies have arisen due to differences in the methods used to purify and reconstitute the proteins, resulting in incorporation of RyR complexes where

important regulatory proteins have been lost. A number of these regulatory proteins will now be discussed.

1.5.5.1 Calsequestrin, triadin and junctin

Calsequestrin is the major intra-SR Ca^{2+} buffering protein. Overexpression of calsequestrin has been shown to result in severe cardiac hypertrophy with reduced Ca^{2+} transient amplitude and Ca^{2+} spark frequency, while the caffeine-releasable pool of Ca^{2+} was greatly enhanced (Jones *et al.*, 1998). This is probably due to the resultant increased Ca^{2+} buffering capacity of the SR, leading to reduced free Ca^{2+} in the SR. Mutations in calsequestrin have been linked to sudden death (catecholaminergic polymorphic ventricular tachycardia, CPVT); when the mutant forms of calsequestrin were expressed in ventricular myocytes impaired Ca^{2+} handling was observed (Terentyev *et al.*, 2003).

1.5.5.2 FK506 binding proteins (FKBPs)

FKBPs bind to and co-purify with RyRs. Two forms, FKBP12 and FKBP12.6 are expressed in the heart. The immunosuppressant drugs, FK506 and rapamycin, cause dissociation of FKBP12.6 from the RyR and modify RyR gating in bilayer studies (Ahern *et al.*, 1994; Brillantes *et al.*, 1994). FK506 increases the Ca^{2+} sensitivity of RyR gating (Xiao *et al.*, 1997) and increases Ca^{2+} transient amplitude and the frequency of Ca^{2+} sparks while reducing the SR Ca^{2+} content (McCall *et al.*, 1996). The role of FKBP12.6 in regulation of cardiac RyR2 has received much attention since it preferentially associates with RyR2 (Timerman *et al.*, 1996) and its depletion from RyR2 has been associated with heart failure (Marx *et al.*, 2000) and with CPVT (Wehrens *et al.*, 2003). It has been suggested that FKBP12.6 stabilises RyR gating, and

facilitates coupled gating of both individual and adjacent RyR tetramers (Marx *et al.*, 2001). Adenoviral overexpression of FKBP12.6 in rabbit ventricular myocytes was associated with increased SR Ca^{2+} content and amplitude of cell contractions, perhaps as a result of reducing SR Ca^{2+} leak through RyRs (Prestle *et al.*, 2001). Myocytes isolated from FKBP12.6 knockout mice were found to exhibit increased Ca^{2+} spark amplitude and frequency, which was associated with an enhanced CICR gain in comparison to wild type mice (Xin *et al.*, 2002). Although these observations are consistent with a role of FKBP12.6 in regulating cardiac RyRs, it has been reported that FKBP12.6 does not affect RyR open probability in lipid bilayers (Galfre *et al.*, 2012). However, Sitsapesan and colleagues did observe a concentration-dependent increase in RyR2 open probability in lipid bilayers in response to FKBP12.0 (Galfre *et al.*, 2012). These investigators postulated that FKBP12.6 may antagonise the activation of the RyR2 that they observed in the presence of FKBP12.0 (Galfre *et al.*, 2012). This increase in RyR activity in response to FKBP12.0 is controversial, however: overexpression of FKBP12.0 in rabbit ventricular myocytes was found not to alter I_{CaL} or Ca^{2+} transient amplitude, but reduced the ability of I_{CaL} to initiate SR Ca^{2+} release, suggesting that, under these conditions, FKBP12.0 reduces the sensitivity of RyRs to Ca^{2+} (Seidler *et al.*, 2007).

1.5.5.3 PKA

PKA, activated by β-adrenoceptor stimulation, is anchored to RyRs via a leucine zipper motif of muscle A Kinase Anchoring Protein (mAKAP) (Marx *et al.*, 2001). At least two phosphorylation sites for PKA, including Ser-2808 and Ser-2030 have been reported to exist on RyR2 (Xiao *et al.*, 2005), with Ser-2030 being proposed as the major PKA phosphorylation site in response to β-adrenoceptor stimulation (Xiao *et al.*,

2006). Ginsberg and Bers have reported that the major effect of phosphorylation on RyR function is accelerated kinetics of channel opening and closing (Ginsburg *et al.*, 2004). The extent of Ca^{2+} loading in the SR appears to influence the degree of effect of PKA-mediated RyR phosphorylation: in studies on intact myocytes, PKA dependent phosphorylation of the RyR had no effect on Ca^{2+} sparks in the absence of phospholamban phosphorylation (Li *et al.*, 2002).

In addition, it has been observed that phosphorylation of RyR by PKA enhances RyR open probability (Valdivia *et al.*, 1995; Marx *et al.*, 2001). Marx and colleagues have proposed that this occurs through a mechanism involving dissociation of FKBP12.6 from the RyR, although this suggestion is controversial (Xiao *et al.*, 2004). These investigators have also been key proponents of the hypothesis that RyR 'hyperphosphorylation' is a mechanism underlying cardiac dysfunction in heart failure (Marx *et al.*, 2000). They observed increased PKA-mediated phosphorylation of RyR2, increased sensitivity of RyR2 to Ca^{2+} and reduced FKBP12.6 binding to RyR2 in failing hearts, compared to non-failing hearts (Marx *et al.*, 2000). Interestingly, the extent of RyR2 phosphorylation returned to normal levels after patients with heart failure were treated with a left ventricular assist device (Marx *et al.*, 2000). However, other research groups have been unable to confirm the suggestions of Marx and colleagues, both in terms of whether PKA-dependent phosphorylation causes dissociation of FKBP12.6 from RyR, and whether PKA causes RyR 'hyperphosphorylation' in heart failure (Bers, 2006).

1.5.5.4 Calmodulin-dependent protein kinase (CaMK) II

Calmodulin is a 148 amino acid protein with 4 Ca^{2+} binding EF-hands. The Ca^{2+} binding sites are largely unoccupied at resting [Ca^{2+}], but as [Ca^{2+}] increases during the

Ca^{2+} transient, Ca^{2+} binds cooperatively, facilitating high affinity binding of calmodulin to target proteins, such as calmodulin-dependent protein kinase (CaMK) II. There are four isoforms of CaMKII: the predominant isoform in cardiac muscle is CaMKIIδ (Tobimatsu *et al.*, 1989). When calmodulin binds to the regulatory domain of CaMKII the enzyme becomes activated and catalyses the phosphorylation of various target proteins. Acitvation of CaMKII can also result in autophosphorylation of Thr-287 in the autoinhibitory region. Autophosphorylation increases the affinity of CaMKII for calmodulin, thus calmodulin can remain bound and the enzyme can remain active even after Ca^{2+} levels are reduced (Meyer *et al.*, 1992).

Regulation of RyR function by CaMKII is controversial. It has been reported that CaMKIIδ is physically associated with RyRs, and that AIP (a CaMKII inhibitor) decreased rabbit ventricular myocyte Ca^{2+} spark frequency, duration and width, without affecting SR Ca^{2+} uptake (Currie *et al.*, 2004). Overexpression of CaMKIIδC in mouse ventricular myocytes was associated with decreased SR Ca^{2+} content but increased frequency of Ca^{2+} sparks (Maier *et al.*, 2003). In order to eliminate any possible influence of SR Ca^{2+} content on RyR modulation by CaMKIIδ, Guo and colleagues measured Ca^{2+} spark frequency in phospholamban (PLB; a protein which regulates uptake of Ca^{2+} into the SR through actions on SERCA) knockout mice in the absence and presence of CaMKIIδ overexpression, and demonstrated an increased spark frequency in myocytes overexpressing CaMKIIδ (Guo *et al.*, 2006). These observations are consistent with a role of CaMKII to increase RyR activity. Conversely, expression of a constitutively active form of CaMKII inhibited SR Ca^{2+} release and a CaMKII inhibitor, AC3-I, enhanced SR Ca^{2+} release in rabbit ventricular myocytes (Wu *et al.*, 2001) suggesting negative regulation of RyR under some experimental conditions.

In addition to CaMKII activation, calmodulin may modulate RyR function directly. Binding of calmodulin to RyR can occur at multiple sites, and has been found to decrease RyR open probability and shift the Ca^{2+} dependence of activation to higher levels of Ca^{2+} (Balshaw *et al.*, 2001).

1.6 Mechanism of contraction

Ca^{2+} release from the sarcoplasmic reticulum raises cytosolic Ca^{2+} from resting levels in the region of 100 nM, to over 1 µM (Bers, 2002). This signal is converted into mechanical force and cell shortening by interaction of Ca^{2+} with the protein troponin C (TnC), which allows the cyclical ATP-dependent process of crossbridge formation between actin and myosin to take place as described in the sliding filament theory of muscle contraction (Huxley, 1969; Huxley *et al.*, 1971).

TnC is a Ca^{2+} binding protein located in the troponin complex which also consists of troponin I (TnI, inhibitory subunit that binds actin during diastole) and Troponin T (TnT, tropomyosin binding subunit). The troponin complex is attached to a ribbon like molecule of tropomyosin, which lies in the groove of the actin double helix, overlying 7 globular actin subunits. TnC has 3 binding sites for Ca^{2+}, two of which are saturated at rest. The third (K_d ~500 nM) is responsive to physiological changes in cytosolic [Ca^{2+}], whose binding leads to a conformational change which strengthens the interaction between TnC and TnI, weakening the interaction between TnI and actin. This leads to the movement of the troponin-tropomyosin complex deeper into the actin groove, exposing myosin binding sites on actin (Bers, 2001).

Myosin is a hexameric protein consisting of two heavy chains, each with a globular head and a tail (the tails coil around each other to form an α-helix). The

globular heads form cross bridges with actin and contain sites for ATP hydrolysis. Associated with each globular head are two light chains (one regulatory light chain, and one essential light chain).

Exposure of myosin binding sites on actin allows the globular heads to form crossbridges between the two filaments; force generation occurs as the myosin heads rotate, sliding the myosin filaments along actin. Energy for this process is provided by ATP which is hydroylsed by ATPases in the myosin head. At typical physiological $[Ca^{2+}]_i$ the force generated in cardiac muscle is submaximal; increases in the amplitude of the Ca^{2+} transient lead to the formation of more crossbridges and hence increased force of contraction. Another mechanism by which force generation can be increased is by altering the sensitivity of the myofilaments to Ca^{2+}, as may occur when myofilaments are stretched and sarcomere length increases (de Tombe *et al.*, 2010), or when drugs which modulate sensitivity are applied (Toller *et al.*, 2006).

Crossbridge formation continues until $[Ca^{2+}]_i$ returns to resting levels and Ca^{2+} dissociates from TnC, leading to termination of contraction and initiation of relaxation.

1.7 Mechanism of relaxation

Relaxation of cardiac muscle between beats (diastole) is essential to allow for refilling of the ventricles. Relaxation occurs as Ca^{2+} returns to resting levels and dissociates from TnC, terminating crossbridge formation. Extrusion of Ca^{2+} from the cytosol occurs through four mechanisms, the relative importance of which varies between species (Bers, 2000). Under steady state conditions, the amount of Ca^{2+} removed from the cell, must be equal to that entering on each beat.

1.7.1 Ca^{2+} uptake

Ca^{2+} uptake into the SR is achieved through the action of a Ca^{2+}-ATPase (cardiac isoform SERCA 2a (Brandl *et al.*, 1986)) which is located at the longitudinal and terminal cisternae regions of the SR (Inui *et al.*, 1988). Importantly, SERCA 2a is regulated by PLB (meaning 'phosphate acceptor'), which was first discovered in cardiac SR microsomes as a substrate for phosphorylation by PKA, which resulted in increased Ca^{2+} uptake (Tada *et al.*, 1975). PLB is regarded as a key protein mediating the cardiac β-adrenergic response. In its dephosphorylated state, PLB interacts with and inhibits the Ca^{2+} transport function of SERCA 2a (James *et al.*, 1989), but phosphorylation (at either Ser-16 by PKA or Thr-17 by CaMKII (Simmerman *et al.*, 1986; Fujii *et al.*, 1987)), removes this inhibition leading to increased SR Ca^{2+} uptake. This is a key part of the mechanism by which β-adrenoceptor stimulation (and PKA activation) leads to increased SR Ca^{2+} load and increases the speed of relaxation (lusitropy). Within the SR, 50-90% of Ca^{2+} is bound to the low-affinity buffering protein calsequestrin 2 (Bers, 2001), permitting enough Ca^{2+} for activation of the myofilaments to be stored in a relatively small volume within the cell.

The operation of a ruthenium red-sensitive mitochondrial Ca^{2+} uniporter, closely apposed to the RyR2 has been proposed to make a small contribution to the clearance of Ca^{2+} from the sarcoplasm by facilitating uptake into mitochondria. However this mechanism does not appear to be functional under physiological conditions (Williams *et al.*, 2013).

1.7.2 Extrusion of Ca^{2+} across the sarcolemma

NCX, located predominantly to the T-tubules (Frank *et al.*, 1992; Scriven *et al.*, 2000) is regarded as the primary transsarcolemmal Ca^{2+} extrusion mechanism in cardiac muscle (Bers, 2000). It has a stoichiometry 3 Na^+: 1 Ca^{2+}, with the net movement of one positive charge in the direction of Na^+ transport, although other modes of transport with different stoichiometry have been reported (Kang *et al.*, 2004). The function of NCX is dependent upon local T-tubular Na^+ and Ca^{2+} concentrations, as well as E_m. At resting $[Ca^{2+}]_i$, NCX has a reversal potential of ~ -50 mV, and so at resting E_m (~ -80 mV) Ca^{2+} efflux is favoured. At the upstroke of the AP when E_m rapidly becomes more positive and $[Na^+]_i$ rises rapidly, Ca^{2+} influx on NCX is favoured briefly since E_m exceeds the reversal potential for NCX (which changes throughout the AP due to changing $[Ca^{2+}]_i$) (Bers, 2002). However, as the CICR mechanism is activated early in the AP, Ca^{2+} influx on NCX can only occur for a limited period and extrusion then resumes.

Also contributing to transsarcolemmal Ca^{2+} efflux is the plasma membrane Ca^{2+} ATPase (PMCA), first identified in sarcolemmal membrane vesicle experiments (Caroni *et al.*, 1980). The PMCA makes only a very small contribution to total Ca^{2+} efflux (although this varies between species (Bassani *et al.*, 1994)); it has been estimated that if the PMCA were the only Ca^{2+} extrusion mechanism in cardiac muscle, relaxation would take around 30 seconds (Bers, 1991).

1.7.3 Competition between uptake and extrusion mechanisms

In order to maintain steady state contractions, the same amount of Ca^{2+} released by the SR must be resequestered by SERCA 2a, and the same amount entering across the sarcolemma must be extruded by NCX (and PMCA). Measurement of the rate of

decay of myocyte contractions or Ca^{2+} transients following rapid cooling or caffeine application to trigger SR Ca^{2+} release, together with selective inhibition of each of the uptake/transport mechanisms has allowed the contribution of each to be assessed in different species (Bers, 2000). SR Ca^{2+} accumulation was inhibited by thapsigargin or 10 mM caffeine, NCX by complete removal of extracellular Na^{+} and Ca^{2+}, PMCA by carboxyeosin and the mitochondrial uniporter by FCCP. In rabbit ventricular myocytes, (accounting for cytosolic Ca^{2+} buffering), SERCA 2a was found to remove 70 % of the Ca^{2+} activating the myofilaments, NCX 28 % and the remaining 2 % was found to be removed by PMCA/mitochondrial uniporter (slow systems) (Bassani *et al.*, 1994). Similar contributions of each component were found in guinea pig, ferret and human myocytes (Bers, 2001). In rat and mouse, the contribution of the SR Ca^{2+} ATPase is higher and removal by NCX lower giving a balance closer to 92:7:1 % for SERCA, NCX and slow systems (Bers, 2000).

1.8 Physiological regulation of cardiac function

The human resting heart rate, which is usually around 70 beats per minute, is modified by sympathetic and parasympathetic nerves of the autonomic nervous system which innervate the SAN and AVN (Levick, 1999). Both sympathetic and parasympathetic systems are active under basal conditions; parasympathetic activity predominates at rest, while stress or exercise will favour activity of the sympathetic over the parasympathetic nervous system (Olshansky *et al.*, 2008), leading to increased cardiac output.

1.8.1 The sympathetic nervous system and β-adrenoceptor stimulation

Sympathetic fibres consist of a short pre-ganglionic fibre originating from the spinal cord at segments T1-T5, which synapse in the paravertebral sympathetic ganglia onto much longer post-ganglionic fibres. Fibres originating from the right paravertebral ganglia innervate the SAN, AVN and atria, while those from the left paravertebral ganglia innervate the ventricular muscle (Levick, 1999).

Stimulation of sympathetic nerves results in the release of noradrenaline from postganglionic nerve terminals, which acts upon β_1-adrenoceptors located at the sarcolemma of cardiac myocytes. Although β_1-adrenoceptors are predominant, cardiac myocytes also express β_2- and β_3-adrenoceptors, and also various α-adrenoceptors (Levick, 1999). All are G-protein coupled receptors (GPCRs) which contain 7 transmembrane spanning domains and couple to heterotrimeric G proteins which consist of α and βγ subunits. Binding of an agonist leads to a conformational change of the receptor, resulting in the exchange of GDP for GTP on the α subunit. This triggers dissociation of α and βγ subunits allowing them to stimulate downstream signalling events. The hydrolysis of GTP back to GDP by the α subunit terminates signalling and the G-protein subunits reassociate. The circulating hormone adrenaline, released from the adrenal medulla also activates these receptors.

Activation of β_1-adrenoceptors triggers a highly complex signalling cascade, which ultimately leads to amplification of all processes in EC coupling, and is the predominant physiological mechanism by which cardiac inotropy, lusitropy and chronotropy are regulated (Levick, 1999). β_1-adrenoceptors are coupled to $G\alpha_s$-proteins which stimulate membrane-bound adenylyl cyclases to catalyse the conversion of intracellular adenosine triphosphate (ATP) molecules to cyclic adenosine 3’ 5’

monophosphate (cAMP). cAMP then binds to and activates PKA which phosphorylates numerous intracellular targets (Levick, 1999). In atrial and ventricular myocytes, phosphorylation of LTCCs increases their open-state probability and duration (Hulme *et al.*, 2006) leading to enhancement of I_{CaL} and increased trigger Ca^{2+} for CICR; phosphorylation of I_{Ks} enhances repolarising outward currents (Marx *et al.*, 2002), contributing to rate-dependent shortening of APD and phosphorylation of PLB reduces its inhibitory action on SERCA (Li *et al.*, 2000), producing an effect of 'disinhibition' to increase uptake of Ca^{2+} into the SR to increase rate of relaxation of myocytes. PKA may also phosphorylate RyR such that more Ca^{2+} is released from the SR on each beat (Marx *et al.*, 2000), and TnI (Sulakhe *et al.*, 1995) to reduce myofilament Ca^{2+} sensitivity and facilitate relaxation. In addition to its effects on LTCCs and I_{Ks}, PKA also acts to phosphorylate and modulate the function of other cardiac ion channels including those carrying Cl^- (Vandenberg *et al.*, 1994) and Na^+ ions (Ono *et al.*, 1993), leading to a characteristic elevation of the AP plateau and more defined repolarisation phase.

Activation of β-adrenoceptors increases the rate of cardiac contraction through direct effects on cells of the SAN. For example, cAMP interacts directly with the hyperpolarisation-activated 'funny' current I_f in SAN cells to increase the slope of diastolic depolarisation leading to an increase in heart rate (Accili *et al.*, 2002), in addition to many other PKA-mediated effects on Ca^{2+} handling in node cells.

In order that phosphorylation levels are returned to normal, protein phosphatases e.g. PP1 and PP2A act to dephosphosphorylate PKA target proteins. These protein phosphatases are often found in regulatory complexes with their target proteins, along with PKA and other kinases such that signalling can be efficiently compartmentalised (Levick, 1999).

1.8.2 The parasympathetic nervous system

Parasympathetic fibres originate from vagal motor nuclei in the brainstem. A long preganglionic fibre synapses with a short post-ganglionic fibre within the myocardium rather than in ganglia like the sympathetic fibres. Parasympathetic innervation of the heart is localised to the SAN and AVN, with more sparse innervation of the ventricles (Levick, 1999).

Stimulation of parasympathetic nerves (vagal nerves) triggers release of acetylcholine, the first neurotransmitter to be identified in 1921 by Otto Loewi (Bennett, 2000). Acetylcholine reduces cardiac output primarily by reducing heart rate, but also reducing contractility through actions at muscarinic receptors. In the heart, the predominant subtype of muscarinic receptors expressed is M_2, which are coupled to the inhibitory G protein, G_i, activation of which reduces adenylyl cyclase activity and hence PKA-mediated phosphorylation of target proteins (Dhein *et al.*, 2001). Activation of M_2 receptors can also have direct actions on atrial, SAN and AVN cells through interaction of G protein βγ subunits with G protein coupled inward rectifying K^+ (GIRK) channels carrying the specific $I_{K(ACh)}$ current (Iijima *et al.*, 1985; Ito *et al.*, 1995). The resulting increase in outward K^+ current leads to hyperpolarisation, which reduces membrane excitability in cells of the SAN and AVN (leading to reduced heart rate), and also reduced APD in atrial cells and an indirect reduction in amplitude of contractions. Other agents produced in the heart and present in the circulation, such as adenosine, are capable of exerting similar effects in isolated cardiac cells (Belardinelli *et al.*, 1995).

The electrophysiological effects of acetylcholine and adenosine on single cells depend upon the region of the heart from which the cell is isolated. In ventricular

myocytes of most mammalian species, a reduction in I_{CaL} in response to muscarinic or purinergic receptor activation is typically only observed after myocytes are pre-stimulated with isoprenaline to raise intracellular levels of cAMP (Hartzell, 1988; Belardinelli *et al.*, 1995). In contrast, atrial and SAN myocytes exhibit responses to acetylcholine or muscarinic receptor agonists under basal conditions (Iijima *et al.*, 1985; DiFrancesco *et al.*, 1988; Petit-Jacques *et al.*, 1993; Vandecasteele *et al.*, 1998). Although muscarinic receptor density (as determined by ^{3}H-QNB specific binding) in rabbit ventricular tissue has been reported to be approximately 20 % of that in atrial tissue (Fields *et al.*, 1978), this is consistent with the idea that basal turnover of adenylyl cyclases in atrial and nodal tissue is higher than in ventricular tissue, leading to increased levels of cAMP in these regions (Mery *et al.*, 1997). This has also been measured directly by the Lakatta group, with the finding that basal cAMP levels were highest in SAN regions and lowest in ventricular cells (Vinogradova *et al.*, 2006), and is supported by observations from the Terrar laboratory (Mattick *et al.*, 2007; Collins *et al.*, 2012).

1.9 Novel modulators of cardiac function: Ca^{2+} mobilising second messengers

1.9.1 Inositol Trisphosphate (IP_3)

IP_3 was the first Ca^{2+} mobilising messenger to be discovered after it was shown to accumulate rapidly in blowfly salivary glands after stimulation with 5-hydroxytryptamine (Berridge *et al.*, 1983). It is generated from hydrolysis of the cell membrane phospholipid phosphatidylinositol 4,5-bisphosphate (PIP_2) by the enzyme phospholipase C (PLC) which is stimulated through the binding of specific agonists at

receptors coupled to G_q proteins. IP_3 is widely regarded to mobilise Ca^{2+} through actions at specific receptors located to the endoplasmic reticulum (or SR in muscle cells), but there have also been reports of Ca^{2+} mobilisation from the nuclear envelope (Zima *et al.*, 2007)

IP_3 receptors have been confirmed to be present in the heart (predominantly the type II isoform), with a higher density of receptors being reported in the atria than the ventricles (Perez *et al.*, 1997; Lipp *et al.*, 2000). In atrial myocytes, agonists acting at G_q-coupled receptors (leading to activation of PLC and generation of IP_3) cause a sustained increase in amplitude of Ca^{2+} transients without enhancing SR Ca^{2+} load (Zima *et al.*, 2004; Bootman *et al.*, 2007; Kockskamper *et al.*, 2008), presumably through opening of IP_3 receptors located to the SR leading to enhanced Ca^{2+} release from the SR on each beat. Localised Ca^{2+} signals similar to Ca^{2+} sparks have been observed in atrial myocytes in response to IP_3 in the presence of inhibitors of RyR function; these were termed 'Ca^{2+} puffs', and were proposed to occur through the opening of multiple IP_3 receptors (Zima *et al.*, 2004).

Data from the Terrar laboratory also support a role for IP_3-dependent Ca^{2+} signalling in atrial myocytes. Phenylephrine (an α_1-adrenoceptor agonist, which stimulates PLC activity) caused an increase in Ca^{2+} transient amplitude which was prevented by both the α_1-adrenoceptor antagonist prazosin, and the IP_3 receptor antagonist 2-aminoethoxydiphenylborane (2-APB) (Collins *et al.*, 2012). Furthermore, the phenylephrine-stimulated increase in Ca^{2+} transient amplitude was found to be reduced in the presence of inhibitors of adenylyl cyclases or inhibitors of PKA. It was therefore proposed that localised Ca^{2+} releases from the SR in response to IP_3 activate Ca^{2+}-stimulated isoforms of adenylyl cyclases (isoforms AC1 and AC8) that are present in atrial myocytes, stimulating PKA-mediated phosphorylation of target proteins and

contributing to the increased Ca^{2+} transient amplitude seen with phenylephrine (Collins *et al.*, 2012).

1.9.2 Cyclic Adenosine Diphosphate Ribose (cADPR)

Shortly after the discovery of IP_3, cADPR was found to mobilise Ca^{2+} in sea urchin egg homogenates by Lee and colleagues (Lee *et al.*, 1989).

In cardiac myocytes, introduction of cADPR into cells (either directly via a patch pipette, or through UV photorelease of a caged cADPR analogue) has been demonstrated to increase the amplitude of both contractions and Ca^{2+} transients, and to increase the frequency of Ca^{2+} sparks (Iino *et al.*, 1997; Cui *et al.*, 1999); effects which were sensitive to competitive inhibitors of cADPR (8-amino cADPR and 8-bromo cADPR) and to inhibition of SR function with ryanodine and thapsigargin (Iino *et al.*, 1997; Cui *et al.*, 1999). In detailed experiments by Drew MacGregor of the Terrar laboratory, photorelease of cADPR led to an increase in Ca^{2+} transients which was independent of any effect on I_{CaL} amplitude (Macgregor *et al.*, 2007b), which is consistent with an effect of cADPR to increase the gain of CICR. However, no changes in SR Ca^{2+} load were observed over shorter time periods (Macgregor *et al.*, 2007b). It is thought that an action of cADPR to enhance the Ca^{2+} sensitivity of RyR, through an interaction with FKBP12.6 may contribute to the mechanism of action of cADPR (Zhang *et al.*, 2009).

1.9.3 Nicotinic Acid Adenine Dinucleotide Phosphate (NAADP)

NAADP is the most potent Ca^{2+} mobilising messenger discovered to date, with Ca^{2+} release from intracellular stores being observed at low picomolar to nanomolar

concentrations in sea urchin egg preparations, and at concentrations in the nanomolar range in some mammalian cells (Galione *et al.*, 2009). First discovered as a derivative of $NADP^+$ (Bernofsky, 1980), it wasn't until later experiments by Lee and colleagues that the Ca^{2+} mobilising ability of NAADP was appreciated (Clapper *et al.*, 1987). In a series of experiments on sea urchin egg homogenates, Lee and colleagues demonstrated that $NADP^+$ evoked immediate Ca^{2+} release, and that alkaline treatment greatly increased the amount of Ca^{2+} released. This suggested that it was not $NADP^+$ itself, but a derivative (presumably present as a contaminant in commercially available $NADP^+$), which was responsible for the Ca^{2+} mobilisation observed. This active contaminant was eventually purified, shown to be distinct from $NADP^+$ and NADPH by HPLC, but to have an NMR spectrum identical to $NADP^+$ (Lee *et al.*, 1995). The simplest explanation for these observations was concluded to be the conversion of an amide to a carboxyl group in nicotinamide, making the Ca^{2+} mobilising molecule nicotinic acid adenine dinucleotide phosphate (NAADP) (Lee *et al.*, 1995). The structure of NAADP was later confirmed using a high-resolution mass spectroscopy approach (Chini *et al.*, 1995; Lee, 2002).

1.9.3.1 NAADP synthesis

The first enzyme reported to synthesise NAADP was ADP-ribosyl cyclase (ARC). Originally referred to as NAD^+ glycohydrolase (NADase), and first purified from the sea slug *Aplysia* (Lee *et al.*, 1991), ARCs are present in a wide range of mammalian tissues including rabbit heart, brain, spleen and kidney (Rusinko *et al.*, 1989). Sequence comparison techniques have extended the family of ARCs to include the lymphocyte antigen CD38 (States *et al.*, 1992) and the bone marrow antigen CD157 (Itoh *et al.*, 1994) which display homology with ARC. CD38 has been shown to

synthesise NAADP in a base-exchange reaction whereby the nicotinamide group of $NADP^+$ is substituted by nicotinic acid, a reaction which occurs preferentially at acidic pH in the presence of nicotinic acid (Aarhus *et al.*, 1995). In addition, it has been proposed that CD38 may be capable of producing NAADP from cADPR-P; this reaction is favoured at physiological pH and occurs with subsequent addition of nicotinic acid (Moreschi *et al.*, 2006). It is unclear whether CD157 is also capable of producing NAADP; indeed it is less active than CD38 terms of cADPR synthesis (Hussain *et al.*, 1998).

Some controversy in this area has arisen since CD38 is a membrane-bound enzyme with its catalytic domain on the extracellular surface (Zhao *et al.*, 2012). However, recent evidence suggests that this may be explained by the existence of two opposing orientations of CD38, type II and type III, with the catalytic domain of the type III enzyme located at the intracellular surface (Zhao *et al.*, 2012). Further recent evidence suggests there may also be a novel ARC located to the SR in guinea pig cardiac tissue (Kannt *et al.*, 2012).

ARC activity has been reported to occur in cardiac tissue (Meszaros *et al.*, 1995) and it is possible that it is regulated by β-adrenoceptor signalling (Higashida *et al.*, 1999).

1.9.3.2 Properties of NAADP-mediated Ca^{2+} release

The properties of NAADP-mediated Ca^{2+} release were extensively investigated in sea urchin eggs. Local uncaging of NAADP led to a gradient of Ca^{2+} across the egg, with the highest concentration occurring at the site of photorelease. Global uncaging produced a Ca^{2+} gradient that was the inverse of the response to local uncaging (Churchill *et al.*, 2001b). This 'self-inactivation' property, whereby high concentrations

of NAADP can inhibit its own Ca^{2+} release mechanism, was found to be reversible in these cells.

In mammalian cells, the concentration response curve to NAADP is typically bell-shaped, with micromolar concentrations inactivating the mechanism (Vasudevan *et al.,* 2008). In early experiments (Macgregor *et al.,* 2007a), the self-inactivation mechanism was exploited to inhibit NAADP Ca^{2+} mobilisation in the absence of pharmacological inhibitors of NAADP, which were not developed until later (see section 1.9.3.6). However, it was noted in 1997 that inhibitors of both L-type Ca^{2+} channels, and certain K^+ channels could prevent NAADP-mediated Ca^{2+} mobilisation (Genazzani *et al.,* 1997).

1.9.3.3 NAADP-sensitive Ca^{2+} stores

Investigations into the mechansims of NAADP-mediated Ca^{2+} mobilisation have determined that the mechanism is pharmacologically distinct from cADPR and IP_3-mediated responses. In sea urchin egg homogenates, NAADP-induced Ca^{2+} mobilisation was prevented by prior addition of NAADP (a demonstration of the self-inactivation mechanism), but was not affected by heparin or 8-amino-cADPR (Lee *et al.,* 1995), inhibitors of IP_3 and cADPR signalling respectively. Furthermore, pre-treatment of sea urchin egg homogenates with either thapsigargin or cyclopiazonc acid (CPA) to inhibit SERCA failed to prevent NAADP-mediated Ca^{2+} mobilisation while it abolished that mediated by IP_3 or cADPR (Genazzani *et al.,* 1996). These observations are supportive of the NAADP pathway involving a Ca^{2+} store other than the SR (whose proper functioning, in contrast, is necessary for both IP_3- and cADPR-mediated responses to be observed).

Further support to this suggestion was provided by experiments utilising intact, stratified sea urchin eggs (whereby the cell is elongated on a sucrose cushion that separates the intracellular organelles by density). Photorelease of caged NAADP mobilised Ca^{2+} from the pole containing mitochondria and acidic vesicles, while IP_3 and cADPR mobilised Ca^{2+} from the opposite pole which contained the ER (Churchill *et al.*, 2002). Indeed, it had been demonstrated in the initial experiments by Clapper and colleagues that $NADP^+$-mobilised Ca^{2+} in Percoll-purified intracellular vesicles (from sea urchin eggs) occurred in a fraction which was more dense than the ER-derived fraction, suggesting the ER was not important in this response (Clapper *et al.*, 1987).

With evidence that the site of NAADP-mediated Ca^{2+} release was distinct from the ER, more detailed investigation into the nature of this store was performed by Churchill and colleagues in 2002. A sequential Percoll gradient centrifugation protocol was used to separate the particulate fraction of sea urchin egg homogenate which was sensitive to NAADP but not to IP_3 or cADPR. It was found that this fraction exhibited prominent [32P]-NAADP binding, and was rich in markers for acidic vesicles. LysoTracker Red DND-99 is a fluorescent weak base, which accumulates in and labels acidic compartments. An agent called GPN (Glycyl-L-phenylalananine 2-naphthylamide), which is membrane permeant and regarded to cause osmotic lysis of lysosomes, disrupted the LysoTracker Red labelling observed in the fraction of sea urchin egg homogenate which was sensitive to NAADP. Importantly, GPN prevented NAADP-mediated Ca^{2+} release in both this fraction of sea urchin egg homogenate, and also in intact eggs, while it did not affect Ca^{2+} mobilisation in response to IP_3 or cADPR. Churchill and colleagues therefore proposed that the targets for NAADP-mediated Ca^{2+} release are acidic lysosomal-related organelles (Churchill *et al.*, 2002).

The question arises as to the mechanism for Ca^{2+} sequestration into NAADP-sensitive Ca^{2+} stores, and this was also investigated by Churchill and colleagues. As previously reported, NAADP-mediated responses are insensitive to thapsigargin (Genazzani *et al.*, 1996), thereby discounting the involvement of SERCA, despite ATP being thought to be necessary for maintenance of NAADP-induced Ca^{2} signals (Genazzani *et al.*, 1996). These suggestions were supported in that Churchill and colleagues found that apyrase (which hydrolyses ATP to AMP and inorganic phosphate) inhibited Ca^{2+} uptake into acidic stores, while thapsigargin and the P-type Ca^{2+} ATPase inhibitor vanadate did not (Churchill *et al.*, 2002). The requirement for ATP was demonstrated with the finding that the presence of a proton gradient was necessary for Ca^{2+} uptake into the lysosomal fraction (since uptake was prevented by protonophores such as nigicerin), and that Bafilomycin A, a vacuolar-type H^{+}-ATPase inhibitor, also prevented Ca^{2+} uptake (Churchill *et al.*, 2002). These observations were thought to be consistent with a model whereby a proton gradient drives Ca^{2+} into lysosomes by a Ca^{2+}/H^{+} exchanger (Churchill *et al.*, 2002).

The observation that lysosomes are alkalinised upon addition of NAADP to sea urchin egg homogenates added further support to the suggestion that targets for NAADP are lysosomal compartments (Morgan *et al.*, 2007) This alkalinisation was not apparent with IP_3 or cADPR, suggesting it was specific to the NAADP signalling pathway (Morgan *et al.*, 2007). Similar observations have since been made in atrial (Collins *et al.*, 2011) and ventricular (Elson, DPhil Thesis, 2011) cardiac myocytes.

However, the idea that NAADP mediates Ca^{2+} mobilisation from acidic stores is not accepted by all investigators. For example, in skeletal muscle SR microsomes, NAADP was reported to release Ca^{2+} in a manner sensitive to ryanodine and ruthenium red, implicating the RyR (type 1) as a target for NAADP (Hohenegger *et al.*, 2002).

However, a direct effect of NAADP on both type 1 and type II RyR is controversial (Copello *et al.*, 2001; Pitt *et al.*, 2010).

1.9.3.4 Store interaction: the 'two-pool' hypothesis

It has been observed that NAADP can induce long-term Ca^{2+} oscillations in sea urchin eggs. Despite short-term responses to NAADP clearly being independent of IP_3 and cADPR-mediated signalling pathways, these long-term oscillations were found to be reduced in the presence of heparin or 8-amino-cADPR, and to be completely abolished in the presence of both (Churchill *et al.*, 2001a) suggesting the requirement of IP_3 or cADPR-mediated mechanisms, and therefore the ER, in maintenance of long-term oscillations (Churchill *et al.*, 2001a) Taken in combination with additional observations that treatment with NAADP increased available Ca^{2+} for CICR in sea urchin eggs, it was proposed that NAADP releases Ca^{2+} from a lysosomal compartment (pool 1), which is taken up into, or triggers CICR from the ER (pool 2) (Churchill *et al.*, 2001a). Further support for this suggestion has been obtained in cardiac myocytes and other cell types (Macgregor *et al.*, 2007a; Tugba Durlu-Kandilci *et al.*, 2010; Collins *et al.*, 2011; Park *et al.*, 2013).

1.9.3.5 Molecular targets of NAADP

The evidence presented above points towards the target for NAADP being pharmacologically distinct from any mechanism involving IP_3 or cADPR, and that the major sites of NAADP-induced Ca^{2+} mobilisation are lysosomal acidic organelles. Two candidate receptor types have been put forward as potential mediators of the specific NAADP-induced response.

The transient receptor potential mucolipin 1 channel (TRP-ML1) is a non-selective cation channel located to lysosomes and late endosomes. It has been reported that concentrations of NAADP ranging from 1 nM – 10 μM stimulated TRP-ML1 channel activity in reconstituted lysosomal membrane proteins from rat liver microsomes (Zhang *et al.*, 2007). This response was found to be prevented by a TRP-ML1 blocking antibody, by very high concentrations of NAADP and by inhibitors of LTCCs (diltiazem, verapamil and nifedipine), consistent with previous observations (Genazzani *et al.*, 1997). These observations were taken to support a role for TRP-ML1 as a target for NAADP (Zhang *et al.*, 2007), despite the lack of evidence of Ca^{2+} permeation in these particular studies (Cs^{+} was used as the charge carrier). However, this suggestion is controversial, given the finding that NRK cells overexpressing TRP-ML1 showed no increase in binding or radiolabelled NAADP in comparison to non-transfected cells, and that addition of 250 nM NAADP to oocytes expressing TRP-ML1 did not increase the currents observed (Pryor *et al.*, 2006). Whether the TRP-ML1 channel is a target for NAADP remains unclear. Furthermore, it has become apparent that another family of ion channels, two-pore channels (TPCs) may mediate NAADP responses (Galione *et al.*, 2009).

TPCs were first cloned from rat kidney and comprise two domains, each with six transmembrane segments (S1 – S6) similar to those found in voltage-gated Ca^{2+} and Na^{+} channels. TPC mRNA expression was found in several other tissues including rat liver, lung and spleen (Ishibashi *et al.*, 2000). In sea urchins, and most vertebrate species, three TPC (*Tpcn*) genes are present (designated *Tpcn1 – Tpcn3)* (Calcraft *et al.*, 2009). Interestingly, *Tpcn3* is present in guinea pig but not in human or mouse genomic sequences (Zhu *et al.*, 2010).

The first evidence of a physiological role for TPC proteins came in 2009 from Calcraft and colleagues (Calcraft *et al.*, 2009). Immunocytochemistry techniques revealed the expression of TPC2 proteins in punctate regions of the cytoplasm which overlapped with expression of lysosomal associated membrane protein 2 (LAMP2). In a cell-line expressing HA-tagged TPC2, this protein was found to co-localise with LAMP2 and Lysotracker Red staining, but not markers for early or late endosomes, ER, Golgi or mitochondria. TPC1 and TPC3 proteins were found to be located to late endosomes and other unidentified cellular compartments, and showed little co-localisation with TPC2.

The localisation of TPC2 proteins specifically to lysosomes prompted the authors of this study to test whether TPC2 constituted a binding site for NAADP. Membranes from HEK293 cells expressing HA-tagged TPC2 exhibited at least a three-fold increase in [32P]-NAADP binding when compared to membranes from wild-type cells. In cells expressing HA-TPC2, photorelease of caged NAADP elicited a biphasic Ca^{2+} response, beginning with a slow elevation followed by a larger Ca^{2+} transient, which were both absent in wild-type cells, where only a single, very small Ca^{2+} release event was observed. Both phases were suppressed by bafilomycin, while the second Ca^{2+} transient phase was sensitive to heparin, suggesting that the initial ramp phase occurred as a result of NAADP-mediated Ca^{2+} release and the second Ca^{2+} transient was dependent on IP_3 receptors, presumably activated by the Ca^{2+} released by NAADP (Calcraft *et al.*, 2009). These observations add further support to the 'two pool' hypothesis put forward by Churchill and Galione (Churchill *et al.*, 2001a).

In order to investigate the potential involvement of TPC2 proteins in NAADP responses further, northern blot analysis was carried out and demonstrated that *Tpcn2* mRNA could be detected in most human tissues including liver, kidney, brain, pancreas

and heart. Further, a *Tpcn2* knockout mouse model was generated. A previous finding that NAADP stimulates Ca^{2+} release from a lysosomal compartment in pancreatic β-cells, leading to the activation of a plasma membrane Ca^{2+} sensitive inward current (Masgrau *et al.*, 2003), was replicated in wild-type mice but could not be observed in *Tpcn2*$^{-/-}$ mice (Calcraft *et al.*, 2009). Taken together, these extensive observations raise the possibility that TPC2 proteins are essential for NAADP-induced responses in mammalian cells. In support of this idea, TPC2 proteins have since been proposed to mediate NAADP-evoked contractions in mouse detrusor smooth muscle (Tugba Durlu-Kandilci *et al.*, 2010).

Pitt and colleagues have recently investigated the properties of the TPC2 channel in lipid bilayer experiments. Channels were reported to exist in three states: a constitutively active state, an NAADP-activated state and an NAADP-inactivated state (Pitt *et al.*, 2010). Channels were found to open even in the absence of ligands, but with very low open probability. Nanomolar concentrations of NAADP activated the channels, in a manner sensitive to luminal pH and Ca^{2+} concentration, but not cytosolic Ca^{2+} concentrations. Interestingly, when in the NAADP-activated state, multiple TPC2 channels were observed to open in a synchronised manner. Furthermore, at high concentrations of NAADP, constitutive opening of channels was abolished, and open probability reduced to zero, indicative of an NAADP-inactivated state and providing a possible explanation for self-inactivating properties of NAADP observed in mammalian cells (Macgregor *et al.*, 2007a). Pitt and colleagues also examined the effects of Ned-19, an antagonist of NAADP signalling (see section 1.9.3.6), on channels in lipid bilayers with the finding that micromolar concentrations closed the channel, but that low nanomolar concentrations actually raised its probability of opening (Pitt *et al.*, 2010). These authors believe that Ned-19 is a high affinity activator of TPC2 that closes

the channel at higher concentrations, and that TPC2 proteins are NAADP-sensitive Ca^{2+} release mechanisms.

However, recent controversy has arisen over the nature of the permeability of TPC2 channels and indeed whether these channels can actually be activated by NAADP (Wang *et al.*, 2012b; Cang *et al.*, 2013). However, as outlined in a recent review by Morgan and Galione, there are some limitations in these studies, and there is still a considerable body of evidence pointing towards TPC2 channels as NAADP-gated Ca^{2+} channels (Morgan *et al.*, 2014).

1.9.3.6 Antagonists of NAADP signalling

In the absence of specific pharmacological inhibitors, high inactivating concentrations of NAADP, V-type H^+ ATPase inhibitors (e.g. bafilomycin A), GPN, LTCC and voltage-gated K^+ channel antagonists have all been used to inhibit NAADP-mediated Ca^{2+} mobilisation (Genazzani *et al.*, 1997). However, the use of some of these compounds has been limited by obvious lack of specificity, or poor membrane permeability.

Ned-19 is candidate NAADP antagonist which was identified by the use of ligand-based virtual screening, and is cell permeant (Naylor *et al.*, 2009). Using a large virtual library (called Zinc Is Not Commercial (ZINC)) of chemical entities, Naylor and colleagues were able to screen molecules for their similarity to a known 'query' ligand, in this case NAADP. A comparison of 3D shape was performed using ROCS (Rapid Overlay of Chemical Structures) software. The top 500 hits were then ranked for electrostatic similarity using EON software. The top 10 commercially available hits identified with ROCS, and the top 15 identified with a combination of ROCS and EON were purchased and assessed for their NAADP inhibitory activity in a sea urchin egg

homogenate assay (Naylor *et al.*, 2009). This led to the discovery of Ned-19. The commercially purchased Ned-19 was a mixture of diastereoisomers. Subsequent synthesis of the *trans* diastereoisomer and testing sea urchin egg homogenate assays revealed it was far more potent than the diastereoisomer mix in inhibiting NAADP-induced Ca^{2+} release (IC_{50} 6 nM) than the *cis* isomer (IC_{50} 800 nM) (Naylor *et al.*, 2009). Ned-19 was also used to identify the NAADP binding site in lipid bilayer studies (Pitt *et al.*, 2010).

1.9.3.7 Role of NAADP in the heart

The first evidence of a functional role of NAADP in cardiac myocytes was provided by studies in the Terrar laboratory. In intact guinea pig ventricular myocytes, photorelease of caged NAADP led to an increase in Ca^{2+} transient amplitude, which was not associated with any change in I_{CaL} amplitude, and which occurred progressively over time, being greater 60 s than 20 s after photorelease (Macgregor *et al.*, 2007a). The actions of photoreleased NAADP were prevented by high self-inactivating concentrations of NAADP, by bafilomycin A and by a combination of ryanodine and thapsigargin to inhibit SR function. The effects on Ca^{2+} transient amplitudes appeared to be associated with an increase in SR Ca^{2+} load since the amplitude of Ca^{2+} transients evoked by 10 mM caffeine (to cause rapid release of Ca^{2+} from the SR via RyR) were increased following photorelease of caged NAADP (Macgregor *et al.*, 2007a). Furthermore, a cell permeant analogue of NAADP (NAADP-AM) increased the amplitude of contraction of guinea pig ventricular myocytes, and the frequency and amplitude of Ca^{2+} sparks in rat ventricular myocytes; effects which were sensitive to bafilomycin A. A role for endogenous NAADP was also postulated, since high self-inactivating concentrations of NAADP and bafilomycin A reduced amplitude of cell

contractions and Ca^{2+} transients in guinea pig ventricular myocytes (Macgregor *et al.*, 2007a). Taken together, these data were suggested to be consistent with a model whereby NAADP mobilises Ca^{2+} from bafilomycin sensitive acidic Ca^{2+} stores, which enhances SR Ca^{2+} load, SR Ca^{2+} release and hence Ca^{2+} transients and contractions.

More recently, the role of NAADP in atrial myocytes was investigated by Collins and colleagues in the Terrar laboratory. Photorelease of caged NAADP was found to increase amplitude of Ca^{2+} transients, without affecting amplitude of I_{CaL}. Application of NAADP-AM was associated with an increase in Ca^{2+} spark frequency which was prevented by disruption of lysosomal function by either GPN, bafilomycin or a ryanodine/thapsigargin cocktail (Collins *et al.*, 2011). As reported in ventricular myocytes, an increase in atrial myocyte SR load was associated with NAADP treatment as observed by an increase in the amplitude of Ca^{2+} transients evoked by rapid application of 10 mM caffeine (Collins *et al.*, 2011). NAADP-AM also caused alkalinisation of lysosomal acidic stores as assessed by a reduction in Lysosensor Green fluorescence, and further, was seen after isoprenaline treatment. In addition, the increase in Ca^{2+} transient amplitude in response to isoprenaline was reduced in the presence of bafilomycin A, suggesting a role for NAADP-mediated Ca^{2+} mobilisation in the β-adrenergic response in atrial myocytes. The effects of NAADP in other regions of the heart, particularly the SA node, remain to be investigated.

More recently, Elson and colleagues have assessed the role of TPC1 and TPC2 proteins in mediating NAADP responses in mouse hearts, by utilising mice lacking either protein (Elson, DPhil Thesis, 2011). In ventricular myocytes isolated from *Tpcn2*$^{-/-}$ mice, NAADP-AM was without significant effect in increasing amplitude of contractions, Ca^{2+} transients or frequency of Ca^{2+} sparks; this was in contrast to myocytes from *Tpcn1*$^{-/-}$ mice, where NAADP-AM treatment was associated with

positive inotropic actions (Elson, DPhil Thesis, 2011). Taken together, these data suggest that TPC2, rather than TPC1 is important in modulating EC coupling in mouse myocytes.

Experiments in the Terrar laboratory have also taken forward the idea that NAADP-induced Ca^{2+} mobilisation may be important in mediating the cardiac β-adrenoceptor response. A possible mechanism whereby endogenous levels of NAADP could be elevated by β-adrenoceptor stimulation was first proposed by Higashida and colleagues, involving stimulation of the enzymes synthesising NAADP (ARCs) by β-adrenoceptor stimulation and PKA. Early studies examining the mammalian tissue expression of ARCs demonstrated its presence in extract from rabbit heart (Rusinko *et al.*, 1989). The NAADP-synthesising capacity of cardiac tissue has also been assessed in mouse and rat hearts, with endogenous levels of NAADP being reported as 0.4 nmol/mg protein in mouse hearts and 0.22 nmol/mg protein in guinea pig hearts (Chini *et al.*, 2002; Macgregor *et al.*, 2007a). Isoprenaline was reported to increase the rate of cADPR synthesis (catalysed by ARCs) in crude membrane fractions prepared from rat ventricular myocytes, as measured by the rate of [^{3}H]cADPR formation from [^{3}H]NAD^+ (Higashida *et al.*, 1999), and to stimulate ARC activity in a concentration-dependent manner, which could be mimicked by a non-hydrolysable GTP analogue (GTPγS), but was inhibited by the β-adrenoceptor antagonist propranolol or by pre-treatment with cholera toxin to lead to maximal activation of adenylyl cyclases.

In experiments utilising whole hearts or functional myocytes, Macgregor and colleagues, isoprenaline was found to greatly increase endogenous levels of NAADP in guinea pig hearts. In the presence of isoprenaline, photolysis of caged NAADP produced a smaller increase in guinea pig ventricular myocyte Ca^{2+} transients than in the absence of isoprenaline, which is consistent with the idea that endogenous levels of

NAADP are raised, possibly through stimulation of ARCs, in guinea pig hearts (Macgregor *et al.*, 2007a). In further support of this idea, more recent data from Lewis and colleagues reported an increase in endogenous levels of both NAADP and cADPR in guinea pig hearts stimulated with isoprenaline (Lewis *et al.*, 2012). The increase in NAADP levels were reported to be transient, while those of cADPR were sustained (Lewis *et al.*, 2012).

The functional effects of isoprenaline were recently assessed in mice lacking both TPC1 and TPC2 proteins (Elson, DPhil thesis, 2011), with the finding that isoprenaline-evoked increases in field-stimulated Ca^{2+} transient and contraction amplitudes were substantially reduced in myocytes from *Tpcn2*$^{-/-}$ mice, while there was no significant difference in myocytes lacking TPC1 proteins (Elson, DPhil Thesis, 2011). These data add to the ideas that NAADP is an important player in mediating the cardiac β-adrenoceptor response, and that TPC2 proteins, rather than TPC1, are the target for NAADP in the heart. However, it remains to be seen whether this mechanism involving TPC2 operates at the level of the whole organ, and in addition whether pharmacological inhibitors of NAADP signalling can reproduce the effects of TPC2 knock-out on isoprenaline responses in guinea pig ventricular cells.

Given that NAADP-mediated Ca^{2+} signalling is thought to contribute to cardiac EC coupling, it is tempting to hypothesise that inhibitors of NAADP signalling may provide a novel target for anti-arrhythmic drugs. This has recently been demonstrated with the NAADP antagonist BZ194 (Nebel *et al.*, 2013).

1.10 Novel modulators of cardiac function: the endocannabinoid system

The diverse physiological effects of *Cannabis sativa* have been utilised therapeutically by humans for thousands of years. Cannabis is now the most widely used recreational drug in the world, largely due to its ability to alter sensory perception and induce euphoria (Pacher *et al.*, 2006). The isolation of the principal psychoactive component of the herb, Δ^9-THC (Gaoni *et al.*, 1964), and subsequent cloning of distinct cannabinoid receptor subtypes, namely CB_1 and CB_2 receptors, has led to the discovery of their endogenous ligands, of which arachidonoylethanolamide (AEA; also known as 'anandamide') and 2-arachidonoylglycerol (2-AG) (Devane *et al.*, 1992b; Mechoulam *et al.*, 1995) are the two most extensively studied examples. The concurrent development of highly selective cannabinoid receptor agonists and antagonists has led to considerable progress in unravelling the molecular mechanisms of cannabinoid action. Since their discovery, a complex biochemical pathway for the synthesis, release, transport and degradation of the endogenous or 'endo-' cannabinoids has been described. It is now appreciated that they form part of a widespread signalling system, termed the 'endocannabinoid system', whose actions may have important physiological and pathophysiological implications, and that pharmacological modulation may provide novel therapeutic targets for various diseases (Pacher *et al.*, 2006), including cardiovascular diseases (Montecucco *et al.*, 2012).

1.10.1 Discovery

The isolation (Gaoni *et al.*, 1964) and subsequent chemical synthesis (Mechoulam *et al.*, 1967) of Δ^9-THC, one of at least 66 'cannabinoids' found in the flowers of the plant, paved the way for the discovery of the molecular targets of cannabinoids. Early suggestions that cannabinoids exert their mood altering effects through interacting with and changing the properties of cell membrane lipids (Hillard *et al.*, 1985; Martin, 1986), were eventually overshadowed by two observations which coincided with a growing understanding of G-protein-coupled receptor (GPCR) signalling in the mid-1980s, and suggested that the molecular target for the cannabinoids was in fact a GPCR. Firstly, Δ^9-THC was shown to decrease prostanoid-stimulated cyclic adenosine monophosphate (cAMP) accumulation in intact neuroblastoma cells (Howlett, 1984), with further studies demonstrating that the potency of Δ^9-THC in inducing this effect correlated well with its psychotropic activity in human and animal behavioural studies (Howlett *et al.*, 1984). Secondly, the development of the more potent and enantiomerically pure Δ^9-THC analogue CP55940, allowed a ^{3}[H]-CP55940 binding site to be demonstrated in rat brain (which correlated with sites for psychotropic activity in brain). Crucially, binding was reduced in the presence of guanylylimidodiphospate (a non-hydrolysable guanosine triphosphate (GTP) analogue), while the ability of non-labelled cannabinoid agonists to displace this radioligand from its binding site (CP55940 $\geq$ Δ^9-THC > cannabinol) was consistent with their potencies in assays of biological function (Devane *et al.*, 1988).

Molecular confirmation of the existence of cannabinoid receptors came serendipitously in 1990, after it was noted that ^{3}[H]-CP55940 binding sites corresponded with the localisation of the cDNA of an orphan GPCR (SKR6) in brain

tissue (Herkenham *et al.*, 1990). Matsuda *et al*., then screened mammalian cells and *Xenopus* oocytes transfected with SKR6 cDNA with several possible ligands (including CP55940 and Δ^9-THC), with the finding that both cannabinoids inhibited forskolin-stimulated cAMP accumulation in a dose-dependent, pertussis toxin (PTX)-sensitive and stereoselective manner; a response not observed in non-transfected cells (Matsuda *et al.*, 1990). Furthermore, the order of potency of the cannabinoids in inhibiting cAMP accumulation (Δ^9-THC > cannabinol > cannabidiol) was in agreement with previous data obtained from neuroblastoma cell lines (Howlett, 1987). Together, these data confirmed that SKR6 was indeed a G_i-protein coupled cannabinoid receptor, designated CB_1 (Howlett *et al.*, 2002). The human CB_1 receptor was later cloned from a human brainstem cDNA library (Gerard *et al.*, 1991), on the basis of 98% amino acid sequence homology with the rat brain CB_1 receptor.

A second cannabinoid GPCR sequence (CX5), which shared 44% amino acid sequence homology with the human CB_1 receptor was cloned from the human promyelocytic leukaemic cell line HL60; radioligand binding studies on COS cells transfected with CX5 cDNA confirmed cannabinoid binding (Munro *et al.*, 1993). *In situ* hybridisation studies in rat showed that this receptor, designated CB_2 was expressed by macrophages in the spleen, but not in brain. More recent evidence suggests that there are several other receptor and non-receptor targets for endocannabinoids, which will be discussed later.

Following the molecular characterisation of the CB_1 receptor, the search for endogenous ligands began. A standard approach for identifying new receptor agonists by demonstrating displacement of a labelled probe was used to identify the first endocannabinoid. Based on the fact that plant and synthetic cannabinoids are highly lipophilic, porcine brains were extracted with organic solvents, and the extract

chromatographed in line with standard protocols for the separation of lipids. The resultant fractions were then screened according to their ability to displace radiolabelled HU-243 (a synthetic analogue of THC) (Devane *et al.*, 1992a) from CB_1 receptors in a centrifugation-based ligand binding assay, resulting in the isolation of the first endocannabinoid, AEA (Devane *et al.*, 1992b). AEA is most commonly referred to as 'anandamide' from the Sanskrit word 'ananda' meaning 'eternal bliss', and was shown to bind to the CB_1 receptor with high affinity (with a K_i value of 52 nM) (Devane *et al.*, 1992b). After refinement of the chromatographic procedure, and elimination of various impurities from the anandamide-containing fraction, the structure of anandamide was elucidated using mass spectrometry (MS) and nuclear magnetic resonance (NMR) techniques (Devane *et al.*, 1992b; Hanus *et al.*, 1993; Mechoulam *et al.*, 1995). In a similar manner, and as a result of the discovery of the CB_2 receptor in immune cells, a second endogenous ligand, 2-AG, was isolated from canine gut, an organ with well-established immunological function (Mechoulam *et al.*, 1995).

1.10.2 Cannabinoid receptor signalling

Given the potency of cannabinoids as modulators of behavioural and sensory perception, many of the investigations into cannabinoid receptor signalling pathways have focussed on neuronal cells (or cell lines); indeed, the findings from many of these investigations have now been integrated into a model explaining the activity of endocannabinoids as retrograde messengers in various brain regions (Kano *et al.*, 2009). However it is becoming apparent that cannabinoid receptor signalling may have relevance in other organ systems.

Both CB_1 and CB_2 receptors are GPCRs. The tissue distribution, particularly of CB_1 receptors appears to account for the well-known psychotropic effects of THC;

indeed, the CB_1 receptor is one of the most abundant GPCRs currently known in the central nervous system, with highest expression in the basal ganglia, cerebellum, hippocampus and cortex (Miller *et al.*, 2011). However, there is also significant expression of CB_1 receptors in the peripheral nervous system, and several peripheral organs and tissues including adipose tissue (Bensaid *et al.*, 2003), the liver (Bensaid *et al.*, 2003) and the heart (Weis *et al.*, 2010). CB_2 receptors on the other hand are mostly restricted to cells of the immune system (Miller *et al.*, 2011), but it appears there is some expression in peripheral organs including the heart (Weis *et al.*, 2010). Some of the reported signalling pathways mediated by cannabinoid receptors will now be discussed.

1.10.2.1 Regulation of cAMP

Studies of the CB_1 receptor in brain issue have demonstrated that its response to cannabinoid agonists is an inhibition of cAMP production (Bidaut-Russell *et al.*, 1991; Childers *et al.*, 1994). This has been confirmed in N18TG2 neuroblastoma cells expressing endogenous CB_1 receptors (Howlett *et al.*, 1988; Pinto *et al.*, 1994), and in cell lines expressing recombinant receptors (Matsuda *et al.*, 1990; Felder *et al.*, 1993; Vogel *et al.*, 1993. This response has been confirmed to be PTX-sensitive, confirming the involvement of $G_{i/o}$ proteins (Felder *et al.*, 1995). Similarly, $G_{i/o}$ coupling of the CB_2 receptor to adenylyl cyclases has been confirmed in human lymphocytes, mouse spleen cells expressing endogenous CB_2 receptors, and in Chinese hamster ovary (CHO) cells expressing recombinant CB_2 receptors (Felder *et al.*, 1995; Slipetz *et al.*, 1995; Gonsiorek *et al.*, 2000). In this system, anandamide and (*R*)-(+) methanandamide (a non-hydrolysable analogue of anandamide) partially inhibited forskolin-stimulated cAMP accumulation at high concentrations via the CB_2 receptor

(Felder *et al.*, 1995; Gonsiorek *et al.*, 2000) whereas this response was completely inhibited by anandamide in N18TG2 cell membranes expressing CB_1 receptors (Childers *et al.*, 1994; Pinto *et al.*, 1994) suggesting anandamide is a partial agonist at the CB_2 receptor in terms of inhibiting cAMP accumulation. In contrast, 2-AG was found to behave as a full agonist in inhibiting forskolin-stimulated cAMP accumulation in CHO cells expressing CB_2 receptors (Gonsiorek *et al.*, 2000).

In some cell types, cannabinoid receptor agonists have been reported to increase cAMP production. For example, in rat globus pallidus slices, WIN55,212-2 (a synthetic cannabinoid) caused a concentration-dependent decrease in cAMP after basal levels were elevated by application of forskolin, but in the absence of forskolin, caused an increase in cAMP (Maneuf *et al.*, 1997). Both effects were inhibited by the CB_1 receptor antagonist, SR141716A (Maneuf *et al.*, 1997). Such biphasic responses have been attributed to the presence of constitutively active CB_1 receptors (which have been observed in mutagenesis studies as a result of a single point mutation, and couple to G_s rather than G_i (Abadji *et al.*, 1999)) cell-type specific expression of adenylyl cyclase isoforms (co-expression of AC 1, 3, 5, 6 or 8 with CB_1 or CB_2 receptors has been reported to cause a decrease in cAMP formation, while co-expression with AC 2, 4 or 7 led to increases (Rhee *et al.*, 1998)) and agonist-specific actions leading to coupling of receptors to different types of intracellular G protein (Mukhopadhyay *et al.*, 2000). Others have suggested that the stimulatory G protein response may only occur in PTX pre-treated systems devoid of functional $G_{i/o}$ proteins. In cultured striatal neurons and in CHO cells transfected with human CB_1 receptors, HU-210 caused an increase in cAMP accumulation after pre-treatment of cells with PTX, which was inhibited by the CB_1 receptor antagonist SR141716A (Glass *et al.*, 1997). The abilities of different cannabinoid receptor agonists to elicit this response appears to vary; synthetic

cannabinoids are thought to be full agonists, while anandamide and Δ^{9}-THC are partial agonists (Bonhaus *et al.*, 1998). Only WIN55,212-2 was a full agonist in stimulating the G_s-mediated response after PTX treatment (Bonhaus *et al.*, 1998). Thus, physiologically the inhibition of AC is probably a more relevant effect of cannabinoid receptor stimulation, especially in cells expressing isoforms 1, 3, 5, 6 or 8 (Rhee *et al.*, 1998).

1.10.2.2 Regulation of ion channels

Early findings that anandamide inhibited N- and Q-type voltage-dependent Ca^{2+} channels in cell lines (either transfected with CB_1 receptor cDNA or expressing the native protein) (Mackie *et al.*, 1993; Mackie *et al.*, 1995) in a PTX-sensitive manner (Mackie *et al.*, 1993), and that anandamide enhanced G-protein coupled inwardly rectifying K^+ currents (K_{ir}/GIRK) (Mackie *et al.*, 1995), have now been integrated into models of the actions of endocannabinoids as retrograde transmitters in various brain regions (Kano *et al.*, 2009). CB_1 receptor-mediated inhibition of neuronal P/Q and N-type, but not L-type Ca^{2+} channels has been reported (Ho *et al.*, 2000). In the cardiovascular system, anandamide and WIN55-212,2 have been reported to inhibit LTCCs cat brain arterial smooth muscle cells which endogenously express CB_1 receptors; an effect which was prevented by both PTX and the CB_1 receptor antagonist SR141716A and correlated with relaxation of arterial rings (Gebremedhin *et al.*, 1999). It is possible that net dephosphorylation of channels due to CB_1 receptor-mediated inhibition of cAMP (and therefore a reduction in PKA activity) (Deadwyler *et al.*, 1995) may be responsible for these effects

1.10.2.3 Other signalling pathways

CB_1 receptors have also been reported to modulate intracellular Ca^{2+}. In neuroblastoma cell lines, an increase in intracellular Ca^{2+} was reported in response to treatment with 2-AG, which was inhibited by both PTX and by the phospholipase C inhibitor U73122, suggesting coupling of the CB_1 receptor with phospholipase C and inositol-1,4,5-trisphosphate (IP_3)-mediated release of Ca^{2+} from intracellular stores (Sugiura *et al.*, 1997). A similar response has been demonstrated in cerebellar granule neurons in which cannabinoid agonists augmented the magnitude of an NMDA receptor- or depolarisation-induced intracellular Ca^{2+} transient; a response sensitive to SR141716A, PTX and PLC inhibitors (Netzeband *et al.*, 1999). Cannabinoid receptor agonists have also been shown to activate p42/p44 mitogen-activated protein (MAP) kinase (Sanchez *et al.*, 1998) and to stimulate nitric oxide production (Prevot *et al.*, 1998). Thus, it appears cannabinoid receptor-mediated responses may vary considerably depending on cell type.

1.10.3Synthesis of endocannabinoids

1.10.3.1 Anandamide

Anandamide is a derivative of arachidonic acid, and is a member of a large family of bioactive lipids collectively referred to as *N*-acylethanolamines. These include non-endocannabinoid compounds like the anti-inflammatory compound *N*-palmitoylethanolamide. Early work by Schmid and colleagues revealed the existence of various *N*-acylethanolamines in degenerating tissues, for example, infarcted dog heart which may reach concentrations as high as 500 μM (Epps *et al.*, 1979), but at the time the existence of an arachidonic acid-containing species (i.e. anandamide) was

overlooked because its levels were too low to be detected with the methods used (Sugiura *et al.*, 2002). Schmid and colleagues later detected anandamide in the brains of several species by MS techniques after rapid freezing of the tissue (Schmid *et al.*, 1995), but levels were much lower than those previously reported by Devane and colleagues at the initial discovery of anandamide (Devane *et al.*, 1992b). It was suggested that a considerable amount of anandamide may be formed during the post-mortem period, which may account for the discrepancy (Schmid *et al.*, 1995). Low levels of anandamide have subsequently been detected in both human and rat hearts (~20 pmol/g wet tissue) (Felder *et al.*, 1996; Koga *et al.*, 1997). In heart failure, circulating levels of anandamide were determined to be of the order of 0.3 – 0.5 ng/ml (Weis *et al.*, 2010).

Anandamide is synthesised from the phospholipid precursor, *N*-arachidonoylphosphatidylethanolamine (NAPE). Little is known about the identity of the enzyme responsible synthesis of NAPE in animal cells, but a Ca^{2+}-dependent *N*-acyltransferase (NAT) enzyme, which catalyses the transfer of an acyl group (in the case of anandamide this is an arachidonoyl group) from the *sn*-1 position of a glycerophospholipid (e.g. phosphatidylcholine) to the amino group of phosphatidylethanolamine, has been proposed to catalyse this step (Cadas *et al.*, 1996; Cadas *et al.*, 1997). Ca^{2+}-dependent NAT activity was first observed in subcellular fractions from canine myocardium (Natarajan *et al.*, 1982) and subsequently in other tissues (Cadas *et al.*, 1996; Cadas *et al.*, 1997), but the cDNA of this enzyme has not been cloned. It should be noted that this enzyme is not specific for the synthesis of anandamide; it can catalyse the transfer of any acyl group (not just an arachidonoyl group) to phosphatidylethanolamine and is thus involved in the synthesis of N-acylethanolamines in general. Another more recently identified candidate is a Ca^{2+}-

independent enzyme with NAT activity, RLP-1 (or iNAT) (Jin *et al.*, 2007), although its physiological relevance remains to be determined (Jin *et al.*, 2009).

Other proposed pathways include a two-step pathway involving the conversion of NAPE to glycerophospho-*N*-acylethanolamine (GP-NAE) by the enzyme α/β-hydrolase 4 (Simon *et al.*, 2006), followed by conversion of GP-NAE intermediates to anandamide by glycerophosphodiesterase 1 (GDE1) (Simon *et al.*, 2008); however, only low levels of GDE1 activity were detected in the heart. Another pathway, characterised in lipopolysaccharide-stimulated macrophage-like RAW264.7 cells, involves the hydrolysis of NAPE by phospholipase C, generating phospho-anandamide as an intermediate, which is then dephosphorylated by a protein tyrosine phosphatase (PTPN22) to yield anandamide (Liu *et al.*, 2006). Whether this pathway exists in the heart is unknown.

Given the multiplicity of anandamide synthetic pathways, the question remains as to which pathway is favoured and under which conditions. It is possible that the nature of the acyl chain transferred to phosphatidylethanolamine and the phospholipid membrane composition at the site of synthesis are important factors, but further investigation is required (Muccioli, 2010).

1.10.3.2 2-AG

Long before it was regarded as an endocannabinoid, 2-AG was identified as a possible source of arachidonic acid in thrombin stimulated platelets (Prescott *et al.*, 1983); indeed levels of 2-AG in the brain have been determined to be 200 times higher than those of anandamide (Stella *et al.*, 1997). In terms of 2-AG as a signalling molecule, synthetic pathways are regarded as being stimulus-dependent (Bisogno *et al.*, 1997; Stella *et al.*, 1997). Stella *et al*. Reported the production of 2-AG in hippocampal

slices as a result of depolarisation-induced Ca^{2+} influx, in a pathway whereby diacylglycerol (DAG) is synthesised from phophatidylinositol by phospholipase C activity, with subsequent hydrolysis of DAG to 2-AG by a diacylglycerol lipase (DAGL) (Stella *et al.*, 1997). The cloning of specific sn1-DAGLα and sn1-DAGLβ has been crucial to enhancing understanding of 2-AG biosynthesis (Bisogno *et al.*, 2003). The highest levels of DAGLα mRNA were detected in the brain of both mouse and human, but there was some expression in the heart of both species (Bisogno *et al.*, 2003). In addition, mRNA was detected in macrophages (human) and vascular tissue (mouse) (Bisogno *et al.*, 2003). Levels of 2-AG were enhanced by overexpression of DAGLα and were decreased by the DAGL inhibitor THL, or by RNA interference in ionomycin stimulated neurons (Bisogno *et al.*, 2003). This pathway has also been demonstrated in brain slices after treatment with the glutamate receptor agonist DHPG (glutamate receptors are coupled to $G_{q/11}$ proteins, stimulating phospholipase C directly) (Jung *et al.*, 2005; Maejima *et al.*, 2005).

Another proposed pathway for 2-AG biosynthesis involves the sequential reactions of phospholipase A1, yielding a 2-arachidonoyl-lysophosphatidylinositol (lyso-PI) intermediate, which is then broken down into 2-AG by a lyso-PI specific PLC (reviewed in Sugiura *et al.*, 2002). Other pathways have also been described; it is possible that they are cell-type and/or stimulus-specific (Kano *et al.*, 2009).

1.10.4Metabolism of endocannabinoids

1.10.4.1 Anandamide

FAAH, a serine hydrolase enzyme cloned in 1996 (Cravatt *et al.*, 1996) has received much attention as a candidate enzyme for anandamide hydrolysis, yielding

arachidonic acid and ethanolamine (McKinney *et al.*, 2005). FAAH is widely expressed in brain, spinal cord and liver, for example, but not in heart or skeletal muscle (Cravatt *et al.*, 1996). The brains of FAAH-/- mice display 10- to 15-fold greater levels of anandamide than their wild-type counterparts (Cravatt *et al.*, 2001). Despite a lack of direct visualisation of FAAH mRNA in the heart, levels of endogenous anandamide have been shown to be raised in myocardial tissue from FAAH-/- mice (Pacher *et al.*, 2005). Immunoblotting in myocardial tissue from spontaneously hypertensive rats has suggested there is an upregulation of FAAH in hypertension (Batkai *et al.*, 2004).

A second FAAH enzyme (FAAH-2), which shares 20 % sequence homology with FAAH (which will now be referred to as FAAH-1) has also been discovered (Wei *et al.*, 2006). Interestingly, the FAAH-2 gene was found in human and primate genomes but not those of the mouse or rat (Wei *et al.*, 2006). Unlike FAAH-1, FAAH-2 mRNA was detected in human heart but was not present in brain, small intestine or testis (Wei *et al.*, 2006). Although the enzyme has a higher catalytic activity for oleamide than for anandamide, it is possible that it may play a role in anandamide hydrolysis under certain conditions (Wei *et al.*, 2006). In contrast to endoplasmic reticulum-localised FAAH-1, FAAH-2 was found to be localised to cytosolic lipid droplets (Kaczocha *et al.*, 2010).

A third enzyme reported to hydrolyse anandamide and other NAEs was identified by Ueda and colleagues in human megakaryoblastic cells (Ueda *et al.*, 1999). This enzyme, *N*-acylethanolamine-hydrolysing acid amidase (NAAA), was found to be highly expressed in macrophages, to localise to lysosomes (Tsuboi *et al.*, 2007), and to have an optimal pH of around 5 (Ueda *et al.*, 1999). NAAA actually has a higher activity for palmitoylethanolamide than anandamide, but analysis of tissue mRNA showed widespread distribution, with highest levels detected in lung, and modest levels

in heart (Tsuboi *et al.*, 2005). This distribution was not the same as that reported for FAAH, suggesting the enzymes have distinct roles (Tsuboi *et al.*, 2005).

Anandamide and 2-AG can additionally be metabolised by cyclooxygenase (COX) 2 (Rouzer *et al.*, 2008). When incubated with COX-2 but not COX-1, anandamide is metabolised to compounds known as prostaglandin-ethanolamides or 'prostamides' such as $PGE_{2\alpha}$-ethanolamide (Yu *et al.*, 1997). These molecules have some receptor-mediated actions themselves, but in general COX-2 is not regarded to contribute to termination of endocannabinoid signalling (Muccioli, 2010).

1.10.4.2 2-AG

2-AG metabolism has not been studied as extensively as that of anandamide. The primary candidate enzyme is monoacylglycerol lipase (MAGL), which was first purified and cloned from adipose tissue (Karlsson *et al.*, 1997). Overexpression of MAGL in rat neurons has been shown to lead to reduced accumulation of 2-AG (Dinh *et al.*, 2002). More recently, a functional proteomic approach was used to map enzymes responsible for 2-AG hydrolysis in mouse brain, with the finding that 85 % of hydrolysis was mediated by MAGL, with the remaining 15 % being attributed to two previously uncharacterised enzymes, ABHD12 and ABHD6 (Blankman *et al.*, 2007). All enzymes were shown to exhibit distinct subcellular distributions, leading to the suggestion that they may regulate different pools of 2-AG in the brain (Blankman *et al.*, 2007). Hydrolysis of 2-AG by MAGL yields arachidonic acid and glycerol. In general, MAGL is regarded as having a higher activity for 2-AG over other MAGs but it has been shown that 2-oleyl glycerol is hydrolysed approximately 2-fold faster than 2-AG by MAGL (Dinh *et al.*, 2002).

1.10.5 Cannabinoid receptor-independent actions of endocannabinoids

In addition to actions at cannabinoid receptors, a widespread body of literature describes actions of cannabinoids and their endogenous counterparts in modulating ion channel function directly; that is, independently of any receptor-mediated actions (Oz, 2006). Because of their high lipophilicity (Tian *et al.*, 2005), cannabinoids would be expected to reside within the cell membrane phospholipid bilayer, where they could feasibly interact with ion channels directly, perhaps in a similar manner to general anaesthetics (Hanley *et al.*, 2004). The concentrations of cannabinoids under such conditions are likely to be much higher than in aqueous solutions, and since the time taken for these compounds to reach equilibrium within the membrane bilayer is unknown, it is possible that *in vitro* experiments with low micromolar concentrations of cannabinoids for short time periods (~5 – 10 minutes) may better reflect the actions of cannabinoids in lipid bilayers (Oz, 2006). Since the cloning of cannabinoid receptors, the focus of research has been on receptor-mediated actions of cannabinoids and endocannabinoids, and direct actions are often overlooked, as highlighted in an extensive review on the subject (Oz, 2006).

Prior to the isolation and cloning of the CB_1 receptor, cannabinoids such as THC were thought to exert their effects through interacting with and disrupting the function of the phospholipid bilayer (Lawrence *et al.*, 1975). To this effect, anandamide has been shown to interact directly with LTCCs from rabbit skeletal muscle membranes, with radioligand binding studies demonstrating that anandamide inhibited binding of Ca^{2+} channel antagonists of the 1,4 dihydropyridine, phenylalkyalamine and 1,5-benzothiazapine class (Shimasue *et al.*, 1996). Later studies in membrane vesicles from the same preparation have shown that anandamide (1 – 100 μM) and *(R)-(+)-*

methanandamide inhibited depolarisation-induced Ca^{2+} fluxes in a SR141716A- and PTX-insensitive manner (Oz *et al.*, 2000). Radioligand binding studies were used to confirm a direct interaction of anandamide with LTCCs in this tissue (Oz *et al.*, 2000). It has also been shown that 2-AG can inhibit Ca^{2+} fluxes in skeletal muscle membranes and inhibit binding of radiolabelled dihydropyridine Ca^{2+} channel antagonists (Oz *et al.*, 2004) Interestingly this effect was not reproduced by THC or the synthetic cannabinoids CP55940 or WIN55,212-2 (Oz *et al.*, 2004). Chemin and colleagues have also reported direct inhibitory actions of anandamide on T-type Ca^{2+} channels expressed in various cell lines (Chemin *et al.*, 2001). The observed inhibition was not prevented by GDPβS (an inhibitor of G-protein function) or by inhibitors of PLA_2, PLC or PLD, and it was postulated that a direct interaction of anandamide with the channel occurred from the intracellular surface, since inhibitory effects were also observed in excised inside-out patches from HEK cells (Chemin *et al.*, 2001).

A number of studies have also reported direct actions of endocannabinoids on various types of K^+ channels (these are reviewed in detail in Oz, 2006). The first evidence of a direct action of anandamide with voltage-gated K^+ channels was obtained from a murine fibroblast B82 cell line expressing Kv 1.2 channels (Poling *et al.*, 1996). Anandamide and THC were found to inhibit these channels with comparable potency (IC_{50} ~2.5 μM) in a SR141716A- and PTX-insensitive manner (Poling *et al.*, 1996). An inhibitory effect of anandamide and methanandamide on I_K has also been observed in rat arterial myocytes (Van den Bossche *et al.*, 2000). A maximal effect of ~50 % inhibition of I_K was seen at a concentration of 3 μM, but only when drugs were applied extracellularly, suggesting an extracellular binding site (Van den Bossche *et al.*, 2000)

1.10.6Effects on the cardiovascular system

The effects of cannabinoids on cardiovascular function are complex and occur as a result of actions on the CNS as well as the heart and vasculature. In humans, smoking cannabis results in an acute drop in blood pressure and a compensatory increase in heart rate (Kanakis *et al.*, 1976), while prolonged cannabis use is associated with a reduction in blood pressure and heart rate (Benowitz *et al.*, 1975). The discovery of endocannabinoids raised the question of whether these compounds could also mediate such actions.

1.10.6.1 In vivo studies

The effects of exogenously applied endocannabinoids in the cardiovascular system *in vivo* are complex and appear to depend upon species and experimental conditions. Administration of a bolus dose of anandamide to anaesthetised rats was found to induce bradycardia and a triphasic effect on blood pressure (Varga *et al.*, 1995; Lake *et al.*, 1997). An initial bradycardic and hypotensive response was followed by a brief pressor response, and finally by a third prolonged phase of hypotension and bradycardia (Varga *et al.*, 1995). The initial bradycardia and associated hypotension was inhibited by atropine or by dissection of the vagus nerve, and is therefore thought to be mediated by activity of the parasympathetic nervous system (Varga *et al.*, 1995). It was later shown that this initial phase was mediated by the activity of anandamide at transient receptor potential vanilloid 1 (TRPV1) receptors located on sensory nerve terminals (Malinowska *et al.*, 2001). In contrast the prolonged depressor response was inhibited by the CB_1 receptor antagonist SR141716A, by cervical spinal transection and by α-adrenoceptor antagonists, and has therefore been attributed to CB_1 receptor

mediated inhibition of sympathetic outflow in the periphery (Varga *et al.*, 1995; Lake *et al.*, 1997; Malinowska *et al.*, 2001). Furthermore, this prolonged depressor response to both anandamide and WIN55,212-2 was absent in CB_1 receptor knockout mice (Ledent *et al.*, 1999). In conscious rats however, the effects of anandamide are very different from those seen in anaesthetised animals, where the prolonged depressor response appears to be absent, except at higher doses (Stein *et al.*, 1996).

Surprisingly, given the clear depressor response to application of exogenous anandamide in anaesthetised animals, basal heart rate and blood pressure were found to be normal in CB_1 receptor knock-out mice (Ledent *et al.*, 1999) and in FAAH deficient mice (Pacher *et al.*, 2005), suggesting little or no involvement of the endocannabinoid system in regulation of blood pressure and cardiac contractility under basal physiological conditions. Furthermore, administration of rimonabant (SR141716A) to pithed rats at doses reported to block the effects of exogenously applied cannabinoids, had no effect on sympathetic tone, blood vessel calibre or heart rate in normotensive animals (Pfitzer *et al.*, 2005). However, in hypertensive states, administration of CB_1 receptor antagonists has been shown to cause an increase in blood pressure and cardiac contractility (Batkai *et al.*, 2004). Furthermore, the decrease in blood pressure in response to anandamide was found to be greater in hypertensive than normotensive states, and elevation of endogenous levels of anandamide through administration of an FAAH inhibitor was found to restore blood pressure to normotensive levels (Batkai *et al.*, 2004). Batkai and colleagues concluded that these observations suggested an upregulation, and perhaps protective role of the endocannabinoid system in hypertension; indeed they observed upregulation of cardiac and vascular smooth muscle CB_1 receptors (Batkai *et al.*, 2004), perhaps explaining the increased sensitivity of hypertensive animals to administration of exogenous anandamide.

Given the likelihood that the aforementioned findings are complicated by both centrally- and peripherally-mediated actions of cannabinoids, many *in vitro* studies have been performed in order to unravel the mechanisms of action of endogenous cannabinoids. In fact, studies of localised actions of endocannabinoids are perhaps more important since these compounds are so rapidly degraded and therefore likely to act only in limited areas. A large body of literature concerning the actions of cannabinoids and endocannabinoids on blood vessel preparations exists; far fewer investigations have been carried out using isolated hearts or cardiac myocytes.

1.10.6.2 In vitro studies: the vascular system

Ellis and colleagues were the first to report a local vasodilator action of anandamide in the cerebral vasculature (Ellis *et al.*, 1995), and later reports confirmed this in the rat isolated mesenteric and coronary vasculatures (Randall *et al.*, 1996; Randall *et al.*, 1997). The effects of anandamide and of THC were sensitive to indomethacin in the cerebral vasculature, suggesting that these compounds induced vasodilatation through the generation of vasoactive prostanoids (Ellis *et al.*, 1995). However, studies in other vascular preparations suggested that this prostanoid-mediated mechanism did not occur in all vascular beds (Randall *et al.*, 1996; Randall *et al.*, 1997; White *et al.*, 1997).

The necessity of the endothelium for vasodilator responses to be observed also appears to vary between vascular beds. The general consensus is that most anandamide vasodilator responses are endothelium independent (Randall *et al.*, 1996; White *et al.*, 1997). However, Pratt and colleagues showed in bovine coronary artery that the presence of the endothelium was necessary to see an anandamide-induced response; it was suggested that an endothelial cytochrome p450 mono-oxygenase enzyme was

necessary to break down exogenous anandamide to vasoactive prostanoids and epoxyeicosatrienoic acids (Pratt *et al.,* 1998). Another mechanism reported in vessels of the kidney is thought to involve synthesis of nitric oxide via endothelial cells, since responses to anandamide were inhibited by SR141716A and by the nitric oxide synthase inhibitor, L-NAME, but not by indomethacin (Deutsch *et al.*, 1997). However, this sensitivity of responses to L-NAME has not been seen in other vascular beds (Randall *et al.*, 1996; White *et al.*, 1997).

At least some of the responses to anandamide observed in vascular preparations are thought to occur through activation of TRPV1 receptors (Zygmunt *et al.,* 1999). This suggestion was made following observations in guinea pig basilar artery and rat mesenteric and hepatic arteries, that anandamide-induced vasodilatation could not be inhibited by SR141716A, but could be inhibited by the TRPV1 antagonist capsazepine and by the calcitonin-gene related peptide (CGRP) antagonist CGRP(8-37), and were not mimicked by other cannabinoid receptor agonists including WIN55,212-2 or 2-AG (Zygmunt *et al.*, 1999). The conclusion was made that anandamide was likely to be generating release of CGRP from sensory nerve terminals through actions on TRPV1 receptors located on the nerves themselves (Zygmunt *et al.*, 1999). However, cannabinoid receptors are also located on nerve terminals and their activation can inhibit the release of certain neurotransmitters leading to vasodilatation (reviewed in Ralevic *et al.*, 2002).

In summary, the body of work suggests that actions of cannabinoids in the vascular system are more complex than a simple cannabinoid receptor-mediated response (Hiley *et al.*, 2004; Montecucco *et al.*, 2012).

1.10.6.3 In vitro studies: the heart

Although reports of anandamide and cannabinoid agonists having depressant effects on cardiac contractility and rate *in vivo* are likely to be due to a CB_1 receptor-mediated inhibition of sympathetic outflow (Szabo *et al.*, 2001), the limited number of studies carried out on isolated cardiac muscle preparations suggest that anandamide can have direct depressant effects on the myocardium.

Both CB_1 and CB_2 receptors are reported to exist in cardiac muscle at the level of mRNA and proteins (Bonz *et al.*, 2003; Weis *et al.*, 2010; Wang *et al.*, 2012a). The first report of effects of anandamide and other cannabinoid receptor agonists in isolated hearts was made by Ford and colleagues who observed a concentration-dependent reduction in cardiac contractility and coronary pressure in response to anandamide (Ford *et al.*, 2002). Responses were reported to be submaximal even at the highest concentration of anandamide used (at 3 μM, a reduction in left ventricular developed pressure of ~25% was observed) (Ford *et al.*, 2002). Curiously, the effects of anandamide were inhibited by the CB_1 receptor antagonists SR141716A, AM251 and by the CB_2 receptor antagonist SR144528, but not another CB_2 receptor antagonist, AM630 (Ford *et al.*, 2002). This led the authors to postulate that the negative inotropic actions of anandamide in Langendorff-perfused hearts were mediated by 'one or more novel sites' (Ford *et al.*, 2002).

Bonz and colleagues observed in human atrial muscle preparations that anandamide (0.1 and 1 μM), methanandamide and the CB_1 receptor agonist HU-210 caused a dose-dependent reduction in contractility, which was prevented by the CB_1 receptor antagonist AM251 (Bonz *et al.*, 2003), leading the authors to conclude that the

negative inotropic action of anandamide in atrial muscle was mediated by CB_1 receptors.

More recently, Li and colleagues have investigated the electrophysiological effects of anandamide on rat papillary muscle and isolated ventricular myocytes. These investigators observed a concentration-dependent reduction in AP duration in partially depolarised papillary muscle which was not prevented by the nitric oxide synthase inhibitor L-NAME, the LTCC agonist Bay K 8644, or by tetraethylammonium, a blocker of K^+ channels (Li *et al.*, 2009). In ventricular myocytes, a concentration dependent reduction in amplitude of I_{CaL} was observed, together with an acceleration in the voltage-dependence of inactivation of LTCCs (Li *et al.*, 2009). The reduction in I_{CaL} amplitude was prevented by the CB_1 receptor antagonist AM251 but not the CB_2 receptor antagonist AM630, leading the authors to propose that anandamide causes AP shortening in ventricular muscle through a reduction in I_{CaL} amplitude mediated by CB_1 receptors (Li *et al.*, 2009). The nature of this signalling pathway was not investigated, but assuming G_i protein coupling of the CB_1 receptor, and given other literature concerning the actions of other agonists acting at G_i protein coupled receptors in the ventricle (Hartzell, 1988), the suggestion that CB_1 receptors could regulate I_{CaL} in ventricular myocytes in the absence of β-adrenoceptor stimulation is controversial. Interestingly, these authors observed effects of anandamide at nanomolar concentrations, while most other authors observe actions of anandamide only in the micromolar concentration range (Maingret *et al.*, 2001; Ford *et al.*, 2002; Bonz *et al.*, 2003; Choisy *et al.*, 2004).

In addition to actions on I_{CaL}, there is additional evidence for the modulation of various cardiac K^+ channels by anandamide, which would also affect AP configuration. Anandamide has been shown to inhibit Kv4.3 and Kv1.5 channels in a receptor-

independent manner (Amorós *et al.*, 2010; Barana *et al.*, 2010); these channels are thought to underlie I_{to1} (Dixon *et al.*, 1996) and I_{Kur} (Feng *et al.*, 1997), respectively. In agreement with this, Li and colleagues have observed a reduction in transient outward current (I_{to}) which was not prevented by either AM251 or AM630 and thus was not thought to be cannabinoid receptor-mediated (Li *et al.*, 2012). Additionally, these investigators also observed an enhancement in the ATP sensitive K^+ current (I_{KATP}) in response to anandamide which was sensitive to AM630, leading the investigators to propose the involvement of the CB_2 receptor in this response (Li *et al.*, 2012). However, the nature of the signalling pathway was not investigated. In the same investigation, anandamide was found to be without significant effect on I_{K1} or the steady-state outward current, I_{ss} (Li *et al.*, 2012). However, Choisy and colleagues did previously observe a partial reduction in I_{ss} in the presence of anandamide (Choisy *et al.*, 2004).

To date, there have been no investigations concerning the actions of anandamide in cardiac myocytes which have combined electrophysiological recordings with measurements of functional parameters, such as contraction or measurements of Ca^{2+} transients. Furthermore, the majority of evidence for CB_1 or CB_2 receptor-mediated actions is based on sensitivity of responses to cannabinoid receptor antagonists (many of which have additional non-specific actions (Andrag *et al.*, 2013)), rather than sensitivity to PTX, and so must be treated with caution.

1.10.7Role in cardiac pathologies

1.10.7.1 Ischaemia reperfusion

Ischaemia is an inadequate tissue oxygenation, which may occur in the heart, for example, if coronary arteries become blocked leading to impaired tissue perfusion. The resultant effects are impaired contractility and increased tendency to arrhythmias (Levick, 1999). Reduced contractility largely occurs due to a reduction in mitochondrial oxidative metabolism and decreased intracellular ATP. A reduction in intracellular ATP leads to activation of K_{ATP} channels (located on mitochondria and at the sarcolemma), leading to outward K^+ current which hastens repolarisation; in isolated ventricular myocytes this can occasionally be observed as a rapid reduction in AP duration and hyperpolarisation, such that eventually no more action potentials can be stimulated. This may be a protective mechanism to reduce membrane excitability and reduce risk of arrhythmias. Intracellular acidosis is also a strong feature of ischaemic conditions (due to conversion of pyruvate oxidation to lactic acid formation), and leads to markedly impaired contractility; this may occur at least in part through competition of H^+ ions for Ca^{2+} binding sites on TnC (Levick, 1999). Intracellular acidosis also leads to cellular Ca^{2+} overload through stimulation of reverse mode NCX through increased $[Na^+]_i$: this arises due to efflux of H^+ ions in acidosis via membrane Na^+/H^+ exchangers and because the function of NKA is impaired due to reduced cellular ATP concentrations. All of these effects lead to abnormally high SR Ca^{2+} load, which can trigger arrhythmias (Levick, 1999). Furthermore, under ischaemic conditions, the sympathetic nervous system is activated in an attempt to compensate for impaired cardiac output, leading to further heightened risk of arrhythmias (Levick, 1999).

Levels of anandamide, and of its metabolite arachidonic acid have been shown to be elevated in isachaemic hearts (Engels *et al.*, 1990), and levels of circulating endocannabinoids and of cardiac receptor expression have been reported to be increased (Wang *et al.*, 2012a). Anandamide has been shown to reduce the incidence of arrhythmias associated with ischaemia and reperfusion (Ugdyzhekova *et al.*, 2001; Krylatov *et al.*, 2002). There is also some evidence that cannabinoids may ameliorate the progression of myocardial infarction (Underdown *et al.*, 2005) and increase resistance to the arrhythmogenic effects of adrenaline (Ugdyzhekova *et al.*, 2001). Further, endogenous anandamide and 2-AG are present in rat hearts perfused in vitro, and their levels are maintained during ischaemia and reperfusion (Wagner *et al.*, 2006). However, these findings are controversial: Andrag and colleagues recently reported that any effect of anandamide to have these antiarrhythmic actions was small and insubstantial (Andrag *et al.*, 2013).

Recent studies have suggested that the CB_2 receptor plays a role in reducing infarct size after ischaemia reperfusion: the CB_2 receptor agonist HU308 was reported to reduce infarct size, levels of reactive oxygen species and tumour necrosis factor α (Wang *et al.*, 2012a). Li and colleagues have proposed that anandamide reduces harmful cellular Ca^{2+} overload in rat ventricular myocytes in simulated ischaemic conditions. Under physiological conditions, anandamide was without significant effect on NCX, and interestingly (given these investigators previous report that anandamide inhibits I_{CaL} in rat ventricular myocytes (Li *et al.*, 2009)) on $[Ca^{2+}]_i$ as measured by fura 2-AM fluorescence (Li *et al.*, 2013). However, in ischaemic conditions, these investigators observed a more negative reversal potential of NCX which was normalised by application of anandamide (Li *et al.*, 2013). The increased $[Ca^{2+}]_i$ observed under ischaemic conditions was also reduced in the presence of anandamide.

These authors suggested that effects of NCX under these conditions were mediated by CB_2 receptors since effects of anandamide were prevented by AM630 and PTX, and mimicked by the CB_2 receptor agonist JWH133 (Li *et al.*, 2013). However, the nature of this putative signalling pathway was not elucidated.

1.10.7.2 Hypertension and heart failure

Basal heart rate and blood pressure have been found to be normal in mice lacking the CB_1 receptor (Ledent *et al.*, 1999) and in FAAH deficient mice (Pacher *et al.*, 2005). However, in spontaneously hypertensive rats, the decrease in blood pressure induced by anandamide was shown to be more pronounced than in normotensive rats (Batkai *et al.*, 2004). Administration of the CB_1 receptor antagonists AM251 and SR141716A resulted in an increase in blood pressure and cardiac contractility, while the use of an FAAH inhibitor to elevate endogenous anandamide was found to reduce heart rate and blood pressure to levels seen in normotensive rats (Batkai *et al.*, 2004). This led to the suggestion that there is an upregulation of the endocannabinoid system in hypertensive states, which acts as a protective mechanism to suppress cardiac contractility and prevent blood pressure from increasing further (Batkai *et al.*, 2004). Interestingly, Batkai and colleagues observed an upregulation of cardiac and vascular CB_1 receptors which were thought to account, at least in part, for this effect (Batkai *et al.*, 2004). However, it is possible that mechanisms involving a reduction in sympathetic outflow to the heart played more of a role in this effect than direct effects on cardiac muscle.

In addition to these effects in hypertension, Weis and colleagues recently reported an up-regulation of CB_2 receptors and a downregulation of CB_1 receptors in failing human cardiac tissue (Weis *et al.*, 2010). In addition, circulating levels of both

anandamide and 2AG were found to be elevated in heart failure (Weis *et al.*, 2010). However, the functional consequences of these changes were not investigated.

1.11 Aims

This thesis will present functional evidence for novel mechanisms and substances mediating positive and negative inotropic actions in cardiac ventricular tissue.

In light of evidence that the NAADP pathway may form part of the positive inotropic response to β-adrenoceptor stimulation in cardiac myocytes, and that TPC2 receptors are strong candidates for mediating NAADP-induced Ca^{2+} mobilisation, the aims of chapter 3 were to address the role of TPC2 proteins in β-adrenoceptor responses in isolated myocytes and in whole hearts from *Tpcn2*$^{-/-}$ mice, and to use pharmacological inhibitors of the NAADP pathway to further assess this possible contribution to β-adrenoceptor responses in guinea pig ventricular myocytes.

Given the controversial nature of suggestions that cannabinoid receptors mediate negative inotropic responses in cardiac muscle, the aims of experiments presented in chapters 4 and 5 were to assess the actions of the endogenous cannabinoid anandamide and related cannabinoid receptor agonists on electrical activity and contractions in guinea pig ventricular myocytes in the absence (chapter 4) and presence (chapter 5) of β-adrenoceptor stimulation. The aims of the experiments presented in chapter 6 were to assess the effects of the phytocannabinoid Δ^9-THC on these parameters

Chapter 2

Methods

2.1 Cell Isolation

A major driving force for the development of techniques to study isolated cardiac myocytes was the finding that early electrophysiological investigations on cardiac muscle preparations were made more difficult due to inadequate control of membrane potential during voltage clamp experiments. Early attempts to isolate myocytes were complicated by the 'calcium paradox', an effect similar to that seen by Zimmerman and Hülsman (Zimmerman *et al.*, 1966), whereby exposure of hearts to the Ca^{2+}-free medium which was necessary to disrupt the integrity of cell-adhesion proteins (e.g. N-cadherin) and aid in dispersion of myocytes, resulted in rapid hypercontracture and cell-death upon reintroduction of Ca^{2+}. This led to investigation into the mechanisms underlying the 'paradox' (Reviewed in Farmer *et al.*, 1983; Piper, 2000) and to the development of various techniques to isolate viable, rod-shaped myocytes. One of the earliest successful methods described was by Powell and Twist (Powell *et al.*, 1976), which was then subsequently modified by many groups. Today, isolation methods used vary between laboratories, depending on species being studied and the investigations to be carried out. All single cell experiments presented in this thesis were performed on myocytes isolated from either guinea pig or mouse ventricle, using a collagenase digestion method, as detailed below. The activity of collagenase enzyme varies considerably between batches, and so testing was performed such that the most appropriate batch could be selected. A high yield of quiescent myocytes that are tolerant to physiological Ca^{2+} concentrations is desirable.

2.1.1 Guinea Pig

This method is modified from an original method described elsewhere (Powell *et al.*, 1980). In accordance with Schedule 1 of the Animals (Scientific Procedures) Act 1986 (H.M.S.O), male guinea pigs (300 – 400g) were killed by cervical dislocation followed by stunning. Hearts were rapidly excised and, in order to prevent clots forming in the coronary vasculature, briefly washed in a modified Tyrode's solution (see below) containing EGTA and heparin 10 U/ml. Hearts were then cannulated via the aorta for retrograde perfusion using a Langendorff apparatus. Retrograde perfusion in this manner allows enzymes to access the interstitial space via the capillary bed.

Perfusion was carried out initially with modified, Ca^{2+}-free Tyrode's solution of composition (mM): NaCl 136, KCl 5.4, $NaHCO_3$ 12, Na Pyruvate 1, NaH_2PO_4 1, $MgCl_2$ 1, glucose 5, EGTA 0.04; gassed with 95% O_2 5% CO_2 in order to maintain a pH of 7.4, and warmed to 36ºC. Ca^{2+}-free solution is necessary to disrupt intracellular connections and also to stop contraction, since beating would place unnecessary metabolic demand on cells and compromise their viability after isolation. Coronary flow rate was 2 drops/sec (measured by timing drops of solution falling from the apex of the heart). After approximately 3 minutes, the perfusion solution was changed to 50 ml of a pre-warmed (36ºC), pre-gassed (95% O_2 5% CO_2) solution of identical composition, but which lacked EGTA and instead contained 0.1 mM $CaCl_2$ and 20 – 30 mg collagenase from *Clostridium histolyticum* (type II, Worthington Biochemical Corp., Lakewood, NJ, USA). This solution was allowed to run through the Langendorff apparatus for 3 minutes at a coronary flow rate of 1 drop/sec (again measured by the drop rate of solution from the apex of the heart), and then recirculated using a peristaltic pump for 24 – 30 minutes, maintaining a coronary flow rate of 1 drop/sec. Care was taken to

ensure that any residual blood in the coronary circulation, which can sometimes become dislodged as collagenase begins to perfuse the heart, was not allowed to recirculate with the collagenase enzyme. Concentrations of collagenase solution and time of recirculation varied depending on the particular batch of collagenase used, but were within the ranges stated.

Once enzymatic digestion was complete, the heart was removed from the cannula and ventricles separated from atria. Ventricular tissue was cut into 4 pieces and placed in a mechanical stirrer (warmed to 36^{o}C) for 5 minutes with collagenase solution (10 ml) that had been recirculated through the Langendorff apparatus during the isolation. The remainder of the recirculated collagenase solution was placed into a water bath at 36^{o}C and gassed with 95% O_2 5% CO_2. After stirring, the solution containing ventricular tissue was filtered through a 250 µm mesh into a 15 ml test tube. A further 10 ml pre-warmed, pre-gassed collagenase solution was added to the remaining ventricular tissue for another 5 minutes stirring; this process was repeated once more so that a total of three 15 ml test tubes of cell suspension were obtained. Cell suspensions were centrifuged slowly for 1 minute, the supernatants discarded, and the remaining pellets re-suspended in 10 ml Dulbecco's Modified Eagle's Medium (DMEM; modified in that it contained low glucose (5.5 mM), pyruvate (1 mM), and HEPES 25 mM). Myocytes were stored at room temperature in this solution; storage on ice would inhibit the Na^+/K^+-ATPase and perhaps lead to Ca^{2+} overload and cell death. Viable ventricular myocytes could be identified by their rod-like shape and clear cross-striations. Those that had been damaged during the isolation procedure appeared rounded, with no apparent organisation in terms of striations. All experiments in this thesis were performed on viable, rod-shaped myocytes. Freshly isolated myocytes typically only retain normal electrophysiological, contractile and morphological

properties for 8 – 12 hours after isolation (Mitcheson *et al.*, 1998), and so experiments were only performed on the day of cell isolation.

2.1.2 Mouse

Mice (13 – 18 weeks) were killed by cervical dislocation (following stunning) in accordance with Schedule 1 of the Animals (Scientific Procedures) Act 1986 (H.M.S.O). Hearts were excised, cannulated via the aorta and perfused retrogradely through the coronary circulation. Initial perfusion of the hearts, for approximately 30 seconds, was performed using a 1 ml syringe attached to the cannula. The syringe contained a pre-gassed (95 % O_2 5 % CO_2) solution of composition (mM): NaCl 125, $NaHCO_3$ 25, KCl 5.4, NaH_2PO_4 1.2, $MgCl_2$ 1, $CaCl_2$ 1, glucose 5.5 (pH 7.4), with the addition of heparin (10 U/ml) or streptokinase (10 U/ml) to minimise the formation of clots in the small coronary vessels, which could impede perfusion. The syringe was then removed and the cannula mounted onto a Langendorff perfusion system where the heart was perfused with pre-warmed (36ºC) pre-gassed solution comprising (mM): NaCl 130, KCl 5.4, $MgCl_2$ 3.5, glucose 10, HEPES 5, NaH_2PO_4 0.4; pH 7.4. After 3 minutes, this solution was replaced with a solution of identical composition but which also contained 0.1 M $CaCl_2$ and 0.3 mg/ml collagenase type II (Worthington, NJ, USA). Following enzymatic digestion (for no longer than 7 minutes), the heart was removed from the cannula. The ventricles were then cut into pieces and stored at room temperature in a solution containing (mM): NaCl 130, KCl 5.4, $MgCl_2$ 3.5, $CaCl_2$ 0.1, NaH_2PO_4 0.4, glucose 10, HEPES 5, taurine 20; 0.1 % bovine serum albumin; pH 7.4, gassed with 95% O_2/5% CO_2. Mouse cell isolations were performed with the assistance of Sam Lin Wee Khang of the Terrar laboratory.

2.2 Cell superfusion

For electrophysiological investigations, freshly isolated ventricular myocytes suspended in DMEM were plated onto a glass coverslip (22 x 50 mm, Menzel-Gläser) which had been attached to the base of a Perspex tissue bath using silicone grease (RS Components Ltd., Northants), and the cells left to adhere for 10 minutes. The bath was placed at the stage of an inverted microscope (Nikon Diaphot 200). During experiments, cells were superfused (via a gravity-fed perfusion system) with a physiological salt solution (PSS), of composition (mM): NaCl 125, $NaHCO_3$ 25, KCl 5.4, NaH_2PO_4 1.2, $MgCl_2$ 1, glucose 5.5, $CaCl_2$ 1.8, pH to 7.4 with NaOH and oxygenated with 95% O_2 5% CO_2. Temperature was maintained at 36^oC throughout experiments by means of a heating block surrounding the inflow of the tube just before it entered the bath. Solution was removed from the tissue bath by suction through a small outflow placed at the opposite side of the bath attached to a peristaltic pump. Bath exchange to alternative reservoirs of PSS or PSS containing drugs of interest was achieved by a series of voltage activated, 3-way solenoid valves (Lee Products Ltd., UK). Solution flow rate was 2 – 4 ml/min, with care being taken to ensure equal flow-rates from each reservoir and therefore stable temperature control. Under these conditions, solution exchange was achieved within 30 seconds or less.

2.3 Electrical field stimulation

In some experiments, cells were stimulated to contract by electrical field stimulation. Cells were allowed to adhere to a cover slip placed at the stage of an inverted microscope as described in section 2.2. The incorporation of carbon fibre electrodes into the sides of the tissue bath allowed 25 - 35 V depolarising current pulses

(2 ms duration, frequency 1 Hz) to be delivered to the plated cells in order to stimulate contractions. Provided solution depths are kept consistently low to minimise capacitance, this technique is relatively simple to perform. One downside of this technique is that cells can become more prone to arrhythmogenic oscillations, especially if field stimulation is performed for longer than 5 minutes. Potential explanations for this are: 1) that there is a non-uniform flow of ionic currents into and out of the cell upon stimulation such that the side of the cell facing the cathode depolarises, and the side facing the anode hyperpolarises (Cheng *et al.*, 1999), and 2) that harmful substances are released from carbon-fibre electrodes as a consequence of electrolysis of the solution.

2.4 Electrophysiology

Electrophysiological experiments were carried out using an Axoclamp 2 amplifier (Axon Instruments, USA).

2.4.1 Sharp microelectrodes

Microelectrodes were pulled from 1.5 mm (external diameter), 0.86 mm (internal diameter), thick-walled, filamented borosilicate glass capillary tubing (GC150F-15; Harvard Apparatus Ltd., Kent) using a vertical electrode puller (Narishige, Japan). Settings were adjusted to produce electrodes with resistances in the range 40 – 70 MΩ for action potential experiments, and 35 - 40 MΩ for dSEVC experiments when filled with solution of composition (M): $KMeSO_4$ 1, KCl 0.01. The advantage of sharp microelectrodes is that the small, high resistance tip permits experimentation with minimal dialysis of intracellular contents, facilitating accurate

measurements of cell contraction, which are not always possible with whole-cell patch experiments where intracellular contents are disturbed. Care was taken to produce microelectrodes with small tips and gradual, uniform tapers, since these cause less damage to cells when they are impaled. Microelectrodes which possess a 'shoulder' where the taper is suddenly larger should be avoided since, once a cell is impaled, it will expand as the membrane seals around the microelectrode and an abruptly expanding taper may cause damage. Although microelectrodes with small tips are advantageous in that they produce less damage to cell membranes, they do have the disadvantage of producing much higher electrical resistances which can make recordings of cell membrane currents noisier and more difficult. It is necessary to obtain a balance between these considerations when deciding whether to use a sharp electrode or a patch electrode.

2.4.2 Patch electrodes

Isolated ventricular myocytes were patched in either the whole-cell or perforated (amphotericin, 240 U/ml) configuration using patch electrodes pulled from 1.5 mm (external diameter), 1.17 mm (internal diameter) thin-walled, filamented borosilicate glass capillary tubing (GC 150TF, Harvard Apparatus Ltd, Kent) using a vertical electrode puller (Narishige, Japan). Electrodes were pulled in a two stage process producing resistances in the range 3.0 – 3.5 MΩ when filled with patch pipette solution. Patch solution contained (in mM): K^+ Aspartate 110, KCl 10, NaCl 5, $MgCl_2$ 5.2, HEPES 5, K_2ATP 5, pH to 7.2 with KOH. For experiments in which Ca^{2+} currents were studied in the absence of contaminating K^+ currents, a Cs^+-containing patch solution was used. This solution contained (in mM): Cs^+ Aspartate 120, TEACl 20, $MgCl_2$ 1.0, MgATP 5, HEPES 20, EGTA 5; pH to 7.2 with 1 M CsOH.

2.4.3 Setup for electrophysiological recording

All electrophysiology recordings presented in this thesis were made using an Axoclamp 2 amplifier (Axon Instruments, USA). Microelectrodes were placed into a Perspex holder, which was itself mounted into a ×1 HS-2A headstage (Axon Instruments, USA). Electrical contact between the headstage and the electrode filling solution was made with an Ag/AgCl-coated wire. All measurements of electrical potential were made with reference to a probe (Ag/AgCl pellet) placed in the bath, such that contact was made with the solution superfusing the myocytes. Microelectrodes were positioned in the perfusing solution, above the cell of interest by use of a micromanipulator (Narishige, Japan).

After the microelectrode was lowered into the cell superfusion solution, the 'input offset' command was used to zero the voltage output of the amplifier with respect to the potential of the bath solution such that recordings of membrane voltage can be made with respect to the 'zero current potential' (Neher, 1992). When the solution inside the pipette is identical to that of the bath, this procedure leads to recording of a voltage which can be considered to accurately reflect the zero current potential. However, when the two solutions are different, a liquid junction or 'tip' potential is generated between the pipette filling solution and superfusion solution (Neher, 1992). The tip potential can be thought of as an imbalance of charge which arises due to more mobile ions diffusing more rapidly across the concentration gradient at the interface of the two solutions (Neher, 1992). In conventional sharp microelectrode recordings, problems with voltage offset due to tip potentials are minimised by using a concentrated KCl solution to fill the microelectrode; KCl is chosen as both K^+ and Cl^- have similar ionic mobility, and so tip potentials are of the

order of 1 mV or less (Neher, 1992). In all sharp microelectrode experiments presented here, a filling solution containing (M): $KMeSO_4$ 1, KCl 0.01 was used, since highly concentrated KCl solutions can cause 'blebbing' of cell membranes (Terrar, personal communication). However, in patch experiments, where the choice of pipette filling solution is dictated by the needs of the experimenter and by the ionic properties of the intracellular contents, more complex solutions are needed which can lead to tip potentials of around 2 – 12 mV (Neher, 1992). This leads to an offset in the apparent voltage being recorded, and must be compensated for in patch experiments (see later).

Since V=IR, the application of current across the resistance of a microelectrode leads to the generation of an artefactual voltage drop which would prevent cell membrane potentials from being recorded faithfully (although this error is minimised by using the Axoclamp amplifier, as opposed to an Axopatch amplifier, where the headstage contains an IV converter rather than a voltage follower). In order to eliminate this error, electrode resistance was compensated for before cells were impaled or patched, by means of the 'bridge balance' circuit. This was done with the amplifier in 'bridge' mode, whereby the microelectrode voltage is continuously recorded while current is injected (current clamp). 1 nA current pulses (200 ms duration) were passed through the electrode while it was in solution, during which adjustment of the 'bridge balance' control allowed a signal of the appropriate amplitude to be subtracted from the amplifier output. The term 'bridge balance' comes from early electrophysiological measurements, where a 'Wheatstone bridge' circuit was used to generate the subtraction. Once the bridge was balanced, a readout of the microelectrode resistance could be taken from the bridge balance control. As previously stated, sharp microelectrodes typically had resistances of 35 – 70 MΩ; patch electrodes 3 – 3.5 MΩ.

The main problems with electrophysiological recordings are those of capacitance and electrical noise. Capacitance is the ability of a body to store electrical charge. In an electrophysiological system it reduces the speed with which recordings can be made, and may prevent fast responses from being detected accurately. Capacitance can arise from various sources including transmural capacitance across the glass wall of the immersed part of the microelectrode and the input capacitance of the amplifier. Transmural capacitance was minimised by keeping superfusing solution depth to a minimum and by using microelectrodes containing minimal amounts of filling solution. In some patch electrode experiments, particularly those where membrane currents were recorded, the tip of the microelectrode was coated with Sigmacote (Sigma Aldrich, UK) which prevents superfusing solution rising up the sides of the microelectrode such that solution depth stays low and capacitance is minimised. Problems of electrical noise were minimised by carrying out all experiments within a Faraday cage. Furthermore, all electrical equipment was grounded to a 'star' earth. The microscope and the stage upon which the microelectrode holder was mounted were supported on an air table which minimised vibrations, which can compromise the stability of the microelectrode and reduce experimental success rate.

2.4.4 Impalement of cells using a sharp microelectrode

Following the aforementioned steps (input offset and bridge balance) which were carried out after the microelectrode tip had been dipped into solution, any remaining capacitance within the system was reduced using a 'capacitance compensation' mechanism built into the Axoclamp amplifier. This anticipates and injects the current required to charge and discharge the input capacitance during signal changes. Capacitance compensation was carried out in discontinuous current clamp

(DCC) mode, where current pulses were injected into the microelectrode and the voltage response monitored using an oscilloscope, connected to the headstage monitor output of the amplifier. The capacitance neutralisation control was dialled up as far as possible to maximise the rate of rise of the voltage response, without generating an overshoot. The fine movement of the micromanipulator was then used to position the microelectrode above the cell of interest, and then lower it down slowly onto the surface of the cell. Contact was indicated by a small offset in the voltage recording, evident as a readout on the amplifier and also as a change in audio tone, which had been set up as a function of recorded voltage. Penetration of the cell membrane was achieved through application of a high frequency oscillatory current 'buzz' through the microelectrode for 5 ms using a remote control box. This step required that the capacitance neutralisation control had been dialled up optimally, such that the capacitance compensation circuitry could be oscillated. Application of several 5 ms 'buzzes' usually results in destruction of the cell, therefore if repeated 'buzzes' were necessary, their duration could be reduced to 1 ms using the control box. Successful impalement of the cell resulted in the generation of stable resting membrane potentials in the range -75 to -85 mV; those not meeting this criterion were discarded. The application of a small amount of hyperpolarising current (up to 0.3 nA) was often useful in achieving good cell penetrations; once a stable impalement had been achieved, negative current was switched off. If greater amounts of negative current were required to keep the cell membrane potential at -75 to -85 mV, it was likely that the cell was not healthy enough for experimentation.

2.4.5 Patching of cells in whole-cell or 'permeabilised' configuration

The setup for patch electrode experiments was similar to that of sharp electrode experiments, except that after the 'bridge balance' and 'input offset' steps, there was no need to dial up the capacitance compensation of the amplifier since there was no requirement to penetrate through the cell membrane by oscillation of the capacitance compensation circuitry. 1 nA hyperpolarising current pulses of 200 ms duration were applied, and contact with the cell membrane indicated by an offset in the voltage recording as with sharp electrodes. Once contact was achieved, gentle but rapid suction was applied by pulling the plunger on a 10 ml syringe (attached by rubber tubing, internal diameter 1.5 mm). The generation of a high resistance seal was evident as an increase in the amplitude of the voltage recording in response to constant current pulses. Once an initial seal had formed, the current pulse was reduced to 0.1 nA until the voltage recording displayed an amplitude of around 200 mV, indicating the formation of a high resistance seal ('gigaseal'). On formation of a stable seal, additional suction could be applied to achieve the 'whole-cell' configuration, indicated by the voltage recording in response to current pulses becoming a flat line, at around -70 to -80 mV. In permeabilised patch experiments, the second stage of suction was not performed; rather, electrical contact with the cell was made by perforation of the cell membrane with amphotericin over a period of 5 to 10 minutes.

2.4.6 Protocol for the recording of action potentials

Single myocytes were stimulated to fire action potentials by 2 ms depolarising current pulses (2 – 5 nA) at a frequency of 1 Hz. Action potentials (APs) were recorded in 'bridge' mode, in which voltage is recorded continuously and current can be injected.

The measurements recorded were action potential duration at 90% (APD_{90}) 50% (APD_{50}) and 20% (APD_{20}) repolarisation, resting membrane potential (RMP) and peak amplitude of the AP.

2.4.7 Protocols for the recording of L-type Ca^{2+} currents

The L-type Ca^{2+} current (I_{CaL}) was activated by 200 ms step depolarisations from a holding potential of -40 mV to 0 mV at a frequency of 0.2 - 0.3 Hz. It is necessary to hold the cell membrane potential at -40 mV in order to inactive Na^{+} currents and also T-type Ca^{2+} currents, which are present to a small degree in guinea pig ventricular cells (Nilius *et al.*, 1985) while the low frequency of stimulation is necessary to allow Ca^{2+} channels to recover completely from inactivation. Current-voltage relations were constructed from a series of step depolarisations from -40 mV to a range of potentials from -30 mV to + 60 mV. The amplitude of the inward current was measured as either the difference between peak inward current and holding potential, or the difference between peak inward current and current at the end of the pulse.

Under some conditions, a rundown of I_{CaL} was observed. In order to correct for this, a correction factor was applied, on the assumption that run-down was always linear. The correction factor was calculated using the following equation, with the example that the current exhibited a rundown of 1.5% per minute and the measurement was made at 15 minutes: 100/(100 – (1.5 x 15)) = correction factor of 1.29. This correction factor was then applied to all measured data points, for example in plots of current voltage relationships.

In some experiments, a double pulse protocol (applied at a frequency of 0.2 Hz) was used to measure inactivation of LTCCs. An initial pre-pulse of 500 ms duration,

from a holding potential of -40 mV to a range of potentials from -50 mV to + 60 mV at 5 mV increments was applied prior to a 200 ms test pulse from -40 mV to 0 mV. Inactivation experiments were performed using a patch electrode (whole-cell configuration, in the presence of Cs^+ to reduce influence of contaminating K^+ currents, or amphotericin-permeabilised in the absence of Cs^+). The amplitude of the test pulse was measured as peak current less current at the end of the pulse, and was then plotted as a fraction of the maximal current amplitude occurring after the pre-pulse.

2.4.8 Protocol for the recording of delayed rectifier K^+ currents

The delayed rectifier K^+ current (I_K) was activated by step depolarisations from a holding potential of -40 mV to + 40 mV for 10 – 800 ms at a frequency of 0.1 Hz, and was measured as outward tail currents upon repolarisation to -40 mV. Several additional currents can be activated during the step depolarisations, including NCX, Ca^{2+}-activated non-specific current (I_{ns}) and Ca^{2+}-activated Cl^- current (Ehara *et al.*, 1988; Beuckelmann *et al.*, 1989; Terrar *et al.*, 1989b; Zygmunt *et al.*, 1991; Sipido *et al.*, 1993; Heath *et al.*, 1996). For this reason, tail currents upon repolarisation were therefore used as a measure of I_K, since any residual Ca^{2+} current would be expected to inactivate much more rapidly than I_K and currents associated with NCX or Ca^{2+}-activated currents are expected to be inward and of much shorter duration.

2.4.9 Data acquisition and analysis

Electrophysiological recordings were detected and digitised by a Digidata 1322A (Axon Instruments, USA) for detection by Clampex software (Axon Instruments, USA), and analysed using Clampfit software (Axon Instruments, USA).

Analogue signals were sampled at a rate of 100 kHz. Action potentials were filtered at a rate of 30 kHz; measurements of I_{CaL} and I_K at 0.3 kHz using the inbuilt filtering of the AxoClamp amplifier.

2.5 Measurement of cell contractions

Two methods were used to measure amplitude of contraction: firstly a video 'edge detection' system, with methods similar to those reported previously (Annetts *et al.*, 1990), and secondly the Ionoptix software for measurements of sarcomere length.

For edge detection experiments, images of single ventricular myocytes were captured by a camera (JAI PulNix PE2010; Brian Reece Scientific Ltd., U.K.) mounted on an inverted microscope with a ×20 objective lens to collect the image of the cell. Cells were stimulated to contract by a 2 ms depolarising current pulse delivered via a microelectrode. The video image of the cell of interest was rotated such that it was horizontal onscreen, and adjusted so that it appeared dark against a light background. Two vertical cursor lines were then positioned over either end of the cell, to define a window for measurement, and cell edges were detected as abrupt changes in light intensity across a single, horizontal line positioned across the long axis of the cell. Each frame of the video image captured was divided into four component fields, allowing a fourfold increase in temporal resolution to 5 ms per sample point (200 Hz). One set of experiments was performed at a lower temporal resolution than this (20 ms per sample point; see Figure 4.9). Data were digitised and recorded using a Digidata 1200 analogue-digital (A/D) converter and Clampex software (Axon Instruments, USA), and analysed using Clampfit software (Axon Instruments, USA).

For measurements of sarcomere length, cells were visualised via a ×40 objective lens using an IonOptix MyoCam (IonOptix Corp.) which sampled images at a frequency of 240 Hz. Optical density traces (which arise from the alternating light and dark bands of the contractile machinery and are sinusoidal in nature, with the wavelength of the sine representing sarcomere length), were then computed into a signal of sarcomere length by application of a fast Fourier transform (FFT) by the IonWizard sarcomere length acquisition software (IonOptix Corp.). Vertical cursors defined the number of sarcomeres used for this calculation (minimum 7 sarcomeres). Length measurements were calibrated using a stage micrometer with 2 μm graduations such that the number of pixels/μm recorded by the MyoCam could be entered into the software as a fixed value. Amplitude of sarcomere shortening was calculated by deduction of systolic from diastolic sarcomere length and expressed either in microns or as a percentage of resting sarcomere length. Analysis was performed using IonWizard 5 software (IonOptix Corp.). All values represent an average of 10 contractions.

2.6 Fluorescent indicators for ions

Fluorescence is defined as the emission of one or more photons of light by a molecule or atom (i.e. the fluorescent probe) activated by the absorption of a quantum of electromagnetic radiation. Fluorescent indicators designed for use in biological studies respond to a specific stimulus, for example the selective binding of an intracellular ion (e.g. Ca^{2+}). Absorption of a photon by a fluorescent indicator results in its transition from a ground to an excited state. The probe exists in an excited state only very briefly (~ 20 nanoseconds) and then returns to its ground state after photons are emitted. Emitted photons are usually lower in energy and longer in wavelength than excitation photons as some energy is dissipated during the excitation of the probe (for

example, through vibration transferring heat to the surrounding solution) (Lakowicz, 2006).

Many of the Ca^{2+} fluorescent probes used in biological studies are related to the Ca^{2+} chelators EGTA and BAPTA. Work by Roger Tsien and colleagues demonstrated that by attaching a fluorescein group to BAPTA, it was possible to detect the binding of Ca^{2+} to the molecule by measuring changes in emitted light (Minta *et al.*, 1989). With excitation light at 488 nm, and in the absence of Ca^{2+} very little light was emitted, but in the presence of Ca^{2+} a dramatic shift in the wavelength of emitted light (~ 510 nm) was observed (Minta *et al.*, 1989). This work led to the development of one of the earliest Ca^{2+} sensitive probes, fluo-3 (Minta *et al.*, 1989).

2.6.1 Choice of Ca^{2+} sensitive fluorescent probe

Since the development of fluo-3 (Minta *et al.*, 1989) additional probes have been developed and optimised to measure Ca^{2+} signals with different properties (for example, Ca^{2+} transients or Ca^{2+} sparks). The major ways in which these probes differ are: 1) binding affinity for Ca^{2+}, 2) excitation light wavelength(s), and 3) emission wavelength(s). Excitation and emission wavelengths obviously influence the experimental apparatus that can be used (and conversely, availability of apparatus can limit the choice of probe), but perhaps the most important consideration is the binding affinity of the dye for Ca^{2+}. If the affinity is too high, there is a chance that Ca^{2+} can be significantly buffered (leading to loss of contractile responses), and that signals can become saturated. The affinities of dyes reported in manufacturers' literature are dependent on specific experimental conditions, and may differ under alternative conditions. It is therefore necessary to perform tests to determine the most appropriate selection for the desired experimental conditions.

For the measurement of Ca^{2+} transients in this thesis, fluo-5F (excitation peak at 494 nm, emission peak at 518 nm and K_d ~2.3 µM at 22°C) was determined to be an appropriate choice of probe. Fluo-5F is based upon structural modifications of fluo-3 (excitation peak at 506 nm, emission peak at 530 nm and K_d ~325 nM at 22°C). Fluo-3 was originally developed by Tsien and colleagues for use in flow cytometry and laser-scanning confocal microscopy experiments (Minta *et al.*, 1989). Structural modification of fluo-3 (substituting two chlorine atoms for fluorines) yielded fluo-4 (excitation peak at 494 nm, emission peak at 516 nm and K_d ~345 nM at 22°C), which displayed higher fluorescence intensity at 488 nm, allowing lower concentrations to be used to achieve the same fluorescence intensity as with fluo-3, and making it suitable for use with argon-ion laser sources (Gee *et al.*, 2000). Fluo-5F in this respect is very similar to fluo-4, but possesses lower Ca^{2+}-binding affinity (i.e. a higher K_d), making it suitable for detecting intracellular Ca^{2+} concentrations which would saturate the responses of fluo-3 and fluo-4; changes in intracellular Ca^{2+} concentrations in ventricular myocytes range from 100 nM at rest, to over 1 µM at the peak of the Ca^{2+} transient (Bers, 2008). In addition, fluo-5F provides very good resolution of Ca^{2+} signals since it exhibits very large (100-fold or greater) fluorescence intensity increases.

Although Ca^{2+} probes in the fluo class enable the detection of changes in Ca^{2+} concentration, it is difficult to directly relate the intensity of emitted light to an absolute concentration of Ca^{2+}. One reason for this is that the intensity of emitted light is influenced not only by binding of Ca^{2+} but also by amount of dye present in the cell. Over time, many cell types, including cardiac myocytes, very efficiently extrude dye from their intracellular space via anion transporters; this is a particular problem for experiments performed at physiological temperature (Takahashi *et al.*, 1999). Furthermore, dyes are subject to 'bleaching' as a result of continued exposure to

excitation light (Takahashi *et al.*, 1999). Together, these factors contribute to a reduction in the effective concentration of dye present, and therefore a gradual reduction in fluorescence intensity over time that is independent of any real changes in intracellular [Ca^{2+}]. Most experiments in this thesis required an experimental time period of at least 15 minutes, and so it was important to consider ways of overcoming these artefactual changes.

One approach considered was the use of ratiometric Ca^{2+} sensitive probes. These probes differ from the fluo series of dyes in that they can be either excited by two different wavelengths of light, or emit two different wavelengths on binding of Ca^{2+} which enables a ratio of either emission or excitation wavelengths to be calculated. In theory, this ratio should remain constant independent of how much dye is present in the cell, and should therefore only change if the amount of Ca^{2+} binding changes (Bootman *et al.*, 2013). The two most commonly used classes of ratiometric dyes are the indo series (dual emission) and the fura series (dual excitation). In the case of indo dyes, a single wavelength of excitation light is necessary (optimal excitation would occur at ~340 nm, although 365 nm is more commonly used in practice). In the absence of Ca^{2+}, peak emission wavelength is close to 405 nm, but on binding of Ca^{2+}, the spectrum shifts so that the peak is close to 485 nm. Conversely, the fura series of dyes are excited at two wavelengths (340 nm and 380 nm) and emit at a single wavelength (~510 nm). Upon binding of Ca^{2+} there is a shift in excitation spectrum (from a maximal excitation wavelength of 340 nm in the absence of Ca^{2+}) to wavelengths close to 380 nm. In practical terms, both methods are challenging in that they require UV excitation light. It is often very difficult to transmit such wavelengths through microscope objective glass, requiring a high intensity of excitation light. UV excitation light can damage cells, and this risk is heightened if high intensity light is required. Furthermore, in the case of fura

dyes, a method of rapidly switching the wavelength of excitation light and recording the amount of emitted light generated by each wavelength is required. In light of these difficulties, it was decided that the fluo-5F was the most appropriate choice, and that the method of application to cells would be optimised in order to reduce artefactual errors arising from dye extrusion and/or photobleaching.

2.6.2 Loading of cells with fluorescent probes

In initial experiments, loading of myocytes with Ca^{2+} indicators was achieved by incubation of cells with the acetoxymethyl (AM) esters of these probes. The esterified form of the dye is uncharged and hydrophobic, and thus readily membrane permeant. Once inside the myocyte, the AM group is rapidly cleaved as a result of actions of intracellular esterases, leaving the cell impermeant 'free' form of the dye (e.g. fluo-5F) in the cell cytoplasm. Stock solutions of fluo-5F AM were prepared in anhydrous dimethylsulphoxide (DMSO) at a concentration of 100 µM, aliquoted, and frozen at -20^{o}C, protected from light. To load cells, stock fluo-5F AM was defrosted, and added to a given volume of cell suspension to achieve a final concentration of 1.5 - 4µM. Cells were incubated for 10 minutes at 30^{o}C, before plating onto a glass coverslip at the stage of an inverted microscope as described previously. An advantage of this method is the ease with which the dye enters cells, but as previously discussed, Ca^{2+} sensitive probes are readily extruded from cardiac myocytes, leading to an artefactual loss of emitted light.

In order to minimise loss of emission signal, all subsequent experiments were performed by introducing the free form of the dye (i.e. fluo-5F pentapotassium salt, which is not membrane permeant) to cells via a patch pipette. In this method the dye is present in the patch pipette at a much larger volume than the intracellular compartment,

and dye is therefore assumed to be replaced from the contents of the patch pipette at a much higher rate than it can be extruded by cell membrane anion transporters. Stock solutions of fluo-5F pentapotassium salt were prepared in double-deionised water (ddH_2O) at a concentration of 1 mM, aliquoted (10 µl), and frozen at -20ºC, protected from light. When required, aliquots were diluted with patch solution (composition outlined in section 2.4.2) to give a final concentration in the patch pipette of 75 µM.

2.6.3 Measurements of whole-cell Ca^{2+} transients

Two methods were used to detect emitted light from Ca^{2+} sensitive probes. Initially, a photomultiplier system (Cairn Research Ltd., UK) was used. Cells (which had been incubated with cell permeant fluo-5F AM for 10 minutes) were superfused with PSS as described previously and a cell of interest viewed using an inverted microscope (Leica DMIRB-E) and a Zeiss 40× oil immersion lens. By means of a video monitor, an aperture was manipulated so as to obscure the area around the cell in question. Excitation light was provided by a xenon arc lamp. Light from the arc lamp was routed initially through a bandpass interference filter, to select for light of wavelength 475 +/- 15 nm. A liquid light guide then directed the light to the back of the microscope and a dichroic mirror reflected excitation light through the objective lens to the cell (the dichroic mirror reflected short wavelength light and passed longer wavelengths, with a cut-off of 505 nm). The longer wavelength emitted fluorescence light passed through the objective and dichroic mirror to an additional mirror in the base of the microscope that reflected the emitted light to the microscope side port. Mounted on the side port was another dichroic mirror, which reflected light of wavelengths less than 600 nm, so that the required emitted fluorescence passed through a long-pass filter (520 nm) to a photomultiplier. The output of the photomultiplier passed through an

amplifier and electronic filter system (low pass 50 Hz cutoff), before being recorded and analysed using pClamp 7 software.

In another set of experiments designed to measure Ca^{2+} transients over a time course of at least 10 minutes, cells were patched in the whole-cell configuration to introduce Fluo-5F salt to the cytoplasm. An EMCCD camera (Luca R; Andor Technology plc., UK) was used to detect emitted fluorescence at a frame rate of at least 12.4 frames per second. In this system, cells were placed at the stage of a Nikon Diaphot 200 inverted microscope, and excitation light provided by a 470 nm LED (OptoLED system; Cairn Research Ltd., UK). Cells of interest were viewed using a Nikon ×40 oil immersion objective lens. The excitation light was delivered to a Cairn filter cube which was equipped with a filter (to select for wavelengths of 475 ± 15 nm) and a dichroic mirror which reflected excitation light up towards the cell of interest. The emitted light was then passed through a mirror at the base of the microscope which directed light out towards the side port, towards the camera. The camera was attached to an A/D interface card (National Instruments, UK). Data acquisition and analysis was performed using WinFluor software (John Dempster, University of Strathclyde, UK), or Clampfit software (Axon Instruments, USA).

2.7 Measurement of coronary perfusion pressure, force and rate of contraction in Langendorff-perfused mouse hearts

Mice were killed in accordance with Schedule 1 of The Animals (Scientific Procedures) Act 1986 (HMSO). Hearts were carefully excised and perfused for 30 seconds with PSS solution containing streptokinase (10 U/ml) via a syringe connected to the cannula. All heart dissections and cannulations were performed with the

assistance of Prof Derek Terrar. After initial perfusion, the syringe was removed and the cannula mounted on a Langendorff apparatus. The heart was retrogradely perfused via the aorta with pre-warmed (36^{o}C) pre-gassed PSS at a constant flow-rate of 3.5 ml per minute, which was controlled by means of a peristaltic pump. Exchange of superfusate was controlled by a series of voltage-activated, 3-way solenoid valves (Lee Products Ltd.), which permitted selection between reservoirs containing PSS with and without drugs of interest at selected concentrations.

Hearts were allowed to beat spontaneously. A small hook, placed through the ventricles near the apex of the heart was attached to a tension transducer to measure force of ventricular contraction. Resting tension was set between 0.5 and 1.0 g at the start of the experiment. Heart rate was calculated from the force signal (triggering a timing system from the upstroke of force development, and measuring rate as the reciprocal of the time interval between contractions). Inflow pressure at the level of the aorta was measured using a pressure transducer positioned close to the heart, so that changes in coronary artery resistance could be measured as pressure changes at a constant perfusion flow rate. Pressure calibrations of this system were performed at the start and end of each experiment. Data were acquired and analysed using Chart software (ADInstruments, UK), with a data acquisition sampling rate of 1 kHz. To minimise the influence of the pulsatile flow of the peristaltic pump, smoothing was applied to the pressure signal (51 points in the smoothing algorithm of the Chart software, amounting to a running average over 0.5 s). The tension signal was low-pass filtered with a cut-off frequency of 50 Hz.

2.8 Drugs

Listed below are details of the salts, fluorescent indicators and drugs used in the experiments presented in this thesis.

Amphotericin B from *Streptomyces* sp., **aspartic acid, CsOH, DMSO** (dimethylsulphoxide), **E-4031, EGTA** (ethylene glycol-bis-(β-aminoethyl ether)N,N,N',N'-tetraacetic acid), **HEPES** (N-[2-hydroxyethyl]piperazine-N'-[2-ethanesulphonic acid]), **heparin**, **(-)-isoprenaline**, **K_2ATP, MgATP**, **Na pyruvate**, **nifedipine, streptokinase from β-haemolytic *Streptococcus*** and **TEACl** were obtained from Sigma, Poole, UK.

Collagenase (type II) was obtained from Worthington Biochemical Corporation, Freehold, New Jersey, USA.

Dulbecco's MEM (minimal essential medium), **Fluo-5F AM** and **Fluo-5F pentapotassium salt** were obtained from Invitrogen, UK.

NaCl, **KCl**, **$NaHCO_3$**, **NaH_2PO_4**, **$MgCl_2.6H_2O$**, **$MgSO_4.6H_2O$**, **KH_2PO_4** **$CaCl_2$**, **KOH** and **glucose** were obtained from VWR International, UK, and were of analaR grade, with the exception of glucose used for solutions employed during isolation of myocytes, which was of aristaR grade.

Adenosine, 2-arachidonoylglycerol, anandamide (supplied pre-dissolved in ethanol), **AM281, AM630, bafilomycin A1 (Streptomyces griseus), (*R*)-(+)-methanandamide** (supplied pre-dissolved in ethanol)**, Δ^9-tetrahydrocannabinol** (supplied pre-dissolved in ethanol), ***trans* Ned-19** and **pertussis toxin** were obtained from Tocris Bioscience.

Unless otherwise stated, drugs were dissolved in double de-ionised water that had been passed through a Milli-Q Biocel water purification system (Millipore, UK). Adenosine, AM281, AM630, Fluo-5F AM, *trans* Ned-19 and nifedipine were dissolved in DMSO, aliquoted and stored at -20^{o}C prior to experimental use. 2-AG was dissolved in DMSO and stored at -80^{o}C. Amphotericin was also dissolved in DMSO, immediately before experiments. (-)-Isoprenaline was dissolved in double de-ionised water containing ascorbic acid on the day of experiments, and stored at 4^{o}C until use.

2.9 Statistics

Statistical comparisons were made using either Student's paired or unpaired *t*-test as appropriate. Where more than three comparisons were made (either multiple time points against a single set of controls, or a single time point across multiple groups), analysis of variance (ANOVA) was used, followed by Dunnett's or Bonferroni post-hoc tests as appropriate.

Chapter 3

Novel pathways in the positive inotropic response to isoprenaline in ventricular muscle

3.1 Introduction

Recent evidence presented from the Terrar laboratory points towards NAADP as an important mediator in both ventricular (Macgregor *et al.*, 2007a) and atrial cell (Collins *et al.*, 2011) excitation contraction coupling. Furthermore, it has been demonstrated that NAADP signalling may be enhanced following β-adrenoceptor stimulation, via stimulation of the enzymes which synthesise NAADP, ARCs (Higashida *et al.*, 1999; Macgregor *et al.*, 2007a; Lewis *et al.*, 2012).

TPC proteins have recently been postulated to be strong candidate targets for NAADP (Calcraft *et al.*, 2009). In sea urchins and most vertebrate species, three *Tpcn* genes (*Tpcn1-3*) are present (Calcraft *et al.*, 2009); humans and some rodent species (but not guinea pig) lack *Tpcn3* (Zhu *et al.*, 2010). These genes are predicted to encode three proteins, TPC1-3 with approximately 35 % sequence homology (Brailoiu *et al.*, 2009).

The first report of a functional role for mammalian TPCs was made by Calcraft and colleagues (Calcraft *et al.*, 2009). Membranes from HEK293 cells expressing HA-tagged TPC2 showed at least a three-fold increase in [^{32}P]-NAADP binding when compared with membranes from wild-type cells. In cells expressing HA-TPC2, photorelease of caged NAADP led to the generation of a slow ramp-like increase in $[Ca^{2+}]_i$, followed by a large Ca^{2+} transient, which was prevented by bafilomycin A and high 'self-inactivating' concentrations of NAADP, and was not present in wild-type cells (Calcraft *et al.*, 2009). Application of 10 nM or 1 μM NAADP via a patch pipette evoked a similar Ca^{2+} release signal in HA-TPC2-expressing cells, and this was prevented not only by bafilomycin A or self-inactivating concentrations of NAADP, but also by transfection of cells with a short hairpin RNA against *Tpcn2* (Calcraft *et al.*,

2009). Calcraft and colleagues also examined the role of TPC2 proteins in a more physiological system, utilising *Tpcn2*$^{-/-}$mice, which lack TPC2 proteins, and their wild-type counterparts. In wild-type mice, application of NAADP to pancreatic β-cells elicited Ca^{2+} release from a lysosomal intracellular compartment, which led to activation of a cell membrane Ca^{2+}activated inward cation current. In *Tpcn2*$^{-/-}$ mice, NAADP failed to activate this inward current (Calcraft *et al.*, 2009). Taken together these data provide evidence that TPC2 proteins are a molecular target for NAADP and are a requirement for physiological processes involving NAADP signalling.

This evidence led Elson and colleagues in the laboratory of Prof Derek Terrar, to investigate the role of TPC2 in cardiac ventricular EC coupling, in the absence and presence of isoprenaline, utilising *Tpcn2*$^{-/-}$ mice. Under basal conditions, there were no significant differences detected in cell contraction, Ca^{2+} transient amplitude or Ca^{2+} spark frequency between ventricular myocytes isolated from wild-type and *Tpcn2*$^{-/-}$ hearts (Elson, DPhil Thesis, 2011). However, in ventricular myocytes isolated from wild-type mice, application of the cell-permeant AM ester of NAADP (NAADP-AM) was found to increase Ca^{2+} spark frequency and amplitude of field-stimulated contractions; these effects were abolished in myocytes from *Tpcn2*$^{-/-}$ mice (Elson, DPhil Thesis, 2011). These data suggest that TPC2 proteins are necessary for NAADP-mediated responses in mouse ventricular myocytes. Furthermore, Elson and colleagues also provided the first evidence that TPC2 proteins form an important component of the β-adrenoceptor signalling pathway in response to isoprenaline (Elson *et al.*, 2010). In myocytes lacking TPC2 proteins, field-stimulated Ca^{2+} transient and contractile responses to isoprenaline were found to be significantly reduced in comparison to their wild-type counterparts (Elson *et al.*, 2010). Taken together with the observations of Macgregor and colleagues in the Terrar laboratory (Macgregor *et al.*, 2007a), these

observations suggest that NAADP signalling via TPC2 proteins forms an important additional component of the β-adrenoceptor signalling pathway in ventricular myocytes.

The aims of the experiments presented in this chapter were to extend the observations of Elson and colleagues in ventricular myocytes from *Tpcn2*$^{-/-}$ mice (Elson *et al.*, 2010), by investigating the effects of isoprenaline on contractions (stimulated by an electrode, rather than an electric field) in ventricular myocytes from *Tpcn2*$^{-/-}$ mice, and on coronary pressure, force and rate of contraction in Langendorff-perfused hearts from *Tpcn2*$^{-/-}$ mice. Further aims were to investigate the effects of pharmacological inhibition of NAADP signalling with either bafilomycin A or Ned-19 on responses to both low (2 – 3 nM, to induce positive inotropic effects) and high (50 nM, to induce arrhythmias) concentrations of isoprenaline in guinea pig ventricular myocytes.

3.2 Methods

Mice lacking TPC2 proteins (*Tpcn2*$^{-/-}$) were generated from an embryonic cell stem cell line (YHD437) containing a gene trap mutation in the *Tpcn2* gene (Calcraft *et al.*, 2009). *Tpcn2*$^{-/-}$ mice were kindly donated by Margarida Ruas da Silva of the laboratory of Prof Antony Galione, Department of Pharmacology, University of Oxford.

Single ventricular myocytes were isolated from *Tpcn2*$^{-/-}$ mice and age- strain- and sex-matched wild-type controls (13 – 18 weeks) or guinea pigs as described in detail in chapter 2. Cells were superfused with PSS (in single cell mouse ventricular myocyte experiments, PSS contained 1 mM Ca^{2+} rather than 1.8 mM, as used in all other experiments), gassed with 95% O_2 5% CO_2 to maintain a pH of 7.4, and patched in the permeabilised configuration (Axoclamp 2 amplifier, amphotericin-permeabilised,

240 U/ml). Cells were stimulated to contract at 1 Hz via the patch pipette, and sarcomere length measured using the Ionoptix system. APs were also recorded and analysed using Clampfit software.

In Langendorff experiments described in detail in chapter 2, whole hearts from *Tpcn2*$^{-/-}$ mice and age- strain- and sex-matched wild-type controls were carefully excised and cannulated via the aorta for mounting on a constant-flow Langendorff-perfusion system. Force of contraction was measured via a tension transducer attached to the apex of the heart by means of a small hook. Resting tension was set between 0.5 g and 1.0 g, and once resting tension was set, a 30 minute equilibration period was allowed before the application of drugs. Heart rate was calculated from the interval between beats shown on the force signal. Inflow pressure at the level of the aorta was measured using a pressure transducer positioned close to the heart, so that changes in coronary artery resistance could be measured as pressure changes at a constant perfusion flow rate.

3.3 Results

3.3.1 The contractile response to β-adrenoceptor stimulation was blunted in ventricular myocytes from Tpcn2$^{-/-}$ *mice*

Figure 3.1 shows the effects of isoprenaline on sarcomere shortening of myocytes stimulated at 1 Hz by a 2 ms depolarising pulse delivered by a patch electrode (perforated configuration). It can be seen that the increases in contraction amplitude caused by 3 nM isoprenaline were greatly reduced in myocytes from *Tpcn2*$^{-/-}$ mice as

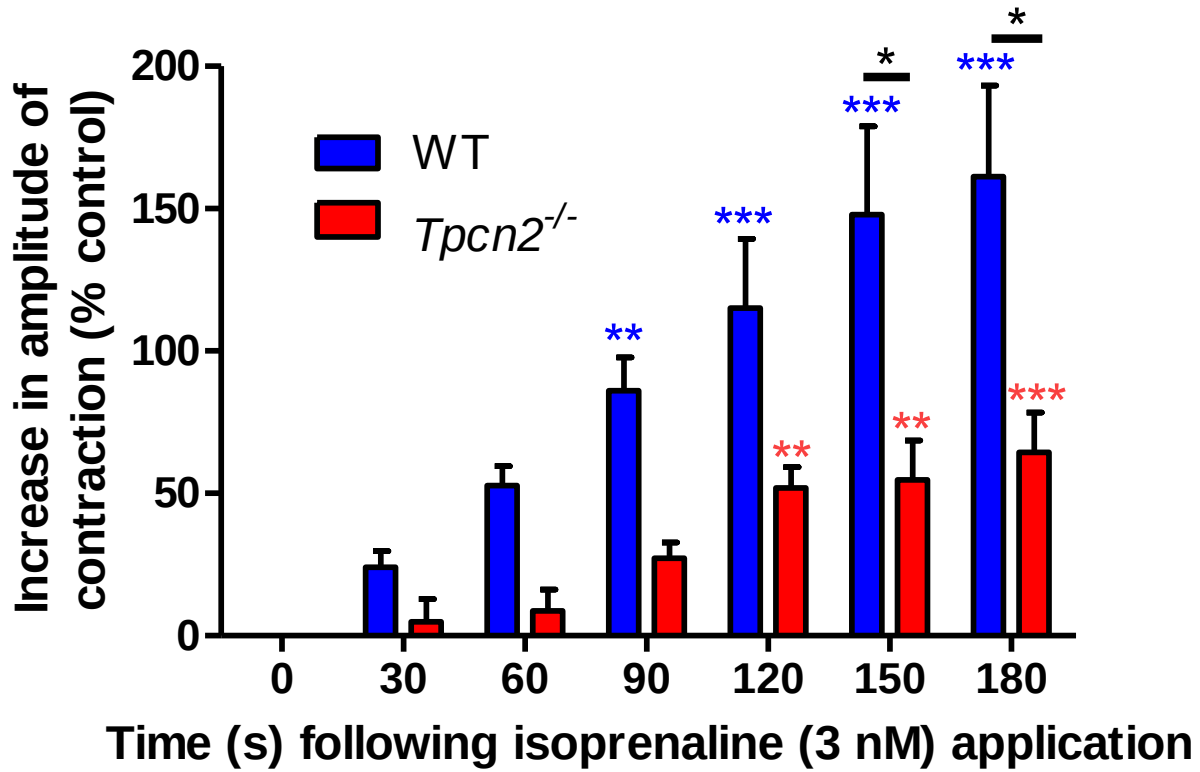


Figure 3.1 Mean data showing the blunted contractile response to isoprenaline in ventricular myocytes from *Tpcn2-/-* mice

Mean data showing the blunted effect of isoprenaline in ventricular myocytes isolated from mice lacking TPC2 proteins (*Tpcn2*$^{-/-}$). After 3 minutes superfusion with isoprenaline (3 nM) sarcomere shortening was increased by 164 ± 32 % in wild-type cells (n = 13, $P < 0.001$), and by 64 ± 14 % in cells lacking TPC2 proteins (n = 7, $P < 0.001$, ANOVA with repeated measures, followed by Dunnett's post-hoc test). These values were significantly different ($P < 0.05$, ANOVA followed by Bonferroni post-hoc test). * denotes $P < 0.05$, ** denotes $P < 0.01$, *** denotes $P < 0.001$.

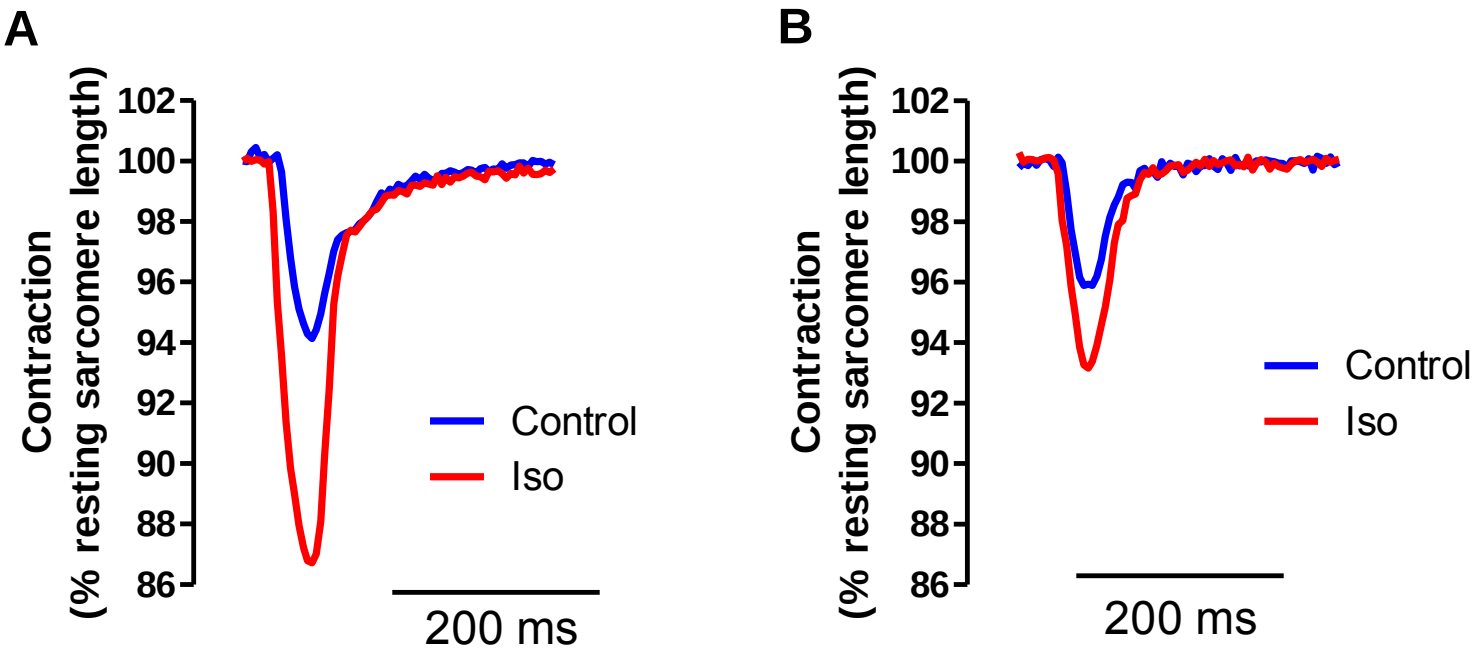


Figure 3.2 Representative contraction traces showing the response to 3 nM isoprenaline a cells from *Tpcn2*$^{-/-}$ and wild-type mice.

Representative contraction traces showing the effect of 3 minutes superfusion with 3 nM isoprenaline on sarcomere shortening in A: a ventricular myocyte isolated from a wild-type mouse, and B: a ventricular myocyte isolated from a *Tpcn2-/-* mouse.
All cells were stimulated to contract at 1 Hz by a 2 ms depolarising current pulse delivered by a patch electrode (amphotericin permeabilised).

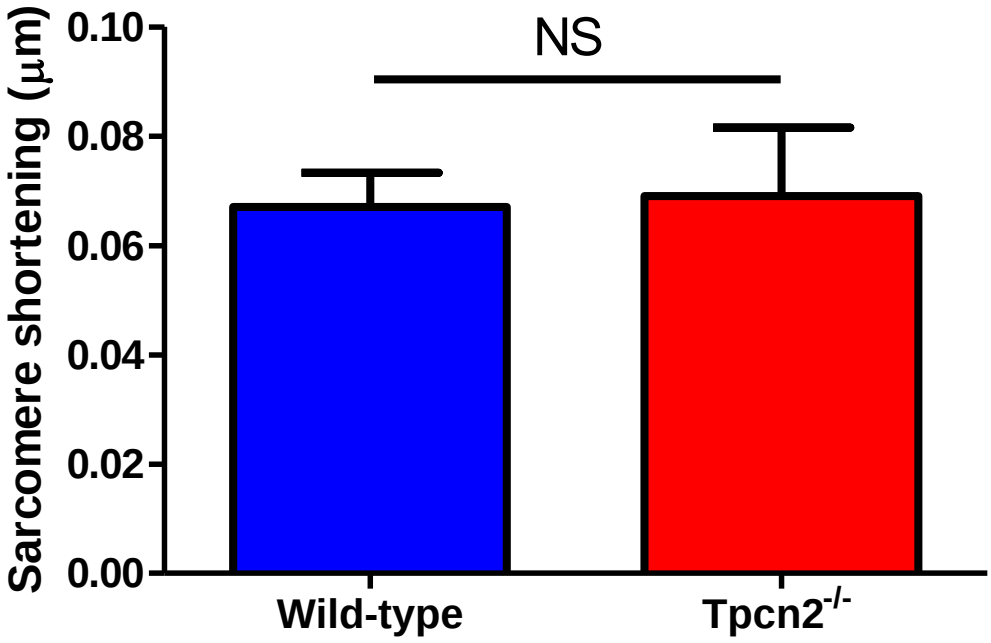


Figure 3.3 Mean data showing lack of difference in basal force of contraction between wild-type and *Tpcn2*$^{-/-}$ myocytes.

Mean data showing magnitude of sarcomere shortening in *Tpcn2-/-* myocytes (n = 7) compared to age-matched wild-type controls (n = 13) in the absence of isoprenaline. There was no difference in magnitude of sarcomere shortening between groups ($P > 0.05$, Student's unpaired *t* test).

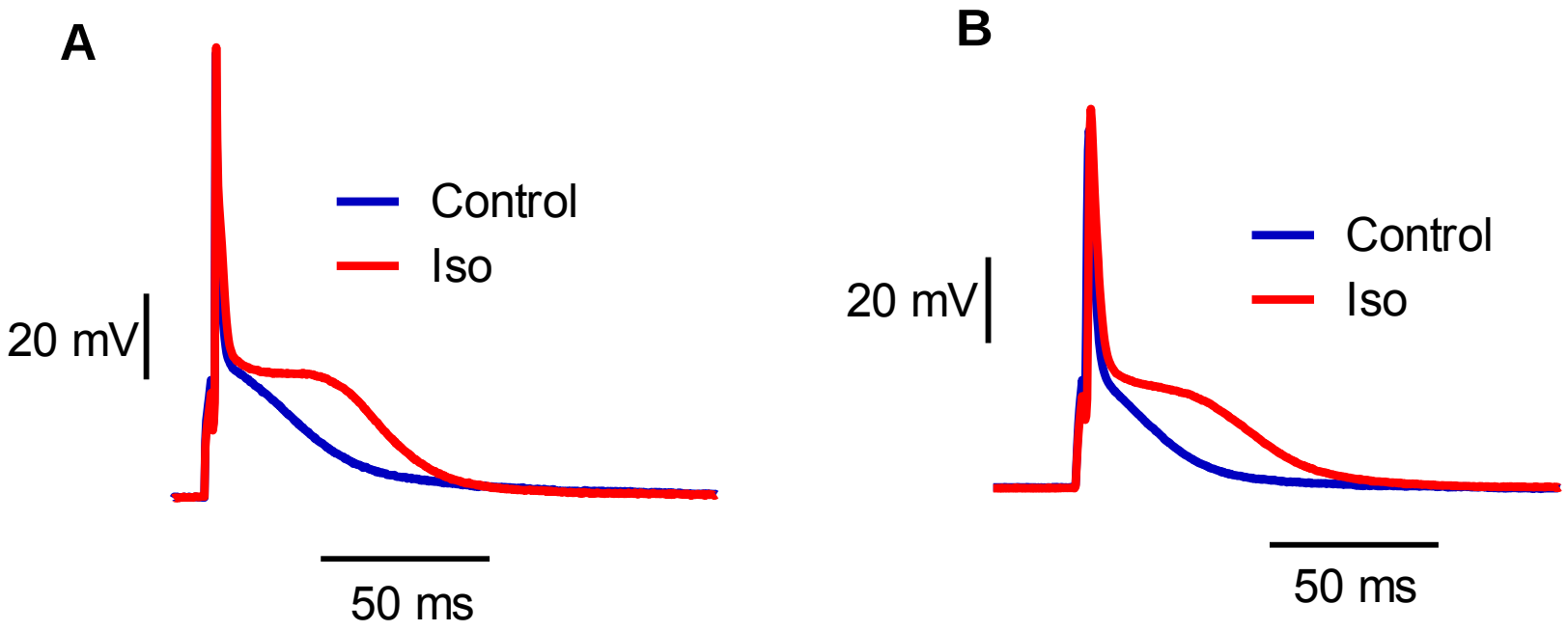


Figure 3.4 Representative action potential traces showing the effects of 3 nM isoprenaline in wild-type and *Tpcn2*$^{-/-}$ cells.

Representative contraction traces showing the effect of 3 minutes superfusion with 3 nM isoprenaline on action potential configuration in A: a ventricular myocyte isolated from a wild-type mouse, and B: a ventricular myocyte isolated from a *Tpcn2*$^{-/-}$ mouse.
All cells were stimulated to contract at 1 Hz by a 2 ms depolarising current pulse delivered by a patch electrode (containing amphotericin to achieve permeabilised configuration).

compared with the increases observed in wild-type myocytes (161 ± 32 %; n = 13 in WT; 64 ± 14%; n = 7 in *Tpcn2*$^{-/-}$; $P < 0.05$). Representative contraction traces are shown in Figure 3.2. No differences in amplitude of contraction before addition of isoprenaline (Figure 3.3) or in AP configuration between *Tpcn2*$^{-/-}$ and wild-type myocytes in response to isoprenaline were observed. Representative AP traces from the same cells illustrated in Figure 3.2 are shown in Figure 3.4.

3.3.2 The contractile response to β-adrenoceptor stimulation was blunted in Langendorff-perfused hearts from Tpcn2$^{-/-}$ *mice*

The observations in myocytes from *Tpcn2*$^{-/-}$ mice were complemented by observations in whole hearts perfused by the Langendorff technique. In preliminary experiments investigating the response to isoprenaline in CD1 mouse Langendorff-perfused hearts, it was found that contractile responses to isoprenaline peaked rapidly (within 2 minutes of application of isoprenaline), and then decayed rapidly. However, the isoprenaline-induced reduction in coronary perfusion pressure (which occurs via a β -adrenoceptor-mediated pathway) and increase in spontaneous beating rate took longer to recover to basal levels. In addition, subsequent applications of isoprenaline were found to elicit smaller responses in all parameters measured. Therefore, a protocol was devised where three separate doses of 5 nM isoprenaline would be applied, each with a washout period of at least 30 minutes in between doses, to begin once maximal responses to isoprenaline had been achieved. All data reported here are therefore the mean values of three separate doses of isoprenaline applied during a time period of up to 2 hours. Any hearts with a spontaneous beating rate lower than 300 bpm and a force of contraction lower than 0.7 g were discarded.

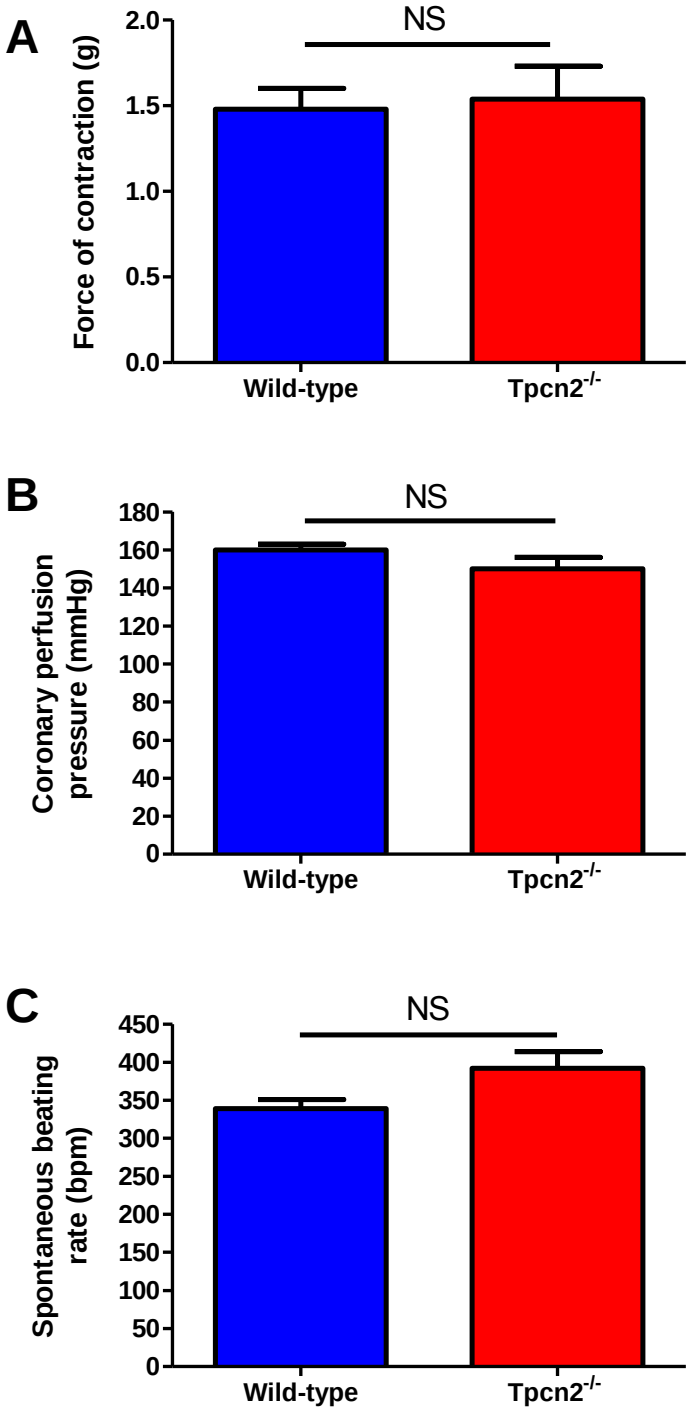


Figure 3.5 Mean data showing the similarities between wild-type and *Tpcn2*$^{-/-}$ Langendorff-perfused hearts in the absence of isoprenaline.

Mean data showing A: force of contraction, B: coronary perfusion pressure, C: spontaneous beating rate, in Langendorff perfused hearts in the absence of isoprenaline. All data are the mean of three measurements made before addition of 5 nM isoprenaline and at least 30 minutes after wash-out of the previous dose of isoprenaline. There were no significant differences between wild-type (n = 5) and *Tpcn2*$^{-/-}$ hearts (n = 7) in any parameters studied ($P > 0.05$, Student's unpaired *t* test).

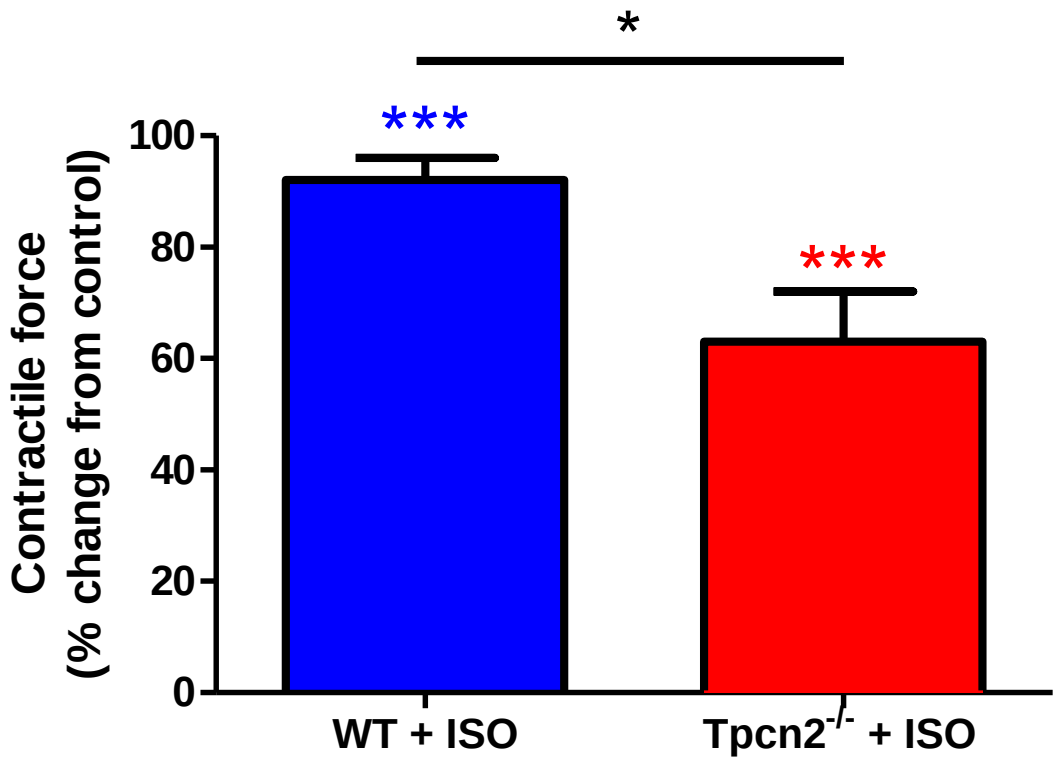


Figure 3.6 Mean data showing the blunted contractile response to isoprenaline in Langendorff-perfused *Tpcn2*$^{-/-}$ hearts.

Mean data showing a blunting of the contractile response to 5 nM isoprenaline in Langendorff-perfused hearts from mice lacking TPC2 proteins (n = 7) compared to age-matched wild-type controls (n = 5). In wild-type hearts 5 nM isoprenaline elicited a 92 ± 4 % increase in force of contraction ($P < 0.001$, Student's paired *t* test). In *Tpcn2*$^{-/-}$ hearts this was 63 ± 9 % ($P < 0.001$), significantly smaller than the increase seen in wild-type hearts ($P < 0.05$, Student's unpaired *t* test). All data were calculated as the mean of three consecutive doses of isoprenaline in each heart.

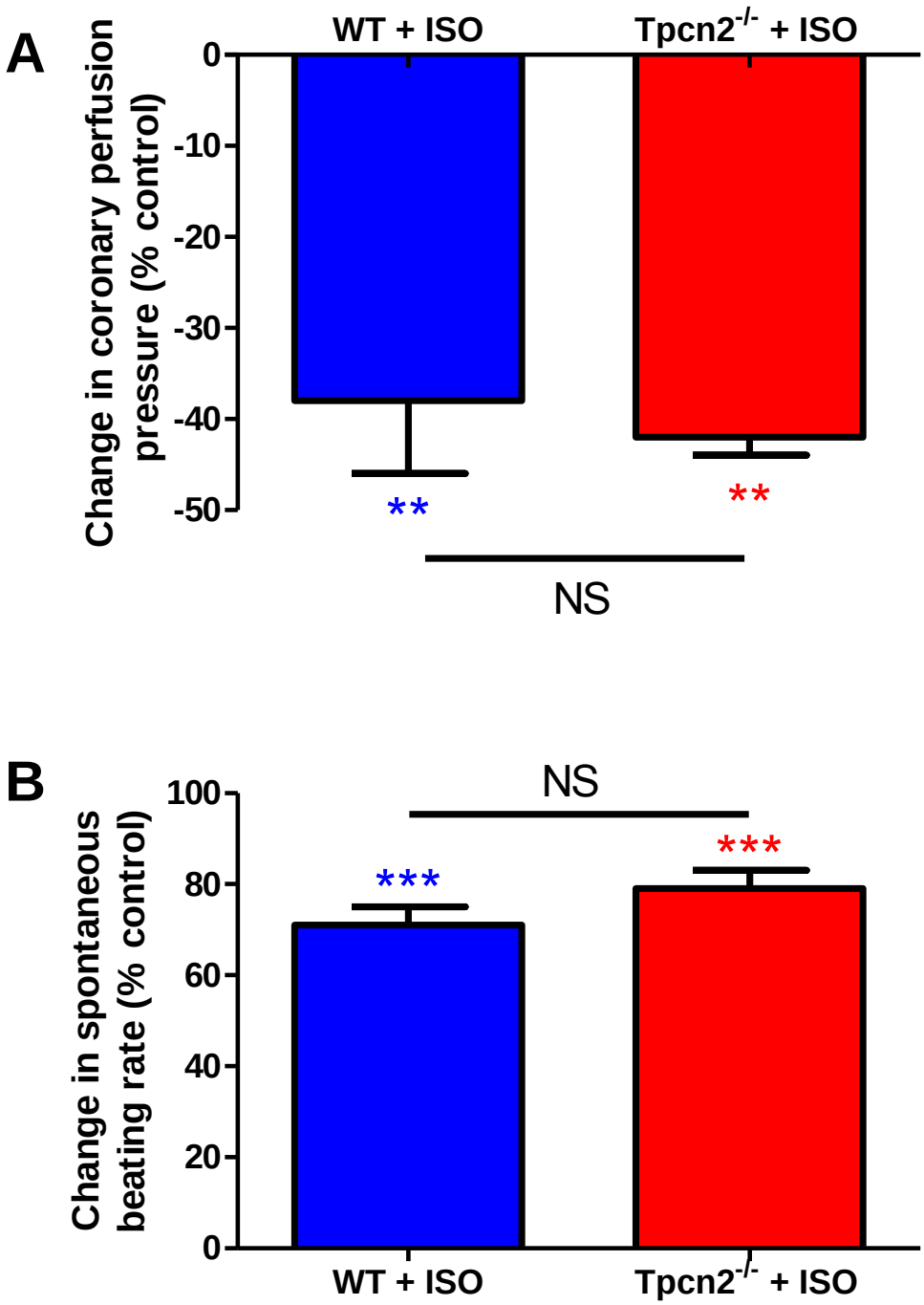


Figure 3.7 Mean data showing the effects of isoprenaline on coronary perfusion pressure and spontaneous rate in wild-type and *Tpcn2*$^{-/-}$ hearts.

Mean data showing the lack of difference in the effects of 5 nM isoprenaline on A: coronary perfusion pressure, and B: spontaneous beating rate, in Langendorff-perfused hearts from wild-type mice (n = 5) and mice lacking TPC2 proteins (n = 7). ** denotes $P < 0.01$, *** denotes $P < 0.001$.

In terms of basal levels of contractility, coronary perfusion pressure and spontaneous rate, there were no differences between wild-type and *Tpcn2*$^{-/-}$ mice (see Figure 3.5). However, three doses of 5 nM isoprenaline led to a mean increase in force of ventricular contraction of 92 ± 4% (n = 5, $P < 0.001$) in age-matched wild-type controls compared with only 63 ± 9% (n = 7, $P < 0.001$) in hearts from *Tpcn2*$^{-/-}$ animals, a significant reduction in animals lacking the TPC2 protein ($P < 0.05$, Figure 3.6). In contrast to force responses, there were no significant differences between wild-type and *Tpcn2*$^{-/-}$ hearts in terms of coronary perfusion pressure and rate responses after isoprenaline application ($P > 0.05$; Figure 3.7). Coronary perfusion pressure was reduced by 38 ± 8 % in wild type hearts (n = 7, $P < 0.01$) and by 42 ± 2 % in *Tpcn2*$^{-/-}$ hearts (n = 5, $P < 0.01$; Figure 3.7A). Rate was increased by 71 ± 4 % in wild-type animals (n = 5, $P < 0.001$) and by 79 ± 4 % in *Tpcn2*$^{-/-}$ hearts (n = 7, $P < 0.001$; Figure 3.7B).

3.3.3 The contractile response to β-adrenoceptor stimulation was blunted in guinea pig ventricular myocytes pre-treated with bafilomycin

Bafilomycin A is an inhibitor of vacuolar-type H^+ ATPases, which are thought to be responsible for the acidification of lysosomes, maintaining the proton gradient necessary for lysosomal accumulation and storage of Ca^{2+}. Previous studies in guinea pig ventricular myocytes have shown that 5 minutes superfusion with bafilomycin A (100 nM) results in a reduction in the amplitude of Ca^{2+} transients, which would suggest that lysosomal Ca^{2+} signalling is active under basal conditions in guinea pig ventricular myocytes (Elson, DPhil Thesis, 2011). Further experiments carried out in the Terrar laboratory during the course of this thesis have shown that patch-applied bafilomycin (1 μM) reduced the effect of isoprenaline to increase the amplitude of the

Ca^{2+} transient, compared with control cells (Bayliss, DPhil Thesis, 2013). However, the effects of bafilomycin on the contractile response to isoprenaline have not previously been investigated. Because contractions cannot reliably be measured using whole-cell patch due to dialysis of intracellular constituents, a pre-incubation protocol (15 minutes, such that bafilomycin could cross cell membranes and access the cytosol) was carried out in order to assess the effects of 1 μM bafilomcyin on contractions in the presence of isoprenaline. Under these conditions, no significant differences in basal amplitude of contraction were detected between bafilomycin-treated and untreated cells (sarcomere shortening of 0.14 ± 0.02 and 0.15 ± 0.02 μm respectively, both n = 11). Figure 3.8 shows the mean increases in contraction after application of 3 nM isoprenaline to 11 guinea pig ventricular cells pre-treated with bafilomycin, and 11 control cells (treated with 0.3 % DMSO vehicle). After 90 seconds superfusion with isoprenaline, sarcomere shortening was increased by 145 ± 37 % in control cells, compared to 43 ± 19 % in cells pre-treated with bafilomycin A ($P < 0.05$, ANOVA with Bonferroni post-hoc test).

3.3.4 There was a trend towards a blunting of the contractile response to β-adrenoceptor stimulation in guinea pig ventricular myocytes pre-treated with Ned-19

Trans Ned-19 is an antagonist of NAADP signalling (Naylor *et al.*, 2009). Previous studies in the Terrar laboratory have demonstrated that *trans* Ned-19 reduces the amplitude of contraction in guinea pig ventricular myocytes without affecting AP configuration or amplitude of I_{CaL} (Elson *et al.*, 2011).

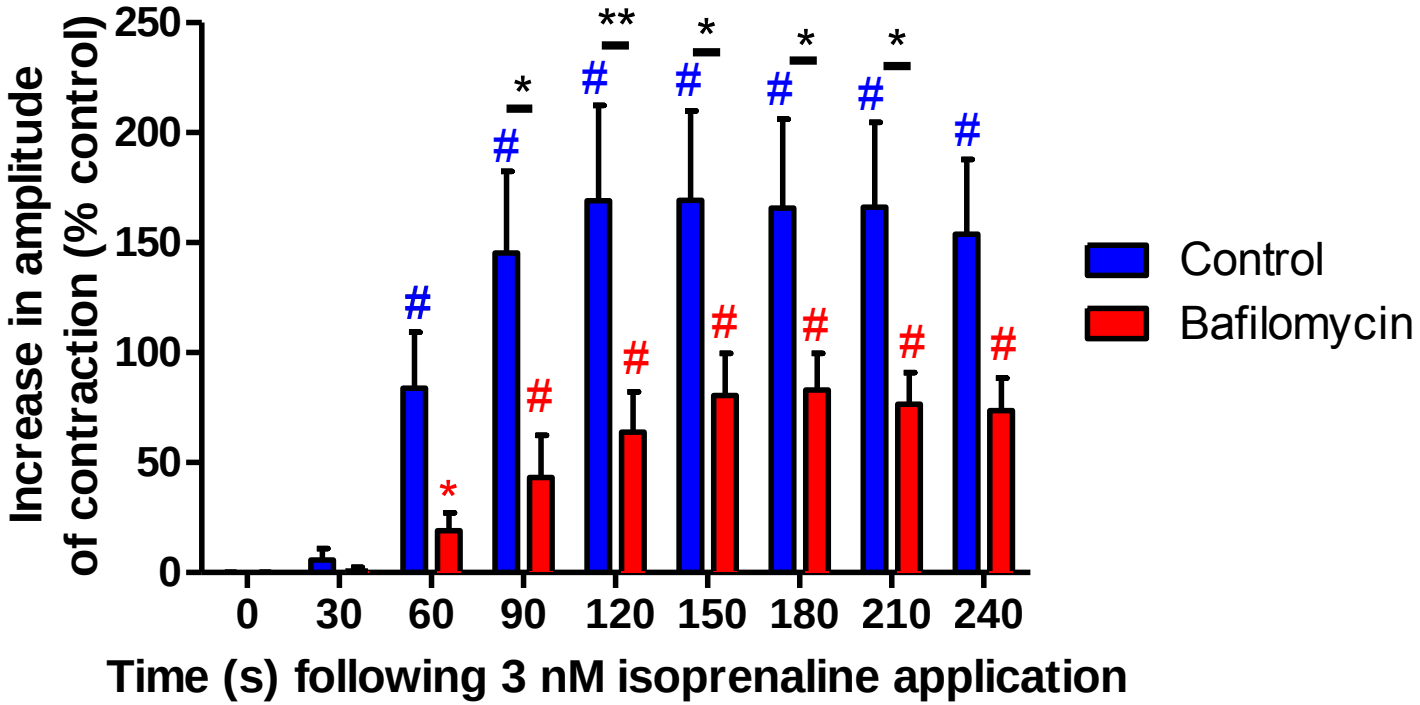


Figure 3.8 Mean data showing the effects of bafilomycin on contractile responses to isoprenaline in guinea pig ventricular myocytes.

Mean data showing the effect of 15 minute preincubations of cells with 1 µM bafilomycin (or 0.3 % DMSO) on the contractile response to 3 nM isoprenaline. After 2 minutes superfusion with isoprenaline, sarcomere shortening was increased by 169 ± 43 % in DMSO-treated cells (n = 11, $P < 0.001$) and by 64 ± 18 % in bafilomycin-treated cells (n = 11, $P < 0.001$, ANOVA with repeated measures followed by Dunnett's post-hoc test). These differences were significantly different ($P < 0.01$, ANOVA followed by Bonferroni post-hoc test). * denotes $P < 0.05$, ** denotes $P < 0.01$ and # denotes $P < 0.001$.

In addition, further experiments carried out during the course of this thesis have demonstrated that patch-applied *trans* Ned-19 (1 µM) reduced the effect of isoprenaline to increase the amplitude of the ventricular cell Ca^{2+} transient (Bayliss, DPhil Thesis, 2013). In order to investigate the effects of *trans* Ned-19 on the amplitude of contractions in the presence of isoprenaline, a pre-incubation protocol (15 minutes) was carried out, using a concentration of 10 µM *trans* Ned-19. Cells were stimulated to contract at 1 Hz via a patch electrode (permeabilised configuration). It was noted that in 6 out of the 13 cells treated with Ned-19, contractions in the absence of isoprenaline were particularly small (sarcomere shortening < 0.05 microns). In these cells, application of isoprenaline resulted in exceptionally large (> 500 %) increases in sarcomere shortening. Mean data showing the responses to isoprenaline in all cells pre-treated with Ned-19 (or 0.1 % DMSO vehicle) are shown in Figure 3.9. A subsequent analysis was carried out where any cells, including those pre-incubated with DMSO, which exhibited particularly small contractions in the absence of isoprenaline (sarcomere shortening < 0.05 microns) were discarded. 3 out of the 11 cells pre-treated with DMSO and 6 out of the 13 Ned-19-treated cells were discarded. These data are summarised in Figure 3.10. After 2 minutes superfusion with 3 nM isoprenaline, the amplitude of contraction in cells pre-treated with Ned-19 was increased by 80 ± 15 % ($n = 7$, $P < 0.01$), while in untreated cells it was 118 ± 23 % ($n = 8$, $P < 0.01$). However, these differences did not reach statistical significance ($P > 0.05$; 95 % confidence interval was -17 to 169).

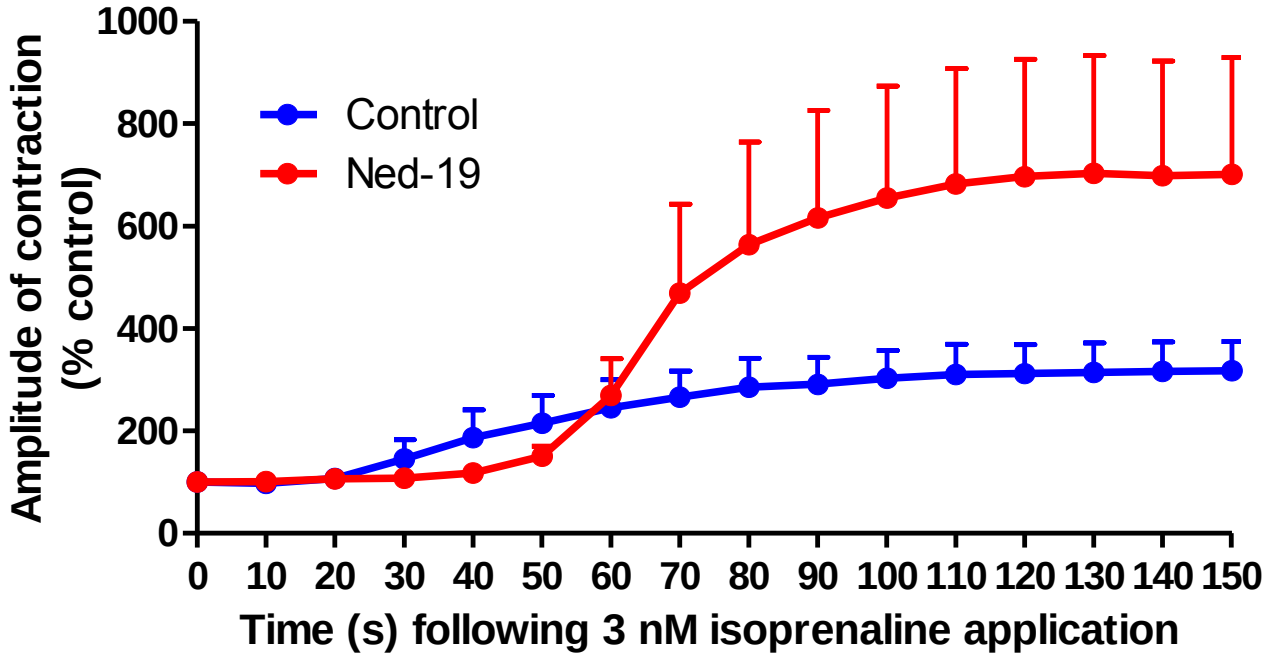


Figure 3.9 Mean data showing the effect of Ned-19 pre-incubation on contractile responses to isoprenaline in guinea pig ventricular myocytes.

Pre-incubation of cells with 10 µM *trans* Ned-19 (n = 13) resulted in an almost complete suppression of contraction in the absence of isoprenaline, which then resulted in a particularly large isoprenaline response (in percentage terms; red line) in comparison with DMSO-treated cells (n = 11; blue line). After 2 minutes superfusion of Ned-19-treated cells with 3 nM isoprenaline, contraction was 697 ± 229 % of control values. In DMSO-treated cells this was 312 ± 56 % of control values.

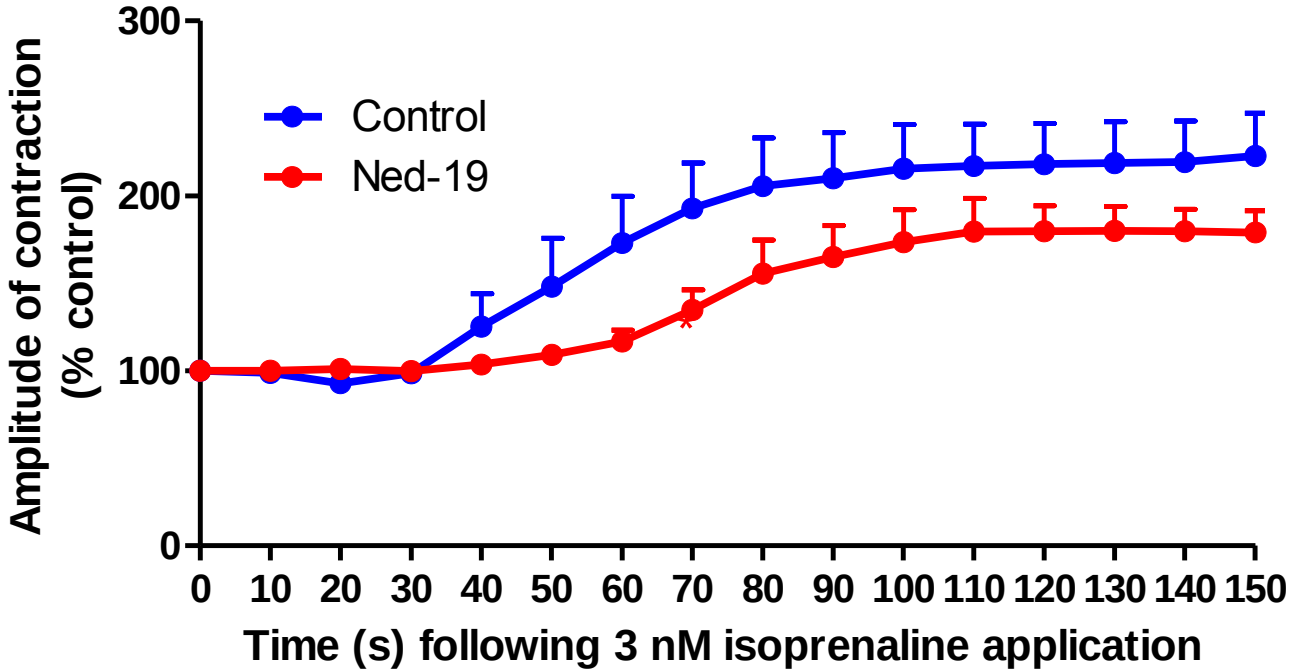


Figure 3.10 Mean data showing the effect of Ned-19 on contractile responses to isoprenaline with the application of exclusion criteria.

Exclusion criteria were applied such that any cells exhibiting particularly small contractions (sarcomere shortening < 0.05 microns) were discarded. After 2 minutes superfusion with 3 nM isoprenaline, the amplitude of contraction in cells pre-treated with Ned-19 was increased by 80 ± 15 % (n = 7, $P < 0.01$), while in untreated cells it was 118 ± 23 % (n = 8, $P < 0.01$). However, these differences did not reach statistical significance ($P > 0.05$; 95 % confidence interval was -17 to 169).

3.3.5 Bafilomycin exerted an anti-arrhythmic action in the presence of high-dose isoprenaline

Since bafilomycin suppressed the effect of 3 nM isoprenaline to increase the magnitude of ventricular cell contractions, the possibility was considered that it may also suppress the effect of high dose isoprenaline (50 nM) to induce arrhythmias. Cells were incubated for 15 minutes with either bafilomycin (1 µM) or 0.3 % DMSO, before being superfused with PSS and stimulated to contract at 1 Hz (via a patch electrode). Superfusion with PSS was carried out until AP recordings were stabilised, at which point superfusion was switched to 50 nM isoprenaline. Initially, small transient depolarisations appeared, which rapidly increased in magnitude until they were large enough to elicit spontaneous action potentials and contractions. Figure 3.11 shows the cumulative proportion of cells showing spontaneous APs and contractions at specified time points after application of 50 nM isoprenaline. Cells pre-incubated with bafilomycin (n = 10) took longer to develop spontaneous APs than those pre-incubated with DMSO (n = 11).

3.4 Discussion

The data presented in this chapter are the first to examine the role of TPC2 proteins in the positive inotropic response to isoprenaline in mouse hearts, and suggest that the effect of isoprenaline to increase contractility in both ventricular myocytes and Langendorff-perfused hearts involves TPC2 channels. In addition, acidic endolysosomal Ca^{2+} stores appear to contribute to the increase in contractility observed

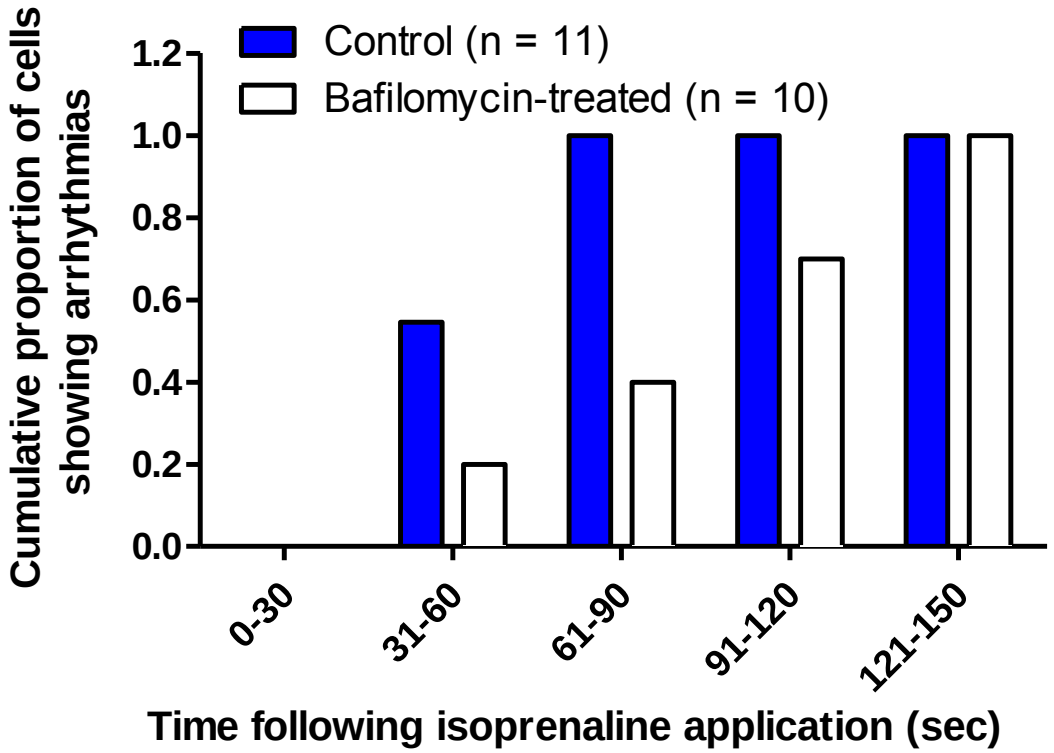


Figure 3.11 Bar graph showing the cumulative proportion of bafilomycin- and DMSO-treated cells showing arrhythmias after application of 50 nM isoprenaline.

The application of 50 nM isoprenaline to cells stimulated at 1 Hz (patch electrode, amphotericin-permeabilised) resulted in the generation of spontaneous action potentials and contractions in between stimulations. The cumulative proportion of cells showing events is shown here; cells pre-treated with bafilomycin took longer to exhibit such spontaneous events than DMSO treated cells.

in guinea pig ventricular myocytes in response to isoprenaline, and preliminary evidence presented here suggests that inhibition of Ca^{2+} storage in endolysosomes may provide a novel target for anti-arrhythmic drugs. Some of these data have been presented in the form of an abstract (Bolton *et al.*, 2013).

Numerous observations made in the Terrar laboratory point towards a role for endogenous NAADP in augmenting the amplitudes of Ca^{2+} transients and contractions in both ventricular (Macgregor *et al.*, 2007a; Elson, DPhil Thesis, 2011) and atrial (Collins *et al.*, 2011; Bayliss, DPhil Thesis, 2013) myocytes isolated from guinea pigs. If it were the case that endogenous NAADP functions to augment the amplitude of contractions and Ca^{2+} transients in mouse cardiac muscle it would be expected that there might be a difference in functional characteristics between wild-type and *Tpcn2*$^{-/-}$ myocytes and Langendorff-perfused hearts in the absence of isoprenaline. However, data presented here show there were no differences in ventricular myocyte contractility between *Tpcn2*$^{-/-}$ and wild-type myocytes in the absence of isoprenaline (Figure 3.3). Furthermore, no differences in the contractility, spontaneous rate or coronary perfusion pressure of Langendorff-perfused hearts was detected (Figure 3.5). These findings would be consistent with the idea that NAADP-mediated Ca^{2+} mobilisation does not contribute to the generation of contractile force in mouse cardiac muscle under basal conditions. Another possibility is that any differences are just too small to detect under the conditions of these experiments. One way of testing whether the NAADP signalling pathway is active under basal conditions in mouse ventricular myocytes would be to preincubate wild-type and *Tpcn2*$^{-/-}$ myocytes with bafilomycin and measure contractions. If the NAADP signalling pathway is active, presumably bafilomycin should lead to reduced contraction amplitudes in wild-type cells, while it should have no effect on *Tpcn2*$^{-/-}$ cells.

Exposure of ventricular myocytes from *Tpcn2*$^{-/-}$ mice to isoprenaline elicited significantly smaller increases in amplitude of contraction than seen in wild-type mice (Figure 3.1and Figure 3.2). Additional observations made in parallel to those presented here also demonstrated a blunted Ca^{2+} transient response to isoprenaline in myocytes lacking TPC2 proteins in terms of Ca^{2+} transient responses (Sam Lin Wee Khang, personal communication); these findings are in agreement with those previously reported from the Terrar laboratory (Elson *et al.*, 2010). The data presented here are the first to show that the contractile response to isoprenaline is blunted in Langendorff-perfused hearts from *Tpcn2*$^{-/-}$ mice (Figure 3.6), providing additional evidence that Ca^{2+} mobilisation via TPC2 channels may constitute an additional mechanism by which force of cardiac contractility in response to β-adrenoceptor stimulation is regulated. In order to provide further convincing evidence of this, it would be beneficial to perform experiments in paced *Tpcn2*$^{-/-}$ Langendorff hearts to rule out possible effects on contractile force which may occur secondary to changes in rate. However, it cannot be ruled out that the differences seen in the experiments prevented here are due, in part, to factors which do not involve the NAADP signalling pathway.

In addition to data obtained using murine hearts lacking TPC2 proteins, experiments were performed using bafilomycin to prevent Ca^{2+} uptake and storage in guinea pig ventricular myocytes. In cells pre-treated with 1μM bafilomycin, the contractile response to isoprenaline was blunted (Figure 3.8) in a similar manner to the effect seen in myocytes from *Tpcn2*$^{-/-}$ hearts (Figure 3.1). Studies performed in the Terrar laboratory during the course of this thesis using patch-applied bafilomycin (1 μM) have shown a blunted Ca^{2+} transient response to isoprenaline in the presence of bafilomycin (Bayliss, DPhil Thesis, 2013). Taken together, these observations provide additional evidence that NAADP-mediated Ca^{2+} mobilisation contributes to the β-

adrenoceptor signalling pathway in guinea pig ventricular myocytes. An additional interesting extension to these observations would be to determine whether application of bafilomycin to Langendorff-perfused murine hearts reduces the contractile response to isoprenaline to levels seen in *Tpcn2*$^{-/-}$ hearts. Preliminary experiments performed as part of this thesis (but not shown) suggested that bafilomycin does not permeate intact tissues as easily as single cells, and so a preincubation protocol would need to be devised. Although technically demanding, this could be achieved by use of a fluid-filled jacket surrounding the heart and a balloon inserted into the left ventricle to measure force of contraction. The use of a fluid filled jacket may also help maintain control of temperature during Langendorff experiments.

Similar experiments were also carried out using a high concentration (10 μM) of the NAADP antagonist *trans* Ned-19 (which has been shown to prevent NAADP-induced activation of TPC2 channels (Pitt *et al.*, 2010)), in an attempt to further verify that the NAADP signalling pathway contributes to the positive inotropic effects of β-adrenoceptor stimulation in guinea pig myocytes. Although there was a trend towards the expected blunting of the response to isoprenaline in cells pre-incubated with Ned-19, the overall effect was not statistically significant (Figure 3.10). It was noted that pre-incubation of some cells with Ned-19 led to an almost complete inhibition of contractility in the absence of isoprenaline, such that when cells were exposed to isoprenaline, the percentage increase in sarcomere shortening was extremely large (Figure 3.9). The utility of this compound as an inhibitor of the NAADP signalling pathway has been tested extensively in the Terrar laboratory (Elson *et al.*, 2011), with the finding that, in addition to preventing the actions of exogenously applied NAADP, superfusion of guinea pig ventricular myocytes with the *cis* isoform inhibited LTCCs, whereas the *trans* isoform (donated by the laboratory of Dr Grant Churchill) did not. It

is therefore possible that the use of high concentrations of *trans* Ned-19 (> 1 μM), applied by superfusion rather than directly into the cytosol leads to additional off-target effects such as inhibition of LTCCs. Indeed, it has been observed that some inhibitors of LTCCs also inhibit NAADP signalling (Genazzani *et al.*, 1997). More recently, experiments performed by Rebecca Bayliss of the Terrar laboratory have shown that patch-applied *trans* Ned-19 prevents the increase in Ca^{2+} transient amplitude in response to photorelease of a caged analogue of NAADP (Bayliss, DPhil Thesis, 2013). Furthermore, patch-applied *trans* Ned-19 reduced the increase in Ca^{2+} transient amplitude in response to superfusion of isoprenaline (Bayliss, DPhil Thesis, 2013); the unclear effects of *trans* Ned-19 presented here are therefore surprising. Potential explanations for this will now be discussed.

Although Ned-19 was initially reported as a membrane permeant inhibitor of NAADP signalling (Naylor *et al.*, 2009), the exact mechanism of transport across the cardiac cell membrane is unknown. It is possible that small amounts of the compound are able to cross the cell membrane freely, or that transporters are necessary for it to cross the membranes of some cells. Interestingly, the experiments of Pitt and colleagues have demonstrated that low concentrations of Ned-19 (in the nM range) actually potentiate NAADP-mediated activation of TPC2 channels, while micromolar concentrations inhibit it in a non-competitive manner (Pitt *et al.*, 2010). It is possible that the lack of clear effect of *trans* Ned-19 to reduce the contractile response to isoprenaline in the experiments presented here (Figure 3.9 and Figure 3.10) is due to poor access of the drug to the cytosol, leading to exposure of intracellular TPC2 channels to unknown (and possibly very low) concentrations of the drug. In order to ensure that high enough concentrations of *trans* Ned-19 reach the cytosol, it would be necessary to measure myocyte contractions while *trans Ned*-19 is introduced directly

into cells. This is technically challenging, since in contrast to Ca^{2+} transients, measurements of contraction over time periods longer than ~3 minutes, cannot easily be obtained using the whole-cell patch technique due to dialysis of intracellular constituents. It may be necessary to use a sharp microelectrode made from theta glass to deliver *trans* Ned-19 to the cytosol while measuring contractions. Another possibility, unrelated to this suggestion, is that Ned-19 can have some direct actions on the myofilaments, perhaps sensitising them to Ca^{2+}.

Finally, the experiments presented here suggest that inhibition of endolysosomal Ca^{2+} storage by use of bafilomycin, reduces the tendency of cells to exhibit arrhythmogenic oscillations in the presence of high dose isoprenaline (Figure 3.11). Presumably, preventing supplementation of SR Ca^{2+} stores with additional Ca^{2+} from endolysosomal stores (in line with the two-pool hypothesis for the mechanism of NAADP actions (Churchill *et al.*, 2001a)) reduces the tendency of the SR to become Ca^{2+} overloaded. The observations presented here are consistent not only with the two-pool hypothesis for NAADP actions (Churchill *et al.*, 2001a; Macgregor *et al.*, 2007a), but also with the hypothesis that β-adrenoceptor stimulation enhances cardiac NAADP signalling (Macgregor *et al.*, 2007a; Lewis *et al.*, 2012). The observation that inhibiting the NAADP pathway could provide a novel target for anti-arrhythmic therapy is consistent with other recent observations (Nebel *et al.*, 2013).

Chapter 4

Effects of endocannabinoids on excitation-contraction coupling in guinea pig ventricular myocytes

4.1 Introduction

Anandamide is a derivative of arachidonic acid, and was discovered as the first endogenous ligand of the cannabinoid CB_1 receptor in porcine brain (Devane *et al.*, 1992b). A second endogenous ligand, 2-AG, was discovered thereafter in canine gut (Mechoulam *et al.*, 1995). Anandamide has been reported to be more selective for CB_1 receptors, while 2-AG is equally potent and efficacious at both binding sites (Howlett *et al.*, 2002). Both CB_1 and CB_2 receptors couple to G_i proteins, but other couplings have been reported (Howlett *et al.*, 2002).

Administration of endogenous cannabinoids *in vivo* causes a complex cardiovascular response, which culminates in a sustained depressant action on cardiac output and reduced blood pressure (Malinowska *et al.*, 2012). At least some of these effects are thought to occur through inhibition of autonomic outflow by actions at pre-synaptic CB_1 receptors (Szabo *et al.*, 2001). However, the confirmation of cannabinoid receptor expression in cardiac muscle itself (Weis *et al.*, 2010), raises questions as to whether their activation can induce direct inotropic actions.

Despite these findings, very few studies have sought to characterise the effects of anandamide and related cannabinoid receptor agonists on electrical activity and contractility in cardiac muscle directly. Ford and colleagues determined that anandamide induced a negative inotropic effect in isolated perfused Langendorff hearts, which could not be attributed to actions at conventional cannabinoid receptors (Ford *et al.*, 2002). In isolated rat atrial muscle preparations, Bonz and colleagues observed a negative inotropic action of anandamide which was prevented by the CB_1 receptor antagonist AM251, leading the authors to conclude that the action was mediated by CB_1 receptors (Bonz *et al.*, 2003). In electrophysiological studies on isolated rat ventricular

myocytes and partially depolarised papillary muscle, Li and colleagues observed an action potential (AP) shortening effect and an inhibition of I_{CaL} which could be prevented by the CB_1 receptor antagonist AM 251 (Li *et al.*, 2009). These investigators therefore concluded that the negative inotropic action of anandamide is mediated by CB_1 receptors (Li *et al.*, 2009). Assuming a G_i protein coupling of the CB_1 receptor, it is interesting to note that the observations of Li and colleagues in ventricular muscle were all made in the absence of β-adrenoceptor stimulation.

In addition to actions at cannabinoid receptors, there is a large body of literature describing direct modulation of ion channels by cannabinoids in various cell types (Oz, 2006). In cardiac muscle, anandamide has been shown to inhibit I_{to1} and I_{Kur} independently of cannabinoid receptors (Amorós *et al.*, 2010; Barana *et al.*, 2010). Very recent studies in rat cardiac myocytes also suggest an inhibition of cell contraction which occurs through a mechanism independent of cannabinoid receptors, arising through inhibitory effects on the Ca^{2+} transient, SR load and NCX (Al Kury *et al.*, 2014a; Al Kury *et al.*, 2014b; Kury *et al.*, 2014). In addition, a whole family of lipid mediators related to anandamide have actions in cardiac muscle which occur through direct inhibition of ion channels (Voitychuk *et al.*, 2012). Furthermore, arachidonic acid (a cell membrane lipid from which anandamide derives), inhibits LTCCs and causes negative inotropic effects in guinea pig ventricular myocytes directly (Mamas *et al.*, 2001).

In light of the inconsistent results from studies investigating the role of cannabinoid receptors in inducing the negative inotropic actions of anandamide, and additional data reporting various effects on ion channel activity which do not depend on cannabinoid receptors, the aim of the experiments presented in this chapter was to investigate the effects of anandamide and related cannabinoid receptor agonists on

electrical activity, Ca^{2+} transients and contraction in ventricular muscle, with the aim of deducing whether a receptor could be involved in the mechanism. This is the first study to utilise guinea pig ventricular myocytes (which, like human, have an AP which plateaus at positive potentials), for this purpose. Further aims were to determine whether 2-AG had any direct inotropic actions in ventricular myocytes.

4.2 Methods

The methods used to perform experiments presented in this chapter are described in detail in chapter 2. Guinea pigs were killed by cervical dislocation and their hearts rapidly excised. To isolate ventricular myocytes, hearts were retrogradely perfused with a modified Tyrode's solution containing collagenase. Cells were plated onto a glass coverslip attached to a perfusion bath and superfused with PSS, which was heated to 36^{o}C and gassed with 95 % O_2 5 % CO_2 in order to maintain a pH of 7.4. Voltage activated switches were used to switch between PSS solutions containing different drugs of interest.

Two methods were used to measure cell contraction in response to electrical stimulation (1 Hz) which was delivered either by carbon fibre electrodes mounted at both sides of the perfusion bath (field stimulation) or via a microelectrode. In most experiments, the IonOptix system was used to measure sarcomere length. Images of ventricular myocytes were captured using the IonOptix MyoCam mounted on a Nikon Diaphot 200 inverted microscope with a ×40 objective lens. In some contraction experiments, cell length was measured using an edge detection system.

For measurement of Ca^{2+} transients, two methods were used. In an initial series of experiments, myocytes were incubated with cell permeant Fluo-5F AM (1.5 – 3 μM)

for 10 minutes, and electrically field stimulated to contract at a frequency of 1 Hz. Whole-cell Ca^{2+} transients were measured using an epifluoresence system. Excitation light was provided by an LED lamp with a bandpass interference filter to select for light of 475 ± 15 nm; emitted light was detected by a photomultiplier after passing through a 520 nm long-pass filter. In a second series of experiments, the pentapotassium salt of Fluo-5F (75 μM) was introduced into cells via a patch pipette, with concurrent measurement of APs. Excitation light was provided by an LED lamp, passed through a filter to select for light of 475 ± 15 nm and collected by an EMCCD camera (Luca R, Andor, UK). Images were analysed using Fluoview software (John Dempster, University of Strathclyde).

Measurements of APs and membrane currents were made using an AxoClamp 2 amplifier (Axon Instruments, USA), with all analysis carried out with Clampfit 9.2 software (Axon Instruments, USA). Cells were impaled with a sharp glass microelectrode as described in chapter 2. In experiments where Ca^{2+} currents were measured in the presence of Cs^{+} to inhibit contaminating K^{+} currents, or where Fluo-5F pentapotassium salt was introduced to myocytes, the whole-cell patch technique was used.

APs were stimulated by 2 ms depolarising current pulses (1 – 5 nA) at a frequency of 1 Hz. I_{CaL} was activated by 200 ms step depolarisations from a holding potential of –40 mV to a range of potentials from –30 mV to +60 mV. In some experiments, a double pulse protocol (applied at a frequency of 0.2 Hz) was used to measure inactivation of LTCCs. An initial pre-pulse of 500 ms duration, from a holding potential of -40 mV to a range of potentials from -50 mV to + 60 mV at 5 mV increments was applied prior to a 200 ms test pulse from -40 mV to 0 mV. The delayed rectifier K^{+} currents I_{Kr} and I_{Ks} were measured by step depolarisations (10 – 600 ms)

from a holding potential of –40 mV to +40 mV. The resulting tail currents were taken to represent I_{Kr} and I_{Ks}.

When using an AxoClamp amplifier, it is not possible to measure cell capacitance directly. Measurements of cell capacitance were therefore estimated during voltage clamp experiments by application of a 10 mV step depolarisation (of 200 ms duration) from a holding potential of –40 mV to –30 mV, during which it would be expected that there would be little or no active current. The capacitive transients occurring at the start and end of the square pulse were then integrated to give an estimate of current flowing per unit time (pA*ms). The following rationale was used:

I (amperes) = Q (coulombs)/ t (seconds)

Therefore, rearranging:

Q = I*t (amp*sec)

Q (amp*sec) = C (Farads)*V (volts)

So, for example, if a value of 2000 pA*ms was obtained on integration of the capacitive transient generated after a 10 mV step depolarisation:

2000 pA*ms = C * 0.01 V

2 pA*s = C * 0.01 V

$2*10^{-12}$A*s = C (Farads) * 0.01 V

$2*10^{-10}$ = C (Farads)

$2*10^{-7}$ = C (mF)

$2* 10^{-4}$ = C (µF)

0.2 = C (nF)

200 = C (pF)

In this case, the cell would have a capacitance of 200 pF.

4.3 Results

4.3.1 Anandamide markedly reduced ventricular myocyte contractility

In isolated ventricular myocytes, field stimulated to contract at a frequency of 1 Hz, anandamide caused a concentration-dependent reduction in magnitude of cell shortening as measured by the Ionoptix system to study sarcomere length; a representative trace is shown in Figure 4.1. After 10 minutes superfusion with 10 µM anandamide, myocyte sarcomere shortening was reduced by 66 ± 4 % of control values (n = 6, $P < 0.001$), and by 37 ± 2 % of control values (n = 6, $P < 0.001$) after 10 minutes superfusion with 3 µM anandamide. 1 µM anandamide was without significant effect on sarcomere shortening (92 ± 5 % of control values; n = 6, $P > 0.05$). Since anandamide was supplied pre-dissolved in ethanol, vehicle control experiments were carried out to rule out any possible effects of ethanol on myocyte contractility. After 10 minutes superfusion with 0.07 % ethanol (~17 mM; the highest concentration used in any of the experiments described in this thesis), there were no significant effects on sarcomere shortening: 94 ± 4 % of control values (n = 6, $P > 0.05$). The effects of anandamide were slow to develop over a 10 minute time-period, and are summarised in Figure 4.2. For a log concentration-response plot, see Figure 5.10 in Chapter 5.

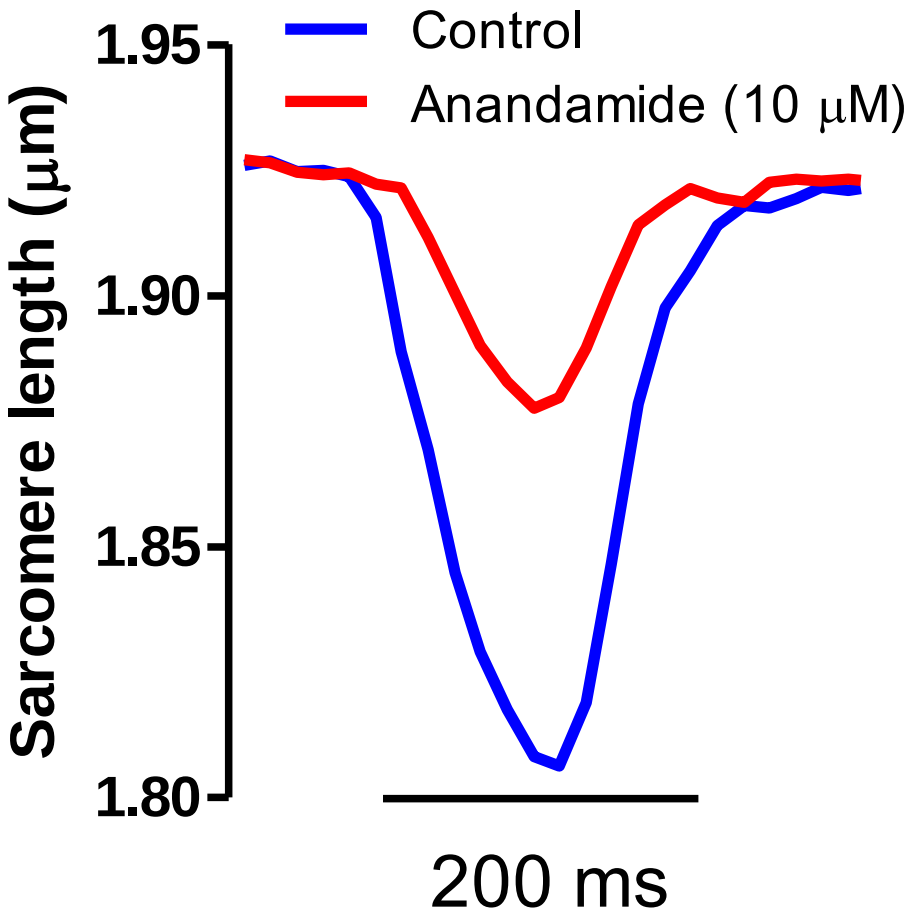


Figure 4.1 Representative contraction after superfusion with anandamide

Representative cell contraction showing the effects of superfusion with 10 μM anandamide for 10 minutes. Cells were electrically field-stimulated at a frequency of 1 Hz, and sarcomere length measured using the Ionoptix system. Anandamide evoked a decrease in amplitude of contraction.

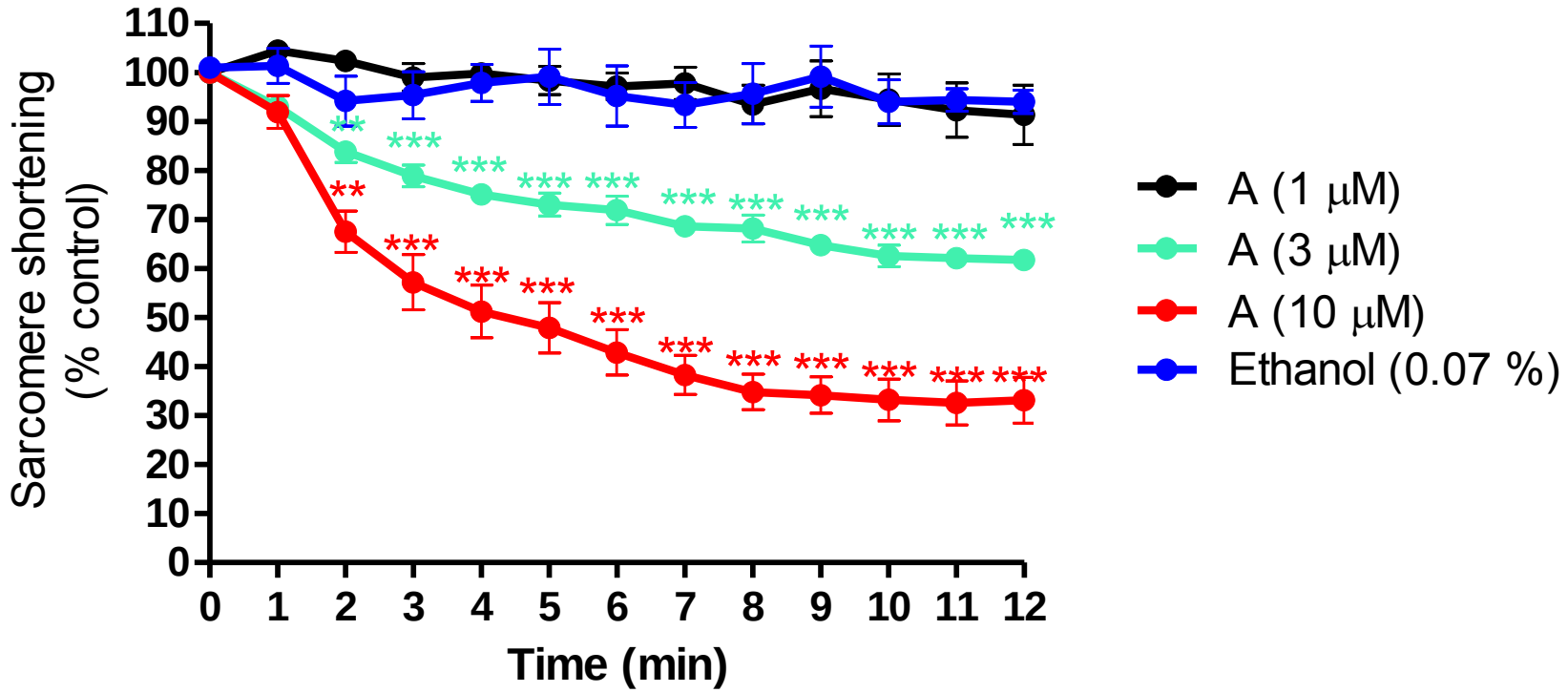


Figure 4.2 Time course of effect of anandamide or ethanol on amplitude of sarcomere shortening

Time course of effect of anandamide (1, 3, 10 μM) and of ethanol vehicle (0.07 %) on mean amplitude of sarcomere shortening in guinea pig ventricular myocytes. Cells were electrically field-stimulated to contract at a frequency of 1 Hz; data are presented as percentage change in sarcomere shortening from control values. Anandamide elicited a concentration-dependent reduction in amplitude of sarcomere shortening. All drugs are n = 6; ** denotes $P < 0.01$, *** denotes $P < 0.001$ relative to control; repeated measures ANOVA with Dunnett's post-hoc test. 1 μM anandamide and ethanol vehicle were without significant effect on sarcomere shortening ($P > 0.05$).

4.3.2 Anandamide reduced amplitude of whole-cell Ca^{2+} transients

In order to investigate whether the effects of anandamide on myocyte contractility were occurring as a result of changes in Ca^{2+} handling, the effects of anandamide on whole-cell Ca^{2+} transients were studied. A representative Ca^{2+} transient measured using fluo-5F as the Ca^{2+} indicator is shown in Figure 4.3A. Superfusion of cells with 10 μM anandamide reduced the amplitude of the Ca^{2+} transient (ΔF/F0) by 28 ± 7 % of control values (n = 5, $P < 0.01$) after 5 minutes. In ethanol vehicle control experiments, no significant changes in Ca^{2+} transient amplitude were observed (96 ± 4 % of control after 5 minutes; n = 6, $P > 0.05$, Figure 4.3B). It is interesting to note that at the 5 minute time point in the previous experiment, the amplitude of contraction was reduced by 52 ± 5 % (n = 6, $P < 0.001$).

As an extension to these experiments, it was decided that a more robust approach to measure Ca^{2+} transients over a 10 minute time period would be to use a patch pipette to introduce the cell-impermeant pentapotassium salt of Fluo-5F into the cytosol. Using this method, any Fluo-5F extruded from the cell is likely to be readily replaced by the large volume of dye present in the patch pipette. Furthermore, this method would permit the concurrent recording of APs. Cells were allowed to load with dye for at least 10 minutes from the time of seal formation. A representative trace is shown in Figure 4.4A. Figure 4.4B shows that after 10 minutes, the amplitude of the Ca^{2+} transient was reduced by 56 ± 2 % (n = 4, $P < 0.001$). APs recorded from these cells revealed that superfusion with anandamide was associated with a shortening of AP duration (APD). APD at 90 % repolarisation (APD_{90}) was reduced by 48 ± 7 % (n = 4, $P < 0.01$) and APD at 20 % repolarisation (APD_{20}) was reduced by 64 ± 5 % (n = 4, $P <$

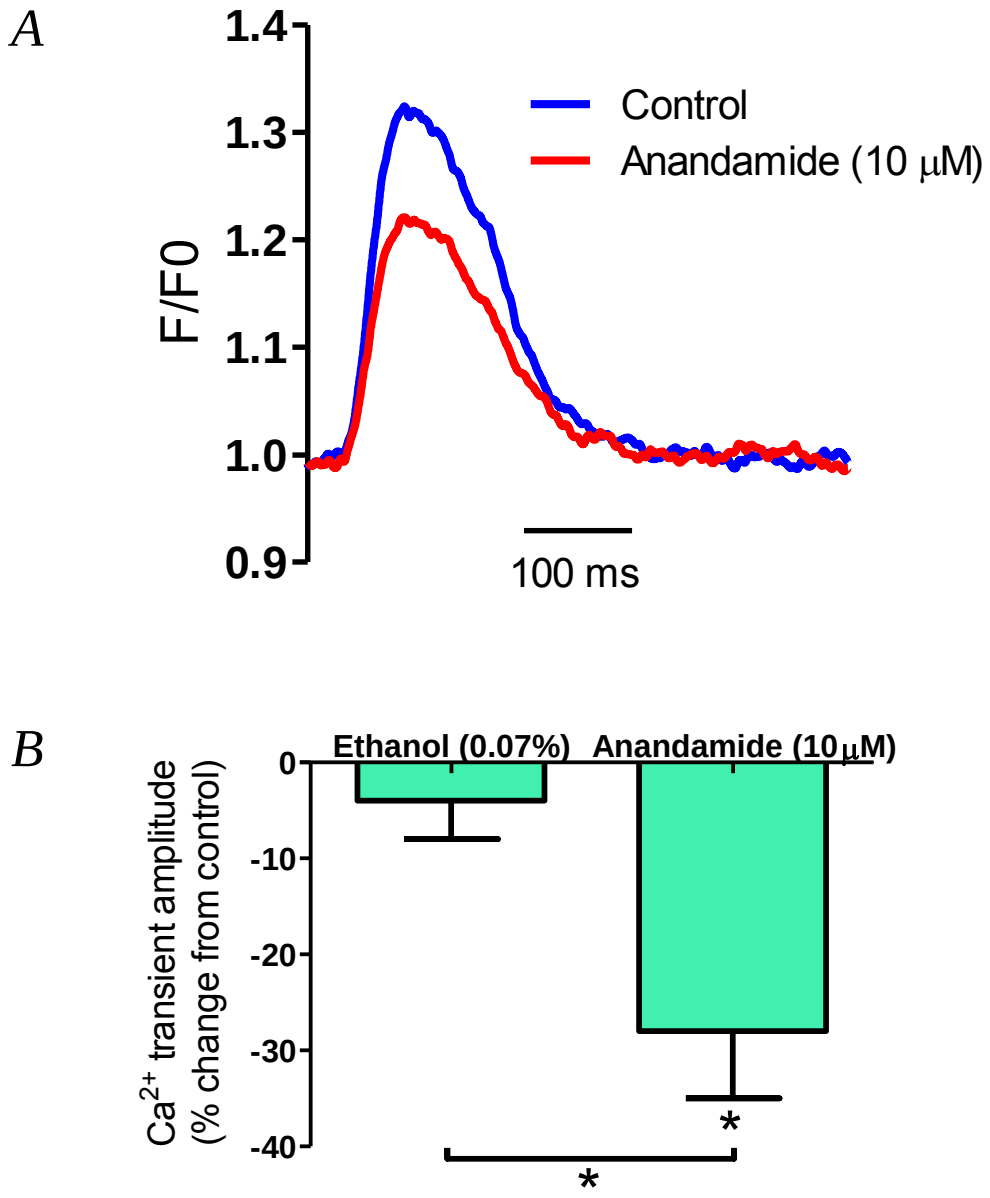


Figure 4.3 Effect of anandamide on Ca^{2+} transient amplitude

Cells were electric field-stimulated to contract at a frequency of 1 Hz.
A: Representative Ca^{2+} transients measured before and after superfusion of the cell with 10 μM anandamide for 5 minutes.
B: Mean changes in Ca^{2+} transient amplitude in cells superfused with either ethanol vehicle or with 10 μM anandamide for 5 minutes. Ethanol was without significant effect on Ca^{2+} transient amplitude (n = 6, $P > 0.05$), while anandamide caused a significant reduction in Ca^{2+} transient amplitude when compared with control and with ethanol vehicle (n = 5, $P < 0.05$); Student's paired and unpaired t-tests respectively. * denotes $P < 0.05$.

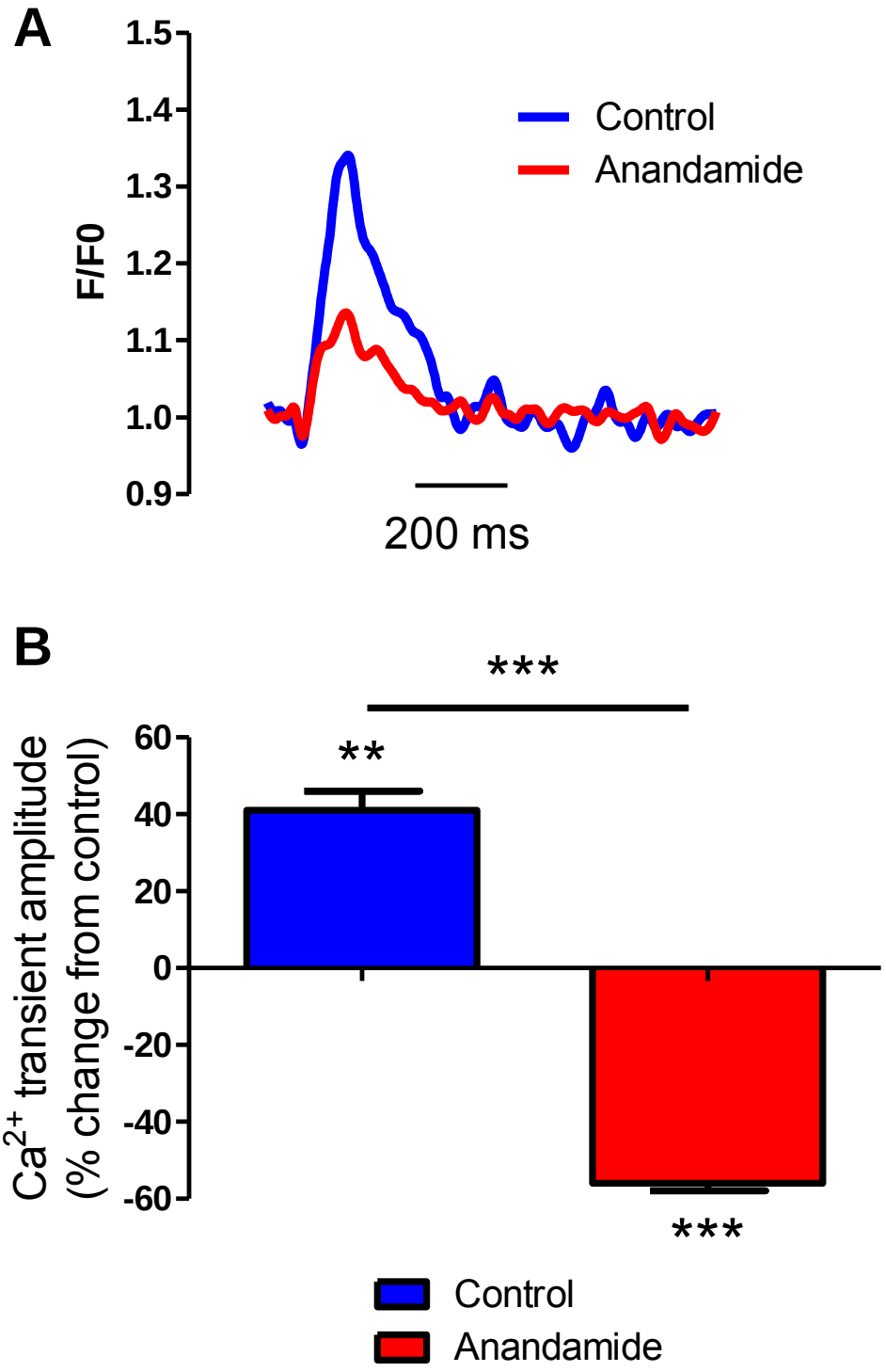


Figure 4.4 Effects of anandamide on Ca^{2+} transient amplitude measured using the pentapotassium salt of Fluo-5F

Cells were patched in the whole-cell configuration with 75 µM Fluo-5F pentapotassium salt included in the patch pipette solution. Ca^{2+} transients were elicited by 2 ms depolarising current pulses delivered via the patch pipette (1 Hz). A: representative Ca^{2+} transient. B: Mean data from control and anandamide experiments (both n = 4). ** denotes $P < 0.01$, *** denotes $P < 0.001$.

0.001). There were no significant effects on peak amplitude of the AP or resting membrane potential (RMP) (n = 4, $P > 0.05$). In time control experiments, where cells were superfused with ethanol (0.07 %) the amplitude of the Ca^{2+} transient was well maintained. Following a period of at least 10 minutes after patching onto the cell to allow for dye loading, measurements were taken. After a further 10 minutes, Ca^{2+} transient amplitude was 141 ± 5 % of control values, n = 4, $P < 0.01$; Figure 4.4B). Once cells had loaded with Fluo-5F (for at least 10 minutes after first patching on to the cell), APD was well maintained. After a further 10 minutes, APD_{90} was 116 ± 14 % of control values (n = 4, $P < 0.05$). However, there was a small reduction in APD_{20}: 20 ± 6 % (n = 4, $P < 0.05$). It is possible that measuring APs using a patch electrode in the whole-cell configuration, and loading with Ca^{2+} indicator may lead to exaggerated changes in AP configuration due to dialysis of intracellular constituents and/or buffering of intracellular Ca^{2+}. However, with Fluo-5F as the Ca^{2+} indicator, (K_d value of ~2.2 μM), any buffering action would be expected to be minimal.

4.3.3 Anandamide reduced action potential duration

Data from the previous set of experiments, in which dye was loaded into cells via a patch electrode in the whole cell configuration, revealed a shortening of the AP in cells superfused with anandamide. It is therefore possible that reductions in amplitude of the Ca^{2+} transient and in myocyte contractility were occurring as a result of reduced Ca^{2+} influx into cells. Because patching of cells in the whole-cell configuration may lead to dialysis of intracellular constituents, another series of experiments was carried out using sharp microelectrodes to more accurately assess the effects of anandamide on ventricular myocyte APs, without the confounding influence of Ca^{2+} indicator being loaded into cells. Parameters studied included APD_{90}, APD_{50} and APD_{20}, RMP and

peak amplitude of the AP. After impalement with a sharp microelectrode, all cells were allowed to settle for at least 5 minutes; any cells not displaying stable AP recordings after this time were discarded. In order to verify the stability of sharp microelectrode recordings and of the superfusion system, initial control experiments were carried out with PSS alone, switching from one reservoir to another in order to detect whether any changes in temperature arising from different flow rates were apparent. All AP parameters were found to remain stable for 10 minutes after the initial 5 minute stabilisation period. These data are summarised in Figure 4.5.

After 10 minutes superfusion with 10 µM anandamide, APD_{90} was reduced by 39 ± 6 % of control, APD_{50} was reduced by 45 ± 8 % and APD_{20} by 42 ± 8 % (all n = 8, $P < 0.001$ relative to control; Figure 4.6A, B, and C). Anandamide was without significant effect on RMP or peak amplitude of the AP (101 ± 1 % and 97 ± 2 % of control respectively, n = 8, $P > 0.05$; Figure 4.6D and E). In a similar manner to the effects of anandamide on cell contraction shown in Figure 4.2, Figure 4.6 shows that the effects of anandamide were slow to develop and were not rapidly reversible on wash. Furthermore, Figure 4.6 also shows that ethanol vehicle (0.07 %; the highest concentration used in any of the anandamide experiments presented in this thesis) was without significant effect on any AP parameters over the time period studied (n = 6, $P > 0.05$). In 6 of the 8 cells impaled with sharp microelectrodes and superfused with 10 µM anandamide, contraction was measured simultaneously using an edge-detection system. After 10 minutes, amplitude of contraction was reduced by 64 ± 8 % ($P < 0.001$); this is in agreement with values obtained with field-stimulated cells and the Ionoptix system shown in Figure 4.2. A representative AP and contraction trace from the same cell are shown in Figure 4.7.

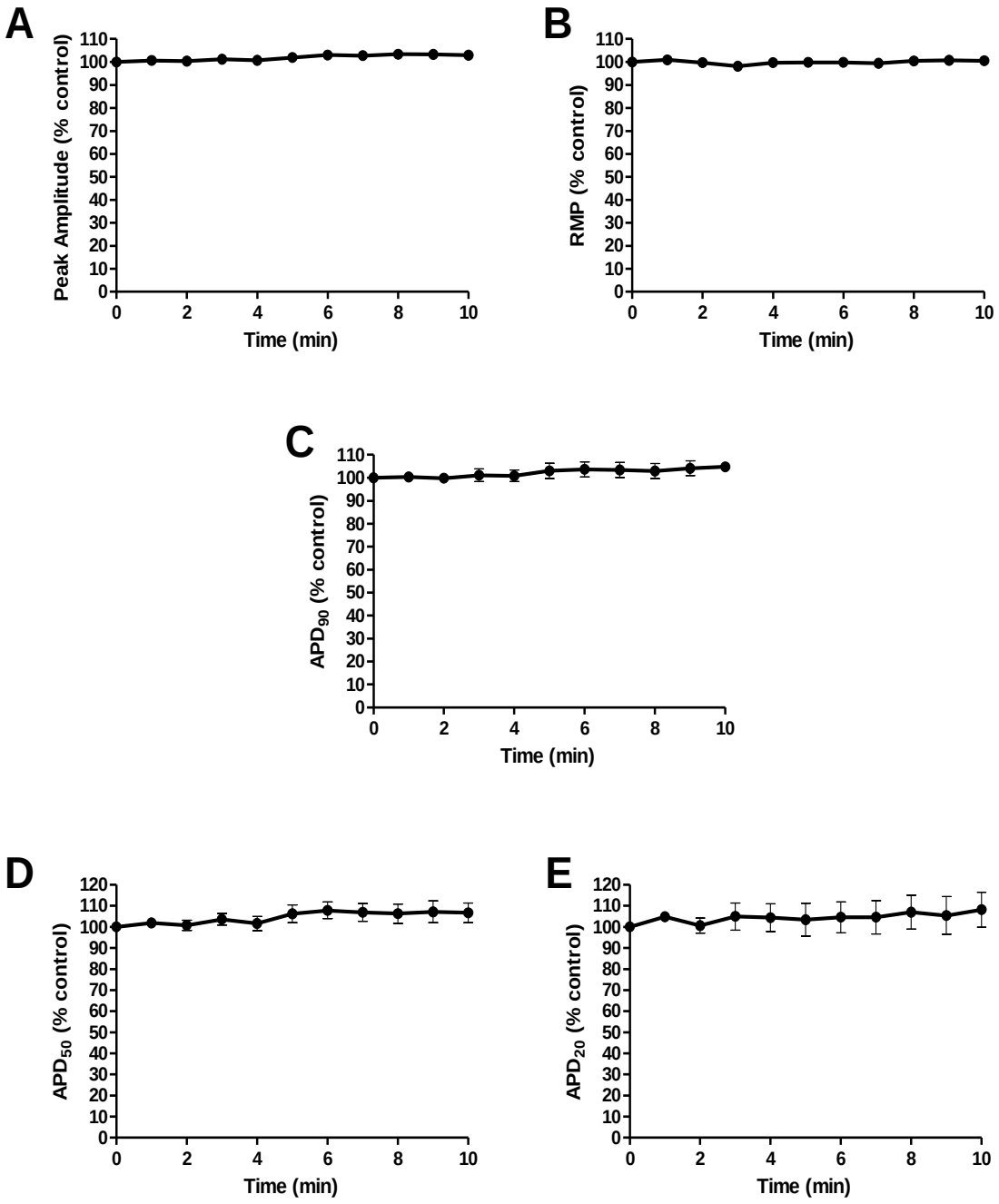


Figure 4.5 Action potential parameters in the absence of drugs

Cells were impaled with a sharp microelectrode and superfused with PSS from reservoir 1 for 5 minutes followed by PSS from reservoir 2 for 5 minutes. No significant effects on any AP parameters were observed (n = 6, $P > 0.05$; repeated measures ANOVA with Dunnett's post-hoc test).
A: Peak amplitude of the action potential.
B: Resting membrane potential.
C: Action potential duration at 90% repolarisation.
D: Action potential duration at 50% repolarisation.
E: Action potential duration at 20% repolarisation.

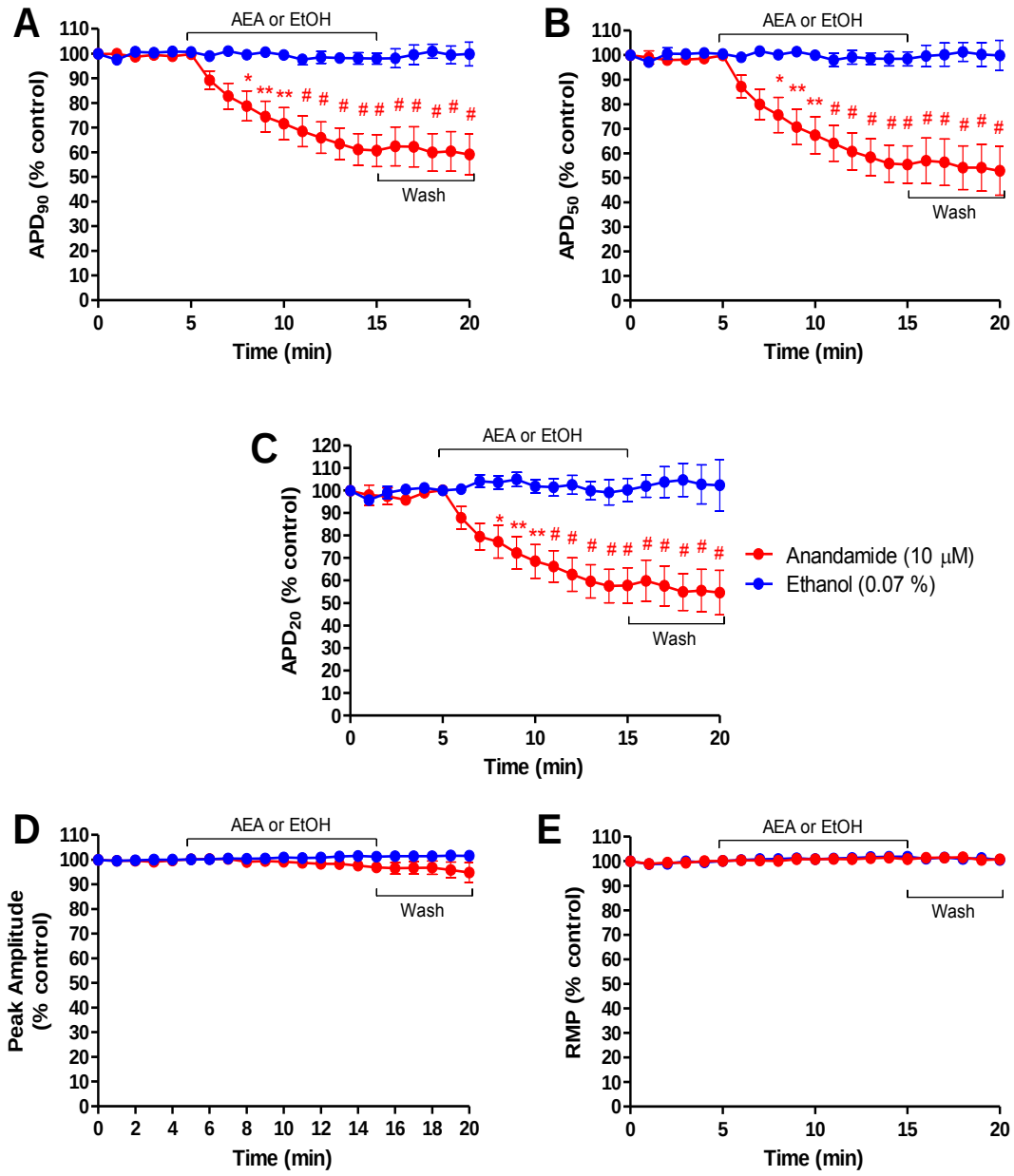


Figure 4.6 Time course of effect of anandamide or ethanol on action potential parameters

A: Action potential duration (APD) at 90 % repolarisation. B: APD at 50 % repolarisation. C: APD at 20 % repolarisation. D: Peak amplitude of the AP. E: Resting membrane potential. Anandamide reduced APD (n = 8, $P < 0.01$), but was without significant effect on peak amplitude of the AP or RMP (n = 8, $P > 0.05$). The effects of anandamide were slow to develop and were not rapidly reversible upon wash. Ethanol vehicle (0.07 %) was without significant effect on any AP parameters over the 10 minute time period studied (n = 6, $P > 0.05$). * denotes $P < 0.05$, ** denotes $P < 0.01$, # denotes $P < 0.001$; repeated measures ANOVA with Dunnett's post-hoc test.

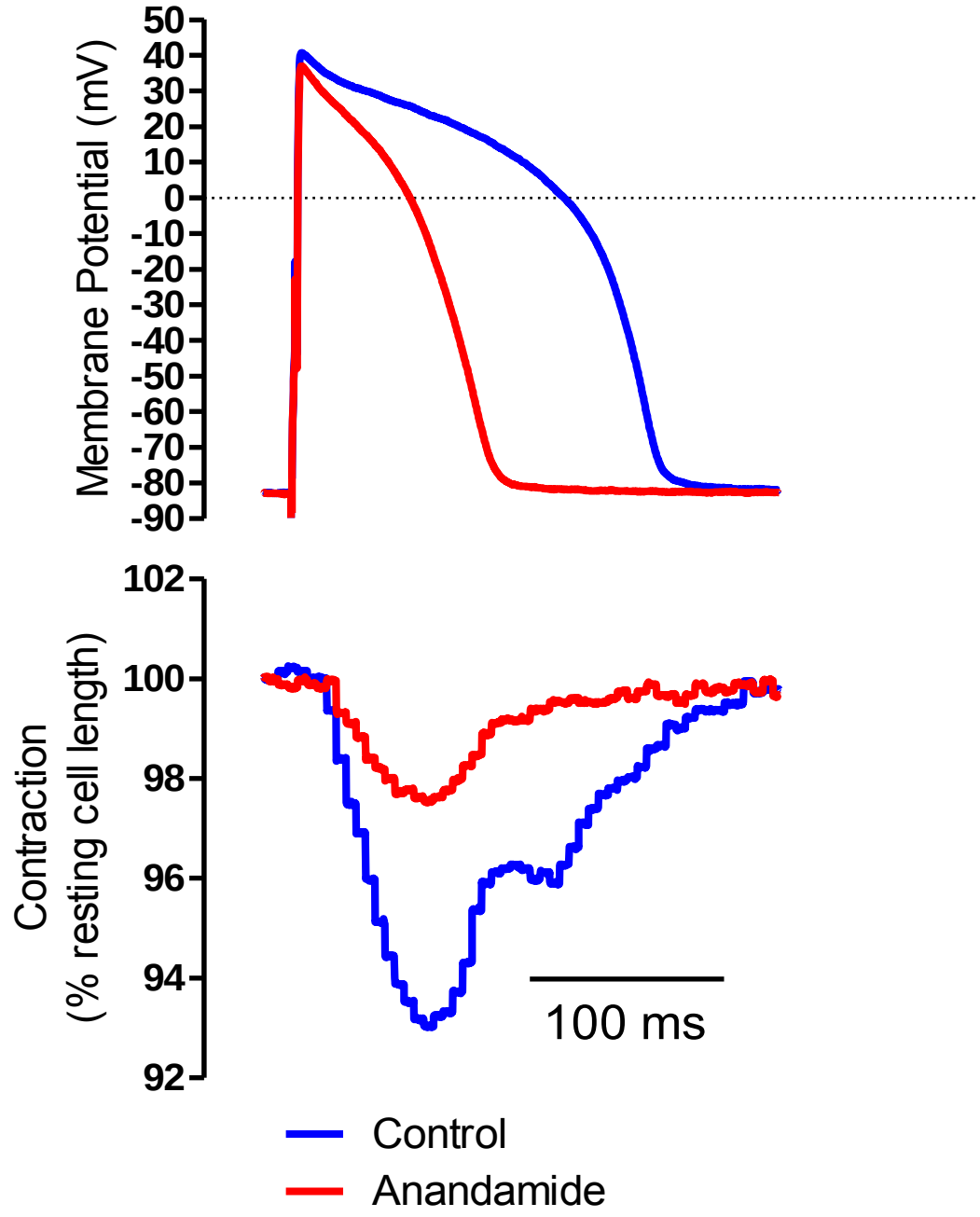


Figure 4.7 Representative action potential and contraction trace from a cell superfused with anandamide for 10 minutes

Cells were stimulated via a sharp microelectrode (2 ms depolarising current pulse at a frequency of 1 Hz.)

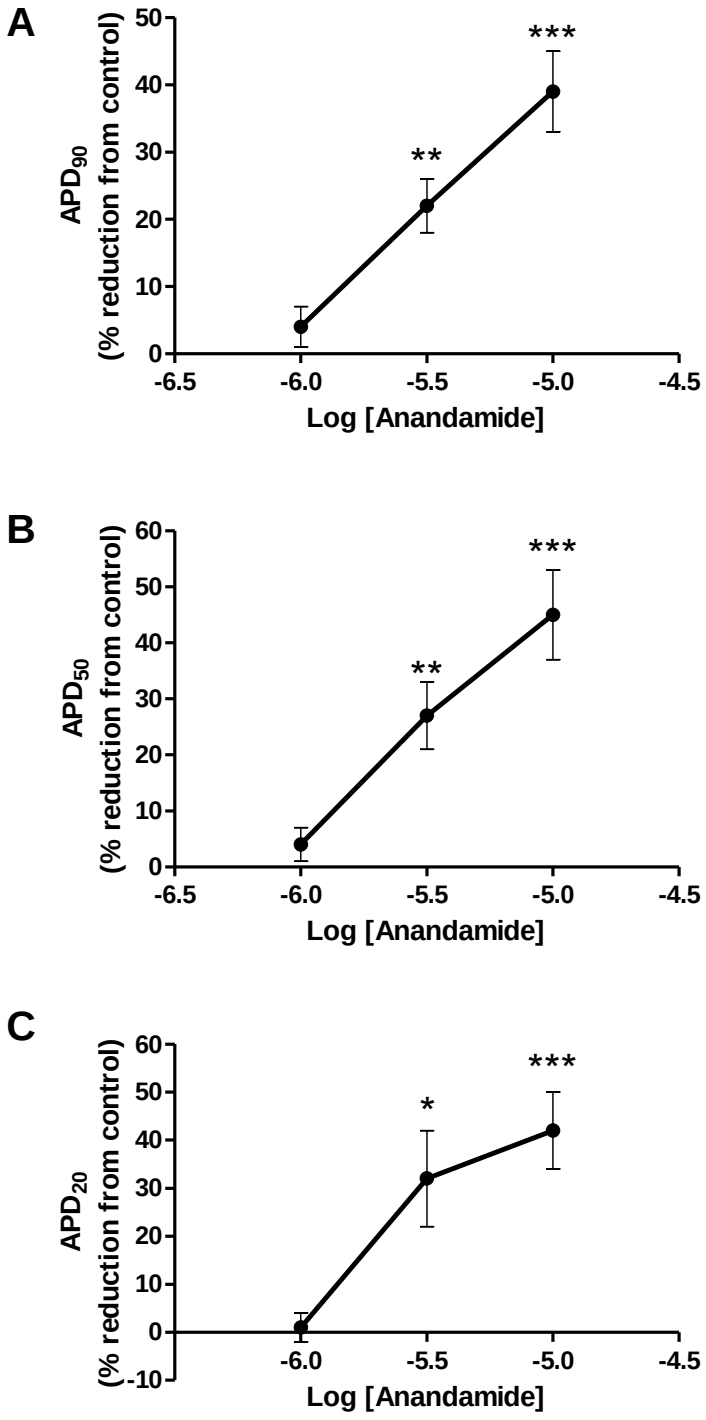


Figure 4.8 Concentration-dependent effects of anandamide on action potential duration

A: Action potential duration (APD) at 90% repolarisation. B: APD at 50% repolarisation. C: APD at 20% repolarisation. 1 µM anandamide was without significant effect on APD (n = 6, $P > 0.05$). Significant reductions in APD with both 3 and 10 µM anandamide were observed (n = 7 and 8 respectively). * denotes $P < 0.05$, ** denotes $P < 0.01$, *** denotes $P < 0.001$ vs control; repeated measures ANOVA with Dunnett's post-hoc test.

In a similar manner to the effects of anandamide on myocyte contractility measured using the Ionoptix system (see Figure 4.2), effects on APD were also concentration-dependent (see Figure 4.8). At a concentration of 3 μM, anandamide reduced APD_{90} by 22 ± 4 % and APD_{50} by 27 ± 6 % after 10 minutes (both n = 7, $P < 0.01$ for both values relative to control). APD_{20} was reduced by 34 ± 10 % (n = 7, $P < 0.05$ relative to control). 3 μM anandamide was without significant effect on RMP or peak amplitude of the AP (99 ± 1 % and 97 ± 1 % of control respectively; n = 7, $P > 0.05$). 1 μM anandamide was without significant effect on any of the AP parameters studied; after 10 minutes, APD_{90} was 96 ± 3 % of control values, APD_{50} was 96 ± 3 %, APD_{20} was 99 ± 5 % of control values, peak amplitude of the AP was 100 ± 0.4 % and RMP was 100 ± 1 % (n = 6, $P > 0.05$; data not shown).

4.3.4 The effects of anandamide on action potential duration and contraction were not due to breakdown to metabolic products

Anandamide is metabolised by FAAH to arachidonic acid and ethanolamine (Cravatt *et al.*, 1996). Since arachidonic acid itself has negative inotropic actions in isolated guinea pig ventricular myocytes (Mamas *et al.*, 2001), a metabolically stable analogue of anandamide, (*R*)-(+)-methanandamide (Abadji *et al.*, 1994) was used to investigate whether the effects of anandamide were occurring through breakdown to arachidonic acid or other metabolites. After 10 minutes superfusion of cells with 10 μM methanandamide, APD_{90} was reduced by 34 ± 6 %, APD_{50} was reduced by 37 ± 6 % and APD_{20} was reduced by 38 ± 6 % (n = 6, $P < 0.01$). The amplitude of contraction was also reduced by 54 ± 9 % (n = 6, $P < 0.01$). These values were not significantly different from those obtained in the presence of 10 μM anandamide ($P > 0.05$, Student's unpaired *t*-test), suggesting that the actions of anandamide were not occurring

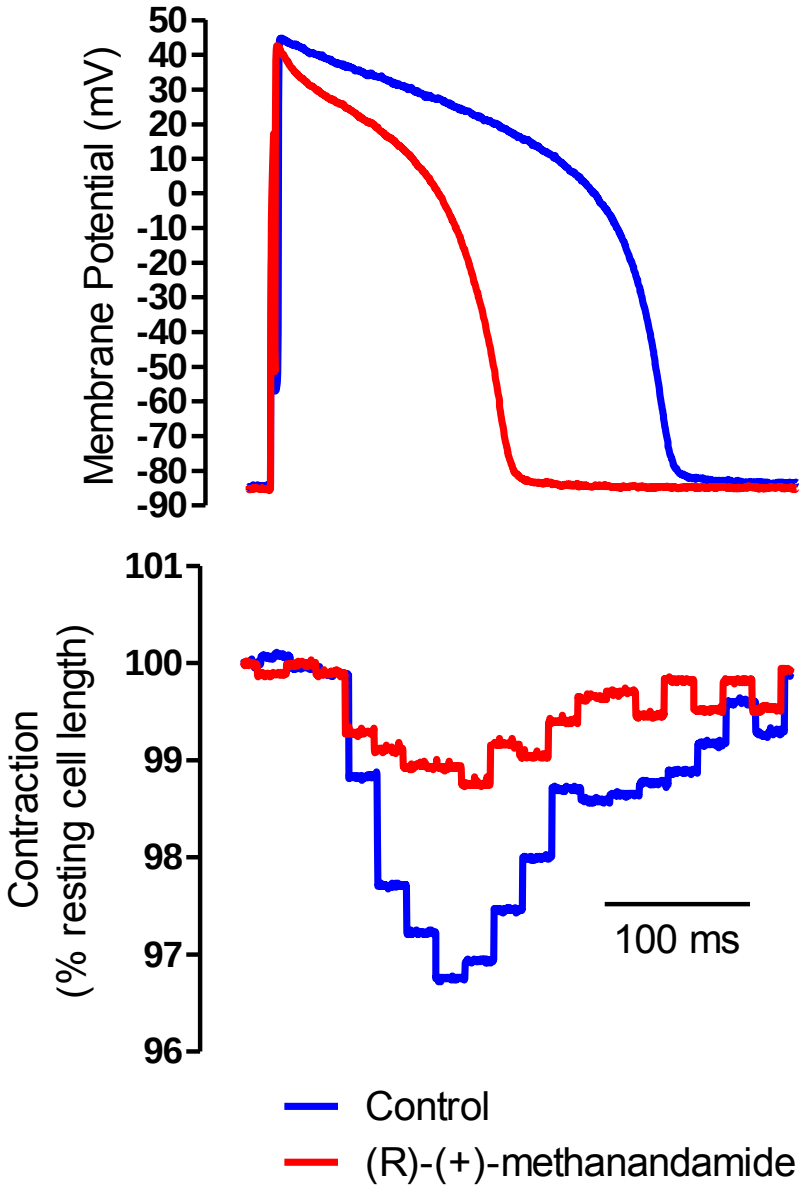


Figure 4.9 Representative action potential and contraction trace from a cell superfused with (R)-(+)-methanandamide

The cell was stimulated to fire action potentials by a 2 ms depolarising current pulse delivered by a sharp microelectrode (1 Hz). Contractions were measured using an edge-detection system. (Resolution was 20 ms per point, rather than 5 ms per point as with previous example for anandamide).

as a result of the actions of metabolic products. In a similar manner to anandamide, (*R*)-(+)-methanandamide was without significant effect on peak amplitude of the AP or RMP, which were 100 ± 1 % and 102 ± 1 % of control respectively (n = 6, $P > 0.05$). A representative AP and contraction trace is shown in Figure 4.9; these recordings were obtained using a sharp glass microelectrode and the edge detection system to measure cell length.

4.3.5 Anandamide inhibited L-type Ca^{2+} currents (I_{CaL})

The observation that anandamide reduced APD, together with a reduction in the amplitude of the Ca^{2+} transient and contraction, is consistent with an action of anandamide to inhibit L-type Ca^{2+} currents (I_{CaL}). The 'switched' voltage clamp technique was used to investigate the effects of anandamide on I_{CaL}, initially with a sharp microelectrode. Two methods were used to determine I_{CaL} amplitude: 1) the peak current was deducted from the holding current, and 2) the peak current was deducted from the current at the end of the step depolarisation. The holding current is largely dictated by fluxes of K^+ through I_{K1} channels which are important in maintaining RMP. The current at the end of the depolarising pulse is influenced by various K^+ currents and also NCX. Therefore, there are arguments for measuring Ca^{2+} current amplitude using both methods. After 10 minutes superfusion with 10 µM anandamide, I_{CaL} amplitude at 0 mV (measured as peak current subtracted from holding current) was reduced by 42 ± 8 % of control (n = 7, $P < 0.001$); when measured as peak current subtracted from the current at the end of the pulse, this value was 36 ± 7 % (n = 7, $P < 0.001$). These effects are shown in Figure 4.10a,b; current voltage relationships are shown in Figure 4.11.

In vehicle control experiments, 0.07 % ethanol was without significant effect on amplitude of I_{CaL}; peak current at 0 mV was 106 ± 4 % of control after 10 minutes

(measured as peak current subtracted from holding current; Figure 4.10A), and 100 ± 7 % (measured as peak current subtracted from current at the end of the pulse; n = 5, $P > 0.05$; Figure 4.10B). Current voltage relationships are shown in Figure 4.12.

As was observed in previous experiments, the effect of anandamide to reduce amplitude of I_{CaL} was slow to develop over a 10 minute time-period (Figure 4.10A,B). Superfusion of cells with 10 μM anandamide also resulted in the current at the end of the pulse becoming more outward in comparison to ethanol vehicle (Figure 4.10C), but there were no clear effects on holding current (Figure 4.10D). A representative Ca^{2+} current trace is shown in Figure 4.13A. Analysis of the time to 50% decay of I_{CaL} showed a reduction in the presence of anandamide from 24 ± 6 ms to 12 ± 3 ms (n = 7, $P < 0.05$; Figure 4.13B). Ethanol vehicle was without significant effect on time to 50 % decay of I_{CaL} (22 ± 6 ms under control conditions, 21 ± 4 ms after 10 minutes superfusion with ethanol; n = 5, $P > 0.05$).

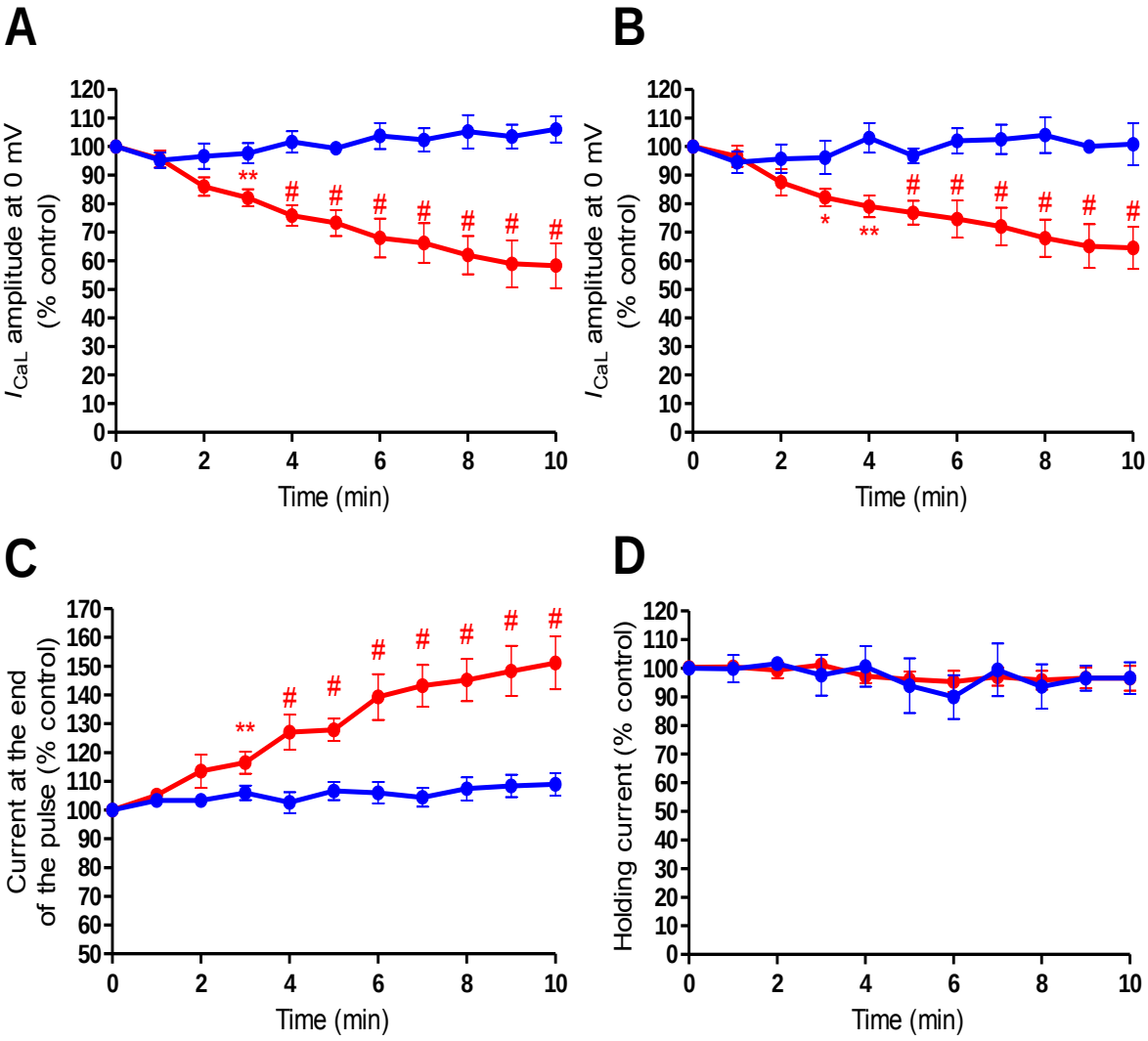


Figure 4.10 Effects of anandamide on I_{CaL} parameters over time

Currents were measured using a sharp microelectrode ('switched' voltage clamp), 200 ms step depolarisations from -40 to 0 mV.
A: Amplitude of I_{CaL} measured as peak current deducted from holding current. B: Amplitude of I_{CaL} measured as peak current deducted from current at the end of the pulse. C: Current at the end of the pulse. D: Holding current.
A significant reduction in amplitude of peak inward current was observed with anandamide (n = 7), as a well as a significant enhancement in the outward direction of the current at the end of the pulse. * denotes $P < 0.05$, ** denotes $P < 0.01$, # denotes $P < 0.001$ vs control; repeated measures ANOVA with Dunnett's post-hoc test. Ethanol vehicle (n = 5) was without significant effect on any I_{CaL} parameters.

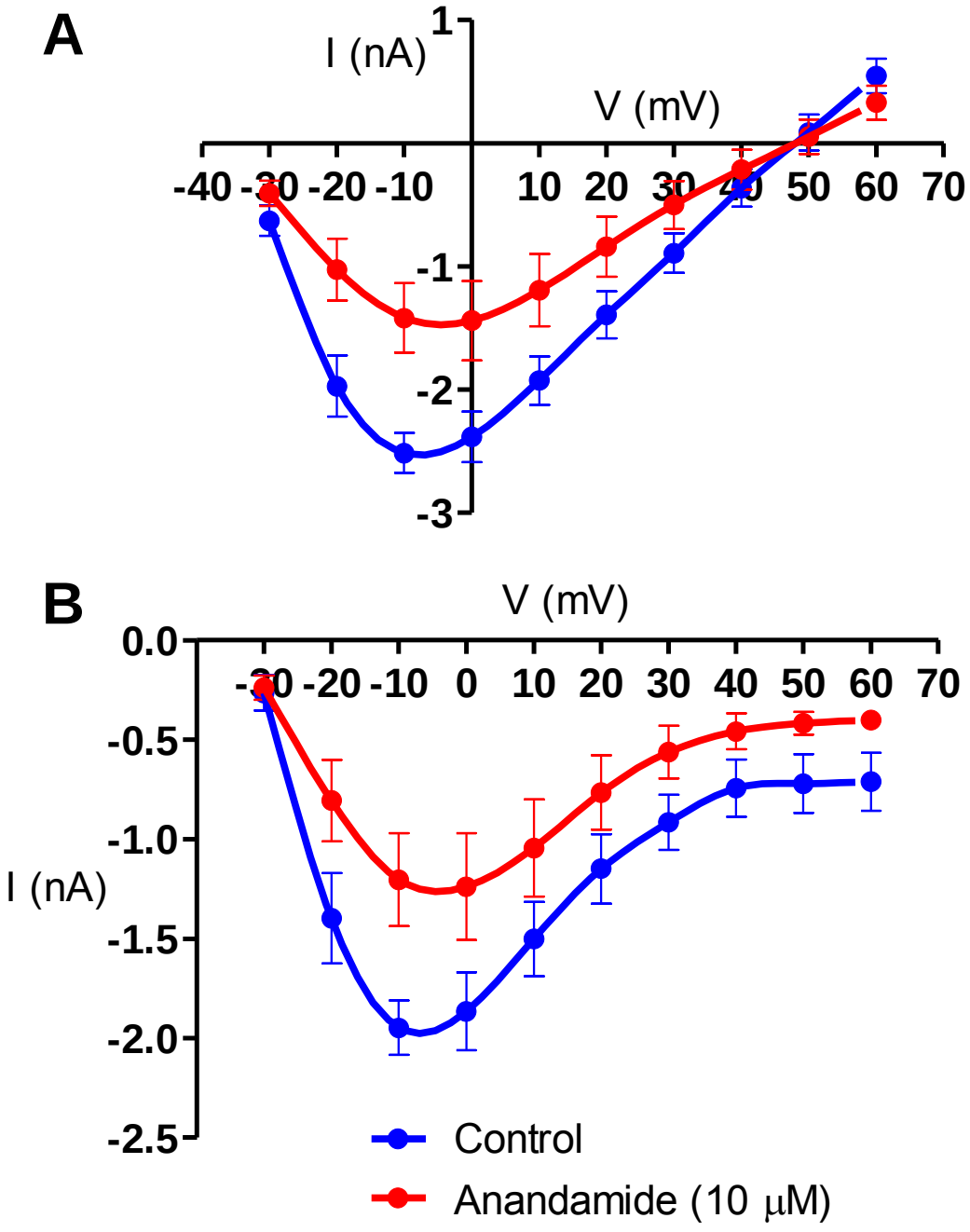


Figure 4.11 Effects of anandamide on current voltage relationship for I_{CaL}

A: Current voltage relationship measured as peak current deducted from holding current.
B: Current voltage relationship measured as peak current deducted from the current at the end of the pulse.

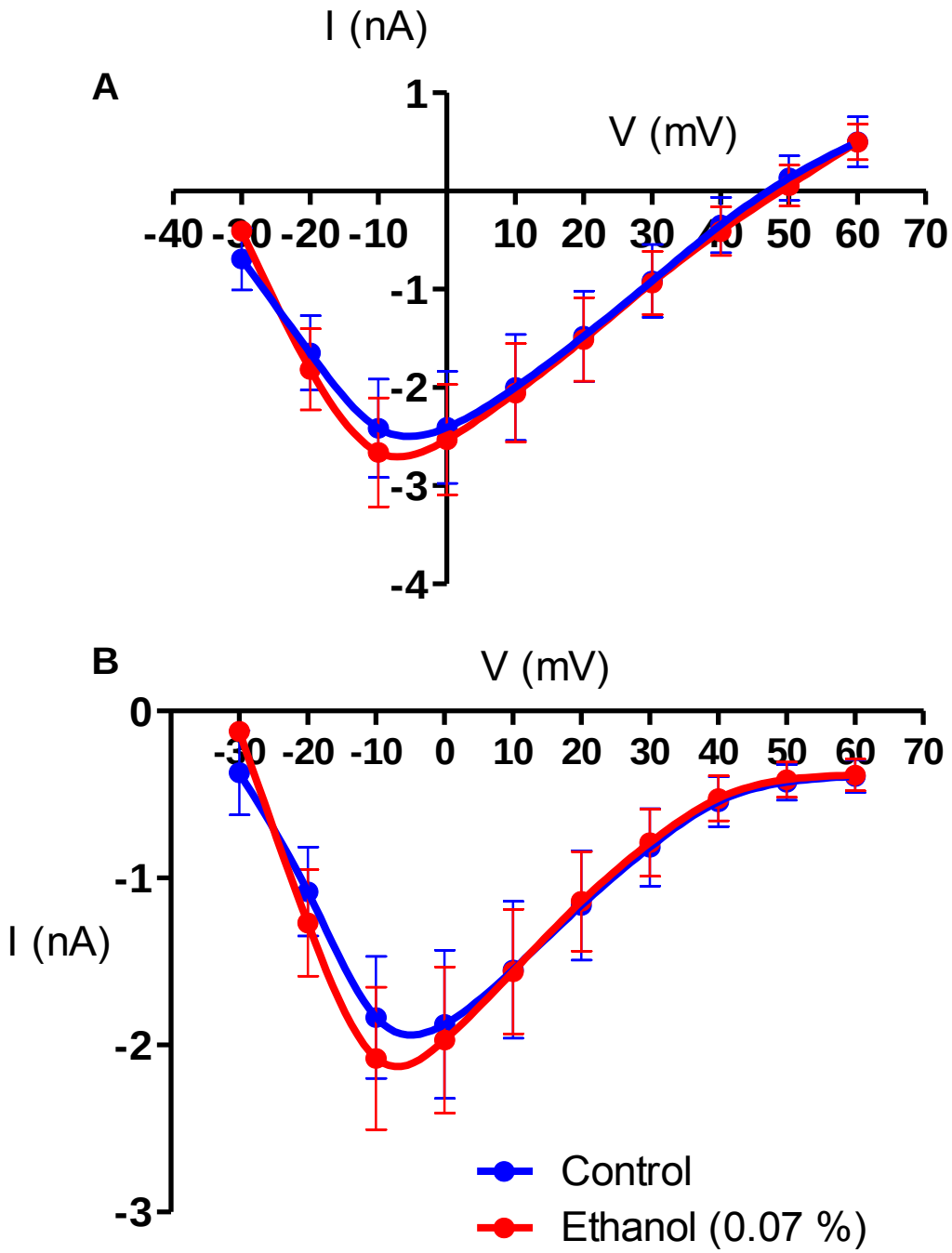


Figure 4.12 Effect of 0.07 % ethanol on current voltage relationship for I_{CaL}

A: Measured as peak current less holding current.
B: Measured as peak current deducted from the current at the end of the pulse

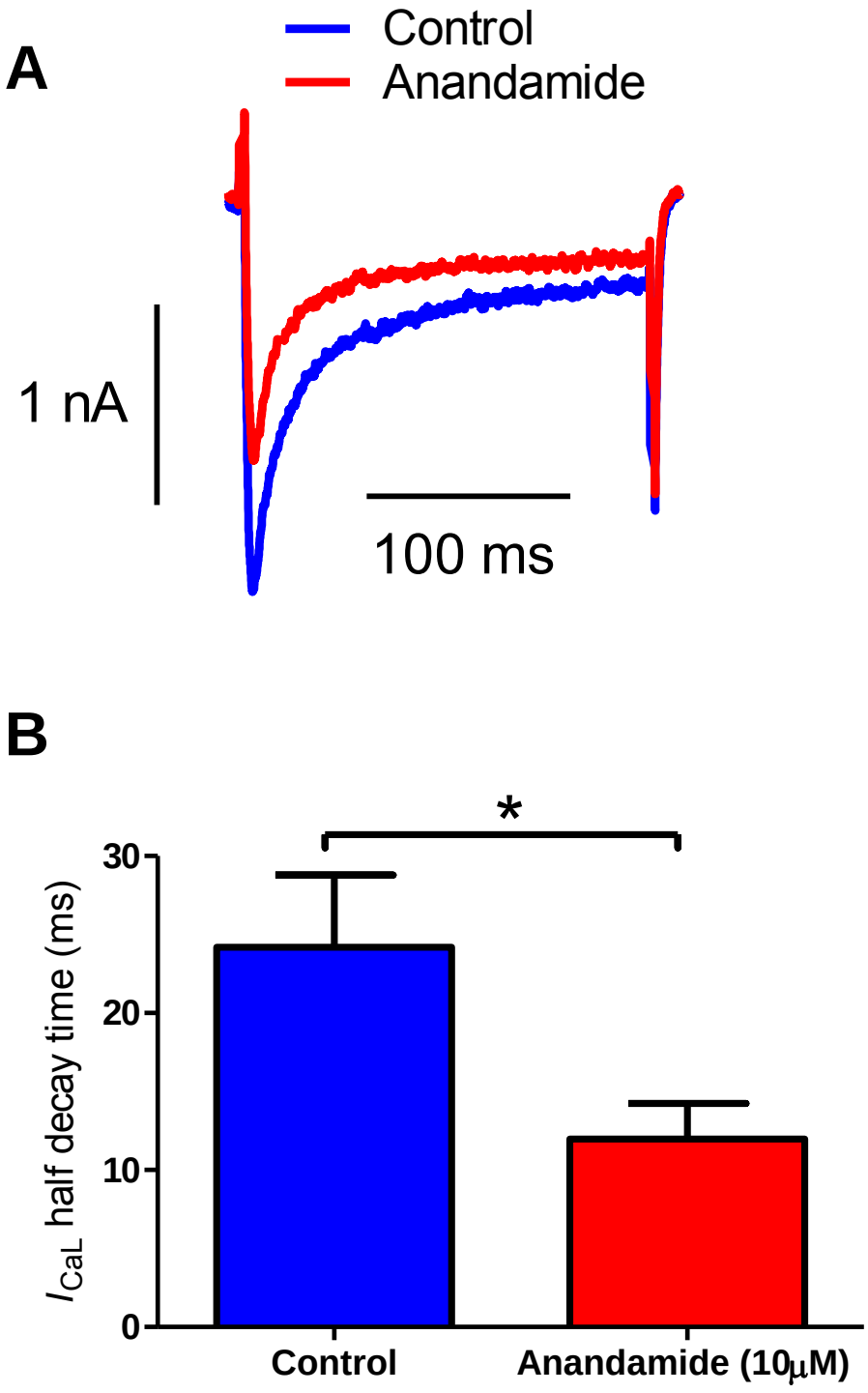


Figure 4.13 Effects of anandamide on I_{CaL} properties

A: Representative trace showing effects of anandamide on I_{CaL} elicited by 200ms step depolarisations from -40 to 0 mV ('switched' voltage clamp).
B: Anandamide reduced 50 % decay time of I_{CaL} (n = 7, $P < 0.05$, Student's paired *t*-test.

4.3.6 Anandamide accelerated inactivation of the L-type Ca^{2+} channel

In order to shed more light on the mechanism by which anandamide may be acting to reduce amplitude of I_{CaL}, further investigations into possible effects on the voltage-dependence of channel inactivation were carried out. These experiments were carried out using a double-pulse protocol delivered via a patch electrode containing Cs^+ in the whole-cell configuration. Because whole-cell patch experiments are sometimes associated with I_{CaL} rundown, time control experiments were first performed with 0.07 % ethanol vehicle. Under these conditions, there was a reduction in amplitude of I_{CaL} at 0 mV of 23 ± 5 % after 10 minutes (n = 5, $P < 0.05$; Figure 4.14). However, there were no significant effects on voltage-dependence of inactivation of I_{CaL} (Figure 4.15 and Figure 4.16). Given this apparent rundown of I_{CaL} under these conditions, it was decided that a correction factor (see section 2.4.7, chapter 2) to account for this should be applied to subsequent experiments with anandamide. Figure 4.17A shows the current voltage relationship under these conditions without application of a correction factor, and Figure 4.17B shows current voltage relationship after application of a correction factor of 1.32, which was calculated based upon a linear decay of I_{CaL} of 2.3 % per minute. The amplitude of I_{CaL} (measured as peak current deducted from the current at the end of the pulse) was reduced by 47 ± 8 % after 10 minutes superfusion with 10 µM anandamide (after application of the correction factor, n = 6, $P < 0.001$); current voltage relationships are shown in Figure 4.17. This is comparable to the 42 ± 8 % reduction in I_{CaL} amplitude observed when cells were impaled with a sharp microelectrode. In addition, after superfusion with anandamide in the presence of Cs^+ the voltage-dependence of

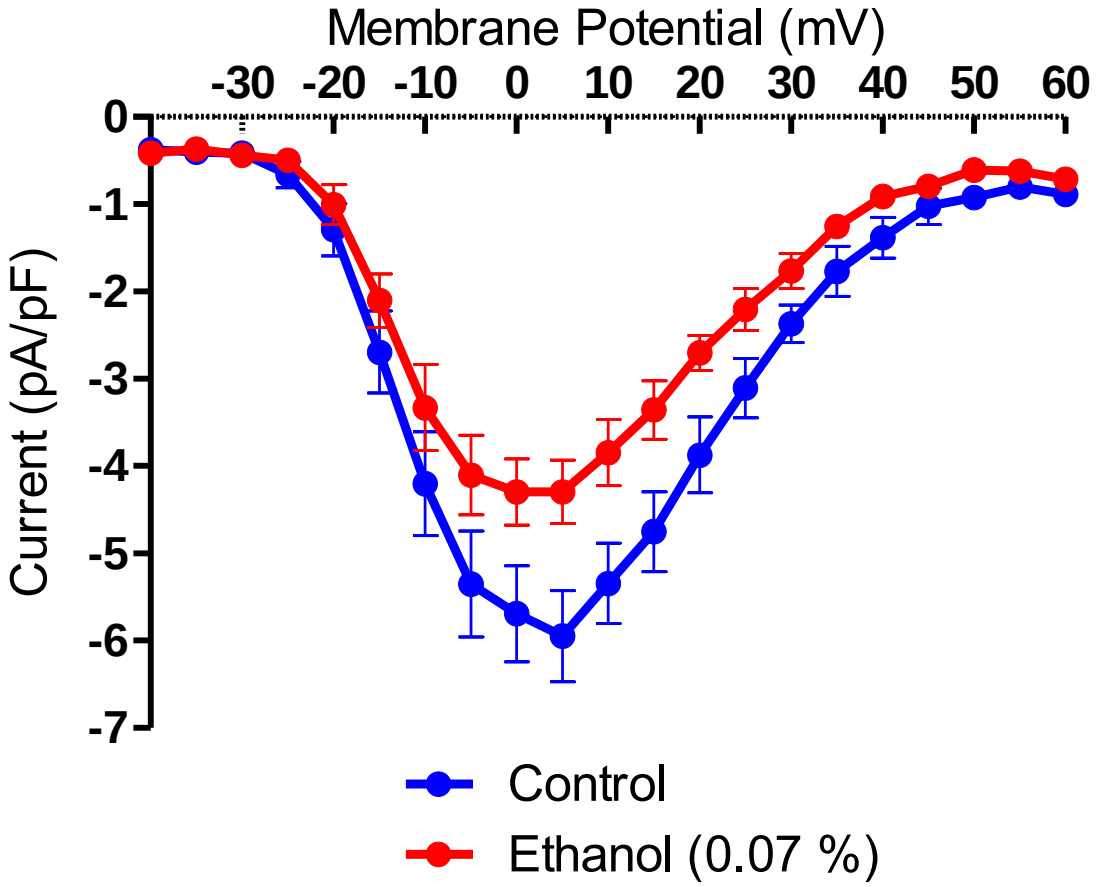


Figure 4.14 Effects of ethanol on I_{CaL} current voltage relationship in the presence of Cs^+

A 200ms test pulse from -40 to 0 mV was applied at 5 mV increments from -40 to + 60 mV; the amplitude of I_{CaL} during the test pulse is plotted as peak current less current at the end of the pulse. The amplitude of I_{CaL} at 0 mV was reduced by 23 ± 5 % (n = 5, $P < 0.05$, Student's paired *t* test).

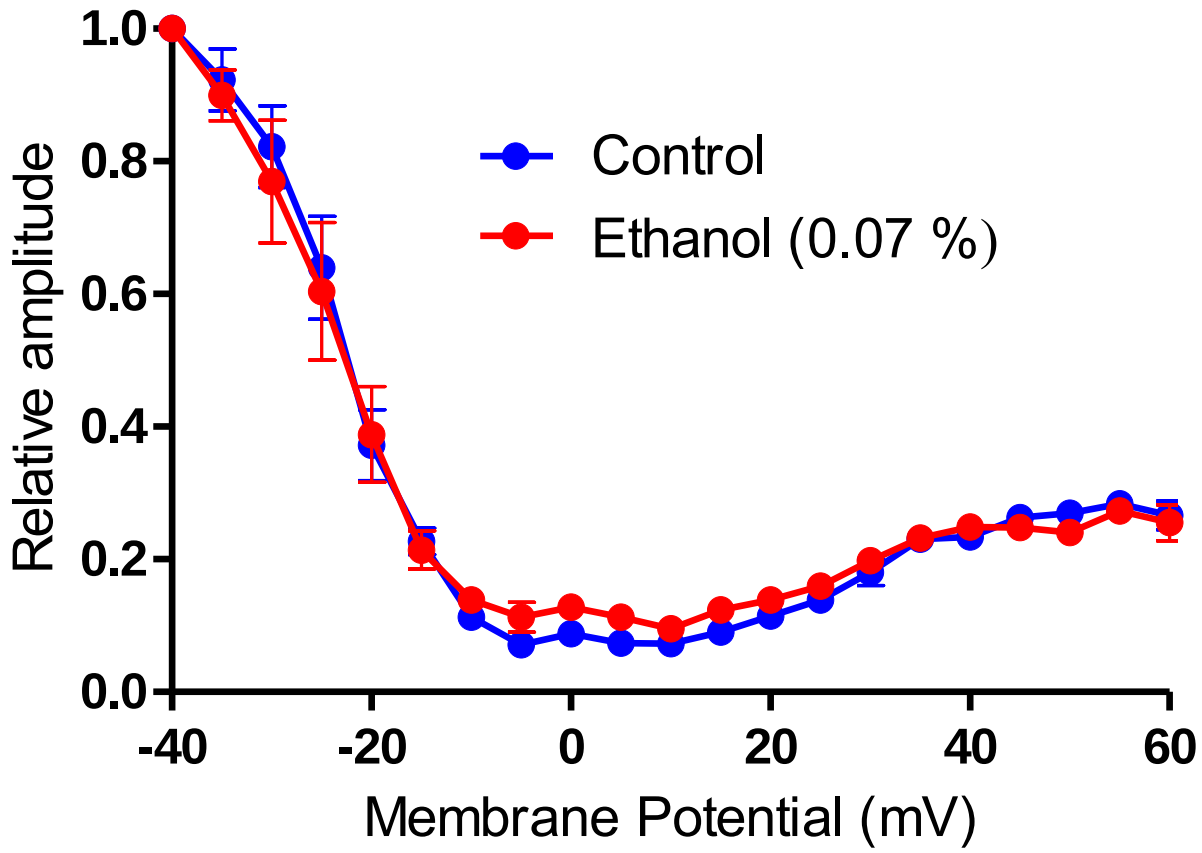


Figure 4.15 Effects of ethanol on voltage-dependence of inactivation of I_{CaL} in the presence of Cs^+.

Inactivation was assessed by a double-pulse protocol delivered via a patch electrode containing Cs^+. A 200ms test pulse from -40 to 0 mV was applied 10ms after a 500ms conditioning 'pre-pulse' applied at 5 mV increments from -40 to + 60 mV; the amplitude of I_{CaL} during the test pulse is plotted as a fraction of its value in the absence of the pre-pulse. $P > 0.05$ at all potentials, ethanol vs control, one-way ANOVA with Bonferroni post-hoc test, n = 5.

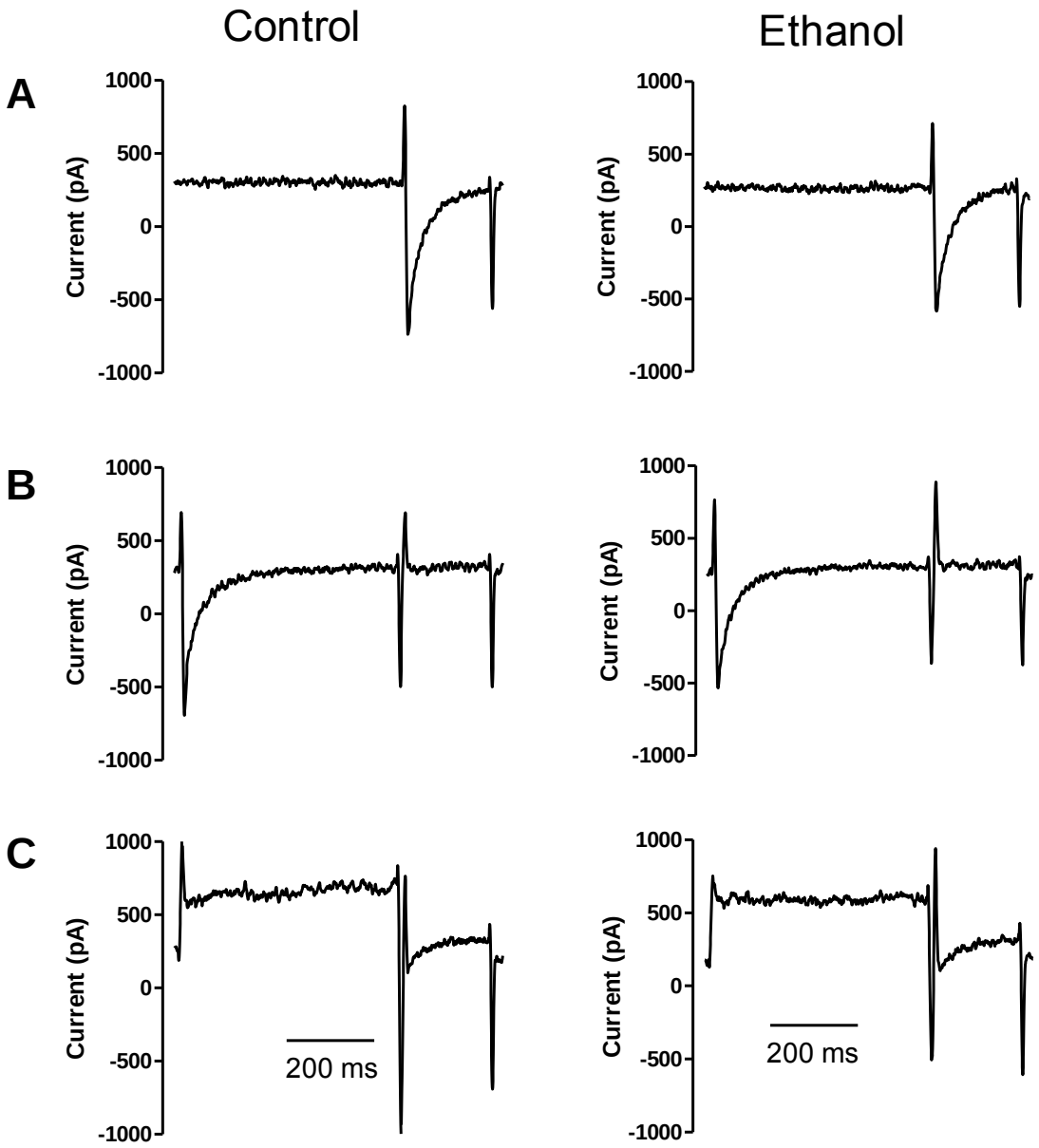


Figure 4.16 Representative traces showing the effects of ethanol on inactivation of I_{CaL} assessed by a double-pulse protocol delivered via a patch electrode containing Cs^+.

Traces on the left were recorded in control, and on the right, after 10 minutes superfusion with 0.07% ethanol. Panel A: prepulse to -40 mV; panel B: prepulse to 0 mV; panel C: prepulse to +40 mV.

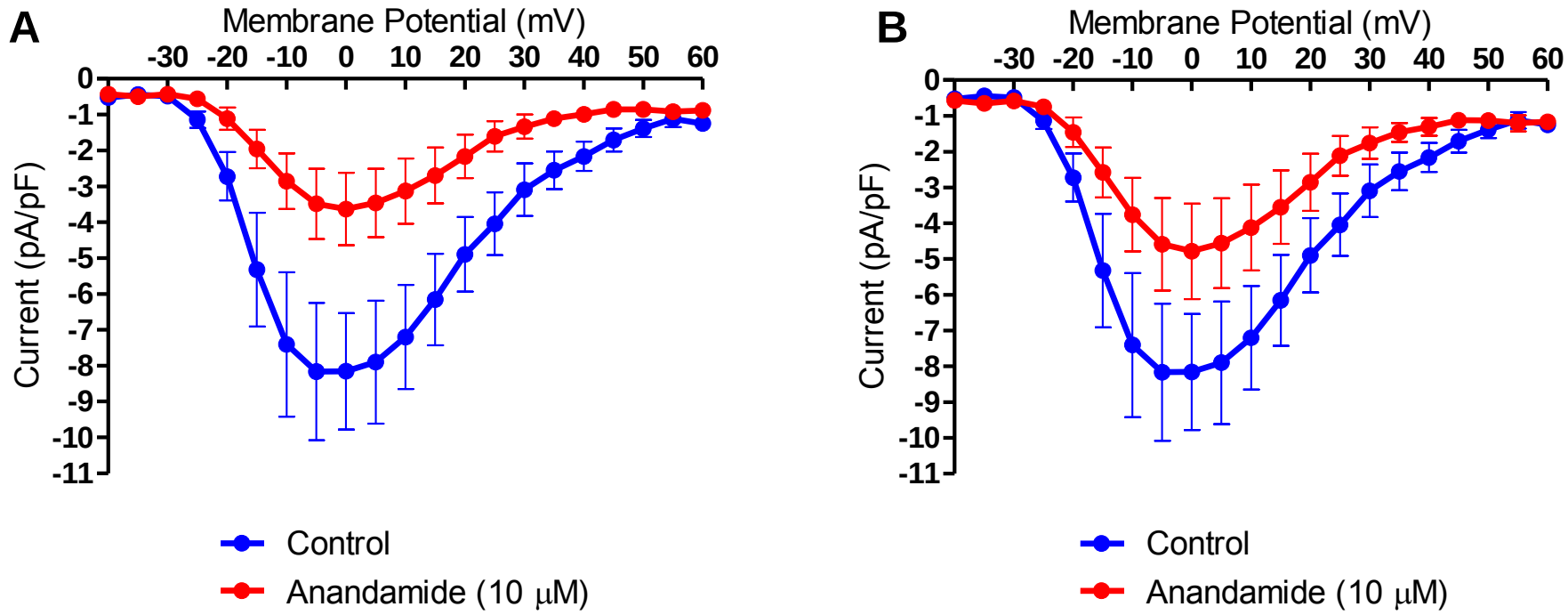


Figure 4.17 Effect of anandamide on I_{CaL} current voltage relationship in the presence of Cs^+

A 200ms test pulse from -40 to 0 mV was applied at 5 mV increments from -40 to + 60 mV; the amplitude of I_{CaL} during the test pulse is plotted as peak current less current at the end of the pulse. A: Current voltage relationship before and after superfusion with anandamide for 10 minutes, without application of a correction for rundown. The apparent reduction in I_{CaL} amplitude at 0 mV was 60 ± 7 % (n = 6, P < 0.001) B: Current voltage relationship with application of a correction for rundown. I_{CaL} amplitude at 0 mV was reduced by 47 ± 8 % (n = 6, P < 0.001).

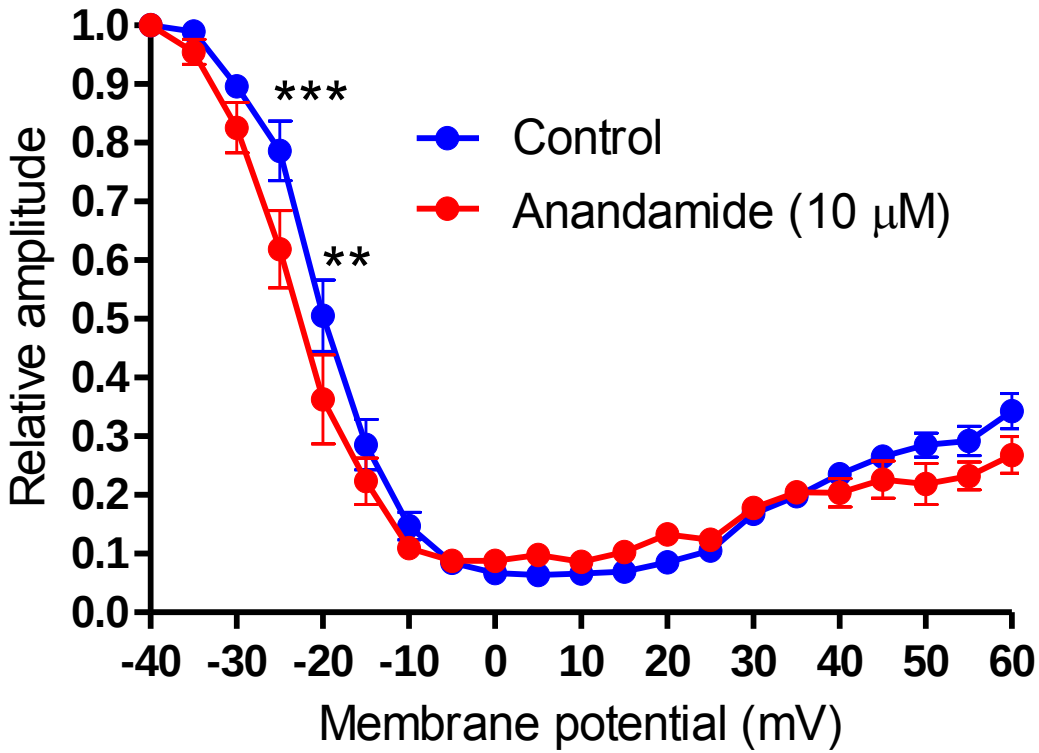


Figure 4.18 Effects of anandamide on voltage-dependence of inactivation of I_{CaL} in the presence of Cs^+

Inactivation was assessed by a double-pulse protocol delivered via a patch electrode containing Cs^+. A 200ms test pulse from -40 to 0 mV was applied 10ms after a 500ms conditioning 'pre-pulse' applied at 5 mV increments from -40 to + 60 mV; the amplitude of I_{CaL} during the test pulse is plotted as a fraction of its value in the absence of the pre-pulse. ** denotes $P < 0.01$, *** denotes $P < 0.001$, anandamide vs control, one-way ANOVA with Bonferroni post-hoc test, n = 5.

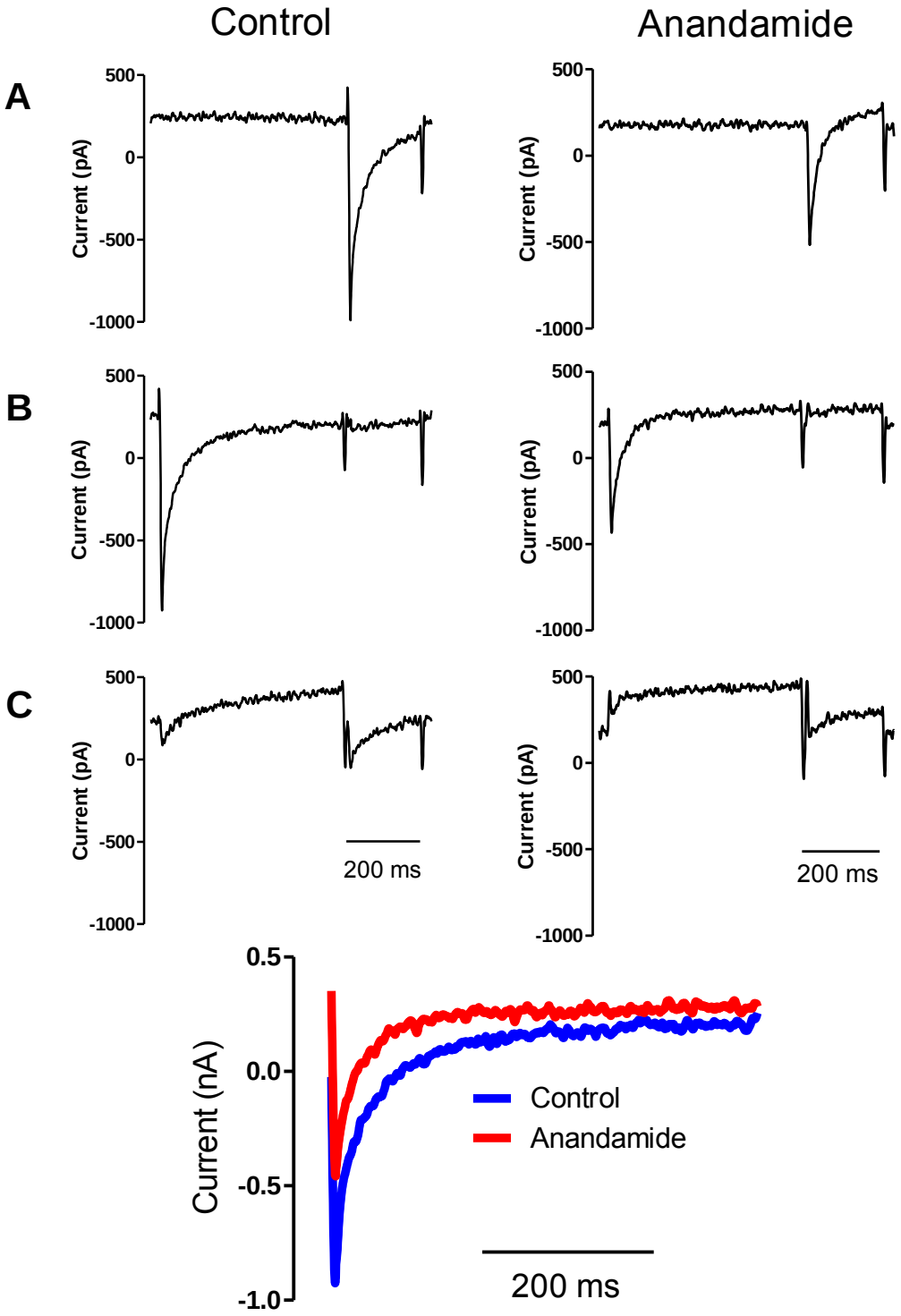


Figure 4.19 Representative traces showing the effects of anandamide on inactivation of I_{CaL} assessed by a double-pulse protocol delivered via a patch electrode containing Cs^+.

Traces on the left were recorded in control, and on the right, after 10 minutes superfusion with anandamide. Panel A: prepulse to -40 mV; panel B: prepulse to 0 mV; panel C: prepulse to +40 mV.

inactivation curve was shifted to the left (Figure 4.18; representative traces in Figure 4.19), providing evidence of an acceleration of the kinetics of LTCC inactivation in the presence of anandamide.

4.3.7 Anandamide inhibited the slowly activating (I_{Ks}) but not the rapidly activating component (I_{Kr}) of the delayed rectifier K^+ current (I_K).

The delayed rectifier K^+ current is crucial in initiating repolarisation of the AP and thus determines APD. A shortening of the AP in response to anandamide could be occurring in part due to an enhancement of outward $I_{K,}$ hastening repolarisation. This hypothesis would also be consistent with the enhancement in current at the end of the pulse in I_{CaL} experiments mentioned previously (Figure 4.10c), although it should be noted that other currents, particularly NCX would also influence the amplitude of this outward current.

In the guinea pig ventricle, I_K can be separated both pharmacologically and kinetically into its slowly and rapidly activating components, I_{Kr} and I_{Ks} (Sanguinetti *et al.*, 1990). Two methods were used to study the effects of anandamide on the different components of I_K. Initially, separation of I_{Kr} and I_{Ks} was achieved by application of depolarising current pulses from -40 mV to +40 mV of varying durations, exploiting differences in the kinetics of activation of I_{Kr} and $I_{Ks,}$ where tail currents after rapid depolarisations (10 – 100ms) comprise mainly I_{Kr}, while those at longer depolarisations are largely $I_{Ks.}$ Figure 4.20 shows a representative family of tail currents before and after superfusion with anandamide, and Figure 4.21 shows the mean effects of 10 µM anandamide on amplitude of tail currents after depolarisations of 10 – 600 ms. The amplitude of the tail current at 600 ms (which would be thought to consist almost

entirely of I_{Ks} (Heath *et al.*, 1996)) was reduced by 41 ± 7 % after 10 minutes superfusion with anandamide (n = 6, $P < 0.05$), while there were no significant effects on tail currents after shorter depolarisations of 100 ms or less (Figure 4.21). Ethanol vehicle was without significant effect on tail currents occurring after depolarisations of any duration (n = 6, $P > 0.05$; Figure 4.22 and Figure 4.23). These observations would be consistent with an inhibitory effect of anandamide on I_{Ks} but not I_{Kr}.

In order to further test this observation, the aforementioned protocol was repeated in the presence of 1 µM E4031 to block I_{Kr} pharmacologically as has been demonstrated previously (Sanguinetti *et al.*, 1990; Heath *et al.*, 1996). Figure 4.24 shows that in the presence of E4031, tail currents generated by depolarisations from 10 – 100 ms were almost completely abolished in the presence of E4031, while those at longer depolarisations remain. Subsequent superfusion of cells with anandamide in the continued presence of E4031 resulted in a reduction in amplitude of the remaining tail currents (which would be expected to consist of I_{Ks} exclusively). The amplitude of the tail current after a 400 ms depolarisation was reduced by 38 ± 8% from the current observed in the presence of E4031 alone (n = 6, $P < 0.01$).

4.3.8 The effects of anandamide did not appear to be mediated by conventional cannabinoid receptors

In order to determine whether the observed effects of anandamide could be attributed to actions at cannabinoid CB_1 and/or CB_2 receptors, APs and contractions were recorded in the presence of the CB_1 receptor antagonist AM 281 (1 µM) and the CB_2 receptor antagonist AM 630 (1 µM). In all antagonist experiments, cells were

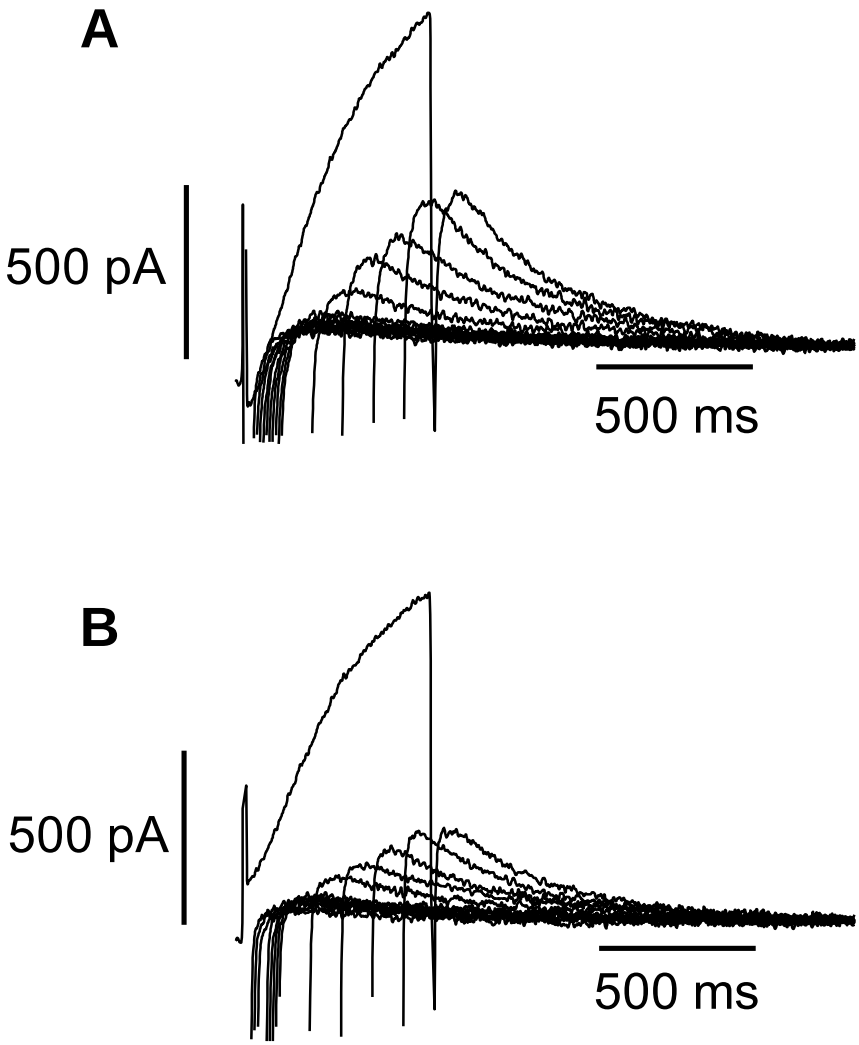


Figure 4.20 Representative traces showing the effects of anandamide on I_K.

I_K was measured as the amplitude of the tail current generated after application of depolarising current pulses from -40 to + 40 mV of varying durations from 10 – 600 ms ('switched' voltage clamp). These traces depict tail currents after steps of all durations. The outward current occurring during the depolarising step of 600 ms is also shown. A: Tail currents occurring in control. B: Tail currents after 10 minutes superfusion with anandamide.

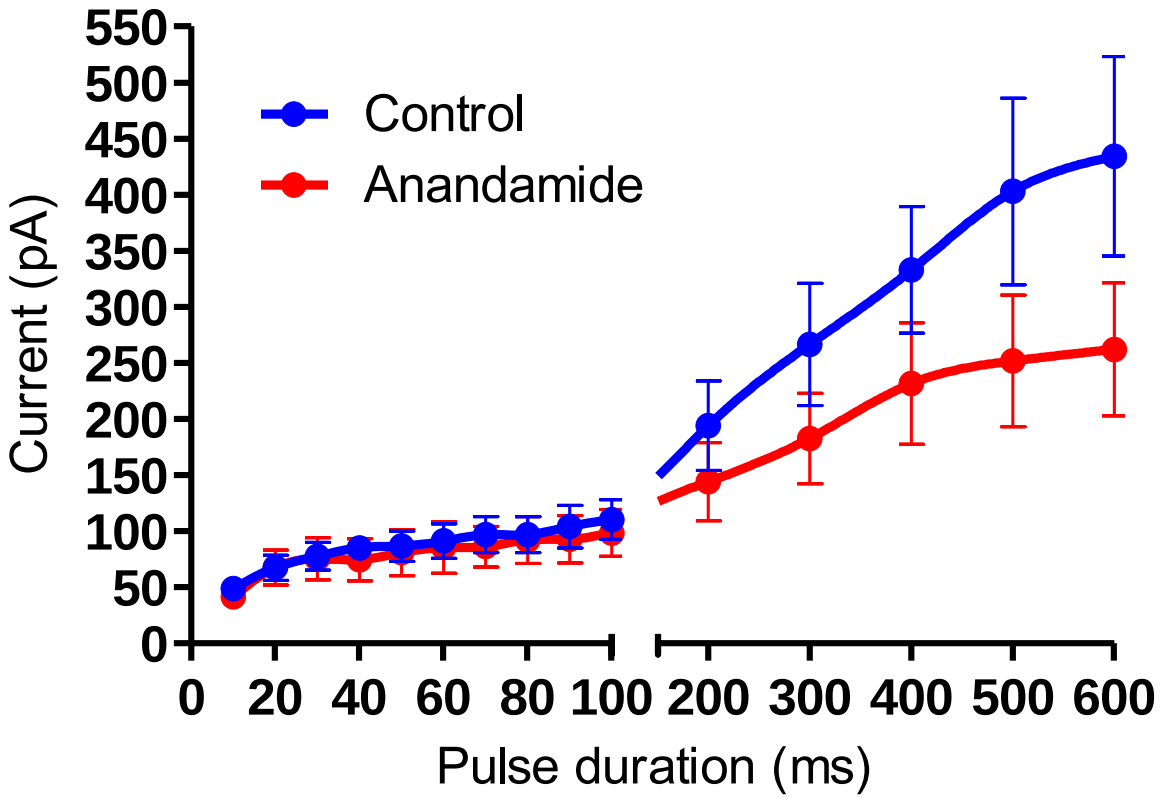


Figure 4.21 Effects of anandamide on I_K.

I_K was measured as the amplitude of the tail current generated after application of depolarising current pulses from -40 to + 40 mV of varying durations from 10 – 600 ms ('switched' voltage clamp). Anandamide reduced amplitude of the tail current at 600 ms was by 41 ± 7 % (n = 6, $P < 0.05$; one-way ANOVA with Bonferroni post-hoc test), but was without significant effect on tail currents generated by shorter duration depolarisations ($P > 0.05$).

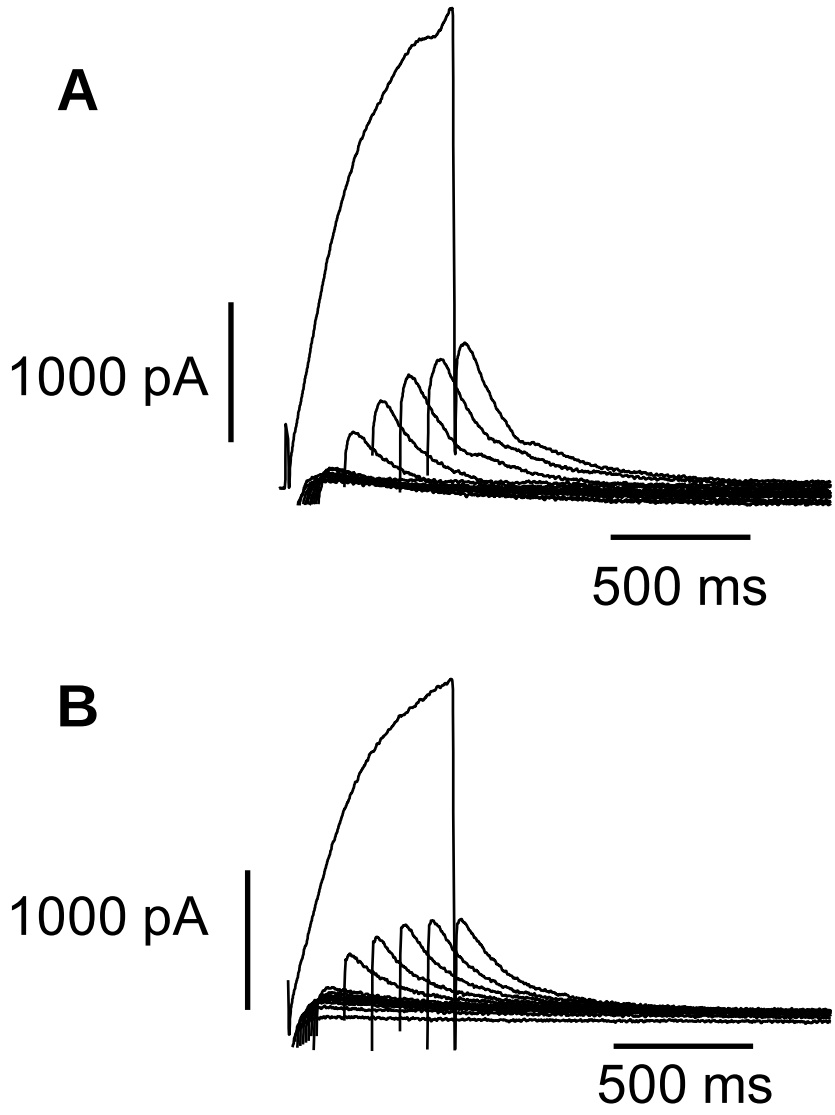


Figure 4.22 Representative traces showing the effects of ethanol on I_K.

I_K was measured as the amplitude of the tail current generated after application of depolarising current pulses from -40 to + 40 mV of varying durations from 10 – 600 ms ('switched' voltage clamp). These traces depict tail currents after steps of all durations. The outward current occurring during the depolarising step of 600 ms is also shown. A: Tail currents occurring in control. B: Tail currents after 10 minutes superfusion with ethanol.

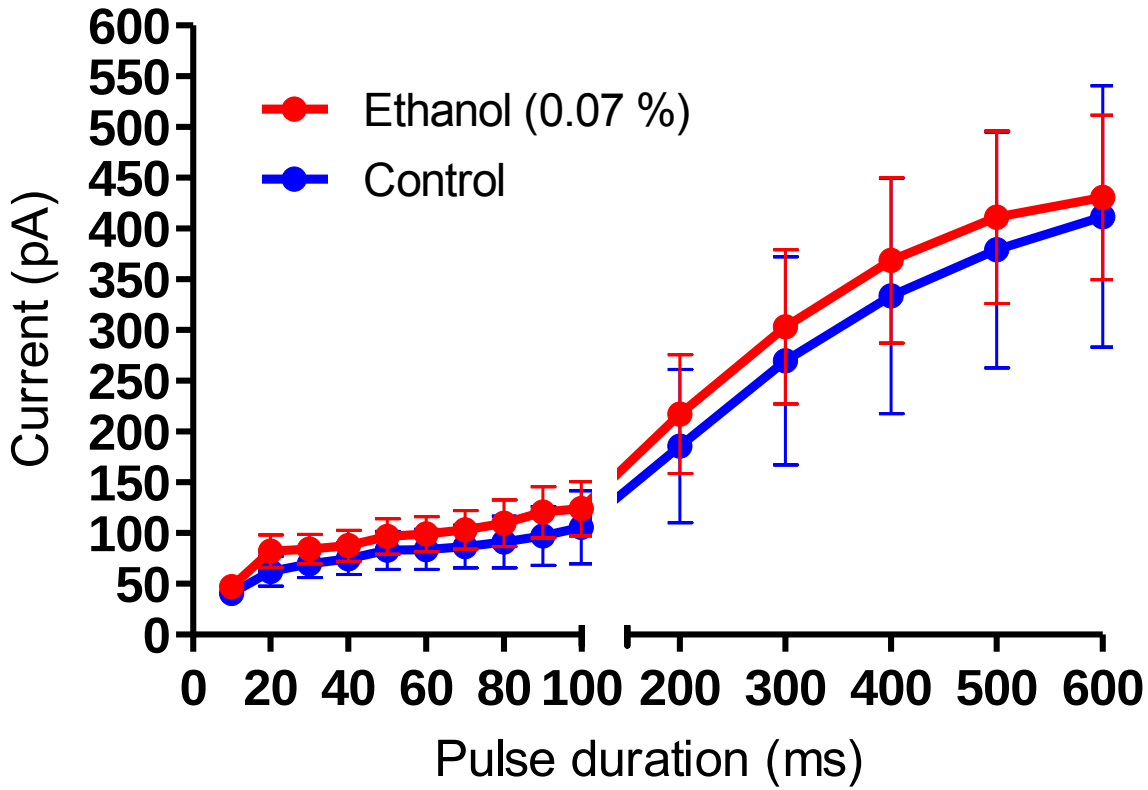


Figure 4.23 Effects of ethanol vehicle on I_K.

I_K was measured as the amplitude of the tail current generated after application of depolarising current pulses from -40 to + 40 mV of varying durations from 10 – 600 ms ('switched' voltage clamp). Ethanol was without significant effect on tail currents (n = 6, P > 0.05; one-way ANOVA with Bonferroni post-hoc test).

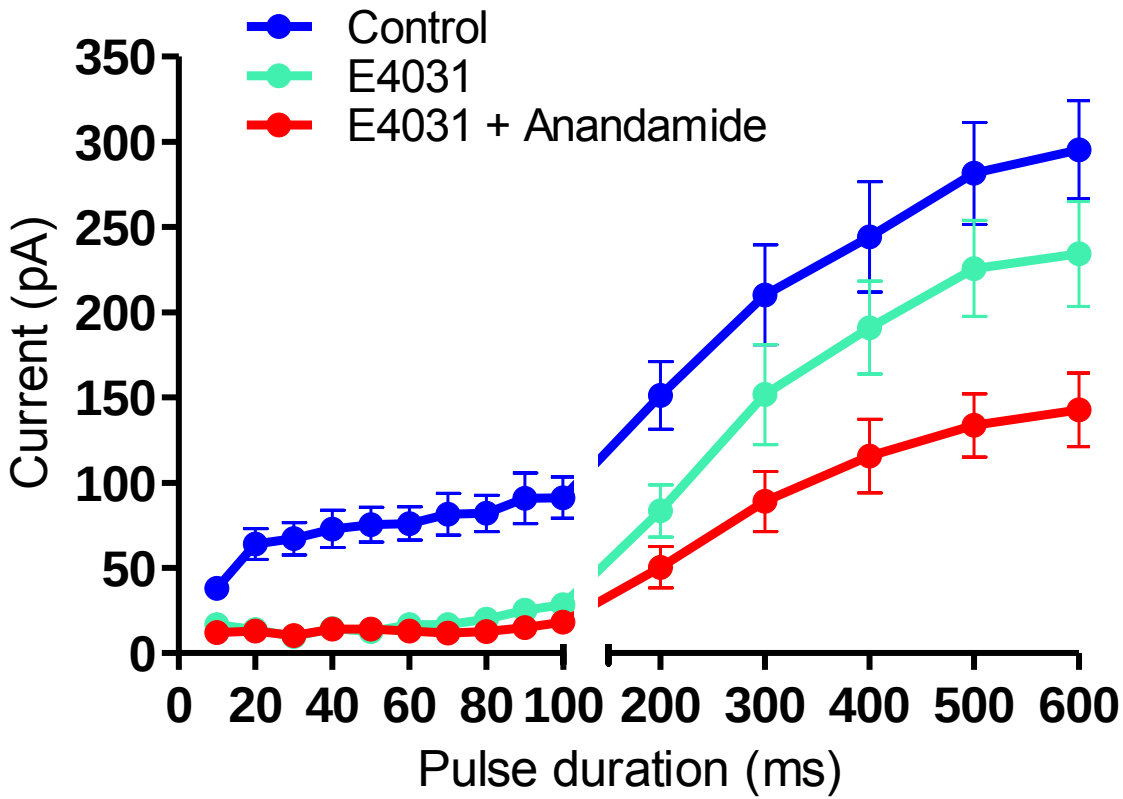


Figure 4.24 Effects of anandamide on I_{Ks}.

I_K was measured as the amplitude of the tail current generated after application of depolarising current pulses from -40 to + 40 mV of varying durations from 10 – 600 ms ('switched' voltage clamp). Cells were initially superfused with 1 µM E4031 to inhibit I_{Kr}; this is evident as a reduction in tail current amplitude after shorter prepulses (10 – 100ms). Subsequent superfusion of cells with anandamide in the continued presence of E4031 reduced amplitude of the tail currents after longer depolarisations. Tail current after a 400 ms depolarisation was by 38 ± 8 % (n = 6, $P < 0.01$; one-way ANOVA with Bonferroni post-hoc test). ** denotes $P < 0.01$ (** in blue denotes control vs E4031), # denotes $P < 0.001$ control vs E4031, *** denotes $P < 0.001$ E4031 vs anandamide + E4031.

superfused with the antagonist of interest alone for 5 minutes prior to superfusion with anandamide (10 μM) in the continued presence of the antagonist. Both AM 281 and AM 630 (1 μM) were without significant effect on any AP parameters or amplitude of contraction relative to control during 5 minutes of superfusion prior to anandamide.

Figure 4.25 shows that in the presence of 1 μM AM 281, superfusion of cells with 10 μM anandamide for 10 minutes resulted in a reduction in the amplitude of contraction of 69 ± 7 % (n = 4, $P < 0.001$) that was slow to develop, and was similar in magnitude to the reduction seen with anandamide alone after 10 minutes (see Figure 4.2). AM 281 also failed to prevent the effects of anandamide on AP duration: APD_{90} was reduced by 41 ± 7 % (relative to values at the end of the 5 minute AM 281 superfusion period), APD_{50} by 48 ± 7%, and APD_{20} by 51 ± 7 % (n = 6, $P < 0.01$; Figure 4.26a-c); anandamide was again without significant effect on peak amplitude of the AP or RMP (n = 6, $P > 0.05$; Figure 4.26d,e).

To establish concentration response-relationships, AP measurements were also made with 3 μM anandamide in the presence of AM281. AM 281 failed to prevent the AP shortening effects of 3 μM anandamide; concentration response relationships are shown in Figure 4.27.

When cells were superfused with 10 μM anandamide in the presence of the CB_2 receptor antagonist AM 630 (1 μM), amplitude of contraction was reduced by 52 ± 8 % (n = 5, $P < 0.001$; Figure 4.28). APD_{90} was reduced by 30 ± 3 % of control values, APD_{50} was reduced by 32 ± 4 % and APD_{20} by 34 ± 5 % (n = 8, $P < 0.01$; Figure 4.29). AP parameters were also measured when cells were superfused with 3 μM anandamide in the presence of 1 μM AM 630 (n = 7); concentration response relationships are shown in Figure 4.30. The effects of anandamide in the presence of AM 630 were not significantly different to those seen with anandamide in the absence of AM 630 ($P <$

0.05), but there did appear to be a trend towards a suppression of the effects of anandamide. In order to investigate whether a more complete inhibition of the response could be observed with longer exposure of cells to the antagonist, a second set of experiments was carried out in which cells were pre-incubated with 1 μM AM 630 for 30 minutes prior to electrophysiological study and exposure to 10 μM anandamide. In these experiments, the reductions in APD caused by anandamide were very similar to those obtained without pre-incubation of cells: APD_{90} was reduced by 23 ± 7%, APD_{50} by 28 ± 9%, and APD_{20} by 31 ± 10 % (n = 6, $P < 0.05$; data not shown). The lack of complete abolition of anandamide responses in the presence of AM 630 would suggest that responses were not occurring through activation of the CB_2 receptor.

4.3.9 Selective cannabinoid receptor agonists failed to mimic the effects of anandamide

In order to verify observations made with anandamide in the presence of cannabinoid receptor antagonists, a series of experiments to investigate the effects of selective cannabinoid receptor agonists on AP parameters and contractions were performed. 10 μM ACEA (a selective CB_1 receptor agonist) was found to be without significant effect on AP parameters or I_{CaL} amplitude (both n = 6, $P > 0.05$). A representative AP trace is shown in Figure 4.31, and current voltage relationships in Figure 4.32). Similarly, the CB_2 receptor agonist HU308 (10 μM) was without significant effect on AP parameters or I_{CaL} amplitude (both n = 6, $P > 0.05$). A representative AP trace is shown in Figure 4.31 and current voltage relationships in Figure 4.33.

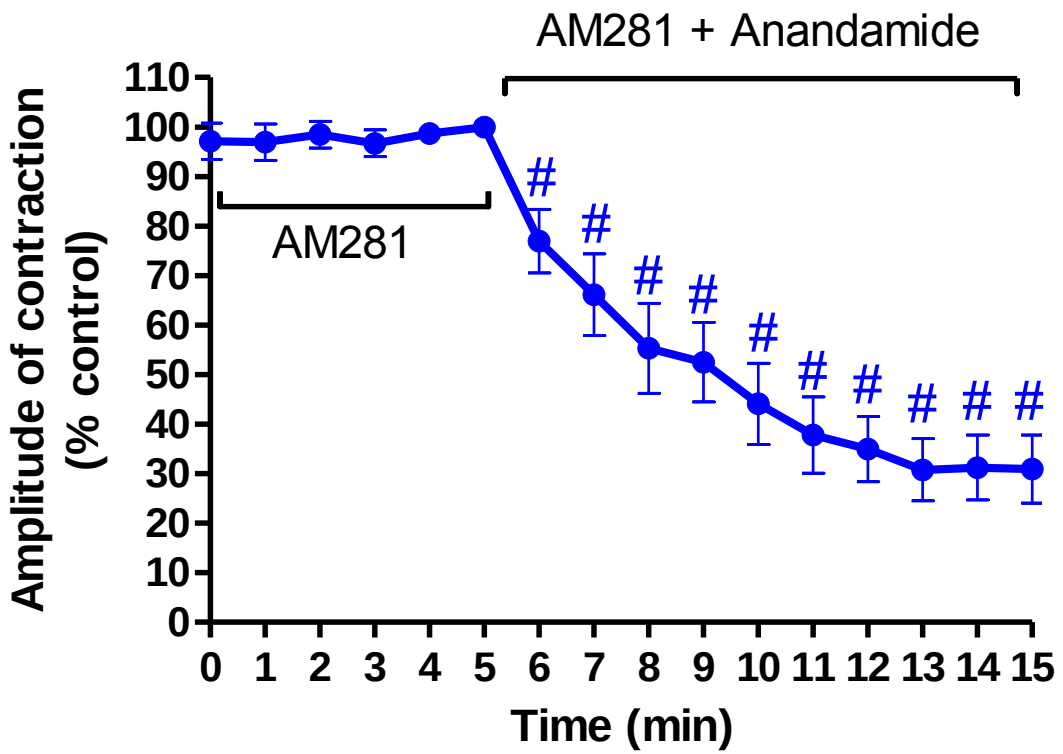


Figure 4.25 Effects of the CB_1 receptor antagonist AM281 on contractile response to anandamide.

Cells were stimulated to fire action potentials (1Hz) by a 2ms depolarising current pulse delivered by a sharp microelectrode, and were superfused with AM 281 (1 µM) for 5 minutes followed by a 10 minute period of superfusion with 10 µM anandamide in the continued presence of AM 281. Contractions were measured using an edge detection system, and are presented normalised to values at the end of the AM 281 superfusion period. AM 281 did not inhibit responses to anandamide; after 10 minutes amplitude of contraction was reduced by 69 ± 7 % (n = 4, $P < 0.001$). # denotes $P < 0.001$ repeated measures ANOVA with Dunnett's post-hoc test.

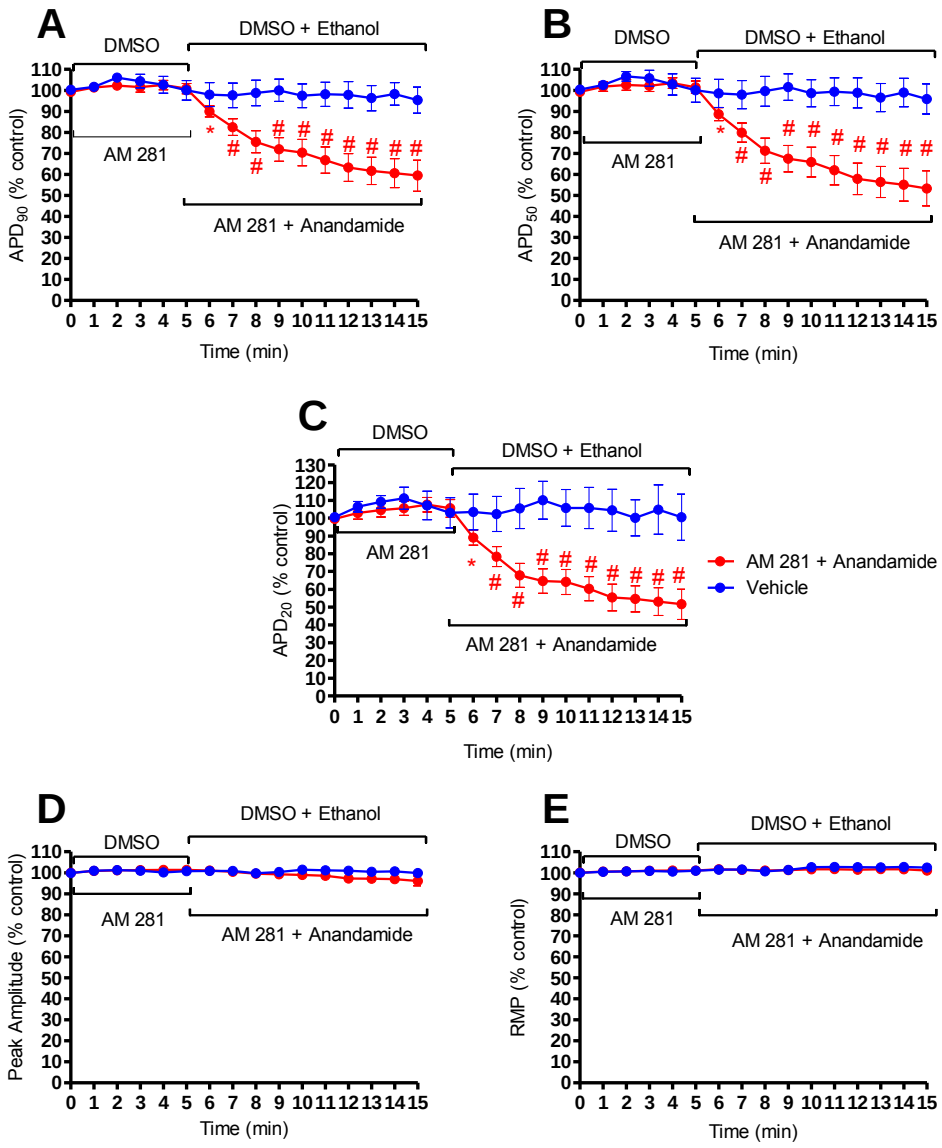


Figure 4.26 Time course of the effects of 10 µM anandamide in the presence of AM 281 (or equivalent concentrations of vehicle) on action potential parameters.

Cells were stimulated to fire APs by a 2ms depolarising current pulse, 1Hz, and were first superfused with AM 281 (dissolved in DMSO) for 5 minutes, followed by 10 minutes superfusion with anandamide (dissolved in ethanol) in the continued presence of AM 281. Control experiments with equivalent concentrations of vehicle are also shown. A: Action potential duration (APD) at 90 % repolarisation. B: APD at 50 % repolarisation. C: APD at 20 % repolarisation. D: Peak amplitude of the AP. E: Resting membrane potential. AM281 failed to inhibit responses to anandamide; APD_{90} was reduced by 41 ± 7 % after 10 minutes superfusion with anandamide in the continued presence of AM 281 (n = 6, $P < 0.001$), DMSO and ethanol vehicles (0.07 %) were without significant effect on any AP parameters (n = 6, $P > 0.05$). * denotes $P < 0.05$, # denotes $P < 0.001$; repeated measures ANOVA with Dunnett's post-hoc test.

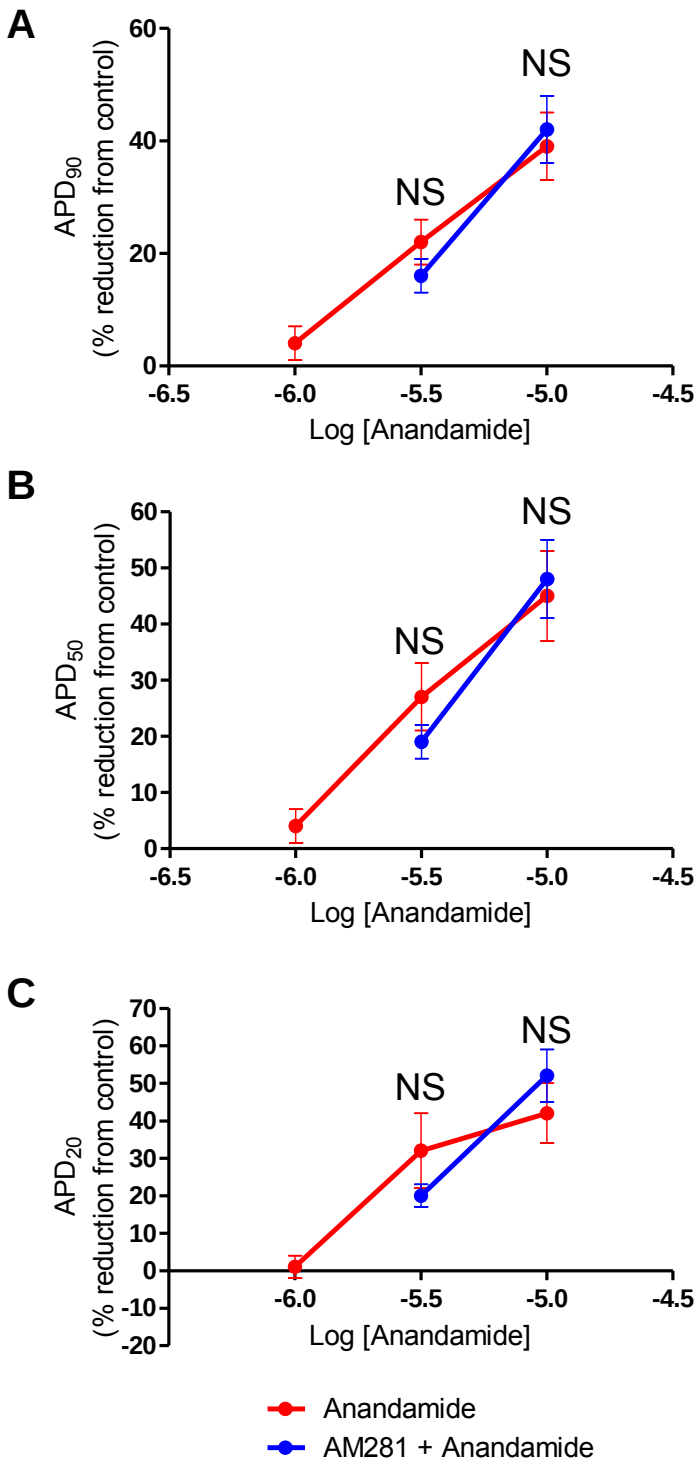


Figure 4.27 Concentration-dependent effects of anandamide on action potential duration in the absence and presence of AM281.

A: Action potential duration (APD) at 90% repolarisation. B: APD at 50% repolarisation. C: APD at 20% repolarisation. AM281 failed to inhibit the reduction in APD in response to both 3 µM (n = 8, $P > 0.05$ vs anandamide alone, n = 7) and 10 µM anandamide (n = 6, $P > 0.05$ Student's unpaired *t* test vs anandamide alone, n = 8).

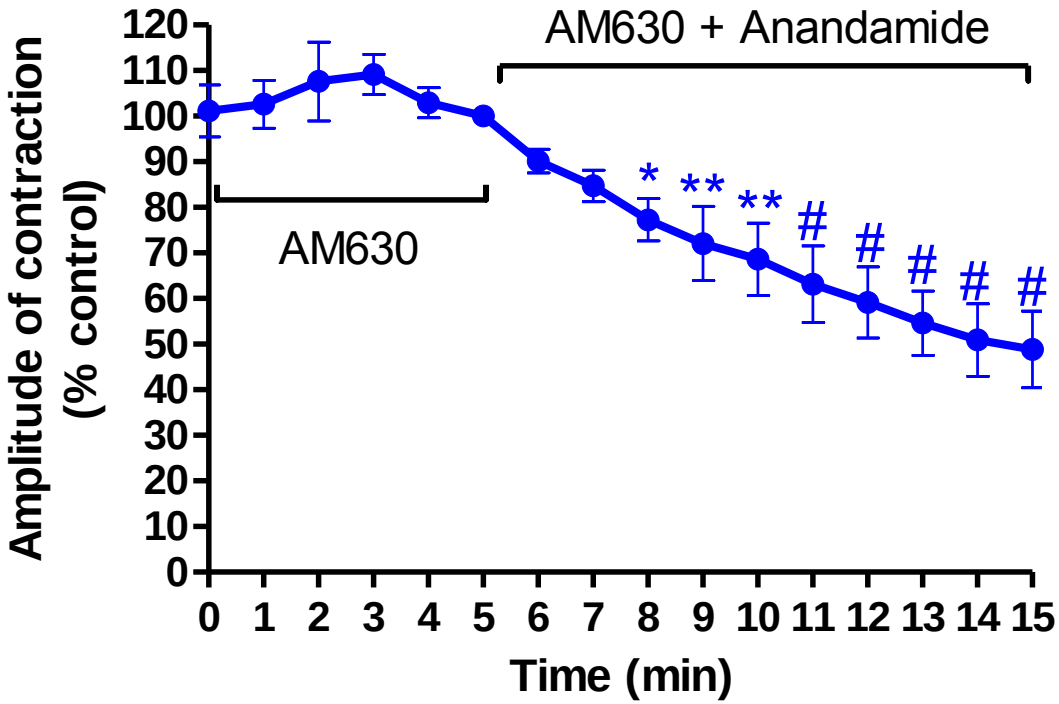


Figure 4.28 Effects of the CB_2 receptor antagonist AM630 on contractile response to anandamide.

Cells were stimulated to fire action potentials (1Hz) by a 2ms depolarising current pulse delivered by a sharp microelectrode, and were superfused with AM 630 (1 µM) for 5 minutes followed by a 10 minute period of superfusion with 10 µM anandamide in the continued presence of AM 630. Contractions were measured using an edge detection system, and are presented normalised to values at the end of the AM 630 superfusion period. AM 630 did not inhibit responses to anandamide; after 10 minutes amplitude of contraction was reduced by 52 ± 8 % (n = 5, $P < 0.001$). * denotes $P < 0.05$, # denotes $P < 0.001$ repeated measures ANOVA with Dunnett's post-hoc test.

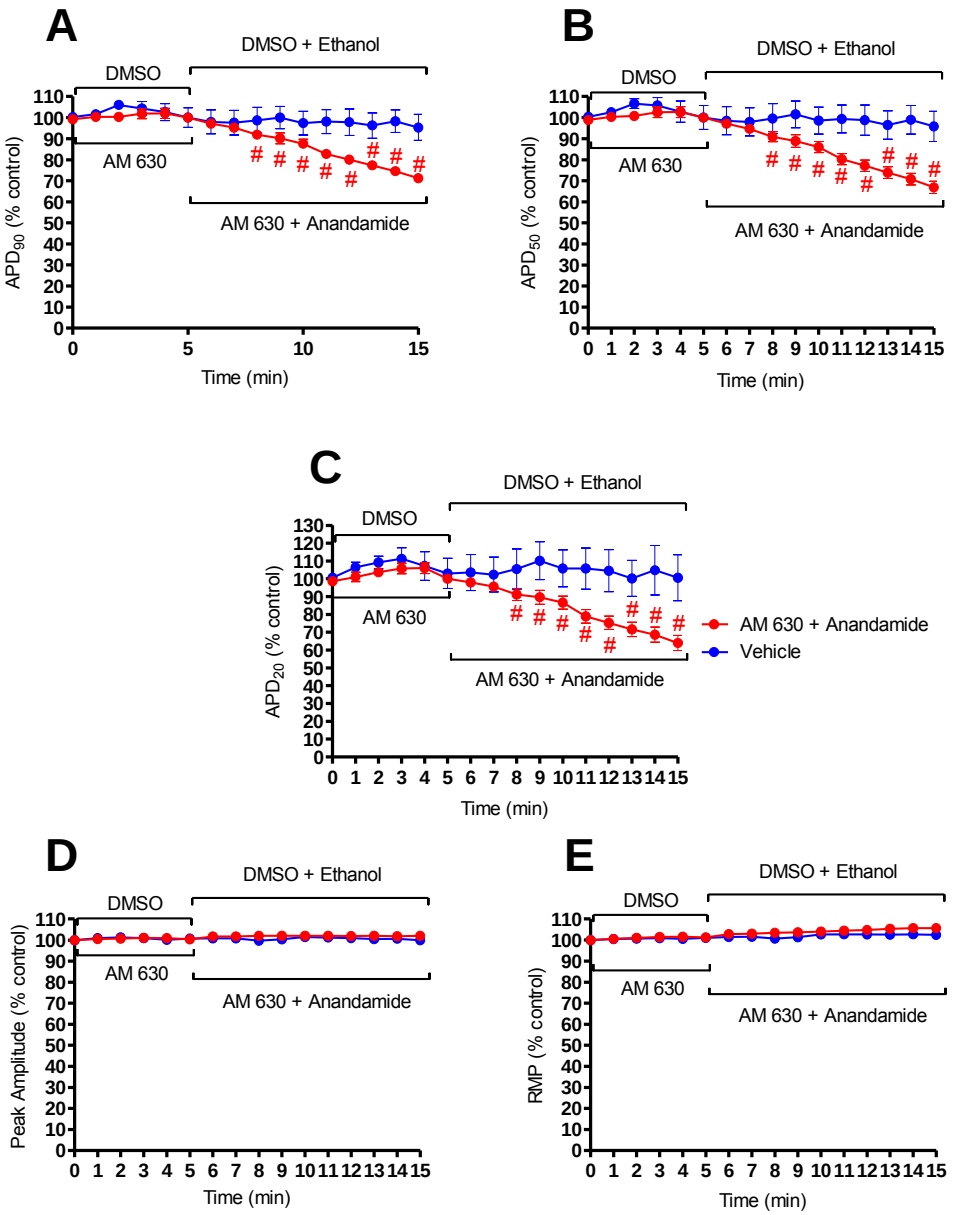


Figure 4.29 Time course of the effects of 10 µM anandamide in the presence of AM 630 (or equivalent concentrations of vehicle) on action potential parameters.

Cells were stimulated to fire APs by a 2ms depolarising current pulse, 1Hz, and were first superfused with AM 630 (dissolved in DMSO) for 5 minutes, followed by 10 minutes superfusion with anandamide (dissolved in ethanol) in the continued presence of AM 630. Control experiments with equivalent concentrations of vehicle are also shown. A: Action potential duration (APD) at 90 % repolarisation. B: APD at 50 % repolarisation. C: APD at 20 % repolarisation. D: Peak amplitude of the AP. E: Resting membrane potential. AM630 failed to inhibit responses to anandamide; APD_{90} was reduced by 30 ± 7 % after 10 minutes superfusion with anandamide in the continued presence of AM 630 (n = 6, $P < 0.001$), DMSO and ethanol vehicles (0.07 %) were without significant effect on any AP parameters (n = 6, $P > 0.05$). # denotes $P < 0.001$; repeated measures ANOVA with Dunnett's post-hoc test.

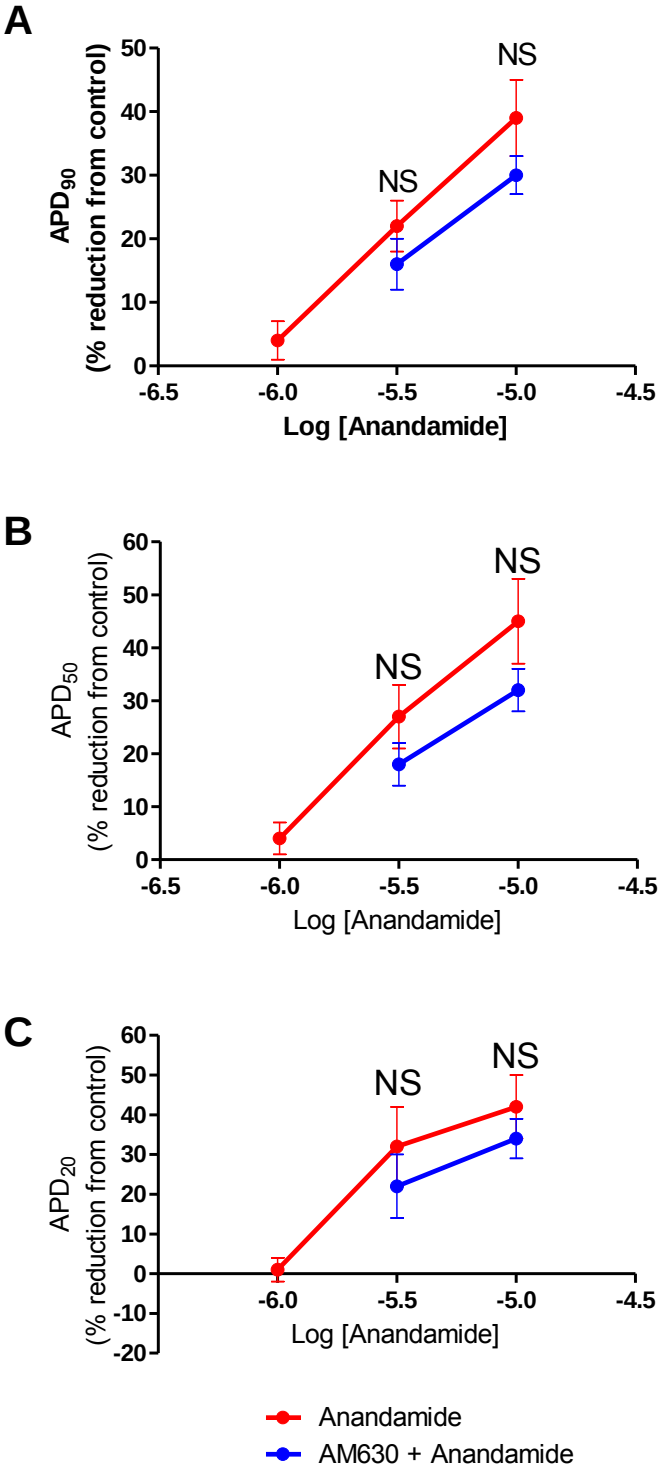


Figure 4.30 Concentration-dependent effects of anandamide on action potential duration in the absence and presence of AM630.

A: Action potential duration (APD) at 90% repolarisation. B: APD at 50% repolarisation. C: APD at 20% repolarisation. AM630 failed to inhibit the reduction in APD in response to both 3 µM (n = 6, $P > 0.05$ vs anandamide alone, n = 7) and 10 µM anandamide (n = 8, $P > 0.05$ Student's unpaired *t* test vs anandamide alone,also n = 8).

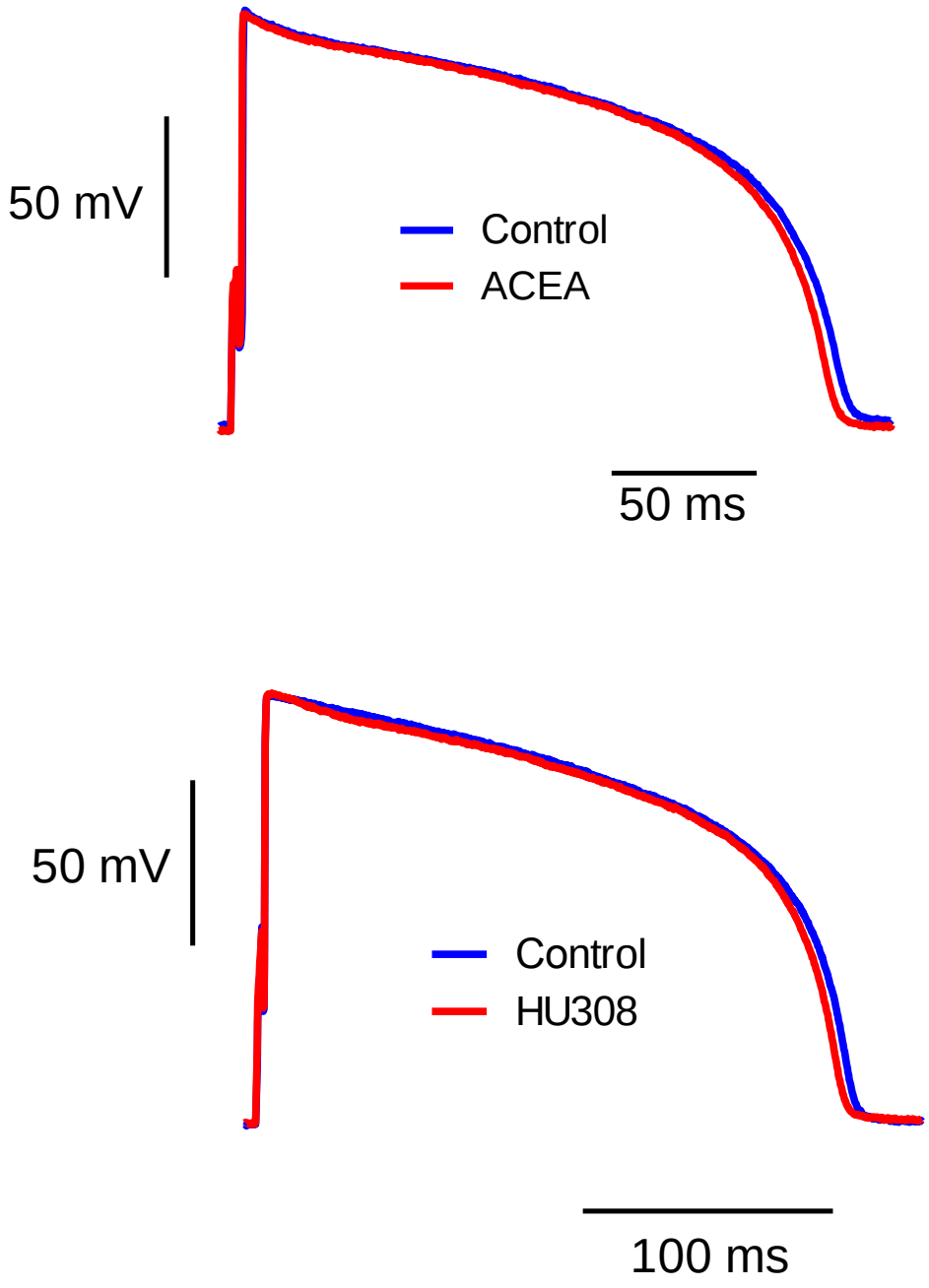


Figure 4.31 Representative action potential traces from cells superfused with cannabinoid receptor agonists

Cells were impaled with a sharp microelectrode and stimulated at 1 Hz.
A: Cell superfused with 10 μM ACEA (CB_1 receptor agonist) for 10 minutes.
B: Cell superfused with 10 μM HU308 (CB_2 receptor agonist) for 10 minutes.

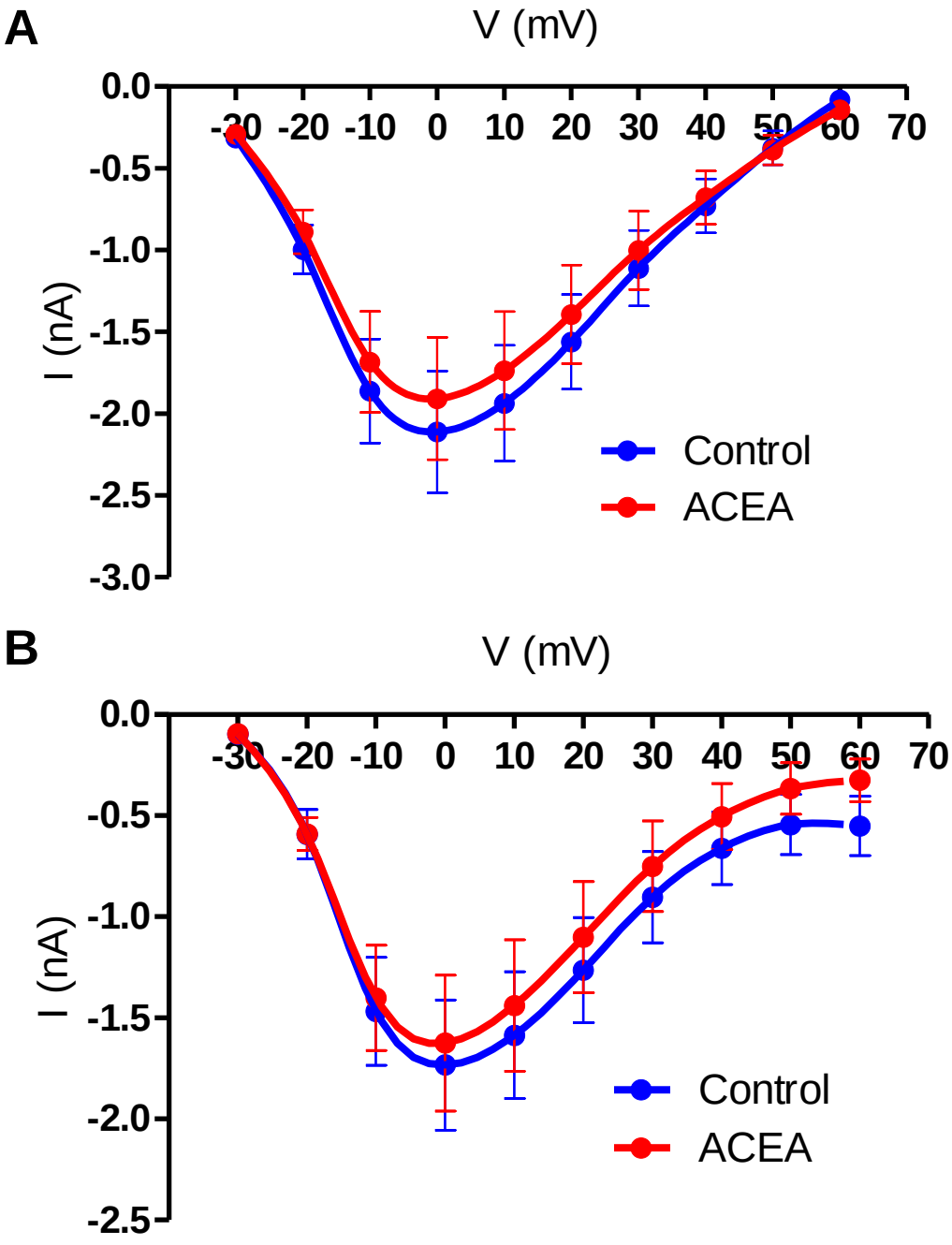


Figure 4.32 Effects of the CB_1 receptor agonist ACEA (10 µM) on current voltage relationship for I_{CaL}.

A: Current voltage relationship measured as peak current deducted from holding current.
B: Current voltage relationship measured as peak current deducted from the current at the end of the pulse.
ACEA was without significant effect on current voltage relationships at all potentials studied (n = 6, $P > 0.05$; ANOVA with Bonferroni post-hoc test).

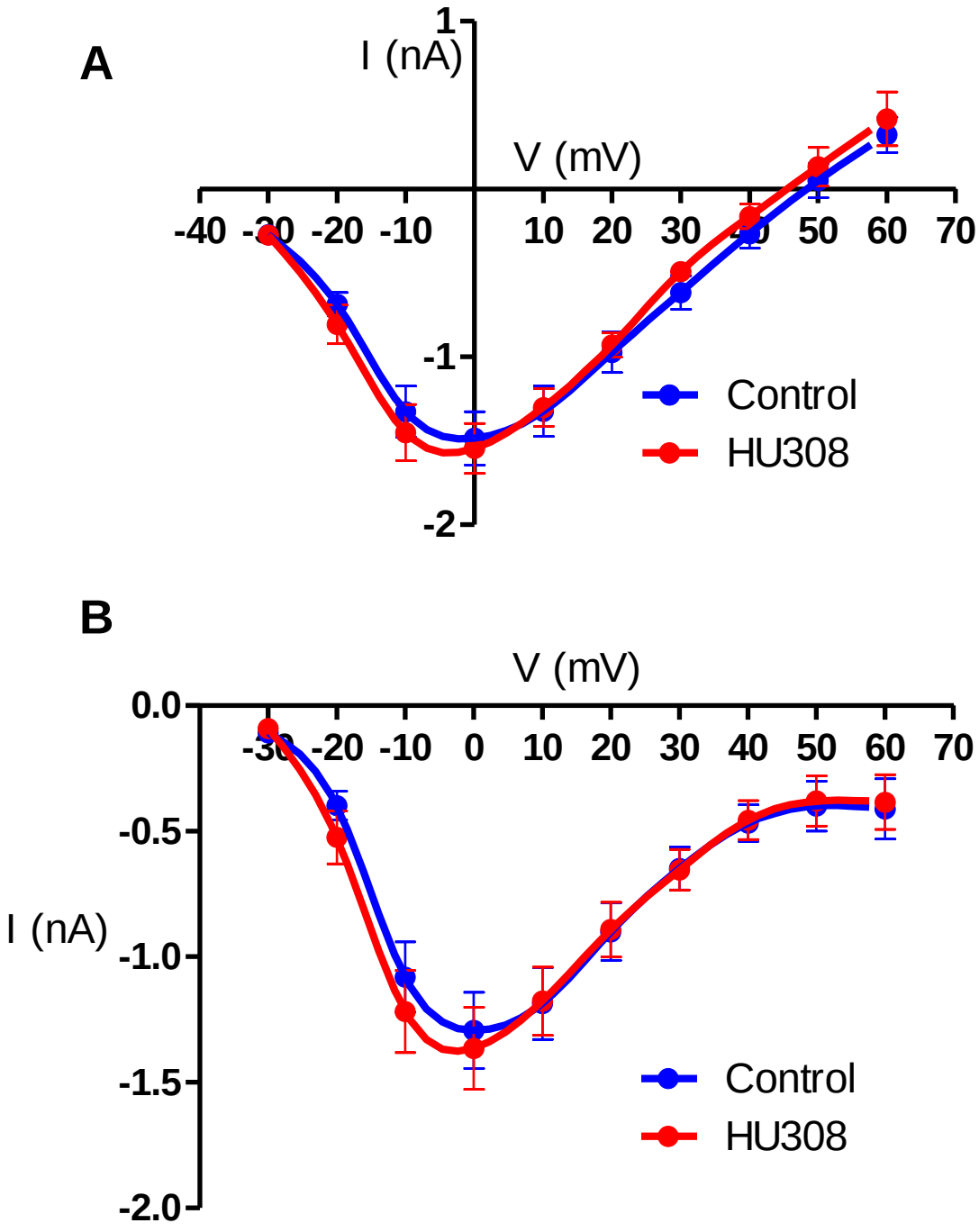


Figure 4.33 Effects of the CB_2 receptor agonist HU308 (10 µM) on current voltage relationship for I_{CaL}.

A: Current voltage relationship measured as peak current deducted from holding current.
B: Current voltage relationship measured as peak current deducted from the current at the end of the pulse.
HU308 was without significant effect on current voltage relationships at all potentials studied (n = 6, $P > 0.05$; ANOVA with Bonferroni post-hoc test).

4.3.10 2-arachidonoylglycerol was without significant effect on ventricular myocyte action potential parameters or contractions

2-AG was the second endogenous cannabinoid to be discovered, and was initially found to have higher activity at the CB_2 receptor (Mechoulam *et al.*, 1995). To my knowledge there are no published reports of the actions of 2-AG in the heart. 2-AG had no significant effects on AP configuration or amplitude of contraction. After 5 minutes superfusion with 10 μM 2-AG, APD_{90} was 99 ± 2 % and APD_{20} was 102 ± 6 % of control values (n = 6, $P > 0.05$). There were also no significant effects on peak amplitude of the AP or RMP (n = 6, $P > 0.05$). The amplitude of contraction (measured using edge-detection) was 100 ± 4 % of control values (n = 6, $P > 0.05$). Representative traces are shown in Figure 4.34.

4.4 Discussion

The data presented in this chapter provide the first evidence that, in ventricular myocytes isolated from guinea pig (a species which, like human, has a ventricular AP which plateaus at positive potentials), anandamide has clear negative inotropic actions. These effects could not be attributed to activation of conventional cannabinoid receptors (CB_1 and CB_2). Anandamide belongs to a family of lipids found in cell membranes called N-acylethanolamines. It has previously been shown in infarcted dog heart that the concentrations of these lipids can be as high as 500 nmol/g (500 μM) (Epps *et al.*, 1979), and so the results presented here may have some significance in cardiac pathologies such as ischaemia. Some of these data have been published in the form of abstracts (Bolton *et al.*, 2011).

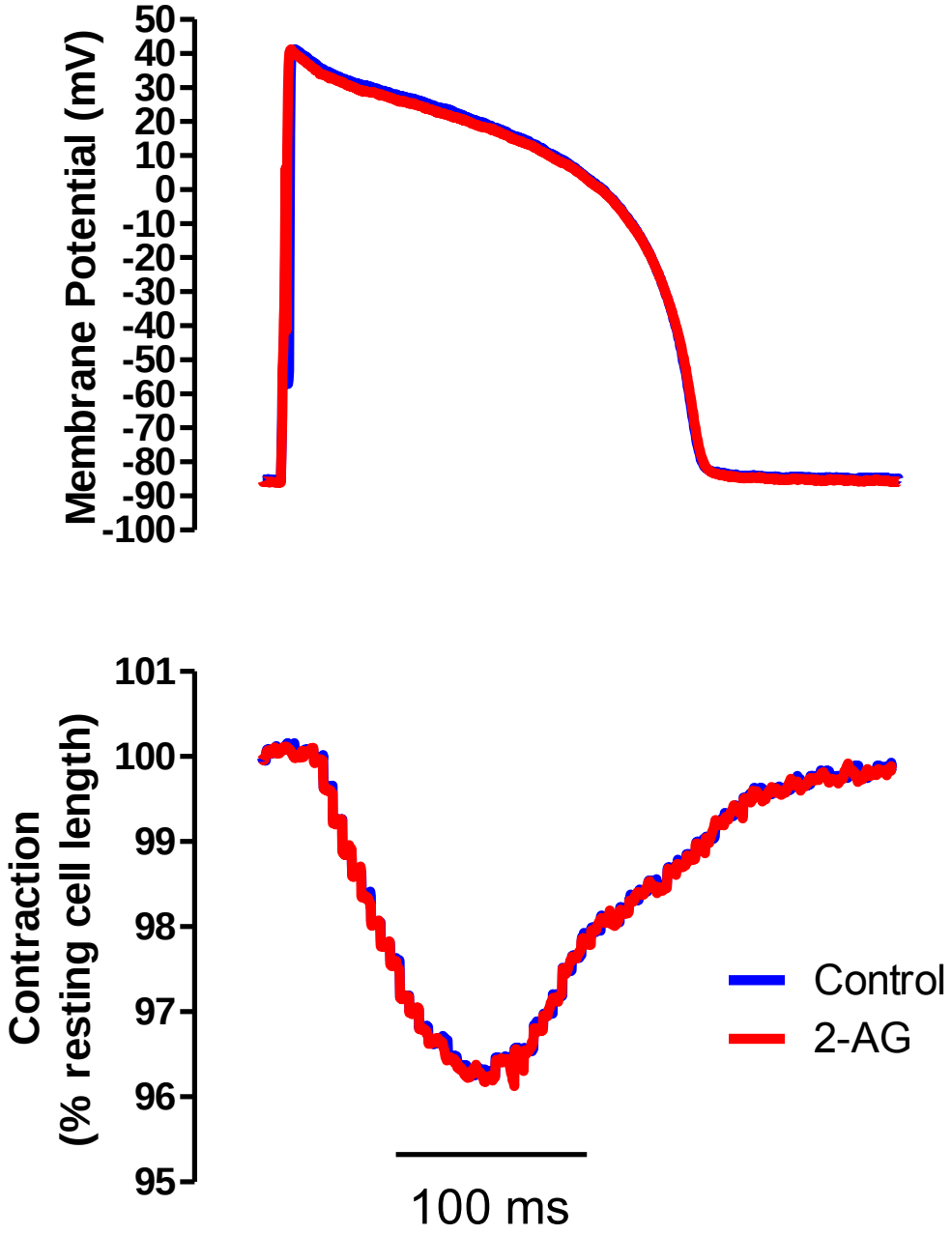


Figure 4.34 Representative traces to show lack of effect of 2-AG on action potentials and contractions.

The finding that anandamide reduced amplitude of cell contractions in a concentration-dependent manner (Figure 4.2) is in agreement with previous data obtained in Langendorff-perfused rat hearts (Ford *et al.*, 2002) and in spontaneously beating atrial muscle preparations (Bonz *et al.*, 2003). Following their study on Langendorff-perfused rat hearts, Ford and colleagues postulated that the negative inotropic action of anandamide (at a concentration of 3 μM, which appeared not to be ,suggestion was based upon the observation that negative inotropic actions were inhibited by the CB_1 receptor antagonists SR141716A and AM251, and by the CB_2 receptor antagonist SR144528, but not another CB_2 receptor antagonist, AM630 (Ford *et al.*, 2002). In addition, the CB_1 receptor agonist ACEA, but not the CB_2 receptor agonist JWH015, was found to induce a small negative inotropic action (Ford *et al.*, 2002) but this was not as great as that observed with anandamide. With this in mind, it is possible that the results obtained using cannabinoid receptor antagonists were misleading the authors, perhaps due to off-target actions (Hiley *et al.*, 2004; Su *et al.*, 2011; Andrag *et al.*, 2013). Very recently, additional evidence was obtained using rat ventricular myocytes which demonstrated a PTX-insensitive negative inotropic action of anandamide which occurred through inhibitory effects on $I_{CaL,,}$ Ca^{2+} transients and NCX (Al Kury *et al.*, 2014a; Al Kury *et al.*, 2014b; Kury *et al.*, 2014).

To my knowledge, the present study is the first to assess the effects of anandamide on contractility in ventricular myocytes isolated from guinea pig. Further, the data presented here are the first to demonstrate a reduction in the amplitude of the ventricular cell Ca^{2+} transient in response to anandamide (Figure 4.3), and would suggest that the reduction in amplitude of contraction occurs as a result of changes in intracellular Ca^{2+} handling, either through an inhibition of Ca^{2+} influx into myocytes or through impairment of SR function. The observations presented here show that the

former is a more plausible explanation. Anandamide was found to reduce APD (Figure 4.6, Figure 4.7 and Figure 4.8); an effect which did not require breakdown to other active metabolic products (Figure 4.9). It appears that a major mechanism by which APD and contraction are reduced is through an inhibition of LTCCs (Figure 4.11).

The suggestion that anandamide reduces amplitude of contraction through an inhibition of I_{CaL} and associated AP shortening, is consistent with the results of Li and colleagues and Al Kury and colleagues, who carried out their electrophysiological investigations in rat ventricular myocytes (Li *et al.*, 2009; Al Kury *et al.*, 2014a; Al Kury *et al.*, 2014b). These investigators determined that the reduction in amplitude of I_{CaL} occurred at least in part through an acceleration of inactivation of I_{CaL}. This is in agreement with the data presented here (Figure 4.18). However, Li and colleagues concluded that this inhibitory effect on LTCCs occurred through an effect of anandamide to activate CB_1 receptors, since responses were suppressed in the presence of the CB_1 receptor antagonist AM251 (Li *et al.*, 2009).

This conclusion is not supported by the results of the present study. Here, the anandamide-induced reduction in amplitude of contraction and in APD were not prevented by the CB_1 receptor antagonist AM281 (Figure 4.25, Figure 4.26 and Figure 4.27), which would in turn suggest that the inhibition of I_{CaL} was not mediated by actions at CB_1 receptors under the conditions of these experiments. AM281 has been reported to act as a competitive antagonist with a K_i value of 12 nM at the CB_1 receptor (Lan *et al.*, 1999), and so at a concentration of 1 µM AM281 (as in these experiments), the log concentration response curve would be expected to be shifted by a factor of 84 (based on a calculation of dose ratio: (1 + (1 µM/ 12 nM)), which is not the case in the experiments presented here (Figure 4.27). Furthermore, the selective CB_1 receptor agonist ACEA was without significant effect on APD or I_{CaL} amplitude in the present

study (Figure 4.31 and Figure 4.32). ACEA, however, was not tested in the experiments of Li and colleagues.

In the present investigation, the CB_2 receptor antagonist AM630 did not significantly attenuate the responses of anandamide (Figure 4.28, Figure 4.29 and Figure 4.30); this is in agreement with the findings of others (Ford *et al.*, 2002; Li *et al.*, 2009). With a K_i value of 32.1 nM (Ross *et al.*, 1999) and assuming competitive antagonism as has been reported previously (Hosohata *et al.*, 1997), it would be predicted that the log concentration response curve for anandamide in the presence of 1 μM AM630 would be shifted by a factor of 33, which is not the case in the experiments presented here (Figure 4.30). Furthermore, the selective CB_2 receptor agonist HU308 was without significant effect on APD, amplitude of contraction or I_{CaL} in the present study (Figure 4.31 and Figure 4.33), but has not previously been tested in other published investigations on cardiac muscle. Ford and colleagues determined that JWH015 did not significantly affect force of contraction in Langendorff-perfused hearts and therefore, taking into account all investigations, it seems reasonable to conclude that CB_2 receptors do not mediate negative inotropy in cardiac muscle.

Findings concerning the CB_1 receptor are however conflicting. A detailed investigation of the putative signalling pathway activated by CB_1 receptors in the study of Li and colleagues was not put forward, but assuming G_i protein coupling of the CB_1 receptor (Howlett *et al.*, 2002), their conclusions are hard to reconcile with a large body of literature surrounding the actions of other agonists which act at G_i protein coupled receptors in ventricular myocytes. In general, other such agonists (for example acetylcholine and adenosine) are without significant effect on ventricular cell contractility or amplitude of I_{CaL} in the absence of isoprenaline (Hartzell, 1988; Belardinelli *et al.*, 1995). However, in the presence of isoprenaline, these substances

potently attenuate the increased amplitude of contraction and amplitude of I_{CaL} observed (Hartzell, 1988; Belardinelli *et al.*, 1995). This has been attributed to an inhibition of adenylyl cyclases by G_i proteins ((Howlett *et al.*, 2002)) and the lack of effect in ventricular myocytes to a very low basal turnover of adenylyl cyclases in the absence of isoprenaline (Mery *et al.*, 1997; Bers, 2001); this has been measured directly by Lakatta and colleagues (Vinogradova *et al.*, 2006). In contrast, these agonists are frequently observed to have actions in atrial muscle in the absence of isoprenaline, usually through activation of I_{KACh} through G_i protein βγ subunits (Ito *et al.*, 1995). Furthermore, the density of such receptors, in particular acetylcholine receptors, is in general regarded as being higher in atrial muscle than in ventricular muscle, in line with a more dense parasympathetic innervation of atria than ventricles. It is possible that a similar situation may arise with CB_1 cannabinoid receptors. In atrial muscle they may couple directly to I_{KACh} channels to cause negative inotropy, and may also be present at a higher density in atrial muscle than ventricular muscle; this may provide an interesting avenue for future research. Pharmacological evidence that CB_1 receptors cause negative inotropy in atrial muscle has been presented by Bonz and colleagues (Bonz *et al.*, 2003); however the mechanisms were not investigated fully and conclusions based upon sensitivity of response to AM251, rather than PTX.

All data so far concerning the actions of anandamide in ventricular muscle, including the data of the present study, have reported negative inotropic actions or AP shortening effects in the absence of isoprenaline. Taking into account the above literature, it seems highly likely that anandamide has additional targets which are not cannabinoid receptors. This is particularly important given the widespread literature concerning direct inhibitory effects of anandamide on ion channels, which are very often overlooked in the endocannabinoid field, as highlighted in a thorough review of

the subject (Oz, 2006). Li and colleagues did touch on the possibility that anandamide could interact with LTCCs directly since they carried out investigations with Bay K 8644, and observed that anandamide still induced an inhibitory action on I_{CaL} (Li *et al.*, 2009). As a result, these authors concluded that a direct interaction of anandamide with LTCCs could not be occurring, however they did not consider that anandamide might bind at a site distinct from the binding site for Bay K 8644. Indeed, anandamide has been shown to bind to not only the DHP binding site on the LTCC but also phenylalkylamine and benzothiazepine binding sites (Shimasue *et al.*, 1996).More recently, Al Kury and colleagues determined that the actions of anandamide were insensitive to PTX (Al Kury *et al.*, 2014a; Al Kury *et al.*, 2014b), as reported here. These investigators demonstrated that an acceleration of I_{CaL} inactivation occurred as a result of a direct interaction of anandamide with the channel, which could be accessed by anandamide during both extracellular and intracellular application (Al Kury *et al.*, 2014b).

Adding further support for a direct inhibitory action of anandamide on ion channels are observations presented here, for the first time, that anandamide inhibits I_{Ks} but not I_{Kr} in guinea pig ventricular myocytes. These data were confirmed by separating the currents both in terms of speed of activation, and pharmacologically using E4031 (Figure 4.21 and Figure 4.24). Although the inhibitory action of anandamide on I_{Ks} would contribute to a lengthening of the AP, it is likely that on balance there is a more significant inhibition of I_{CaL} which leads to the observed AP shortening. The suggestion that anandamide can modulate K^+ currents directly is in agreement with observations in rat ventricular myocytes concerning I_{to1}, I_{Kur} and I_{KATP} (Amorós *et al.*, 2010; Barana *et al.*, 2010; Li *et al.*, 2012).

The present study highlights a marked negative inotropic action of anandamide and associated inhibition of I_{CaL}. Given its highly lipophilic nature, anandamide is perhaps more likely to reside within the cell membrane and interact with ion channels directly; thus it is perhaps unlikely that an intracellular action on SR stores could occur and this avenue of research was not pursued in the present investigation. However, additional actions of anandamide on the SR or myofilaments cannot be ruled out. Interestingly, it has recently been demonstrated that carrier proteins exist for translocation of n-acylethanolamines (like anandamide) to nuclear receptors (Kaczocha *et al.*, 2012). Whether these exist in cardiac myocytes, and could mediate some action of n-acylethanolamines on the SR is currently unknown, and may provide an additional interesting avenue for future research. Interestingly, anandamide has recently been shown to inhibit IP_3-mediated Ca^{2+} signalling through both CB_1 and CB_2 receptors in isolated guinea pig cardiac cell nuclei (Currie *et al.*, 2008); whether this mechanism exists in intact cells is unknown.

However, the possibility remains, that a receptor-mediated mechanism of negative inotropy in response to cannabinoid receptor agonists may occur when adenylyl cyclases are activated in guinea pig ventricular myocytes by isoprenaline. This possibility will be addressed, for the first time, in chapter 5.

Chapter 5

Effects of endocannabinoids on excitation-contraction coupling in the presence of β-adrenoceptor stimulation

5.1 Introduction

It has been suggested that the endocannabinoid system may have a protective role in a number of cardiac pathologies including protection against Ca^{2+} overload in ischaemia (Li *et al.*, 2013) and protection against arrhythmias (Ugdyzhekova *et al.*, 2001; Krylatov *et al.*, 2002). Anandamide has also been shown to reduce infarct size after ischaemia through a CB_2 receptor-mediated mechanism (Lamontagne *et al.*, 2006). Furthermore, circulating levels of anandamide and 2AG are elevated in heart failure, although it is unknown whether this provides protection against the progression of the disease (Weis *et al.*, 2010). All of these conditions are associated with increased activation of the sympathetic nervous system (Levick, 1999).

Stimulation of sympathetic nerves, leading to the release of noradrenaline which acts upon cardiac β-adrenoceptors is the primary mechanism by which force of cardiac contraction (along with rate, and speed of relaxation) is increased in order to meet metabolic demands of organs and tissues (Levick, 1999). To maintain homeostasis, activation of parasympathetic nerves and subsequent release of acetylcholine, leads to rapid attenuation of rate and force of contraction (Levy, 1971; Hartzell, 1988; Lewis *et al.*, 2001). Acetylcholine acts primarily upon M2 receptors, which are negatively coupled to adenylyl cyclases (Brodde *et al.*, 1999). In ventricular muscle, acetylcholine has very little direct effect on electrical activity or contractility, unless adenylyl cyclases are stimulated by treatment of ventricular muscle with β-adrenoceptor agonists, where a reduction in cell contractility (which can be attributed to a reduction in amplitude of β-adrenoceptor stimulated I_{CaL}) is observed (Brodde *et al.*, 1999). Other agents released from cells and present in the circulating blood are also capable of 'anti-adrenergic' effects in ventricular muscle; for example adenosine (Belardinelli *et al.*,

1995) via activation of A1 receptors, also negatively coupled to adenylyl cyclases (Bohm *et al.,* 1989). Notably, adenosine is without significant effect on amplitude of I_{CaL} or contractions in the absence of β-adrenoceptor stimulation (Belardinelli *et al.*, 1995).

Given the reported actions of agonists acting at receptors coupled to inhibitory G-proteins to induce anti-adrenergic effects, one might postulate that G_i protein-coupled cannabinoid receptors may also mediate such actions. For example, these may account for previous observations concerning the protective effects of anandamide against adrenaline-induced arrhythmias (Ugdyzhekova *et al.,* 2001). Although prominent negative inotropic effects were observed in the absence of β-adrenoceptor stimulation (chapter 4) it is possible that these may be enhanced in the presence of isoprenaline to stimulate the β-adrenoceptor signalling pathway. An enhancement of the negative inotropic actions of anandamide when adenylyl cyclases are stimulated would be suggestive of at least some component of the response being mediated by a G_i-protein coupled receptor signalling pathway to reduce the activity of adenylyl cyclases. Furthermore, it is possible that the cannabinoid receptor agonists might possess additional actions which are only evident when β-adrenoceptors are stimulated with isoprenaline.

In light of the data presented in chapter 4, the aim of the work presented here was to investigate whether stimulation of β-adrenoceptors would lead to additional negative inotropic and 'anti-adrenergic' actions of anandamide and other cannabinoid receptor agonists. Further aims were to determine whether any actions observed under these conditions could be mediated by a G_i-protein coupled receptor, by use of pertussis toxin (PTX), rather than cannabinoid receptor antagonists, which may have off-target actions. In order to achieve these aims, initial experiments were performed with

adenosine to determine whether the 'anti-adrenergic' and PTX-sensitive actions of adenosine reported in the literature (Belardinelli *et al.*, 1995), could be reproduced under the conditions of these experiments. This would act as a suitable control to confirm the effectiveness of the PTX pre-treatment protocol for subsequent anandamide experiments.

5.2 Methods

The methods used to perform experiments presented in this chapter are described in detail in chapter 2. Guinea pigs were killed by cervical dislocation and their hearts rapidly excised. To isolate ventricular myocytes, hearts were retrogradely perfused with a modified Tyrode's solution containing collagenase. Cells were plated onto a glass coverslip attached to a perfusion bath and superfused with PSS, which was heated to 36^{o}C and gassed with 95 % O_2 5 % CO_2 in order to maintain a pH of 7.4.

Cell contraction was measured using the IonOptix system to measure sarcomere length. Images of ventricular myocytes were captured using the IonOptix MyoCam mounted on a Nikon Diaphot 200 inverted microscope with a ×40 objective lens.

Electrophysiological measurements of action potentials and membrane currents were made using an AxoClamp 2 amplifier (Axon Instruments, USA), with all analysis carried out with Clampfit 9.2 software (Axon Instruments, USA). Cells were impaled using a sharp glass microelectrode as outlined previously. Action potentials were stimulated by 2 ms depolarising current pulses (1 – 5 nA). L-type Ca^{2+} currents were activated by 200 ms step depolarisations from a holding potential of –40 mV to a range of potentials from –30 mV to +60 mV. All I_{CaL} measurements under conditions of β-adrenoceptor stimulation were taken as holding current less peak current. The holding

current is largely dictated by current passing through I_{K1} channels, while many currents may contribute to the current at the end of the voltage clamp pulse, for example NCX, and various K^+ currents. It was decided that measurements of I_{CaL} taken as holding current less peak current would be simpler to interpret under the conditions of these experiments. Because isoprenaline accelerates activation of I_{CaL} (Bean *et al.*, 1984), peak I_{CaL} occurred at -10 mV rather than 0 mV as in earlier experiments in the absence of isoprenaline (see Figure 5.1 and Figure 5.3 for examples). Therefore, all measurements of I_{CaL} amplitude in the presence of isoprenaline were taken at -10 mV.

In some experiments PTX was used to determine whether inhibitory G-proteins could be involved in mediating observed responses. PTX is an exotoxin produced by the bacterium *Bordetella pertussis*, which causes whooping cough. It is formed from an A subunit and 5 B subunits (Tamura *et al.*, 1982; Stein *et al.*, 1994). The A subunit ADP-ribosylates the α-subunit of inhibitory G-proteins, which leaves the heterotrimeric G-protein locked in its GDP-bound inactive state, preventing dissociation of the α and βγ subunits, rendering it inactive and incapable of inhibiting adenylyl cyclase activity (Burns, 1988). The B subunit mediates binding of the holotoxin to cell membranes via glycoconjugate receptors (Brennan *et al.*, 1988; Witvliet *et al.*, 1989). Once bound, the holotoxin is taken into cells via endosomes, transported to the Golgi and endoplasmic reticulum, where the subunits dissociate and the A subunit is transported to the cell membrane where it inhibits G_i-protein function (Kaslow *et al.*, 1992). This process has been reported to be fully complete within three hours (Katada *et al.*, 1983). Pertussis toxin pre-treatment protocols in cardiac myocytes have varied from incubation at 35ºC for 2 – 6 hours depending on species (Gong *et al.*, 2002). In the present study, prolonged incubations at 36ºC appeared to compromise cell viability and therefore

incubation at 30°C for >4 hours was deemed to be an appropriate compromise, as tested using adenosine as a control (see section 5.3.2).

5.3 Results

5.3.1 Adenosine attenuated the increases in contraction and I_{CaL} amplitude evoked by isoprenaline

Adenosine has been reported to display prominent anti-adrenergic effects to reduce the amplitude of isoprenaline-stimulated contractions and I_{CaL} in ventricular muscle, but is without significant effect on these parameters in the absence of β-adrenoceptor stimulation (Belardinelli *et al.*, 1983). In order to verify that this was reproducible under the conditions of our experiments, cells were first superfused with 50 μM adenosine in the absence of isoprenaline. Under these conditions, adenosine was without significant effect on APD or amplitude of contraction in guinea pig ventricular myocytes. After 10 minutes superfusion with 50 μM adenosine, sarcomere shortening was 96 ± 5 % of control, APD_{90} was 102 ± 7 % and APD_{20} was 109 ± 14 % (n = 5, $P > 0.05$). Furthermore, adenosine was without significant effect on amplitude of I_{CaL}; after 10 minutes, I_{CaL} amplitude at 0 mV was 95 ± 13 % of control (n = 6, $P > 0.05$). Current voltage relationships are shown in Figure 5.1.

In order to confirm the reproducibility of the anti-adrenergic effects of adenosine, cells were superfused with 2 nM isoprenaline for 3 minutes, until a maximal contractile response had been achieved, and then superfused with 50 μM adenosine in the continued presence of isoprenaline. Figure 5.2 shows that, in the presence of isoprenaline, a negative inotropic response to adenosine occurred within 1-2 minutes: after 5 minutes superfusion with 50 μM adenosine in the presence of 2 nM isoprenaline,

sarcomere shortening was reduced by 40 ± 8 % of the peak isoprenaline-stimulated level of sarcomere shortening (n = 6, $P < 0.001$). In isoprenaline and 0.1 % DMSO vehicle control experiments, there was a small but significant reduction in sarcomere shortening. After 5 minutes superfusion with DMSO in the continued presence of isoprenaline, there was a 10 ± 4 % reduction from peak isoprenaline-stimulated contraction (n = 5, $P < 0.01$; Figure 5.2). However, the magnitude of this effect was significantly less than that seen with adenosine at the 5 minute time point ($P < 0.01$; Figure 5.2).

Further confirmation of the anti-adrenergic effects of adenosine was made by measuring the amplitude of I_{CaL} in cells superfused with 2 nM isoprenaline for 3 minutes, such that a maximal I_{CaL} response could be reached, followed by 5 minutes superfusion with 50 µM adenosine in the continued presence of isoprenaline. Because isoprenaline accelerates activation of I_{CaL} (Bean *et al.*, 1984), peak current in the presence of isoprenaline occurred at -10 mV (see Figure 5.3), and so all measurements made in the presence of isoprenaline in this chapter are taken at -10 mV rather than 0 mV as in earlier experiments in the absence of isoprenaline. Figure 5.3 shows that in the presence of 2 nM isoprenaline, superfusion of cells with 50 µM adenosine for 5 minutes resulted in a 40 ± 5 % reduction (n = 6, $P < 0.01$) in the amplitude of peak I_{CaL} at -10 mV. 0.1 % DMSO was without significant effect on isoprenaline pre-stimulated I_{CaL}: after 5 minutes, the amplitude of the current at -10 mV was 96 ± 5 % of the peak isoprenaline-stimulated current (n = 5, $P > 0.05$; Figure 5.4).

5.3.2 The effects of adenosine were pertussis toxin sensitive

In cells that had been pre-treated with PTX, the effect of adenosine to reduce the isoprenaline-stimulated amplitude of contraction was abolished: after 5 minutes superfusion with 50 µM adenosine in the continued presence of isoprenaline, sarcomere shortening was 94 ± 8 % of peak isoprenaline-stimulated contractions (n = 4, $P > 0.05$; Figure 5.2); an effect significantly reduced in comparison to cells which had not been treated with PTX ($P < 0.01$; Figure 5.2). These data are consistent with previous observations in guinea pig ventricular myocytes (Belardinelli *et al.*, 1983).

The effects of adenosine on isoprenaline-stimulated I_{CaL} amplitude were also measured in cells pre-treated with PTX to render inhibitory G-proteins inactive. Current voltage relationships are shown in Figure 5.5. Once a maximal response to isoprenaline had been achieved, a further 5 minutes superfusion with adenosine in the continued presence of isoprenaline resulted in a reduction in I_{CaL} amplitude of 14 ± 4 % of the peak isoprenaline-stimulated response (n = 6, $P < 0.05$). The magnitude of this reduction in I_{CaL} amplitude was significantly reduced in comparison with reductions seen in cells which had not been pre-treated with PTX (Figure 5.6), but was not significantly different from cells pre-treated with DMSO ($P > 0.05$; Figure 5.6).

These data are consistent with reports in the literature, that adenosine acts via PTX-sensitive inhibitory G-proteins to counteract the isoprenaline-stimulated increases in adenylyl cyclase which lead to increased cell contractility and I_{CaL} amplitude (Belardinelli *et al.*, 1983; Belardinelli *et al.*, 1995; Song *et al.*, 1996).

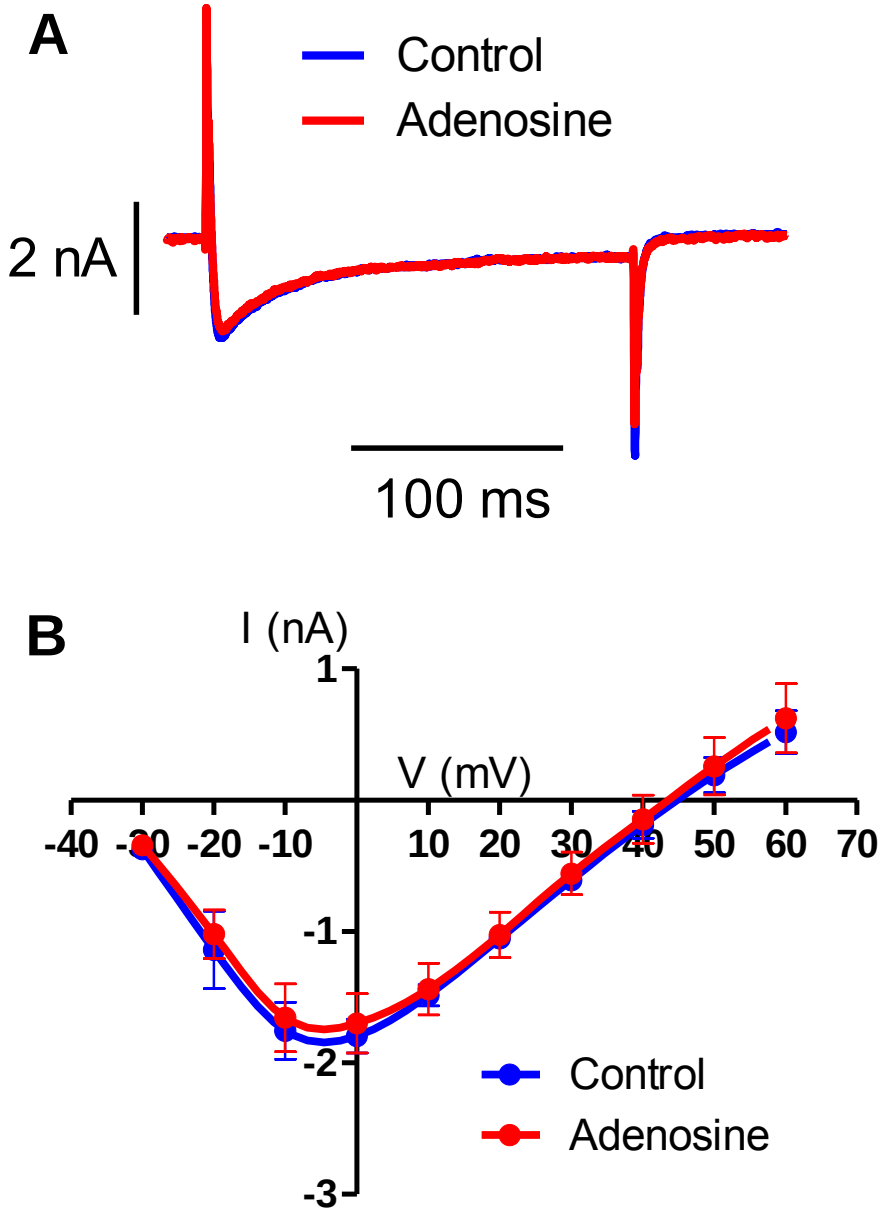


Figure 5.1 Lack of effect of adenosine on I_{CaL} current voltage relationship in the absence of isoprenaline

I_{caL} was measured by 200 ms depolarising current pulses from -40 mV to a range of potentials between -30 and +60 mV. Adenosine was without significant effect on peak I_{CaL} at 0 mV in the absence of isoprenaline (97 ± 12 % of control; n = 6, P > 0.05). A: Representative trace (-40 to 0 mV step). B: IV relationship.

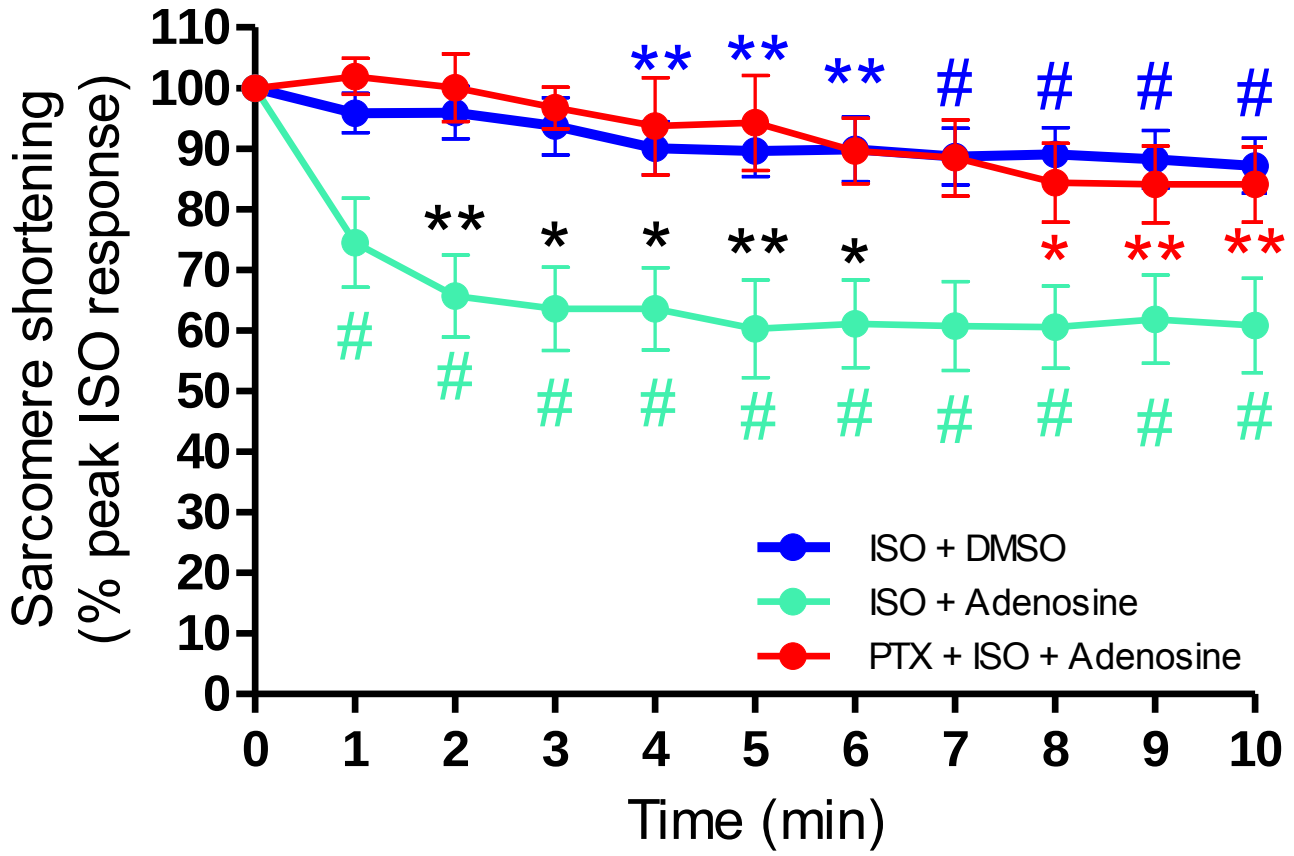


Figure 5.2 Effects of adenosine on sarcomere shortening in the presence of isoprenaline

Cells were stimulated to contract at 1 Hz by a 2 ms current pulse delivered by a sharp microelectrode. * denotes $P < 0.05$, ** denotes $P < 0.01$, # denotes $P < 0.001$. Adenosine reduced amplitude of contraction in the presence of isoprenaline. These effects were prevented by pre-treatment of cells with pertussis toxin. Blue, red and aqua symbols are repeated measures ANOVA followed by Dunnett's test. Black symbols are ANOVA with Bonferroni post-hoc test, PTX-treated vs non PTX-treated cells.

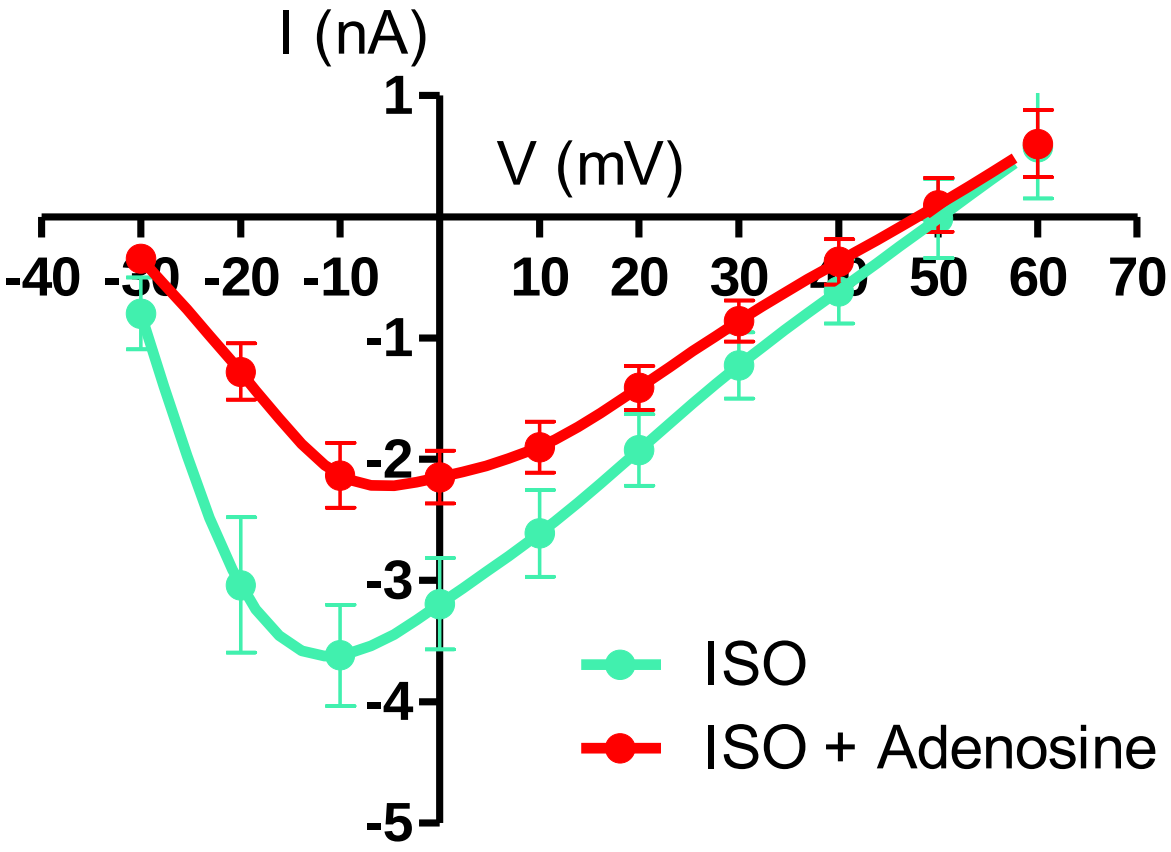


Figure 5.3 Effects of adenosine on isoprenaline-stimulated I_{CaL}

I_{CaL} was measured by 200 ms depolarising pulses from -40 mV to a range of potentials between -30 and +60 mV. Cells were superfused with 2 nM isoprenaline for 3 minutes followed by 50 µM adenosine in the continued presence of isoprenaline. Peak isoprenaline-stimulated I_{CaL} was reduced by 40 ± 5 % after 5 minutes superfusion with adenosine (n = 6, $P < 0.05$).

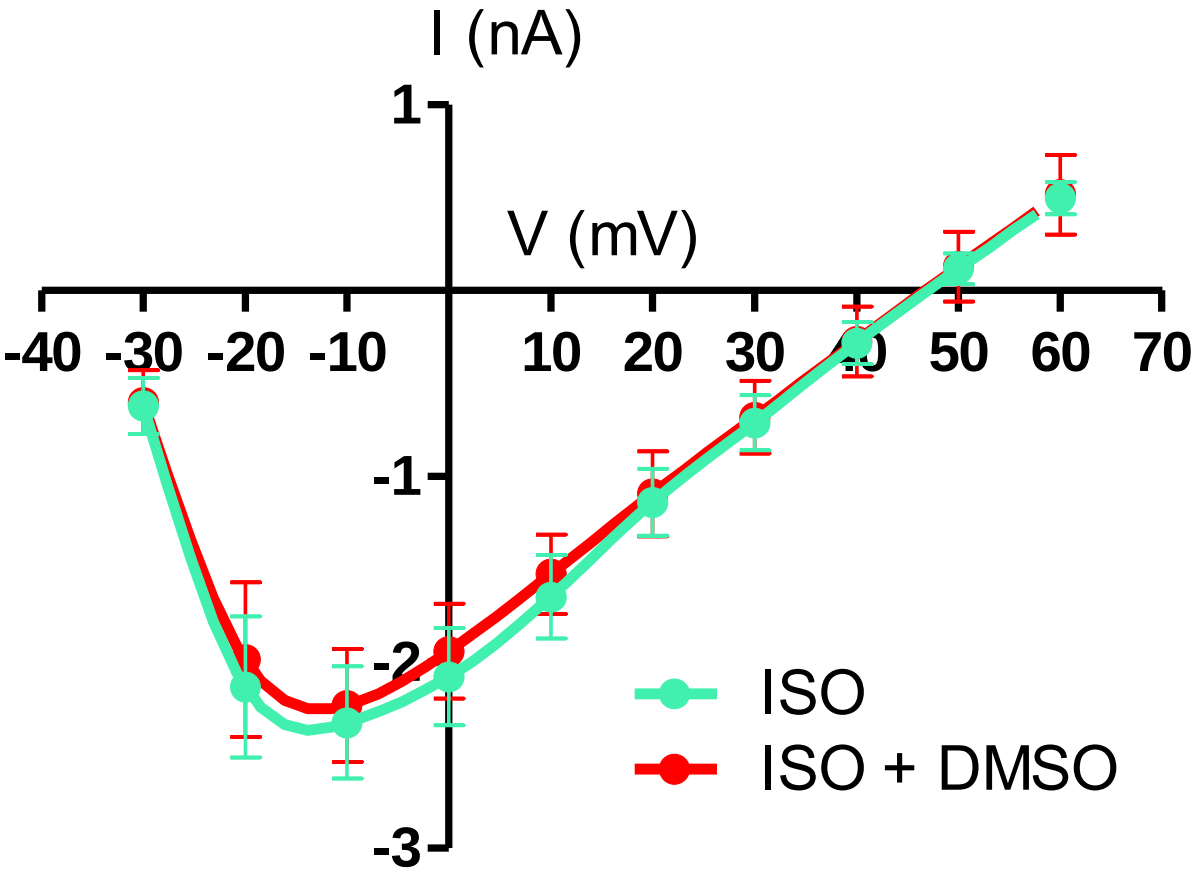


Figure 5.4 Lack of effect of DMSO vehicle on isoprenaline-stimulated I_{CaL}.

I_{CaL} was measured by 200 ms depolarising pulses from -40 mV to a range of potentials between -30 and +60 mV. Cells were superfused with 2 nM isoprenaline for 3 minutes followed by 0.1 % DMSO in the continued presence of isoprenaline. Peak isoprenaline-stimulated I_{CaL} was 96 ± 5 % after 5 minutes superfusion with DMSO (n = 5, $P > 0.05$).

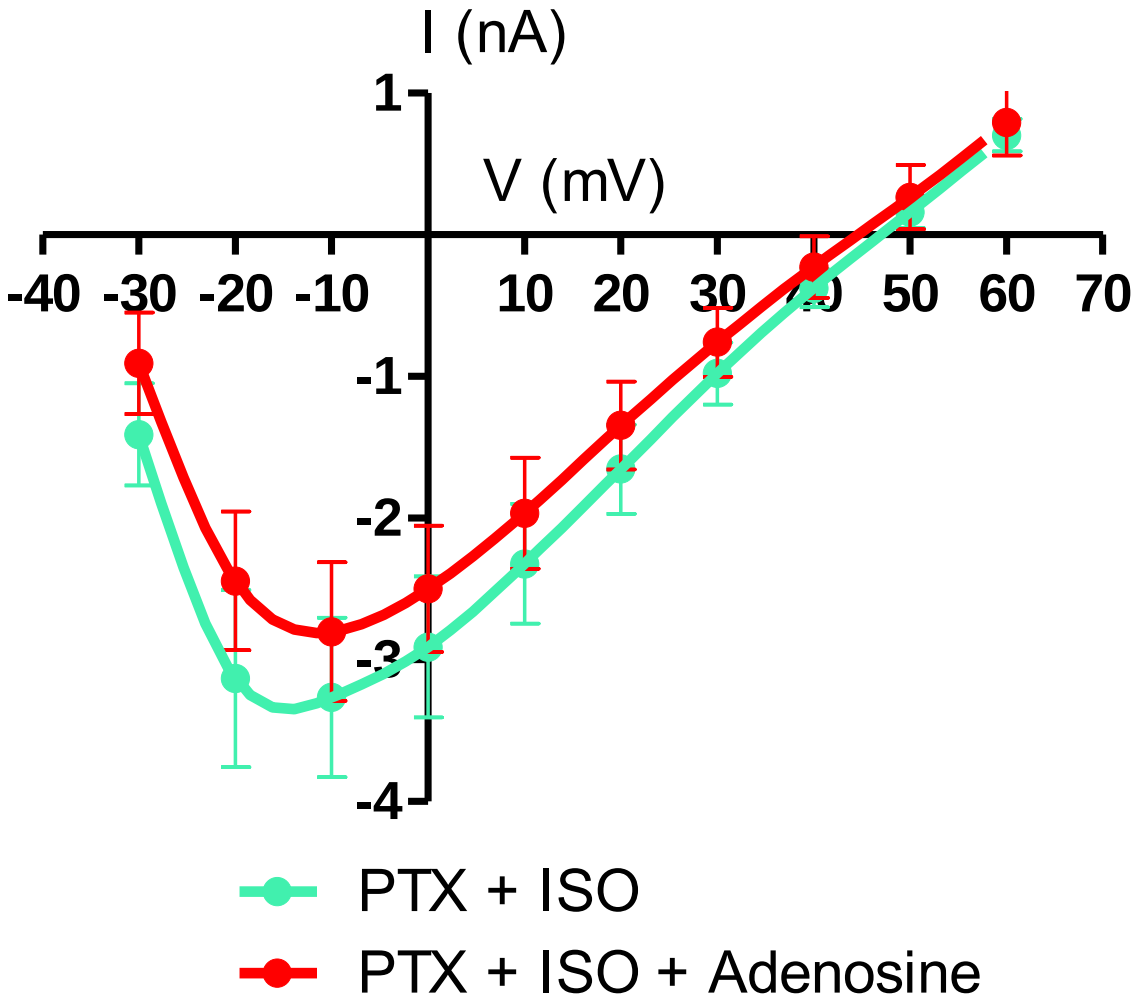


Figure 5.5 Lack of effect of adenosine on isoprenaline-stimulated I_{CaL} in cells pre-treated with pertussis toxin

I_{CaL} was measured by 200 ms depolarising pulses from -40 mV to a range of potentials between -30 and +60 mV. Cells were treated with PTX for at least 4 hours at 30°C and then superfused with 2 nM isoprenaline for 3 minutes followed by 50 µM adenosine in the continued presence of isoprenaline. Peak isoprenaline-stimulated I_{CaL} was reduced by 14 ± 4 % after 5 minutes superfusion with adenosine (n = 6, $P < 0.05$).

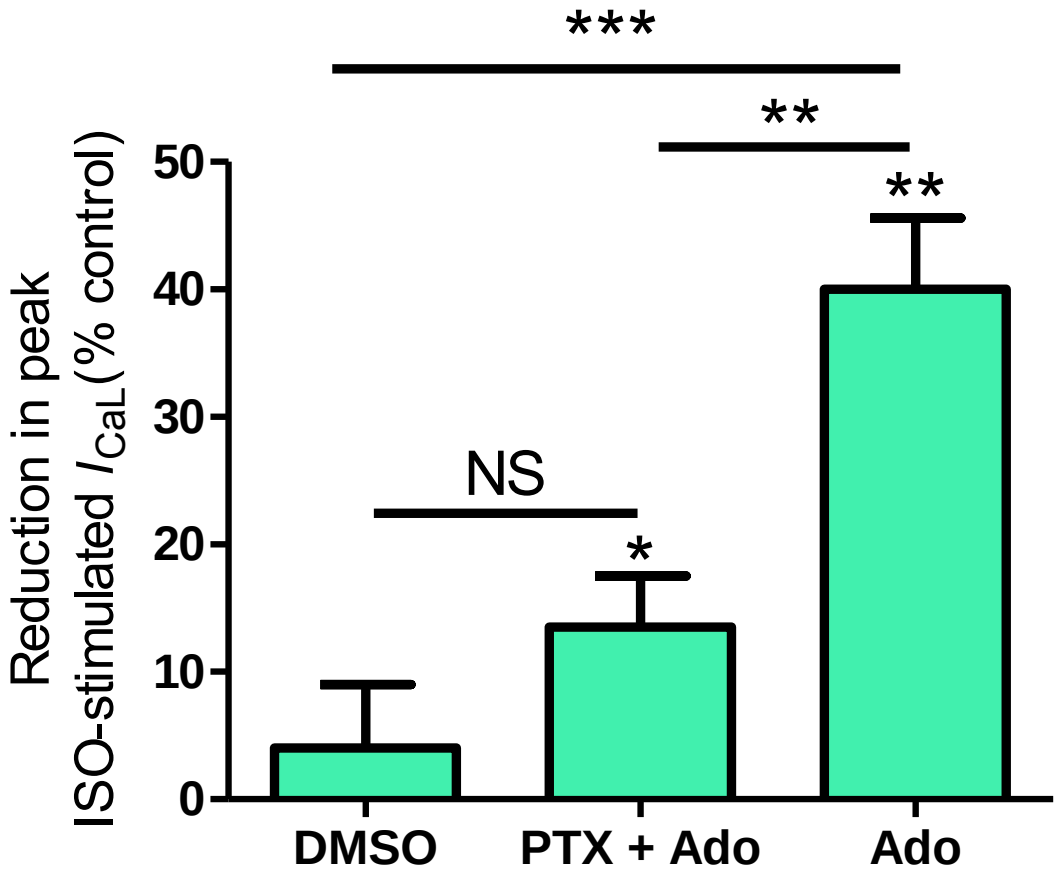


Figure 5.6 Mean effects of adenosine on isoprenaline-stimulated I_{CaL} amplitude in the absence and presence of pertussis toxin

Cells were superfused for 3 minutes with 2 nM isoprenaline followed by the drug of interest in the continued presence of isoprenaline. After 5 minutes, there was a 40 ± 8 % reduction in the amplitude of isoprenaline-stimulated I_{CaL} (n = 6, $P < 0.001$). This effect was prevented by pre-treatment of cells with PTX where I_{CaL} amplitude was reduced by 14 ± 4 % (n = 6, $P < 0.05$). ** denotes $P < 0.01$, *** denotes $P < 0.001$, one-way ANOVA with Bonferroni post-hoc test.

5.3.3 The effects of anandamide to reduce myocyte contractility and action potential duration were smaller in magnitude in the presence of isoprenaline

Following effective confirmation of the PTX-sensitive anti-adrenergic effects of adenosine, and of an effective PTX pre-treatment protocol, the effects of anandamide under conditions of β-adrenoceptor stimulation were studied. The possibility that anandamide may have additional receptor-mediated actions when adenylyl cyclase activity is stimulated was first tested by the measurement of action potentials and contractions in the presence of 2 nM isoprenaline. Figure 5.7A shows that in 6 cells superfused with isoprenaline for 3 minutes, sarcomere shortening was increased by 76 ± 29 % (n = 6, $P < 0.001$), and was then reduced following superfusion with 10 μM anandamide in the continued presence of isoprenaline. After 10 minutes, sarcomere shortening was reduced by 30 ± 4 % ($P < 0.001$ vs peak isoprenaline response; Figure 5.7B). In vehicle control experiments (Figure 5.7A and B), 10 minutes superfusion with 0.07 % ethanol in the continued presence of isoprenaline was without significant effect on sarcomere shortening: 86 ± 8 % of control values (n = 5, $P > 0.05$).

AP parameters were also measured in these cells: a representative trace is shown in Figure 5.8, and Figure 5.9 depicts AP parameters over time. Isoprenaline itself has highly variable effects on the configuration of the ventricular cell action potential which depend on activities of various currents. In some cells, isoprenaline treatment leads to AP lengthening, while in others the AP shortens, perhaps due to a greater sensitivity of repolarising K^+ currents in some cells to enhancement by the β-adrenoceptor signalling pathway. Cells were initially superfused with 2 nM isoprenaline for 3 minutes until a maximal contractile response was achieved: this was not associated with any consistent

effect on APD or RMP (n = 6, $P > 0.05$; Figure 5.8 Figure 5.9A-C). There was a slight elevation in the height of the plateau as shown in Figure 5.8, which is associated with an enhancement of I_{CaL}. Following a further 10 minutes superfusion with anandamide in the continued presence of isoprenaline, APD_{90} was reduced by 15 ± 2 % and APD_{20} by 17 ± 3 % ($P < 0.001$ vs 3 min isoprenaline values, n = 6; Figure 5.9A and B). APD_{20} was reduced by 20 ± 9 % (n = 6, $P < 0.05$ vs 3 min isoprenaline values; Figure 5.9C). There were no significant effects of anandamide on either RMP or peak amplitude of the AP in the presence of isoprenaline (n = 6, $P > 0.05$; Figure 5.9D and E). Ethanol vehicle (n = 5), was without significant effect on any AP parameters studied in the presence of isoprenaline (Figure 5.9A-E, $P > 0.05$).

In order to gain an appreciation of concentration-response relationships to anandamide in the presence and absence of isoprenaline, the aforementioned experiments were also performed with 3 µM anandamide. A concentration-response plot for the effect of anandamide in the absence and presence of isoprenaline on amplitude of contraction is shown in Figure 5.10. After 10 minutes superfusion with 3 µM anandamide in the presence of isoprenaline, sarcomere shortening was reduced by 22 ± 3 % ($P < 0.01$). The negative inotropic effects of anandamide at both 3 and 10 µM appeared significantly reduced in the presence of isoprenaline compared to in the absence of isoprenaline (Figure 5.10). Furthermore, the effect of anandamide to reduce APD was also reduced in the presence of isoprenaline as depicted in Figure 5.11, which shows concentration response plots for APD.

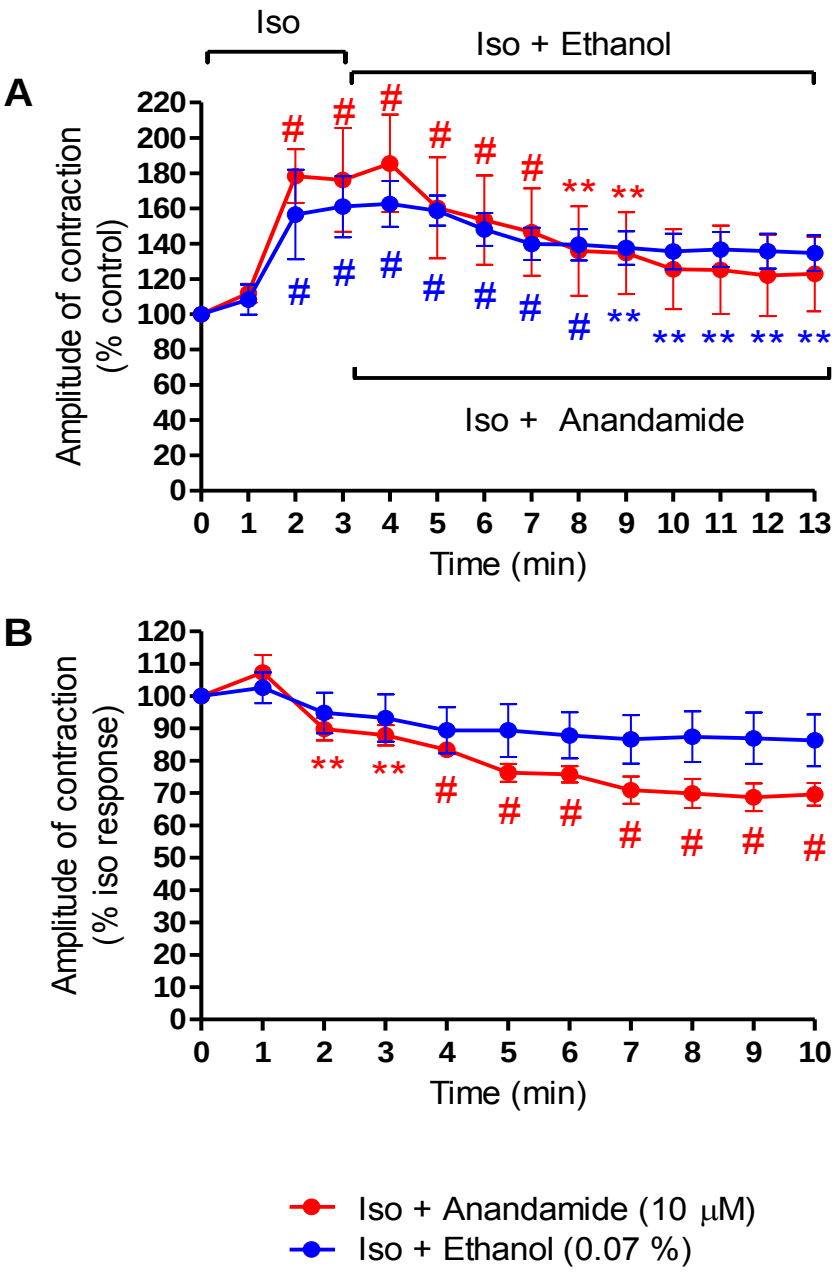


Figure 5.7 Effects of anandamide on amplitude of contraction in the presence of isoprenaline

Cells were stimulated to contract at 1 Hz by 2 ms depolarising current pulses delivered via a sharp microelectrode.
A: Time course of effect of isoprenaline, and then anandamide (n = 6; red line) or ethanol vehicle (n = 5; blue line) in the continued presence of isoprenaline, on amplitude of contraction expressed as a percentage of control (pre-isoprenaline) values.
B: Time course of effect of anandamide in the presence of isoprenaline, expressed as a percentage of peak isoprenaline values.

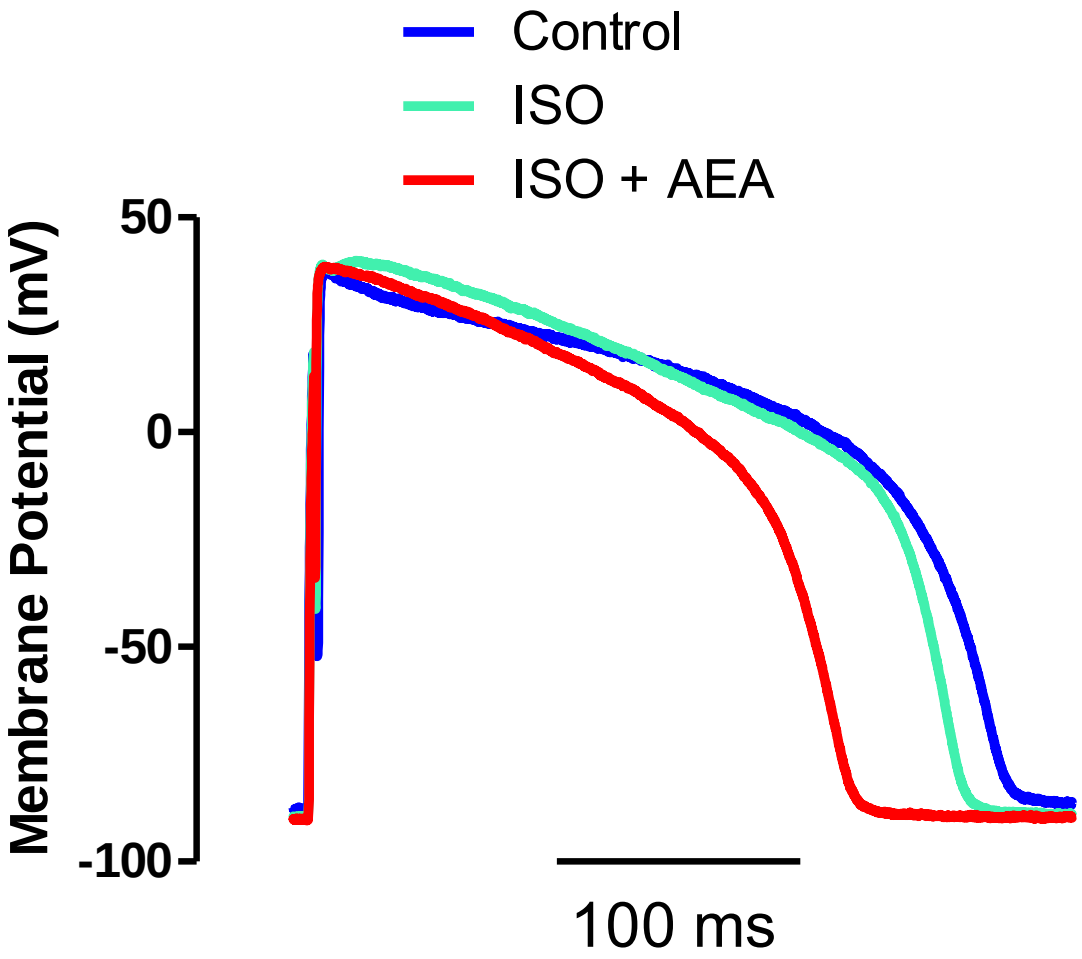


Figure 5.8 Representative action potential trace from a cell superfused with isoprenaline and anandamide

Representative APs from a cell stimulated to fire APs at 1 Hz via a sharp microelectrode and superfused with 2 nM isoprenaline for 3 minutes followed by 10 µM anandamide in the continued presence of isoprenaline for 10 minutes.

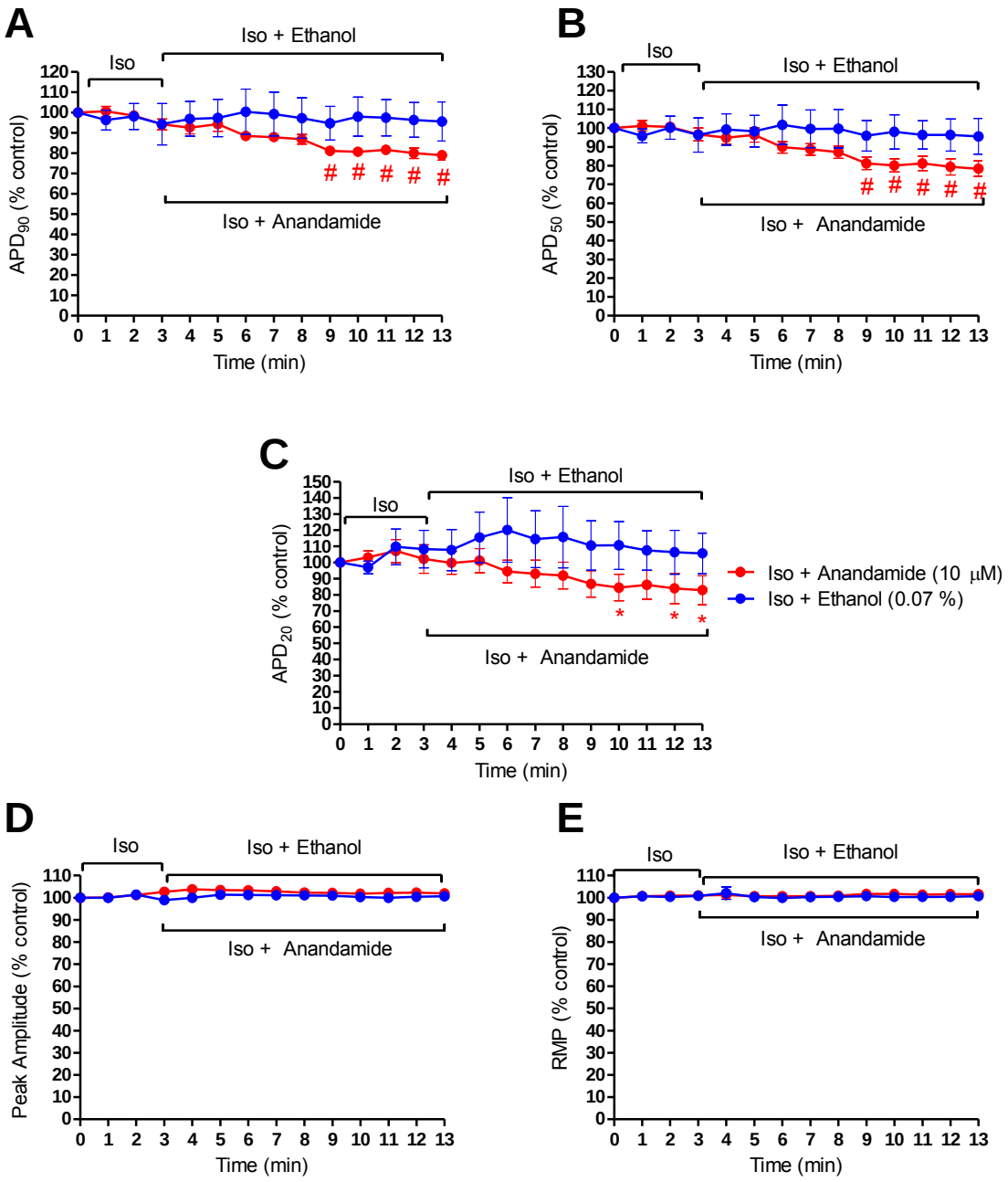


Figure 5.9 Effects of anandamide or ethanol on action potential parameters in the presence of isoprenaline

Cells were superfused with isoprenaline for 3 minutes followed by anandamide (n = 6, red line) or ethanol (n = 5, blue line) and stimulated to fire APs at 1 Hz via a patch electrode.
A: Action potential duration (APD) at 90 % repolarisation; B: APD_{50}; C: APD_{20}; D: Peak Amplitude of the AP; E: Resting membrane potential.

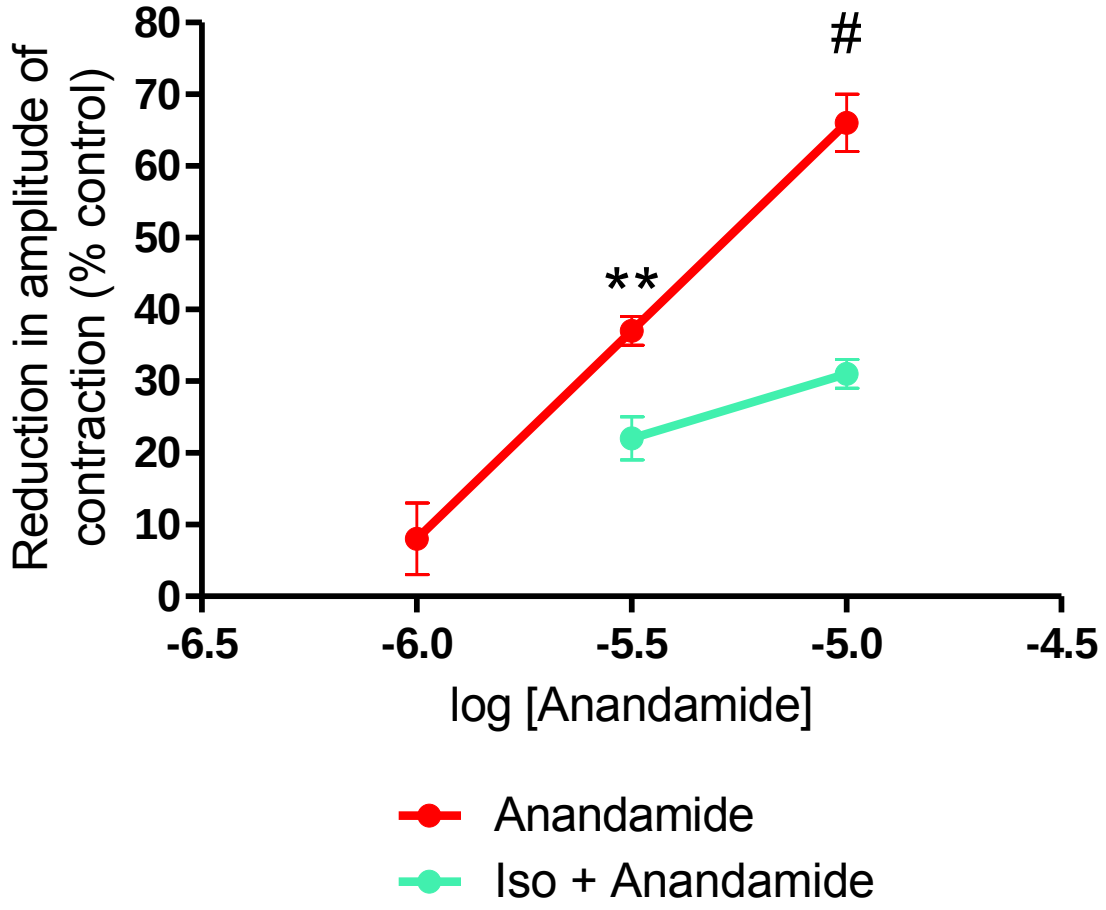


Figure 5.10 Concentration-dependent effects of anandamide in the absence and presence of isoprenaline on amplitude of cell contractions

Effects of anandamide on sarcomere shortening in the absence and presence of isoprenaline. The negative inotropic effect of anandamide (3 and 10 µM) in the presence of isoprenaline (both n = 6) was significantly reduced compared to that observed in the absence of isoprenaline (both n = 6). ** denotes $P < 0.01$, # denotes $P < 0.001$. One –way ANOVA with Bonferroni post-hoc test.

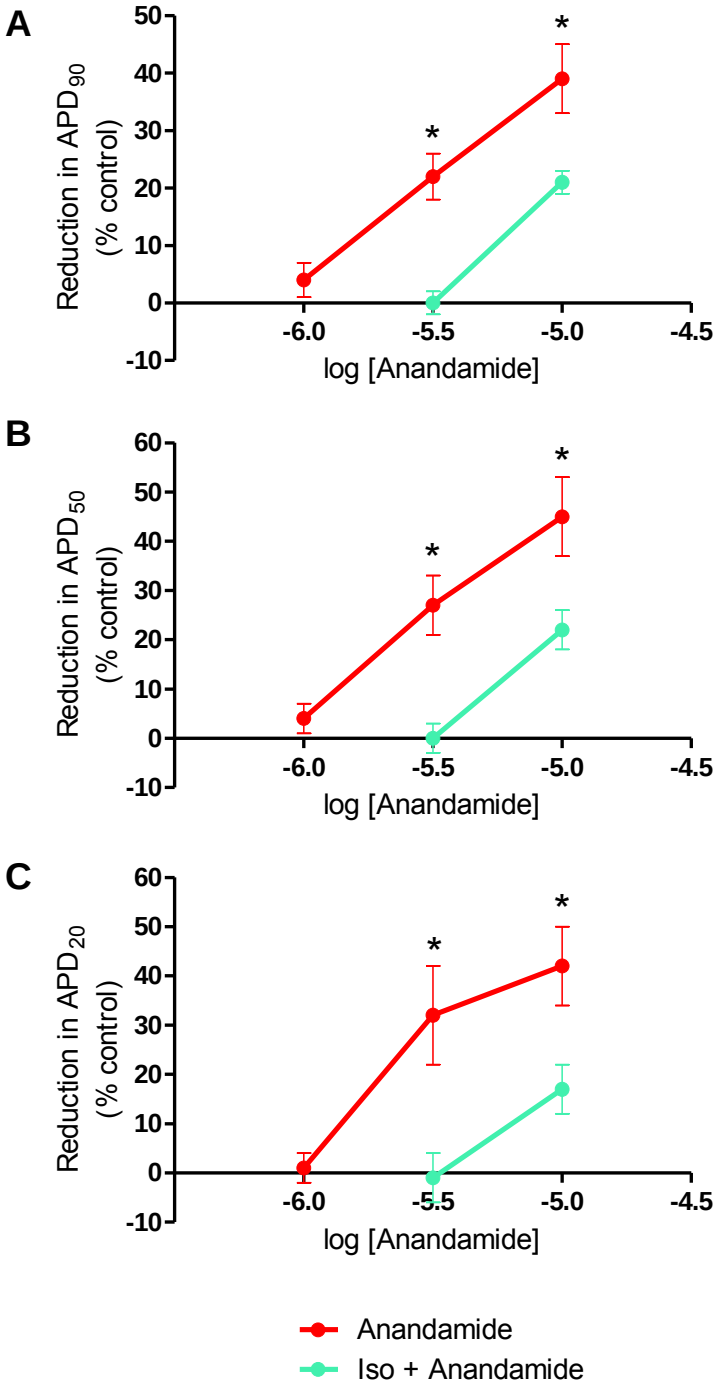


Figure 5.11 Concentration-dependent effects of anandamide on action potential duration in the absence and presence of isoprenaline

Effects of anandamide on action potential duration in the absence and presence of isoprenaline. A: 90 % repolarisation, B: 50 % repolarisation, C: 20 % repolarisation. The effect of anandamide (3 and 10 µM) on APD in the presence of isoprenaline (both n = 6) was significantly reduced compared to that observed in the absence of isoprenaline (both n = 6; data shown previously in figure 4.2). * denotes $P < 0.05$. ANOVA with Bonferroni post-hoc test.

5.3.4 Anandamide inhibited L-type Ca^{2+} currents in the presence of isoprenaline

In order to determine whether the reduced negative inotropic effect of anandamide in the presence of isoprenaline might be due to a reduced inhibitory effect on I_{CaL}, cells were superfused with 2 nM isoprenaline for 3 minutes until a maximal increase in I_{CaL} amplitude had occurred, followed by a further 10 minutes superfusion with anandamide in the continued presence of isoprenaline. Because of the relatively prolonged time course of anandamide action (at least 10 minutes), and the possibility that a rundown of I_{CaL} may be observed during this time, 0.07 % ethanol vehicle controls were first performed in the presence of isoprenaline. Under these conditions, there was a small reduction in amplitude of the isoprenaline-stimulated current. After 10 minutes superfusion with 0.07 % ethanol in the continued presence of isoprenaline a reduction in I_{CaL} amplitude of 16 ± 4 % of the peak isoprenaline-stimulated current was observed (n = 7, $P < 0.05$). Current voltage relationships are shown in Figure 5.12.

Because a reduction in I_{CaL} amplitude was observed after 10 minutes superfusion with ethanol in the presence of isoprenaline, it was decided that a correction factor to account for this should be applied to all subsequent experiments utilising ethanol as the vehicle (this applies to experiments with anandamide and with the CB_1 receptor agonist ACEA, see section 5.3.8). A correction factor of 1.19 was applied, based on a reduction in I_{CaL} amplitude of 1.6 % per minute under these conditions, as reported above. Figure 5.13A shows the effect of anandamide on current voltage relationship for I_{CaL} without application of the correction factor, and with the correction factor in Figure 5.13B. After 10 minutes superfusion with 10 μM anandamide in the continued presence of isoprenaline, the apparent reduction in peak current at -10 mV

was 34 ± 3 % of the peak isoprenaline-stimulated current (n = 10, $P < 0.001$; Figure 5.13A). With application of the correction factor, this value was determined to be 21 ± 5 % (n = 10, $P < 0.01$; Figure 5.13B). Figure 5.14 shows that even without application of a correction factor for I_{CaL} rundown, the effects of anandamide to reduce amplitude of isoprenaline-stimulated I_{CaL} were significantly greater in magnitude than those observed with ethanol vehicle.

It would be expected that, if anandamide were having an effect to reduce the activity of adenylyl cyclases in the presence of isoprenaline, that the effect of anandamide to reduce amplitude of isoprenaline-stimulated contractions and I_{CaL} would be enhanced, in comparison to the effects shown in chapter 4 in the absence of isoprenaline. Figure 5.15A shows that the magnitude of reduction in I_{CaL} amplitude observed with anandamide in the presence of isoprenaline, was no greater than that observed in the absence. Interestingly, when taking into account the correction factor for rundown of I_{CaL} in the presence of isoprenaline, the magnitude of reduction in I_{CaL} amplitude the presence of isoprenaline was significantly smaller than in the absence of isoprenaline (Figure 5.15B). However, it should be noted that, for observations made in the absence of isoprenaline, it was not necessary to correct for rundown of I_{CaL} (Figure 5.15A,B). Thus, the observations presented here are not consistent with the suggestion that anandamide has significant additional anti-adrenergic effects.

5.3.5 The effects of anandamide in the presence of isoprenaline were not prevented by pre-treatment of myocytes with pertussis toxin

Given the apparent lack of additional negative inotropic effects of anandamide under the conditions of these experiments, a receptor-mediated action seems unlikely.

However, in order to further test the hypothesis that anandamide exerts actions at G_i protein-coupled receptors in the heart, a series of experiments was carried out after cells had been pre-treated with PTX to render inhibitory G-proteins inactive.

Action potentials and contractions were measured in a group of PTX treated cells superfused with 2 nM isoprenaline for 3 minutes followed by 10 µM anandamide in the continued presence of isoprenaline. Figure 5.16 shows that after 10 minutes in PTX pre-treated cells, the amplitude of isoprenaline-stimulated contractions was reduced by 31 ± 8 % (n = 7, $P < 0.001$); this effect was slow to develop as had been observed previously. Mean data from this experiment, combined with previous experiments in the absence of PTX are summarised in Figure 5.16 and show that the reduction in isoprenaline-stimulated amplitude of contraction was not significantly different in PTX treated and untreated cells after superfusion with anandamide.

Similar observations were made with measurements of anandamide on isoprenaline-stimulated I_{CaL} amplitude in PTX-treated cells. Current voltage relationships are shown in Figure 5.17. After 10 minutes superfusion with anandamide in pertussis toxin-treated cells, peak I_{CaL} was reduced by 30 ± 5 % of maximal isoprenaline-stimulated I_{CaL} amplitude (n = 6, $P < 0.05$). Mean data from this experiment and comparisons with untreated cells are shown in Figure 5.18. These data, and those discussed previously would be consistent with the suggestion that the major effects of anandamide under isoprenaline-stimulated conditions in guinea pig ventricular myocytes occur independently of pertussis-toxin sensitive inhibitory G-proteins.

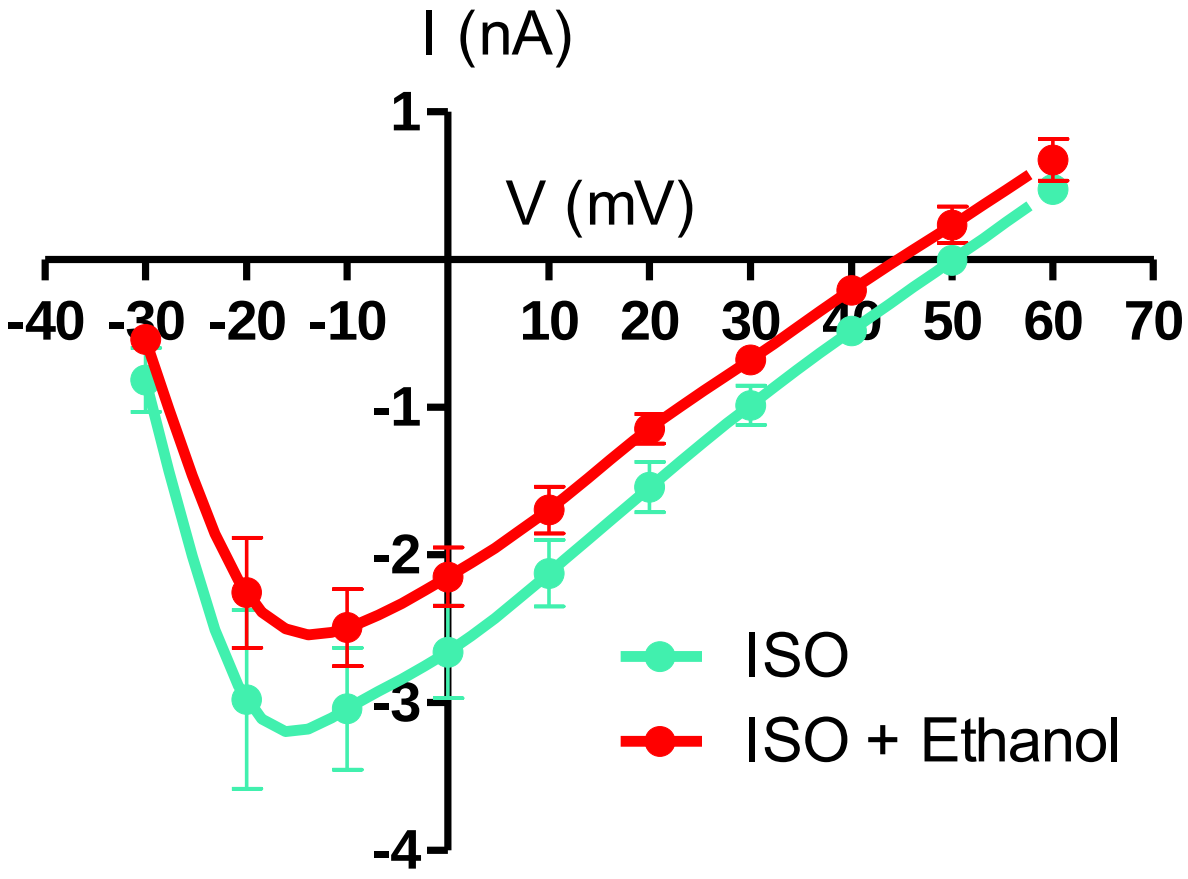


Figure 5.12 Effects of ethanol vehicle on isoprenaline-stimulated I_{CaL}

I_{CaL} was measured by clamping cells at -40 mV and stepping to a range of potentials from -30 to +60 mV for 200 ms. Cells were superfused with 2 nM isoprenaline for 3 minutes (aqua line) followed by 0.07% ethanol for 10 minutes in the continued presence of isoprenaline (red line). After 10 minutes superfusion with 0.07 % ethanol in the continued presence of isoprenaline I_{CaL} amplitude was reduced by 16 ± 4 % (n = 7, $P < 0.05$; Student's paired *t* test vs peak isoprenaline response).

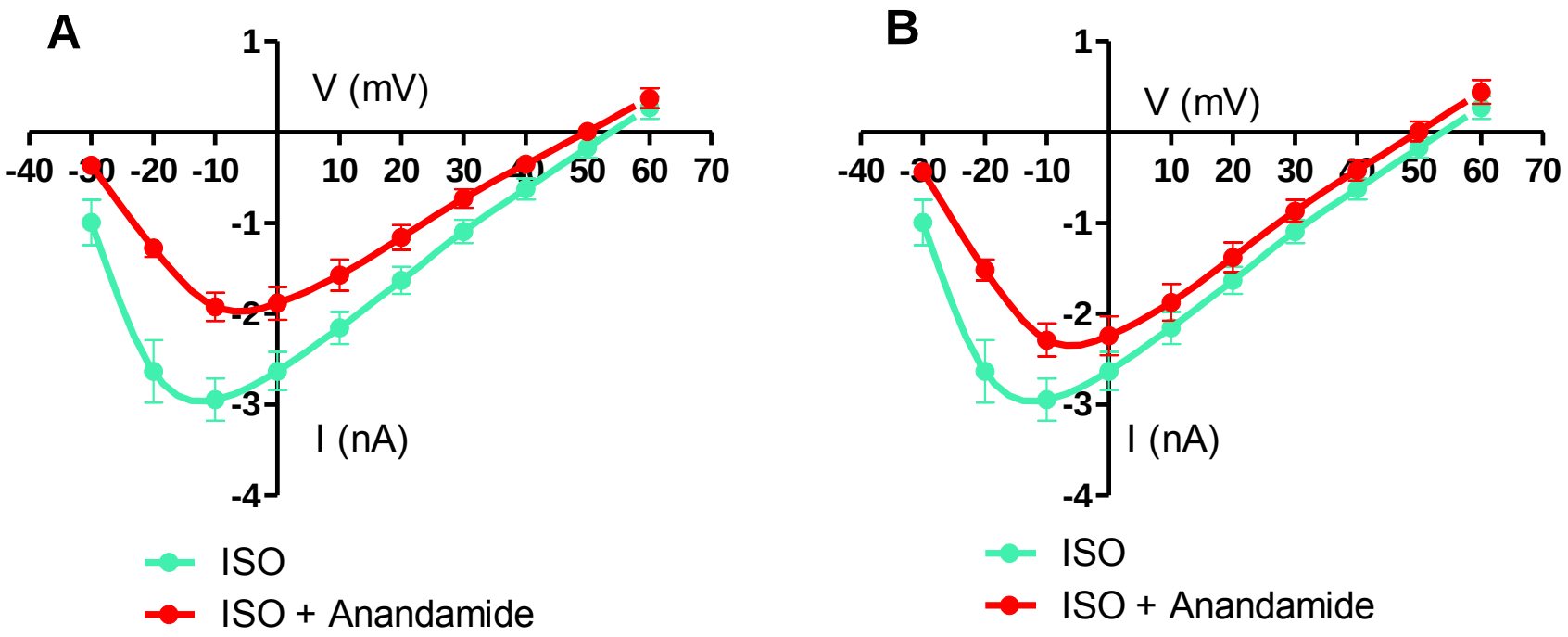


Figure 5.13 Effects of anandamide on isoprenaline-stimulated I_{CaL}

I_{CaL} was measured by clamping cells at -40 mV and stepping to a range of potentials from -30 to +60 mV for 200 ms.
Cells were superfused with 2 nM isoprenaline for 3 minutes followed by anandamide in the continued presence of isoprenaline for 10 minutes.
A: Current voltage relationship without application of a correction factor for I_{CaL} rundown. I_{CaL} amplitude was reduced by 34 ± 3 % (n = 10, $P < 0.001$) from maximal isoprenaline response.
B: Current voltage relationship after application of a correction factor to account for possible I_{CaL} rundown. Peak current at -10 mV was reduced by 21 ± 5 % (n = 10, $P < 0.01$).

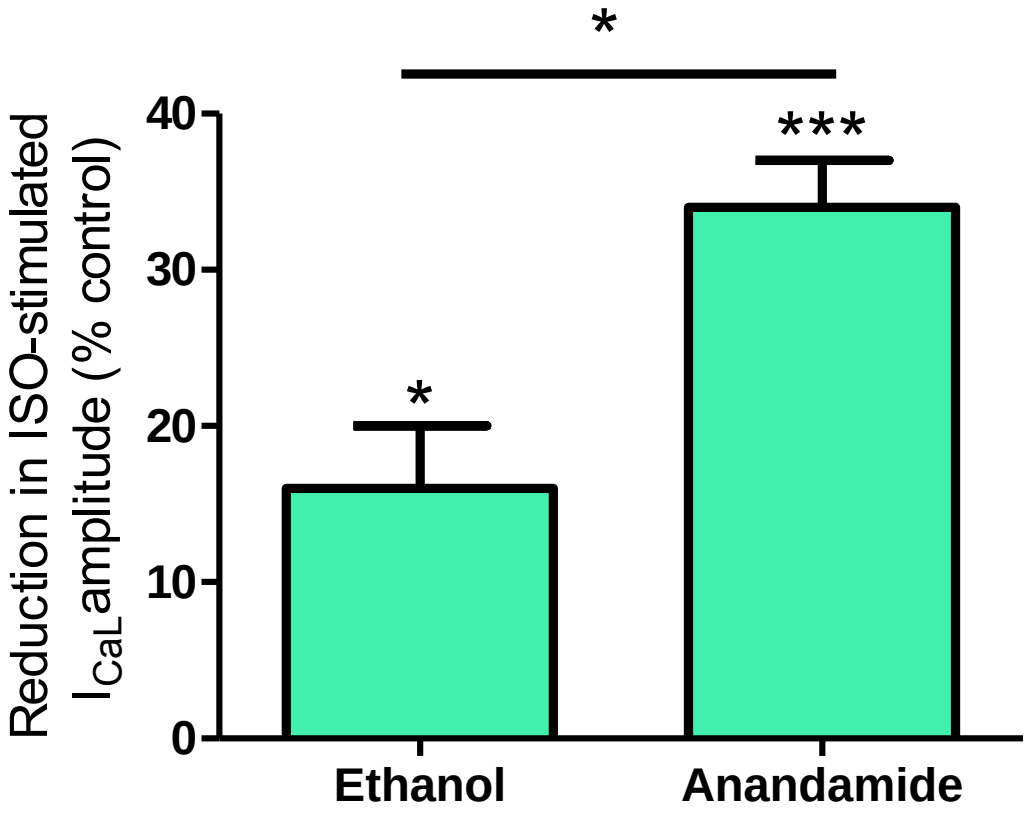


Figure 5.14 Mean data showing comparisons of the effects of anandamide and ethanol to reduce isoprenaline-stimulated I_{CaL}

There was a rundown of isoprenaline-stimulated I_{CaL} after 10 minutes superfusion with 0.07 % ethanol in the continued presence of isoprenaline (reduction of 16 ± 4 %; n = 7, $P < 0.05$). However, this was significantly smaller in magnitude than the reduction in isoprenaline-stimulated I_{CaL} amplitude in cells superfused with 10 µM anandamide (reduction of 34 ± 3 %; n = 10, $P < 0.001$). The correction factor for I_{CaL} rundown was not applied to either data set shown here.

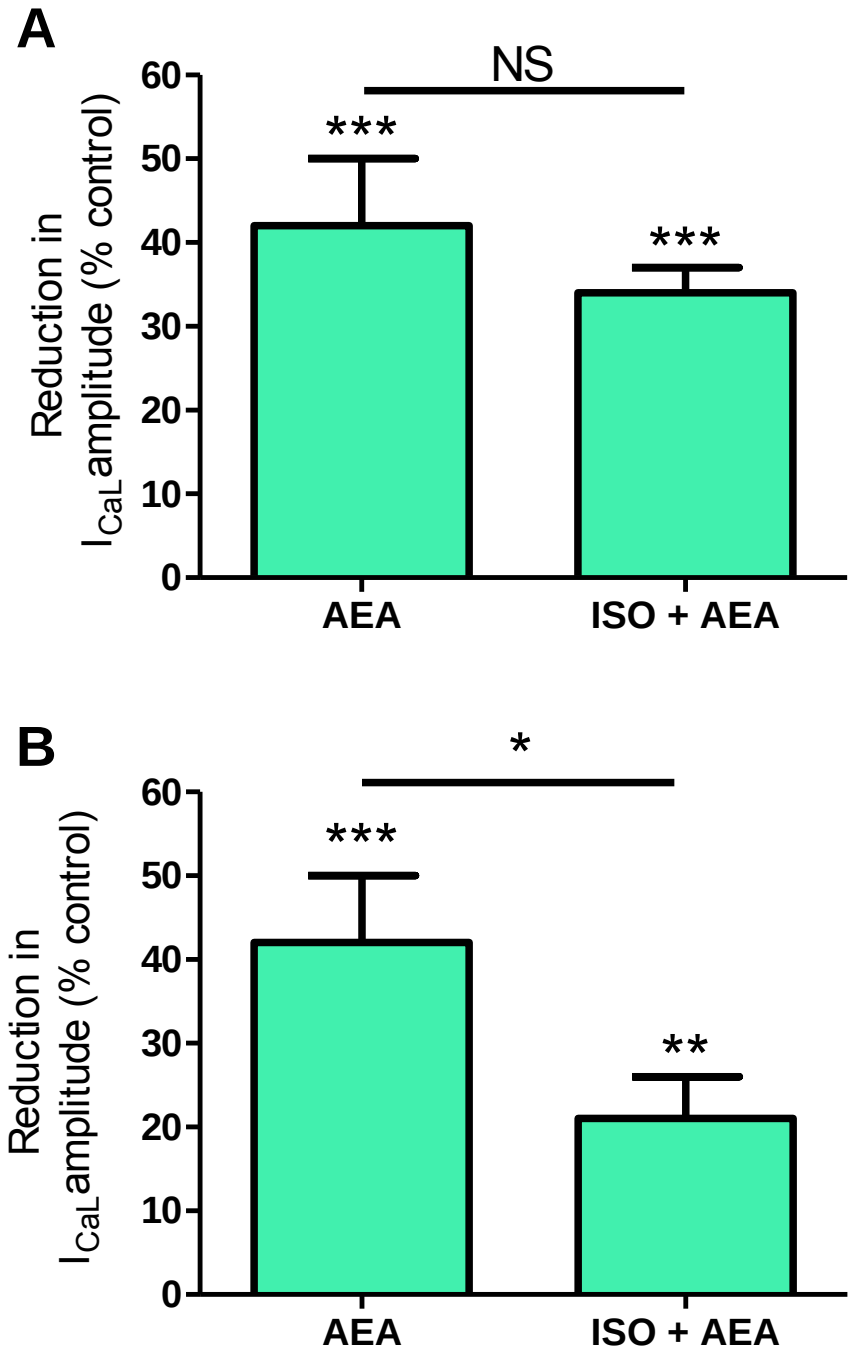


Figure 5.15 Mean reduction in I_{CaL} amplitude in cells superfused with anandamide (AEA) in the absence and presence of isoprenaline

A: Comparison of I_{CaL} reductions in the absence and presence of isoprenaline. The correction factor for rundown has not been applied to the isoprenaline data.
B: As in (A), but the correction factor has been applied to the isoprenaline data. * denotes $P < 0.05$, ** denotes $P < 0.01$, *** denotes $P < 0.001$.

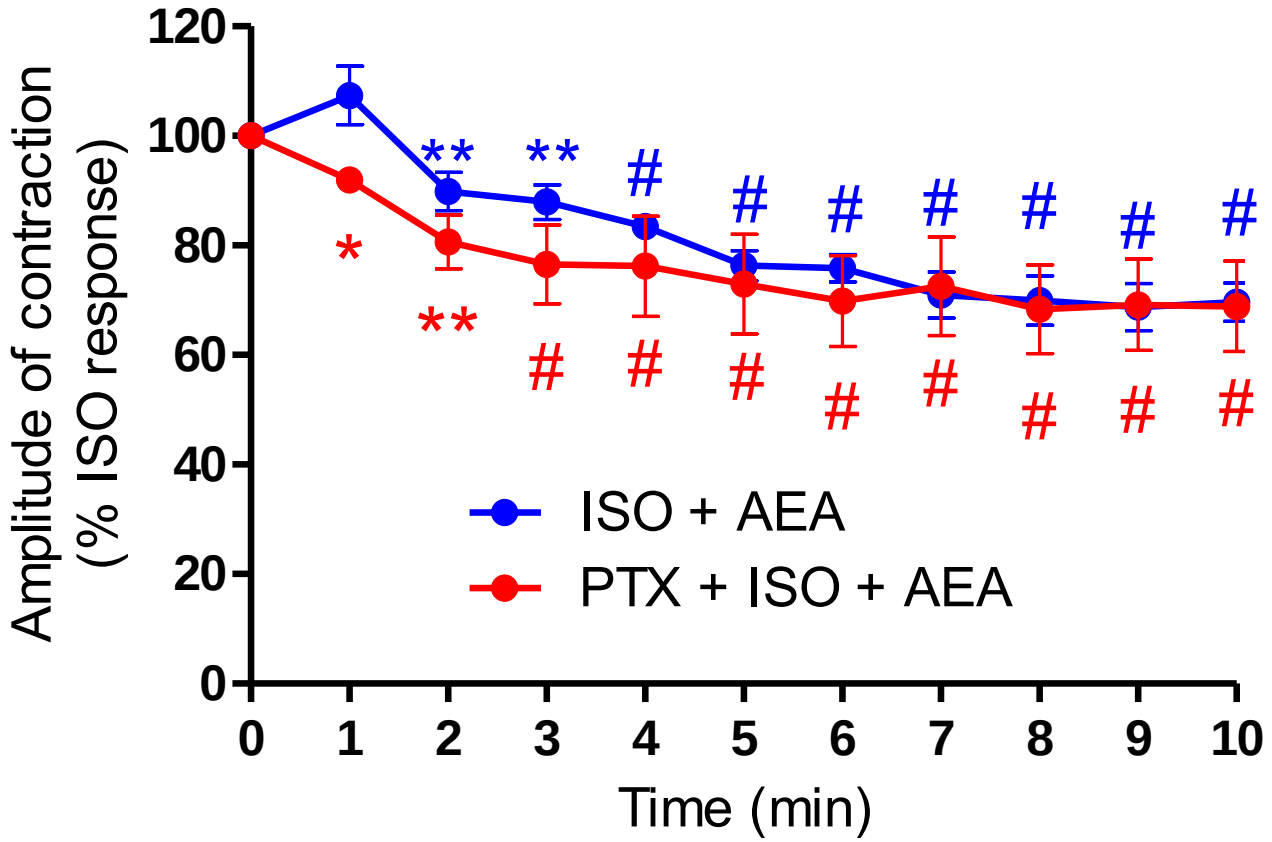


Figure 5.16 Lack of effect of pertussis toxin pre-treatment on the negative inotropic response to anandamide (AEA) in the presence of isoprenaline

Cells were stimulated to contract at 1 Hz via sharp microelectrode. Pre-treatment of cells with PTX for at least 4 hours prior to the start of the experiment did not prevent the negative inotropic response to anandamide. After 10 minutes, amplitude of sarcomere shortening was reduced by 31 ± 8 % (n = 7, $P < 0.001$) in cells which had been pre-treated with PTX, compared to 30 ± 4 % (n = 6, $P < 0.001$). * denotes P < 0.05, ** denotes P < 0.01, # denotes P < 0.001, ANOVA with repeated measures followed by Dunnett's post hoc test.

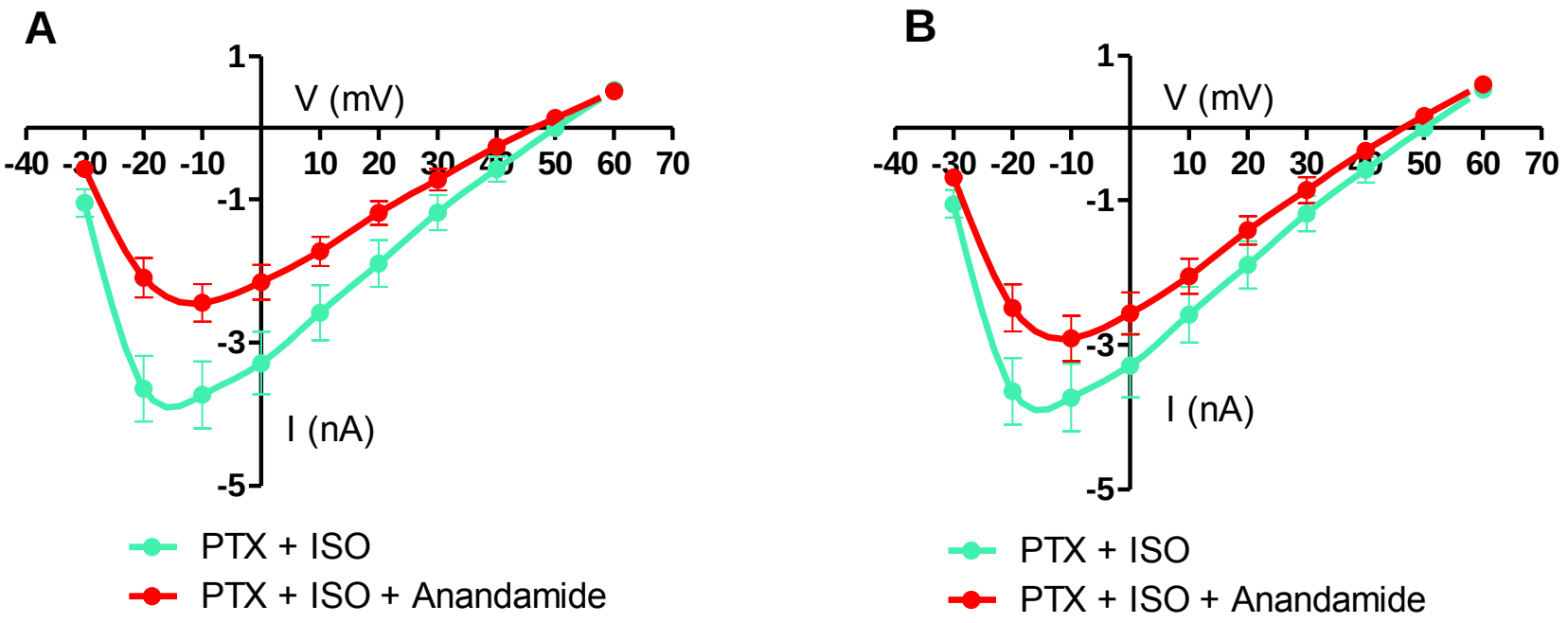


Figure 5.17 Lack of effect of PTX pre-treatment on the effect of anandamide to reduce amplitude of isoprenaline-stimulated I_{CaL}

I_{CaL} was stimulated by 200 ms depolarising current pulses from -40 mV to a range of potentials from -30 mV to +60 mV. Cells were pre-treated with PTX for at least 4 hours, and then superfused with 2 nM isoprenaline followed by 10 µM anandamide in the continued presence of isoprenaline.
A: Current voltage relationship without application of a correction factor to account for I_{CaL} rundown under these conditions.
After 10 minutes superfusion with anandamide, the amplitude of isoprenaline-stimulated I_{CaL} was reduced by 32 ± 5 % of the maximal isoprenaline response (n = 7, $P < 0.01$).
B: Current voltage relationship after application of a correction factor to account for I_{CaL} rundown. The amplitude of isoprenaline-stimulated I_{CaL} was reduced by 19 ± 6 % (n = 7, $P < 0.05$).

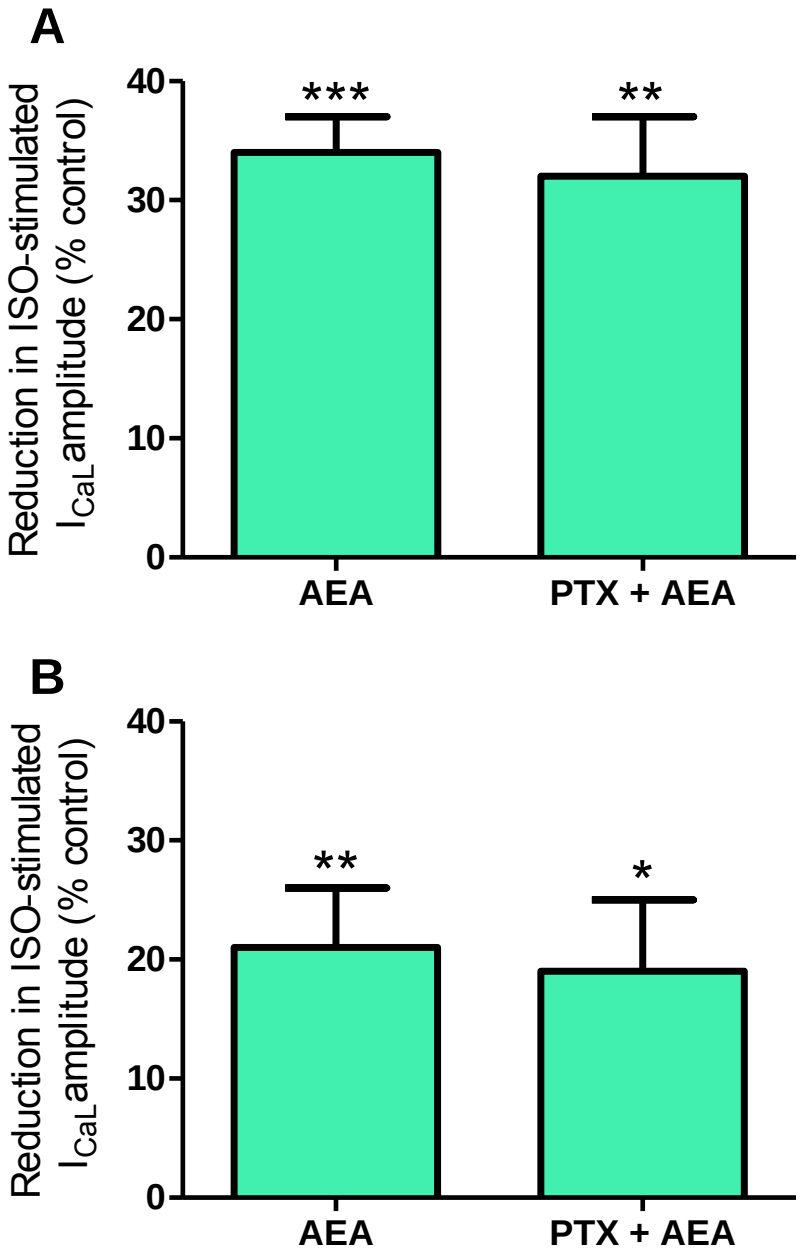


Figure 5.18 Mean data summarising the lack of effect of pertussis toxin in preventing the effect of anandamide (AEA) to reduce amplitude of isoprenaline-stimulated I_{CaL}

A: Apparent reduction in isoprenaline-stimulated I_{CaL} amplitude without application of a correction factor for rundown.
B: Reduction in isoprenaline-stimulated I_{CaL} amplitude after application of a correction factor.
The magnitude of I_{CaL} reduction in cells which had been treated with PTX was equivalent to those which had not.

5.3.6 The negative inotropic effect of nifedipine was reduced in the presence of isoprenaline

It is interesting to note that the effects reported above suggest that the actions of anandamide to reduce amplitude of contraction and I_{CaL} are slightly suppressed in the presence of isoprenaline (for example, see Figure 5.10 and Figure 5.15), compared to effects observed in the absence. Since the actions of anandamide to inhibit amplitude of contraction and I_{CaL} do not appear to be mediated by inhibitory G-proteins (for example, see Figure 5.16 and Figure 5.18), one possibility is that anandamide interacts directly with the LTCC. There are some reports that anandamide weakly interacts with the DHP binding site on the LTCC (Johnson *et al.*, 1993; Shimasue *et al.*, 1996), and that the effects of DHP Ca^{2+} channel blockers to inhibit I_{CaL} are reduced in the presence of isoprenaline (Legssyer *et al.*, 1997; Farkas *et al.*, 2012). Therefore, one explanation for the diminished effect of anandamide to induce negative inotropic responses in the presence of isoprenaline may be that phosphorylation of the LTCC reduces the ease with which anandamide can interact with the DHP binding site on the channel. In order to investigate the feasibility of this suggestion, measurements of cell contractions were made using nifedipine (a DHP Ca^{2+} channel antagonist) in the absence and presence of isoprenaline. Figure 5.19 shows the amplitude of cell contractions measured with 100 nM nifedipine alone, and then 100 nM nifedipine in the presence of 2 nM isoprenaline. 100 nM nifedipine was selected as it produced a reduction in amplitude of contraction similar in magnitude to that observed with 10 μM anandamide (reduction of 76 ± 5 %, n = 5, $P < 0.01$). 100 nM nifedipine caused a marked reduction in amplitude of cell contractions, but the magnitude of this reduction was reduced in the presence of isoprenaline (Figure 5.19).

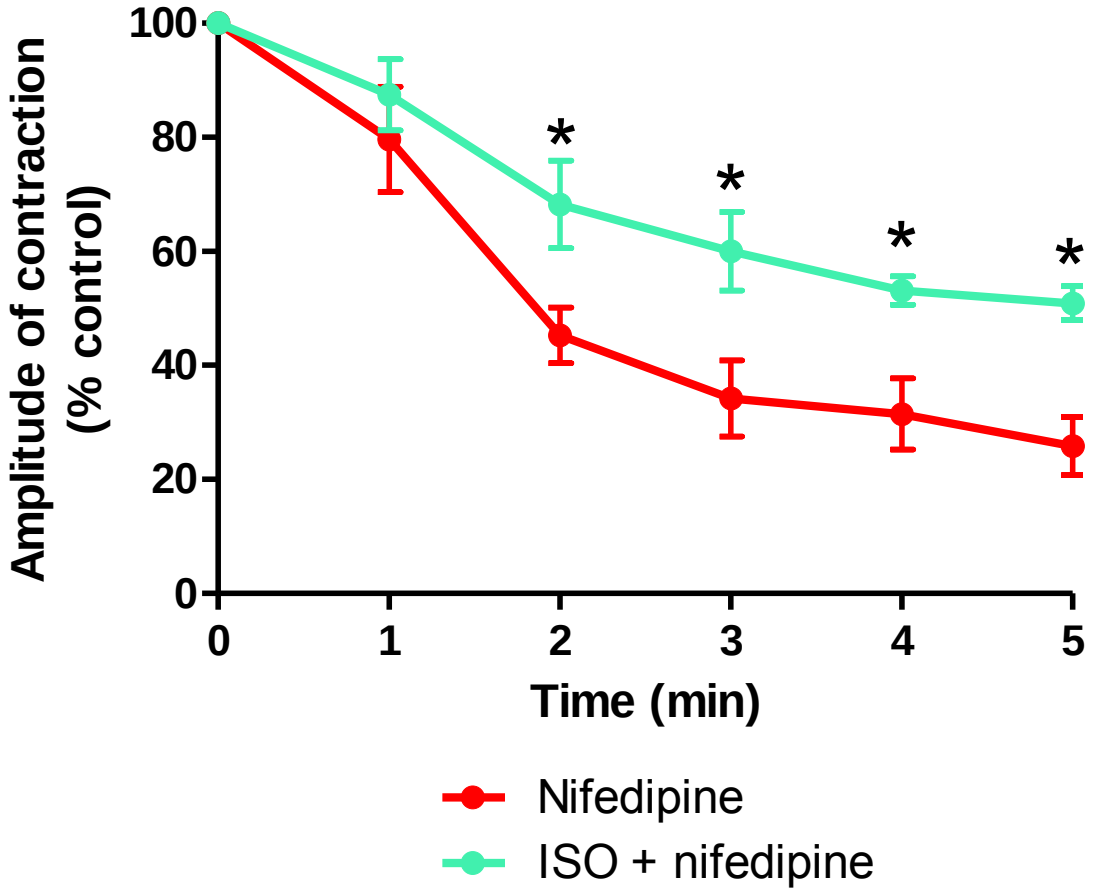


Figure 5.19 Effects of nifedipine on sarcomere shortening in the absence and presence of isoprenaline

Cells were stimulated to contract at 1 Hz via a sharp microelectrode. After 5 minutes superfusion with 100 nM nifedipine, contraction was reduced by 74 ± 5 % reduction in the absence of isoprenaline, and by 49 ± 4 % in its presence. (n = 5 and 4 respectively, both $P < 0.01$ vs control). * denotes $P < 0.05$, one-way ANOVA with Bonferroni post-hoc test.

5.3.7 Anandamide exerted an anti-arrhythmic action in the presence of high dose isoprenaline

Figure 5.20 illustrates the effects of 50 nM isoprenaline to induce spontaneous electrical activity in a cell stimulated to fire APs at 1 Hz. In the absence of drugs, only stimulated APs were observed (Figure 5.20A), but in the presence of 50 nM isoprenaline, small transient depolarisations began to appear in between stimulated APs until they were large enough in magnitude to elicit full spontaneous APs. In the presence of 50 nM isoprenaline alone, this spontaneous activity began to appear within 2 minutes, and was well maintained for a further 10 minutes in all cells studied (n = 5). In a further 6 cells, the effects of 10 μM anandamide on this spontaneous activity were studied. In 3 of 6 cells, spontaneous APs were completely suppressed after 7 minutes superfusion with anandamide. In the remaining 3 cells, spontaneous APs appeared relatively infrequently after 7 minutes but were not completely suppressed during the course of the experiment.

The effects of anandamide on spontaneous electrical activity after 10 minutes were quantified by measuring the number of spontaneous APs occurring over a 5 second period. After 10 minutes superfusion with anandamide in the presence of 50 nM isoprenaline, the number of spontaneous APs was 4.2 ± 0.2 in control and 1.7 ± 0.6 after 10 minutes superfusion with anandamide in the continued presence of 50 nM isoprenaline, (n = 6, $P < 0.05$). In cells superfused with 50 nM isoprenaline in the absence of anandamide, the number of spontaneous APs was well maintained after 10 minutes (4.2 ± 0.4 spontaneous APs in control, and 4.2 ± 0.2 after 10 minutes; n = 5, $P > 0.05$).

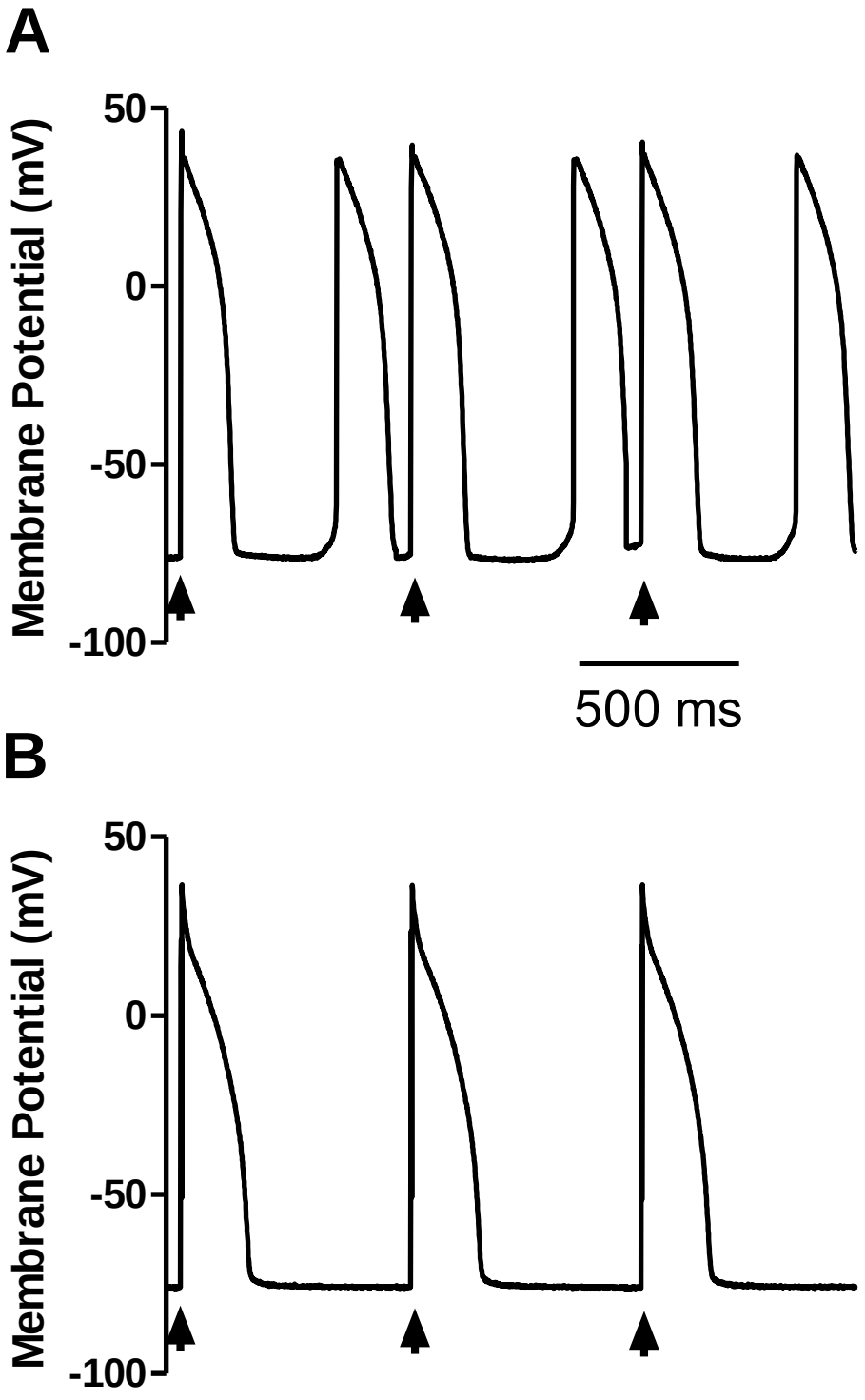


Figure 5.20 Example of spontaneous electrical activity induced by 50 nM isoprenaline and suppressed by anandamide

A: Spontaneous APs occurring after treatment with 50 nM isoprenaline.
B: Abolition of spontaneous APs occurring after 7 minutes superfusion with 10 μM anandamide in the continued presence of 50 nM isoprenaline.

5.3.8 ACEA, a selective CB_1 receptor agonist was without significant effect on I_{CaL} amplitude in the presence of isoprenaline

Taken together, the above data are suggestive of an effect of anandamide which is independent of cannabinoid receptors. However, these receptors have been shown to be expressed in cardiac tissue (Weis *et al.*, 2010), and a cannabinoid receptor-mediated anti-adrenergic action cannot be ruled out on the basis of the above data. In order to determine whether any effects of selective cannabinoid receptor agonists were evident in the presence of isoprenaline, I_{CaL} amplitude was measured in cells superfused with isoprenaline (2 nM) for 3 minutes until a maximal effect was achieved, followed by superfusion with either the selective CB_1 receptor agonist ACEA (10 μM) in the continued presence of isoprenaline.

Figure 5.21A depicts current voltage relationships in 6 cells superfused with isoprenaline and ACEA. After 10 minutes superfusion with ACEA, there was a small but significant reduction (17 ± 6 %; n = 6, $P < 0.05$ vs peak isoprenaline response) in amplitude of isoprenaline-stimulated I_{CaL}. However, since ACEA was dissolved in ethanol, and significant reductions in the amplitude of isoprenaline-stimulated current had previously been observed (Figure 5.12), the correction factor to account for this was applied to ACEA data. Figure 5.21B shows current voltage relationships after application of the correction factor. Isoprenaline-stimulated I_{CaL} was 96 ± 7 % of the peak isoprenaline response after 10 minutes (n = 6, $P > 0.05$). Furthermore, Figure 5.22 shows that there were was no significant reduction in amplitude of contraction, which would be expected if there were a real inhibition of I_{CaL} in response to ACEA (n = 6, $P > 0.05$).

5.3.9 Effect of 2-arachidonoylglycerol on action potentials and contractions in the presence of isoprenaline

In order to conclude this section of work, the effects of 2-AG were also studied in the presence of isoprenaline. APs and contractions recorded from cells superfused with 2 nM isoprenaline for 3 minutes, followed by 10 μM 2-AG for 5 minutes in the continued presence of isoprenaline. Preliminary observations showed that after 5 minutes superfusion with 2-AG, APD_{90} was 99 ± 7 % of control and APD_{20} was 99 ± 10 % (n = 3, $P > 0.05$), and the amplitude of isoprenaline-stimulated contractions was 91 ± 7 % of control values (n = 3, $P > 0.05$).

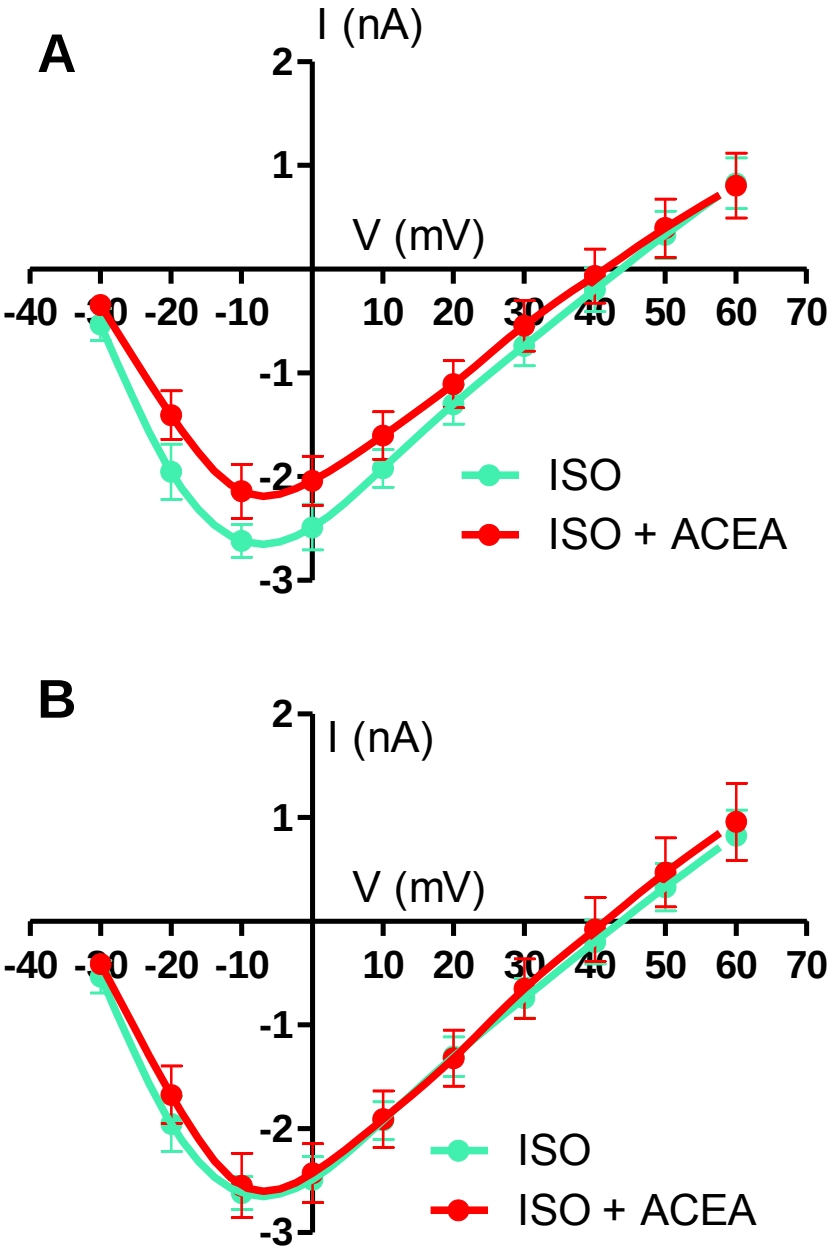


Figure 5.21 Lack of effect of the CB_1 receptor agonist ACEA on isoprenaline-stimulated I_{CaL}

I_{CaL} was elicited by 200 ms step depolarisations from -40 mV to a range of potentials from -30 to +60 mV.
A: Current voltage relationship without correction for I_{CaL} rundown. After 10 minutes superfusion with 10 µM ACEA in the continued presence of 2 nM isoprenaline, the apparent reduction in I_{CaL} amplitude was 17 ± 6 % of the maximal isoprenaline response (n = 6, $P < 0.05$).
B: Current voltage relationship after correcting for I_{CaL} rundown. After correction, there were no significant effects of ACEA on I_{CaL} amplitude: 96 ± 7 % of peak isoprenaline response (n = 6, $P > 0.05$).

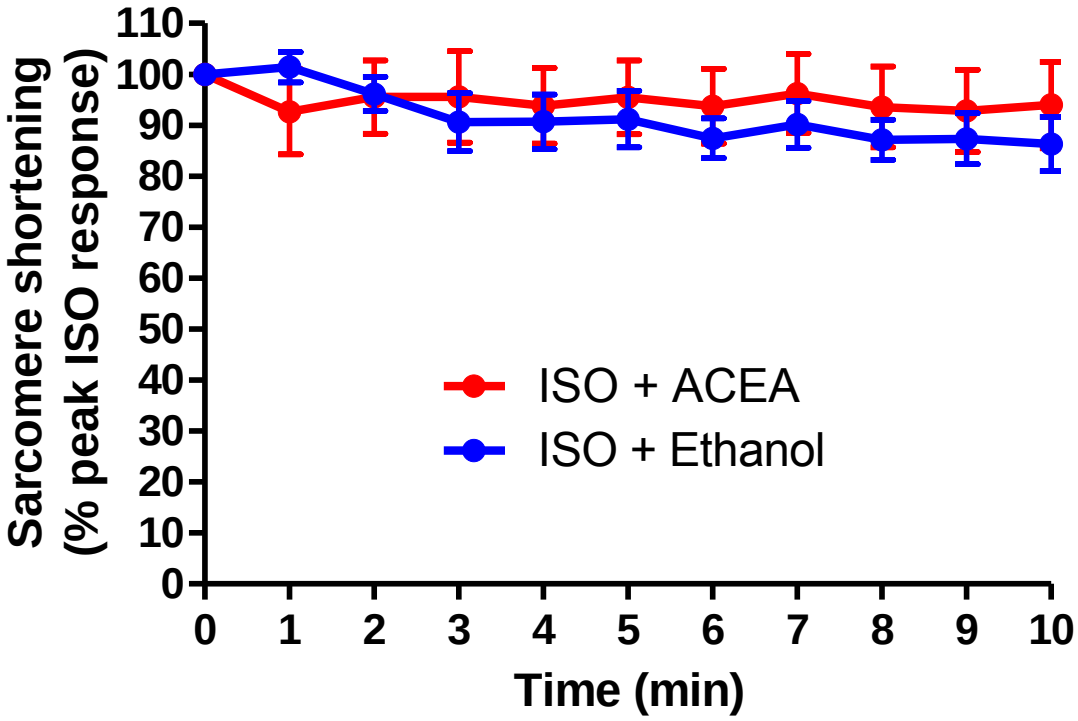


Figure 5.22 Lack of effect of ACEA on isoprenaline-stimulated contractions

Cells were stimulated to contract at 1 Hz via a sharp microelectrode. After 10 minutes superfusion with ACEA, the amplitude of isoprenaline-stimulated contractions was 94 ± 8 % of control (n = 6, $P > 0.05$).

5.4 Discussion

The data presented in this chapter are the first reports of the effects of anandamide on electrical activity and contractions in isolated guinea pig ventricular myocytes in the presence of the non-specific β-adrenoceptor agonist isoprenaline, which raises intracellular cAMP through activation, primarily, of β_1 adrenoceptors. Some of these data have been published in the form of an abstract (Bolton *et al.*, 2012).

In contrast to the marked negative inotropic actions of anandamide reported in the absence of β-adrenoceptor stimulation in chapter 4, adenosine was without significant effect on amplitude of contractions or I_{CaL} in the absence of isoprenaline (Figure 5.1). However, in the presence of isoprenaline, the amplitude of contractions and I_{CaL} were rapidly reduced upon superfusion with adenosine (Figure 5.2 and Figure 5.3). These observations are in agreement with reports in the literature, that agonists acting at G_i protein coupled receptors are without significant effect on ventricular myocyte contractility or I_{CaL} unless adenylyl cyclase activity is stimulated by β-adrenoceptor stimulation (Hartzell, 1988; Belardinelli *et al.*, 1995; Song *et al.*, 1996; Calloe *et al.*, 2013). Furthermore, the effects of adenosine were sensitive to PTX, demonstrating the involvement of inhibitory G-proteins in these 'anti-adrenergic' effects (Figure 5.2, Figure 5.5 and Figure 5.6), which is in agreement with effects reported in the literature (Brown *et al.*, 1990), and confirmed the effectiveness of the PTX pre-treatment protocol for subsequent anandamide experiments. Furthermore, the speed with which responses to adenosine occurred are indicative of a GPCR-mediated mechanism.

Anandamide was found to exert a concentration dependent negative inotropic action in the presence of isoprenaline (Figure 5.10) and a concentration dependent

reduction in AP duration (Figure 5.11). The magnitude of these effects was found to be smaller than the magnitude of equivalent observations made in the absence of isoprenaline (Figure 5.10 and Figure 5.11). It might be expected that if anandamide were acting through a G_i protein-coupled receptor-mediated mechanism, to reduce intracellular cAMP and PKA-mediated phosphorylation of protein targets, that the magnitude of effect observed in the presence of isoprenaline may be greater than that observed its absence. Thus, the observation that this was not the case, is, in itself, suggestive of a mechanism of action of anandamide that is independent of cannabinoid receptors.

Studies of the effects of isoprenaline-stimulated I_{CaL} were made more challenging due to an apparent rundown of the isoprenaline-stimulated current in the presence of ethanol (Figure 5.12). A correction factor was therefore applied to all experiments where ethanol vehicle had been used. The observation that the effect of anandamide to inhibit isoprenaline-stimulated I_{CaL} was certainly no greater in magnitude than the effect seen in the absence of isoprenaline (Figure 5.15), is also suggestive of a mechanism which does not involve inhibitory G-proteins. It may be expected that an effect to reduce intracellular cAMP and thus associated phosphorylation of I_{CaL} would be enhanced when cAMP is elevated in the presence of isoprenaline. However, given that a reduction in I_{CaL} amplitude was still observed, experiments with PTX were carried out as a further test for the involvement of inhibitory G-proteins.

Using the same PTX pre-treatment protocol used to inhibit the responses to adenosine in the presence of isoprenaline, it was determined that the effects of anandamide to reduce amplitude of contraction and I_{CaL} could not be prevented by PTX (Figure 5.16, Figure 5.17 and Figure 5.18). Although this finding was not unexpected

given the data in chapter 4, it gives further weight to the proposal that the effects of anandamide under the conditions of these experiments were largely, if not completely, independent of actions of PTX-sensitive inhibitory G-proteins.

Although the effects of PTX on anandamide actions in cardiac myocytes have not previously been investigated, this finding is in conflict with the conclusions of Li and colleagues who suggested that the effects of anandamide occurred through activation of CB_1 receptors (although these researchers did not investigate the nature of the signalling pathway involved) (Li *et al.*, 2009). It is unclear why the conclusions of Li and colleagues are different from those of the present study, and from the conclusions of Al Kury and colleagues (Al Kury *et al.*, 2014a; Al Kury *et al.*, 2014b). One possibility is that, because these investigators used rat ventricular myocytes, a species difference could underlie differences in the mechanism involved. Interestingly, Li and colleagues observed effects of anandamide at nanomolar concentrations, which were not evident in the present study; one reason for this could be that they used DMSO as the solvent while ethanol was used in the present study. It is possible that the solvent could affect the nature of the interaction between lipid chains and receptors or ion channels.

It is possible that the mechanisms of action of anandamide may vary depending on the region of the heart being studied, and which ion channels are expressed. For example, in the case of adenosine and acetylcholine, direct negative inotropic actions are observed in atrial myocytes due to the activation of a K^+ channel by G-protein $\beta\gamma$ subunits, that is not expressed in as high abundance in ventricular muscle (Iijima *et al.*, 1985; Belardinelli *et al.*, 1995). Activation of this channel leads to AP shortening, and as a result, a secondary reduction in Ca^{2+} influx during the AP and reduced amplitude of contraction (Belardinelli *et al.*, 1995). Bonz and colleagues suggested that anandamide

exerted actions though CB_1 receptors in rat atria (Bonz *et al.*, 2003); indeed basal levels of turnover of adenylyl cyclases in the atria are thought to be higher than in the ventricles (Vinogradova *et al.*, 2006), which may mean that additional receptor-mediated effects of anandamide on membrane currents may be evident in atrial tissue. Furthermore, it is possible that the density of cannabinoid receptors varies depending on region of the heart being studied. The lack of effect of ACEA to reduce the amplitude of isoprenaline-stimulated I_{CaL} in ventricular myocytes in this study (Figure 5.21) would be consistent with the ideas that either CB_1 receptors do not couple to pathways regulating I_{CaL}, or that receptor density is too low in ventricular tissue. Another possibility is that receptor-mediated actions of cannabinoids on cardiac contractility are only observable in disease states; indeed CB_2 receptors are up-regulated in cardiac tissue in heart failure (Weis *et al.*, 2010). Perhaps the density of receptors in non-disease states is just too low to mediate an observable effect. Thus, an interesting potential line of future study may be to examine the effects of cannabinoid receptor agonists and anandamide in diseased cardiac myocytes.

Given that the effects of anandamide under the conditions of the experiments presented here appear to be independent of cannabinoid receptors, other mechanisms of action must be considered. Since anandamide is highly lipophilic, it is possible that it may interact directly with ion channels, or interfere with the cell membrane lipid bilayer. There are some reports that anandamide weakly interacts with the DHP binding site on the LTCC (Johnson *et al.*, 1993; Shimasue *et al.*, 1996). In light of observations reported here, that the effect of nifedipine to reduce the amplitude of cell contractions in the presence of isoprenaline is diminished compared to in the absence of isoprenaline (Figure 5.19), one possibility is that the reduced effects of anandamide in the presence of isoprenaline might be explained by a reduced effect to interact with the LTCC when

it is phosphorylated. Furthermore, other investigators have reported that the magnitude of inhibition of I_{CaL} by nifedipine is reduced in the presence of isoprenaline ((Legssyer *et al.*, 1997; Farkas *et al.*, 2012). Nevertheless, an anti-arrhythmic action of anandamide was still observed (Figure 5.20), and it is possible that this is mediated by dual inhibition of Ca^{2+} and K^{+} channels. In addition, it is possible that an inhibitory effect of anandamide on NCX, recently observed by Al Kury and colleagues (Kury *et al.*, 2014), may also contribute to this mechanism by reducing the effect of NCX to induce delayed after-depolarisations when SR Ca^{2+} load is elevated. However, other actions of anandamide, for example to reduce myofilament Ca^{2+} sensitivity or SR load cannot be ruled out. It is also important to consider that the findings presented here do not necessarily reflect the *in vivo* situation. It is possible that, because of reported actions of anandamide to inhibit sympathetic outflow (Szabo *et al.*, 2001), anti-adrenergic actions may be more pronounced *in vivo*.

Preliminary observations of the effects of 2-AG suggested this endocannabinoid had little or no effect on isoprenaline-stimulated APs and contractions in the present study. It is likely that this endocannabinoid does not share the ability of anandamide to evoke effects at multiple targets (e.g. ion channels). For example, the ability of anandamide to interact directly with T-type Ca^{2+} channels was not shared with 2-AG (Chemin *et al.*, 2001). This may explain why the actions of anandamide have received greater attention in the literature than those of 2-AG.

Chapter 6

Effects of Δ^9-tetrahydrocannabinol on excitation-contraction coupling in guinea pig ventricular myocytes

6.1 Introduction

Δ^9-THC, first isolated, purified and synthesised in the 1960s (Gaoni *et al.*, 1971), is the principal psychoactive constituent of *Cannabis sativa.* In addition to the use of cannabis as a recreational drug, Δ^9-THC and other compounds such as cannabidiol are used therapeutically to treat pain, and to prevent the nausea and vomiting associated with chemotherapy (Pacher *et al.*, 2006). However, medications containing Δ^9-THC are contra-indicated in patients with pre-existing cardiovascular disease (for example, severe heart failure, ischaemic heart disease or poorly controlled blood pressure). Despite the use of this compound as a therapeutic agent, very few studies have sought to address the effects of Δ^9-THC on cardiac muscle directly.

Acute exposure to Δ^9-THC (or cannabis, which contains Δ^9-THC and many other cannabinoids) results in tachycardia (Nahas *et al.*, 1985), but repeated exposure is associated with reduced blood pressure and heart rate, which has been attributed to centrally mediated, reduced sympathetic and enhanced parasympathetic activity (Jones, 2002). Although many of the effects of Δ^9-THC are thought to be mediated by CB_1 and CB_2 receptors (Matsuda *et al.*, 1990; Munro *et al.*, 1993), there is evidence of other non-cannabinoid receptor targets (Pertwee *et al.*, 2010), including direct modulation and inhibition of T-type Ca^{2+} channels (Ross *et al.*, 2008), voltage-gated Na^+ channels (Kumbaraci *et al.*, 1980) and K^+ channels (Poling *et al.*, 1996). This hypothesis would provide support to very early observations that the effects of cannabinoid compounds occur through effects to perturb the cell membrane lipid bilayer (Lawrence *et al.*, 1975), which are very often overlooked (Oz, 2006).

In light of the data concerning endogenous cannabinoids presented in chapters 3 and 4, and because very few, if any published studies have examined the effects of Δ^9-

THC in cardiac muscle, the aim of the experiments presented in this chapter was to determine whether Δ^9-THC modulates the electrophysiological and contractile function of guinea pig ventricular myocytes. Furthermore, the use of Δ^9-THC as a therapeutic agent means that it is of scientific interest to understand whether this compound has direct actions on cardiac muscle.

6.2 Methods

The methods used to perform experiments presented in this chapter are described in detail in chapter 2. Guinea pigs were killed by cervical dislocation and their hearts rapidly excised. To isolate ventricular myocytes, hearts were retrogradely perfused with a modified Tyrode's solution containing collagenase. Cells were plated onto a glass coverslip attached to a perfusion bath and superfused with PSS, which was heated to 36^{o}C and gassed with 95 % O_2 5 % CO_2 in order to maintain a pH of 7.4.

Cell contraction, (in response to electrical stimulation delivered at 1 Hz via a patch electrode with amphotericin to achieve permeabilised configuration) was measured using the IonOptix system to measure sarcomere length. Images of ventricular myocytes were captured using the IonOptix MyoCam mounted on a Nikon Diaphot 200 inverted microscope with a ×40 objective lens.

Electrophysiological measurements of action potentials and membrane currents were made using an AxoClamp 2 amplifier (Axon Instruments, USA), with all analysis carried out with Clampfit 9.2 software (Axon Instruments, USA). Cells were patched using amphotericin (240 U/ml) to achieve the permeabilised configuration, except where Cs^+ was required to be introduced to the intracellular compartment, when whole-cell patch clamp was used. Action potentials were stimulated by 2 ms depolarising

current pulses (1 – 5 nA). I_{CaL} was activated by 200 ms step depolarisations from a holding potential of –40 mV to a range of potentials from –40 to +60 mV at a frequency of 0.2 Hz. In experiments measuring I_{CaL} inactivation, a double pulse protocol (applied at a frequency of 0.2 Hz) was used. An initial pre-pulse of 500 ms duration, from a holding potential of -40 mV to a range of potentials from -50 mV to +60 mV at 5 mV increments was applied prior to a 200 ms test pulse from -40 mV to 0 mV. These experiments were made in the absence and presence of Cs^+. A correction for rundown of the current was made as outlined in chapter 2. Measurements of I_K were made by application of step depolarisations from -40 to +40 mV for 10 – 800 ms, at a frequency of 0.1 Hz. The amplitude of the tail current upon repolarisation was taken to represent I_K.

When using an AxoClamp amplifier to patch cells, it is not possible to measure cell capacitance directly (as is possible, for example with an AxoPatch amplifier). Measurements of cell capacitance were therefore estimated during voltage clamp experiments by application of a 10 mV step depolarisation (of 200 ms duration) from a holding potential of –40 mV to –30 mV, during which no currents should be activated. The resulting capacitive transients were then integrated to give an estimate of current flowing per unit time (pA*ms). The same rationale as outlined previously (chapter 4) was used.

6.3 Results

6.3.1 Δ^9-THC markedly reduced myocyte contractility

Superfusion of ventricular myocytes with Δ^9-THC, resulted in a concentration-dependent reduction in contractility. In a manner similar to the effects of anandamide,

this was slow to develop over the course of a 10 minute experiment. After 10 minutes superfusion with 10 μM Δ^9-THC, the amplitude of sarcomere shortening was reduced by 57 ± 7 % (n = 6, $P < 0.001$). After 10 minutes superfusion with 3 μM Δ^9-THC, this reduction was 33 ± 8 % (n = 5, $P < 0.001$). These data are shown in Figure 6.1. AP parameters were also measured in these cells. After 10 minutes superfusion with 10 μM Δ^9-THC, APD_{90} was 97 ± 2 % and APD_{20} 101 ± 2 % of control values (n = 6, $P > 0.05$). To summarise, Δ^9-THC caused a reduction in contraction, with little or no apparent change in AP configuration. Figure 6.2 shows the apparent lack of effect of Δ^9-THC on AP parameters; a representative AP and contraction trace are shown in Figure 6.3.

6.3.2 Δ^9-THC inhibited the L-type Ca^{2+} current (I_{CaL})

Although Δ^9-THC was not found to significantly alter AP configuration, it is still possible that the reduction in amplitude of contractions may be mediated, at least in part, by a reduction in Ca^{2+} influx via LTCCs, provided that there are additional compensating effects on other currents to maintain action potential shape (see section 6.3.3). In this series of experiments, I_{CaL} was measured using the perforated patch technique (amphotericin 240 U/ml), and control experiments performed using 0.03 % ethanol. Figure 6.4 shows current voltage-relationships before and after superfusion with ethanol for 10 minutes. Under these conditions, the amplitude of I_{CaL} at 0 mV after 10 minutes was 80 ± 6 % of control (n = 7, $P = 0.057$). Because of this apparent run-down under these conditions, it was decided that a correction (as described in chapter 2, section 2.4.7), based on a 2% per minute rundown, must be made in subsequent I_{CaL} experiments utilising the permeabilised patch technique. There were no significant effects on the kinetics of I_{CaL} inactivation in these control experiments (n = 7, $P > 0.05$; Figure 6.5).

Superfusion of myocytes with 10 μM Δ^9-THC, resulted in a reduction in I_{CaL} amplitude measured using the permeabilised patch technique. After 10 minutes, peak current at 0 mV was reduced by 40 ± 7 % (n = 6, $P < 0.01$), without a correction for rundown. When rundown was corrected for, I_{CaL} amplitude at 0 mV was reduced by 28 ± 8 % (n = 6, $P < 0.05$). Current voltage relationships without the correction are shown in Figure 6.6A, and with the correction in Figure 6.6B. In addition, there was a leftward shift of voltage-dependence of inactivation of I_{CaL} after exposure to Δ^9-THC (Figure 6.7).

Additional experiments were then performed using the whole-cell patch technique, such that Cs^+ could be introduced into the intracellular compartment to prevent contaminating K^+ currents interfering with I_{CaL} recordings. Measurements of I_{CaL} made using the whole-cell patch technique are also susceptible to rundown, and so corrections were made based on the control experiments presented in chapter 4, where a rundown of 2.3 % per minute was observed (see section 4.3.6 and Figure 4.17, chapter 4). After 10 minutes superfusion with 10 μM Δ^9-THC in the presence of Cs^+, before the application of a correction for rundown, peak I_{CaL} at 0 mV was reduced by 51 ± 5 % (n = 3, $P < 0.05$); current voltage relationships are shown in Figure 6.8A. When a correction was applied, this reduction was 35 ± 7 % (n = 3, $P < 0.05$; Figure 6.8B), which is comparable to the 28 ± 8 % reduction observed with perforated patch after correction for run down (Figure 6.4). In addition, a leftward shift of the voltage-dependence of inactivation of I_{CaL} was also observed with Δ^9-THC in the presence of Cs^+, as illustrated in Figure 6.9.

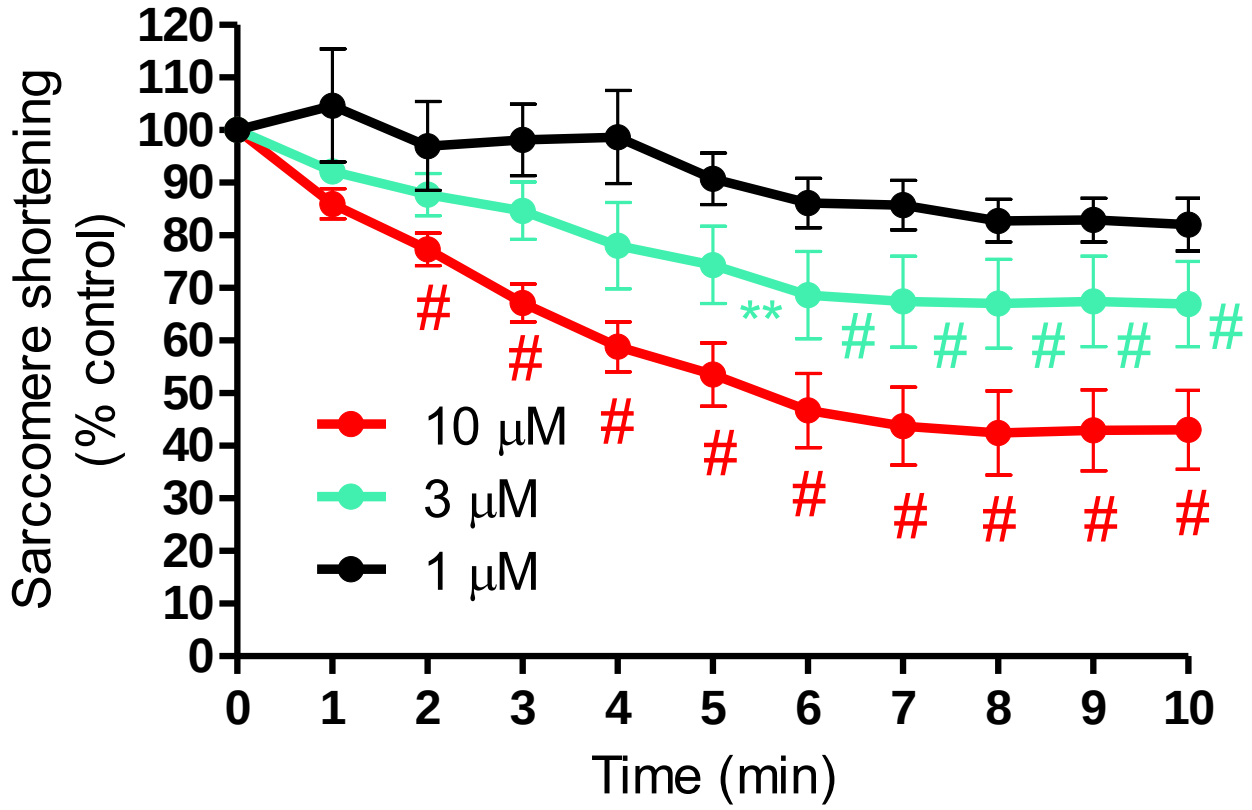


Figure 6.1 Concentration-dependent effects of Δ^9-THC on ventricular myocyte contractility

Cells were stimulated to contract at a frequency of 1 Hz via a patch electrode; data are presented as percentage change in sarcomere shortening from control values. Δ^9-THC elicited a concentration-dependent reduction in amplitude of sarcomere shortening (10 μM, n = 6, 3 μM n = 5). ** denotes $P < 0.01$, *** denotes $P < 0.001$ relative to control; repeated measures ANOVA with Dunnett's post-hoc test. 1 μM Δ^9-THC was without significant effect on sarcomere shortening (n = 4, $P > 0.05$).

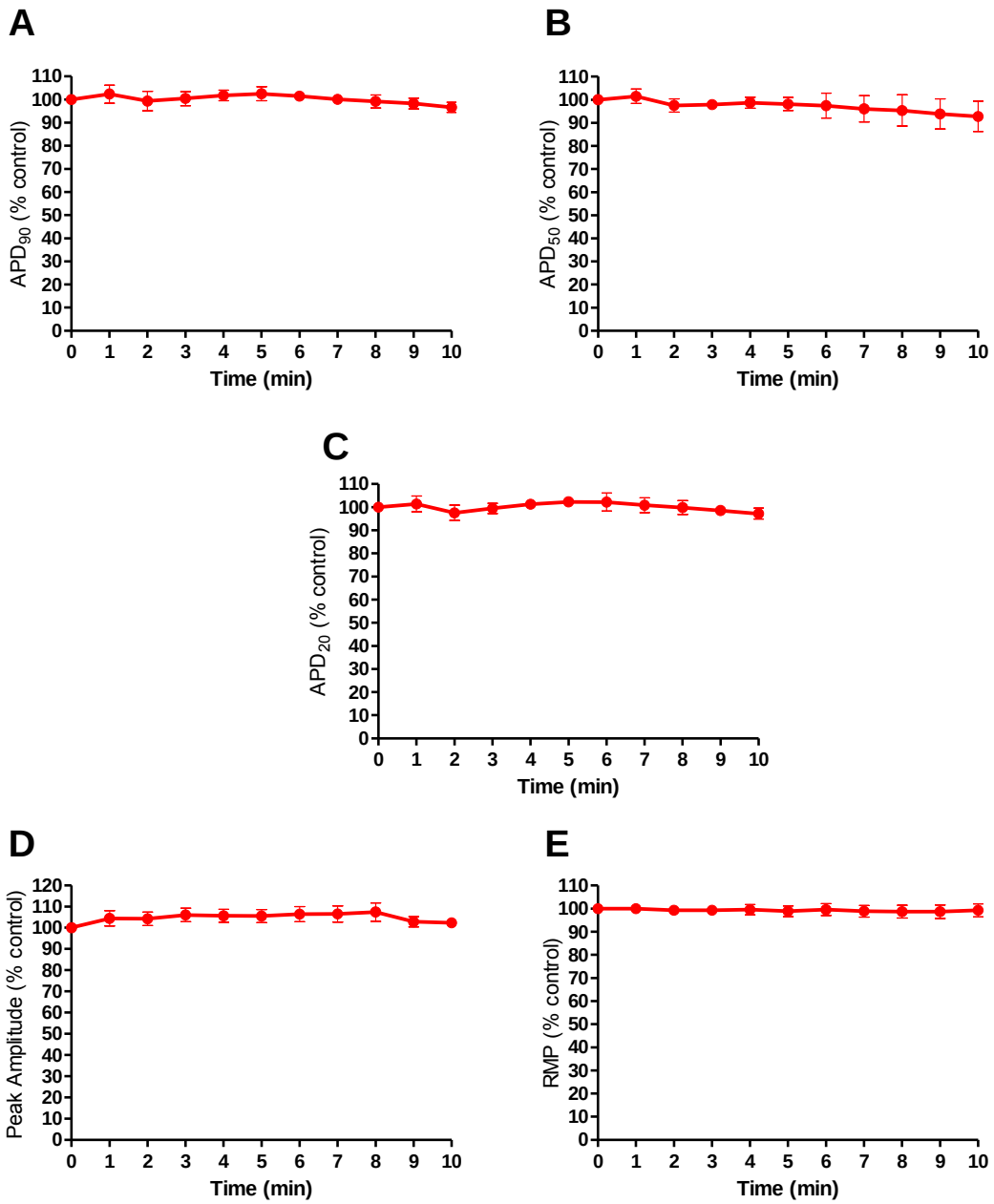


Figure 6.2 Lack of effect of 10 µM Δ⁹-THC on action potential parameters

Cells were patched in the permeabilised configuration and action potentials stimulated at 1 Hz. No significant effects on any AP parameters were observed (n = 6, $P > 0.05$; repeated measures ANOVA with Dunnett's post-hoc test).
A: Peak amplitude of the action potential.
B: Resting membrane potential.
C: Action potential duration at 90% repolarisation.
D: Action potential duration at 50% repolarisation.
E: Action potential duration at 20% repolarisation.

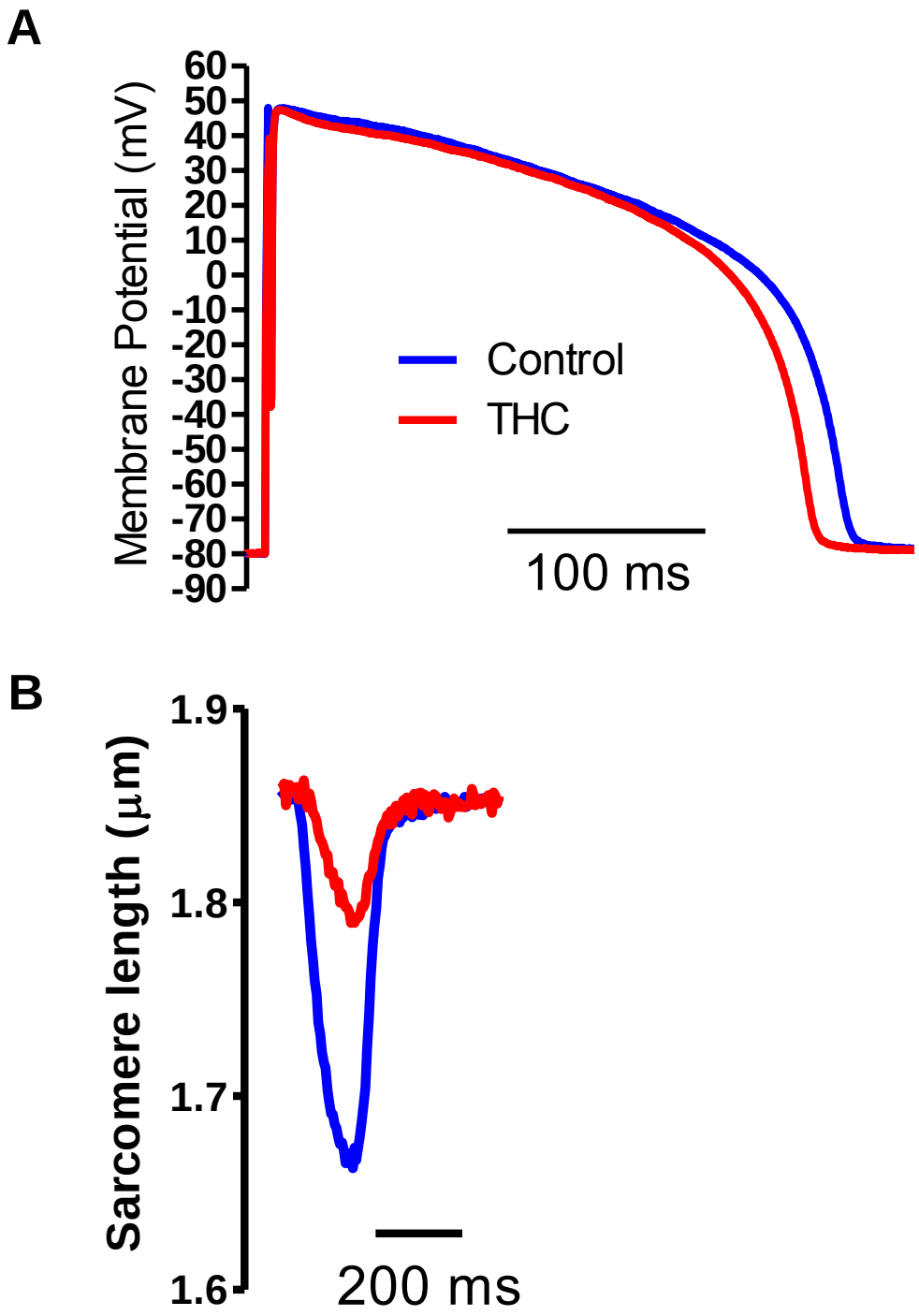


Figure 6.3 Representative traces to show the effect of 10 µM Δ⁹-THC on action potentials and contractions in guinea pig ventricular myocytes

A: Cells were patched in the perforated configuration and stimulated to fire action potentials via a current pulse delivered by the microelectrode (2 ms, 1 Hz). B: Contraction was measured in terms of sarcomere length and recorded using the Ionoptix system. Δ^9-THC evoked a decrease in amplitude of contraction without markedly reducing action potential duration.

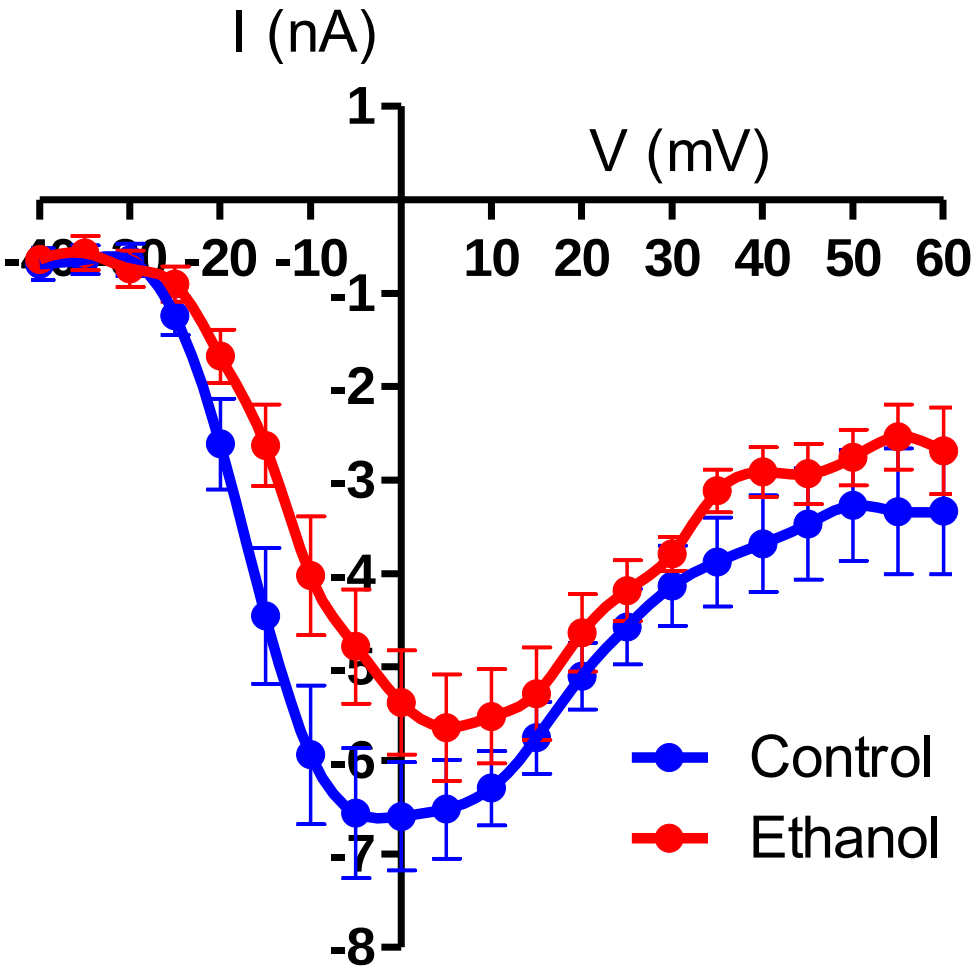


Figure 6.4 Effects of ethanol vehicle on current voltage relationship for I_{CaL} measured using the perforated patch technique

I_{CaL} was elicited by 200 ms step depolarisations (frequency 0.2 Hz) from -40 mV to a range of potentials between -40 and +60 mV at 5 mV increments and measured as peak current deducted from the current at the end of the pulse. After 10 minutes superfusion with 0.03 % ethanol, the amplitude of I_{CaL} at 0 mV was 80 ± 6 % of control (n = 7, *P* = 0.057).

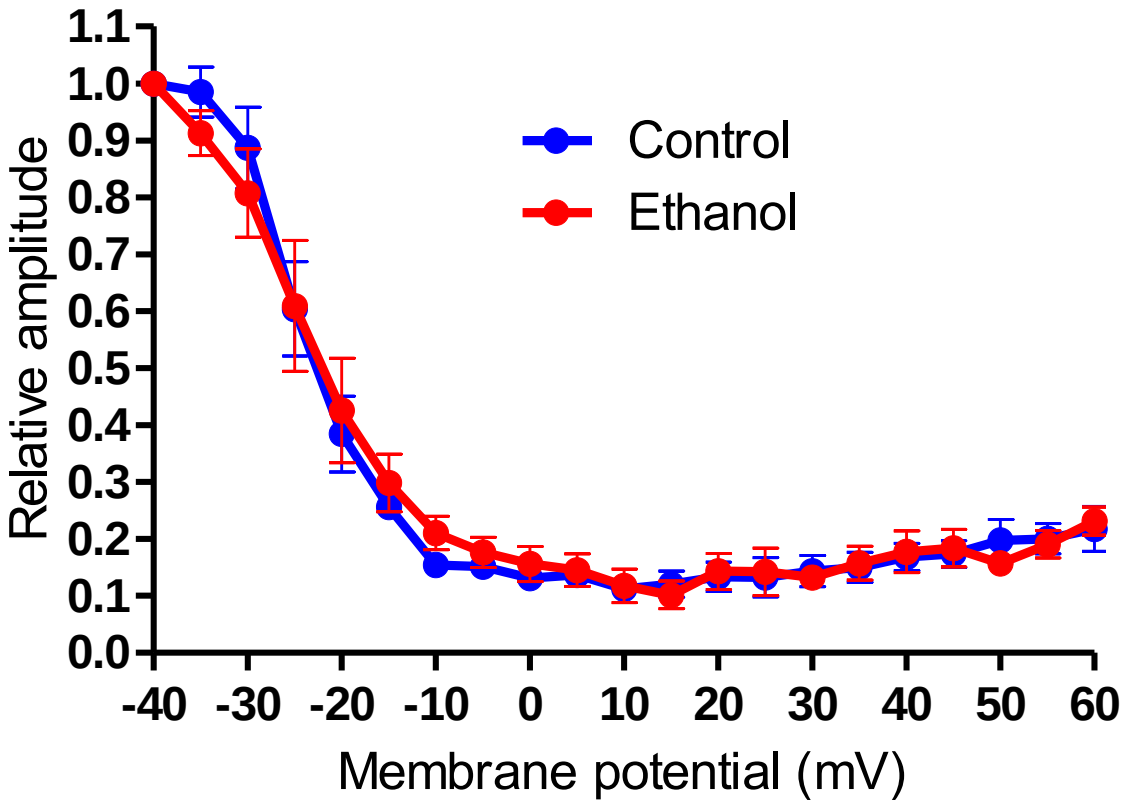


Figure 6.5 Effects of ethanol on voltage-dependence of I_{CaL} inactivation measured using the perforated patch technique

A 200 ms test pulse from -40 to 0 mV was applied 10ms after a 500ms conditioning 'pre-pulse' applied at 5 mV increments from -40 to +60 mV; the amplitude of I_{CaL} during the test pulse is plotted as a fraction of its value in the absence of the pre-pulse. There were no significant differences in relative amplitude of the test pulse at all potentials studied; $P > 0.05$, one-way ANOVA with Bonferroni post-hoc test, n = 7. Representative traces from this protocol are similar to those shown in figure 4.16.

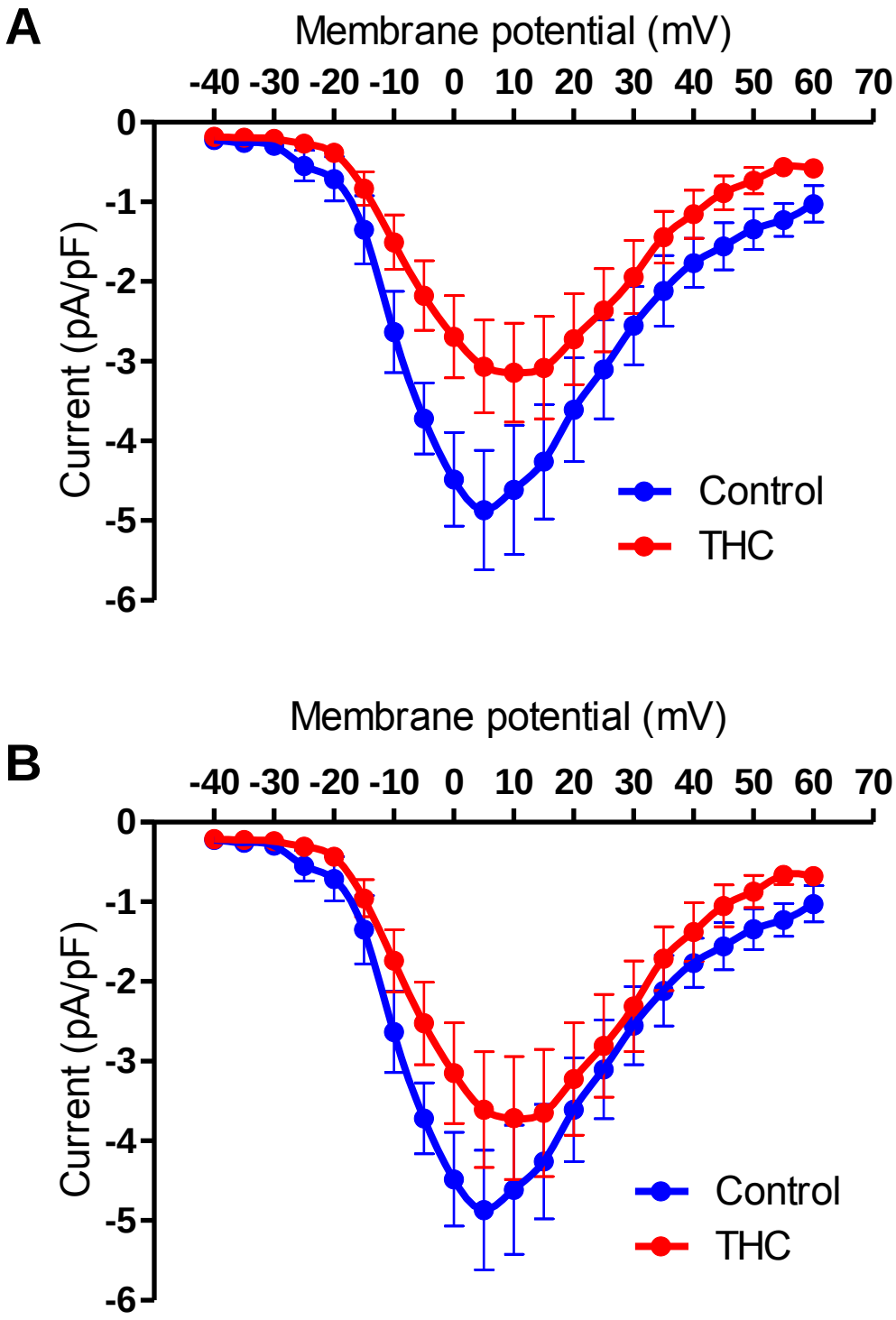


Figure 6.6 Current voltage relationship for I_{CaL} in the presence of 10 µM Δ⁹-THC

I_{CaL} was elicited by 200 ms step depolarisations (frequency 0.2 Hz) from -40 mV to a range of potentials between -40 and + 60 mV at 5 mV increments and measured as peak current deducted from the current at the end of the pulse. A: Without correction for current rundown (reduction at 0 mV of 40 ± 7 %; n = 6, $P < 0.01$). B: With correction for current rundown (reduction of 28 ± 8 %; n = 6, $P < 0.05$).

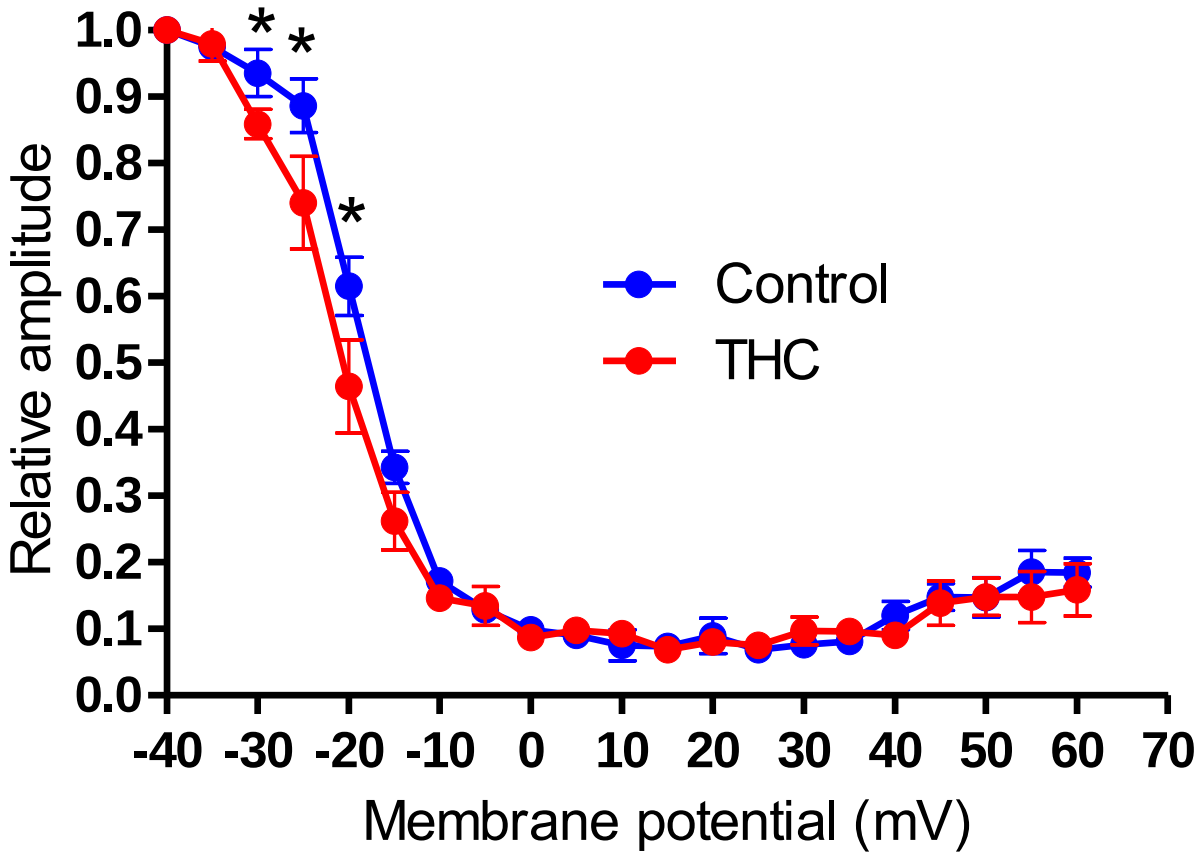


Figure 6.7 Acceleration of the voltage-dependence of inactivation of I_{CaL} in the presence of 10 µM Δ^9-THC

A 200 ms test pulse from -40 to 0 mV was applied 10ms after a 500ms conditioning 'pre-pulse' applied at 5 mV increments from -40 to + 60 mV; the amplitude of I_{CaL} during the test pulse is plotted as a fraction of its value in the absence of the pre-pulse. * denotes $P < 0.05$, one-way ANOVA with Bonferroni post-hoc test, n = 5. Representative traces from this protocol are similar to those shown in figure 4.19.

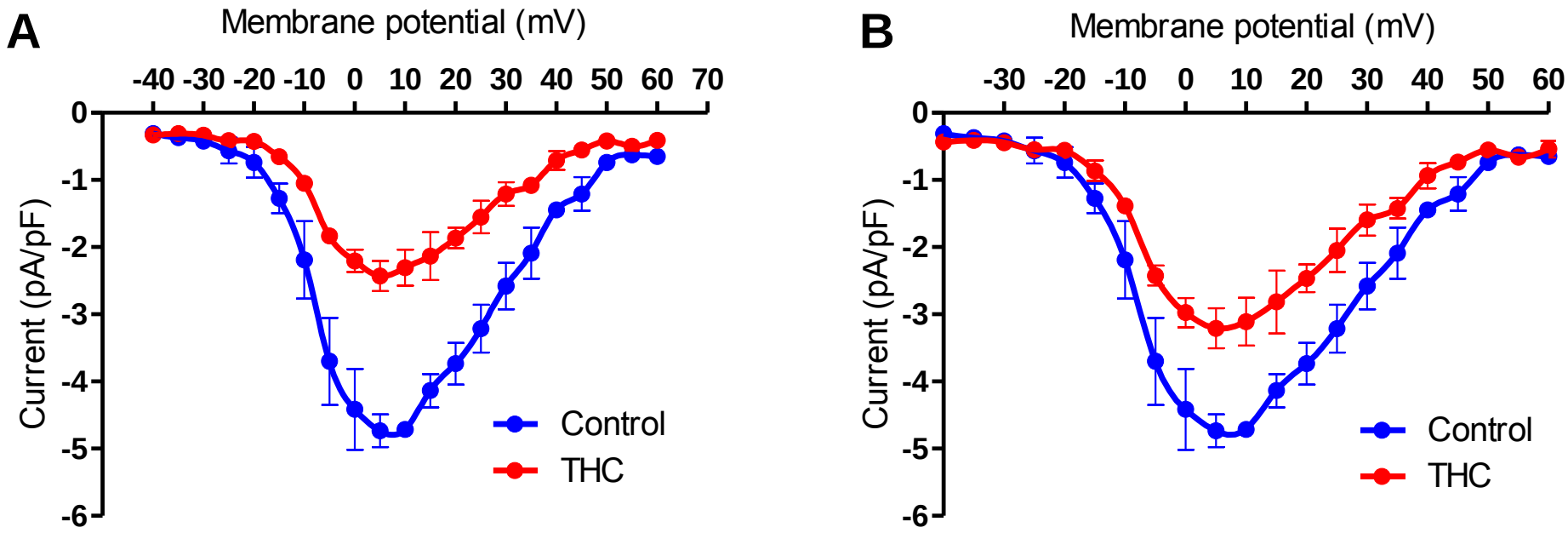


Figure 6.8 Effect of Δ^9-THC on I_{CaL} current voltage relationship in the presence of Cs^+

I_{CaL} was elicited by 200 ms step depolarisations (frequency 0.2 Hz) from -40 mV to a range of potentials between -50 and + 60 mV at 5 mV increments, via a patch electrode in the whole-cell configuration to introduce Cs^+ to the cytosol. Current voltage relationships were measured as peak current deducted from the current at the end of the pulse. A: Current voltage relationship without correction for I_{CaL} rundown under these conditions. Peak I_{CaL} at 0 mV was reduced by 51 ± 5 % (n = 3, $P < 0.05$). B: Current voltage relationship with correction factor for I_{CaL} rundown. After application of the correction factor the apparent reduction in I_{CaL} amplitude was 35 ± 7 % (n = 3, $P < 0.05$).

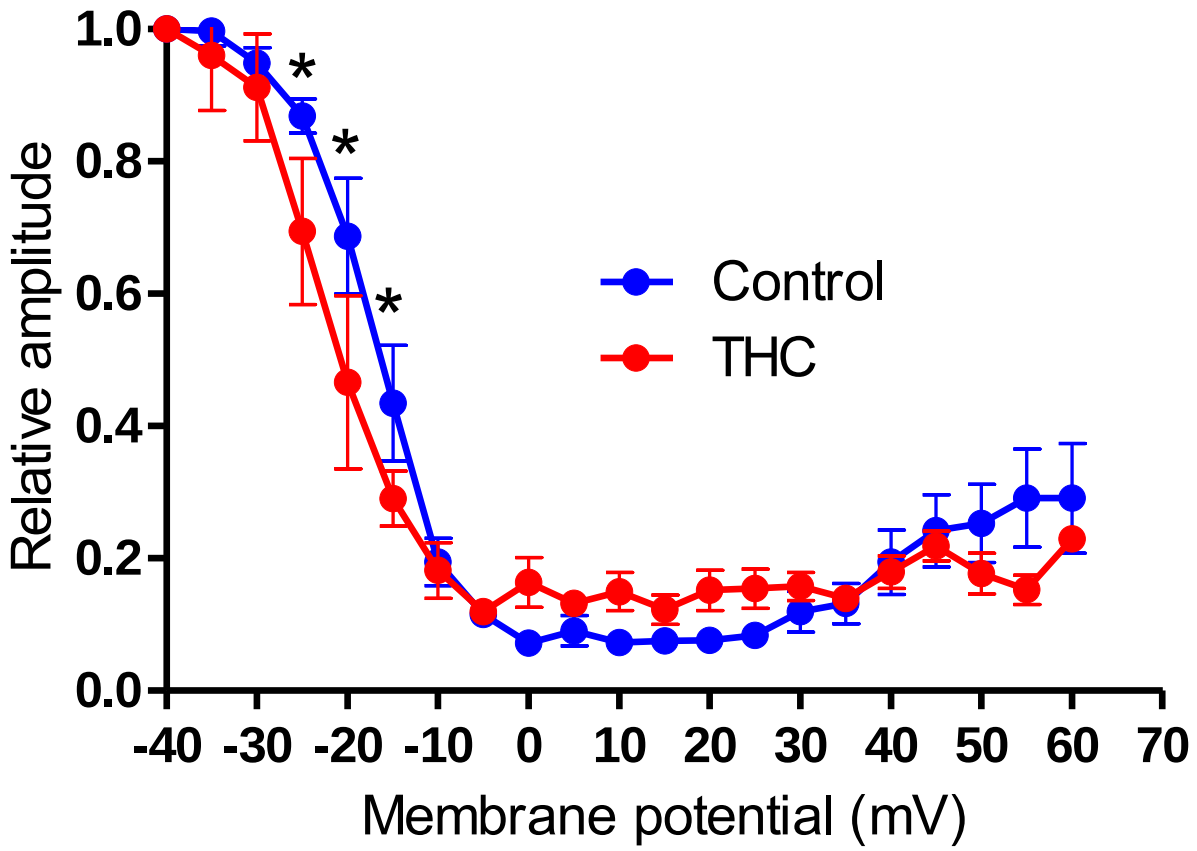


Figure 6.9 Acceleration of the voltage-dependence of inactivation of I_{CaL} in the presence of Δ^9-THC with Cs^+ in the patch electrode

A 200ms test pulse from -40 to 0 mV was applied 10ms after a 500ms conditioning 'pre-pulse' applied at 5 mV increments from -40 to + 60 mV; the amplitude of I_{CaL} during the test pulse is plotted as a fraction of its value in the absence of the pre-pulse. * denotes $P < 0.05$, Δ^9-THC vs control, one-way ANOVA with Bonferroni post-hoc test (n = 3). Representative traces from this protocol are similar to those in figure 4.19.

6.3.3 Δ^9-THC inhibited the slowly activating (I_{Ks}) but not the rapidly activating component (I_{Kr}) of the delayed rectifier K^+ current (I_K)

The observations that Δ^9-THC reduces the amplitude of ventricular myocyte contractions, at least in part through an inhibition of I_{CaL}, but does not markedly reduce the APD, raises the possibility that this compound potently inhibits guinea pig I_K. This would lead to a lengthening of the AP, counteracting the effect of I_{CaL} inhibition to shorten APD. Measurements of I_K were initially made by separating I_{Kr} and I_{Ks} in terms of the speed with which they are activated. Pulses from -40 to +40 mV of 10 – 800 ms duration were applied to cells, with tail currents after pulses from 10 – 100 ms largely consisting of I_{Kr}, and those after pulses from 100 – 800 ms consisting of I_{Ks} (Sanguinetti *et al.*, 1990). The amplitude of tail currents at 600 ms was reduced by 46 ± 7 % (n = 5, $P < 0.05$) in the presence of 10 µM Δ^9-THC. In ethanol vehicle control experiments, there were no significant changes in amplitude of the tail current at 600 ms (93 ± 7 % of control; n = 5, $P > 0.05$). The effects of Δ^9-THC to inhibit I_{Ks}, but not I_{Kr} are shown in Figure 6.10. Ethanol control experiments are shown in Figure 6.11.

A second series of experiments was then performed in the presence of 1 µM E4031, in order to eliminate I_{Kr}. In the presence of E4031, the tail current occurring after pulses of 10 – 100 ms duration was abolished (Figure 6.12). The tail current amplitude after a 600 ms pulse in the presence of E4031 and 10 µM Δ^9-THC was reduced by 56 ± 7 % (n = 4, $P < 0.01$). Compared to the reductions in I_{Ks} amplitude seen with anandamide under these conditions (reduction of 38 ± 8 %; see chapter 4), it appears that Δ^9-THC may more potently inhibit I_{Ks} than anandamide.

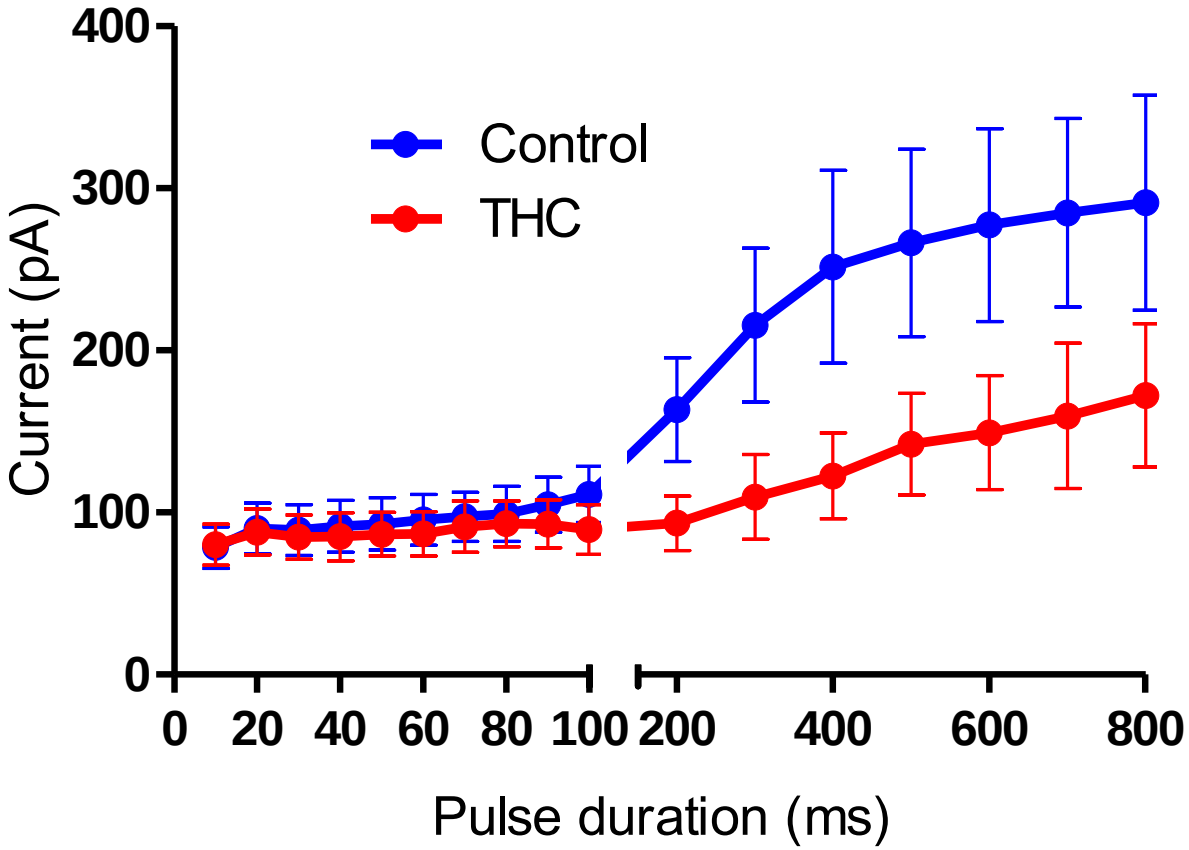


Figure 6.10 Effects of 10 µM Δ^9-THC on amplitude of I_K

I_K was measured as the amplitude of the tail current generated after application of depolarising current pulses from -40 to + 40 mV of varying durations from 10 – 800 ms ('switched' voltage clamp, amphotericin permeabilised patch). Δ^9-THC reduced amplitude of the tail current. At 600 ms it was reduced by 46 ± 7 % (n = 5, $P < 0.05$; one-way ANOVA with Bonferroni post-hoc test). Representative traces from this protocol are similar to those in figure 4.20.

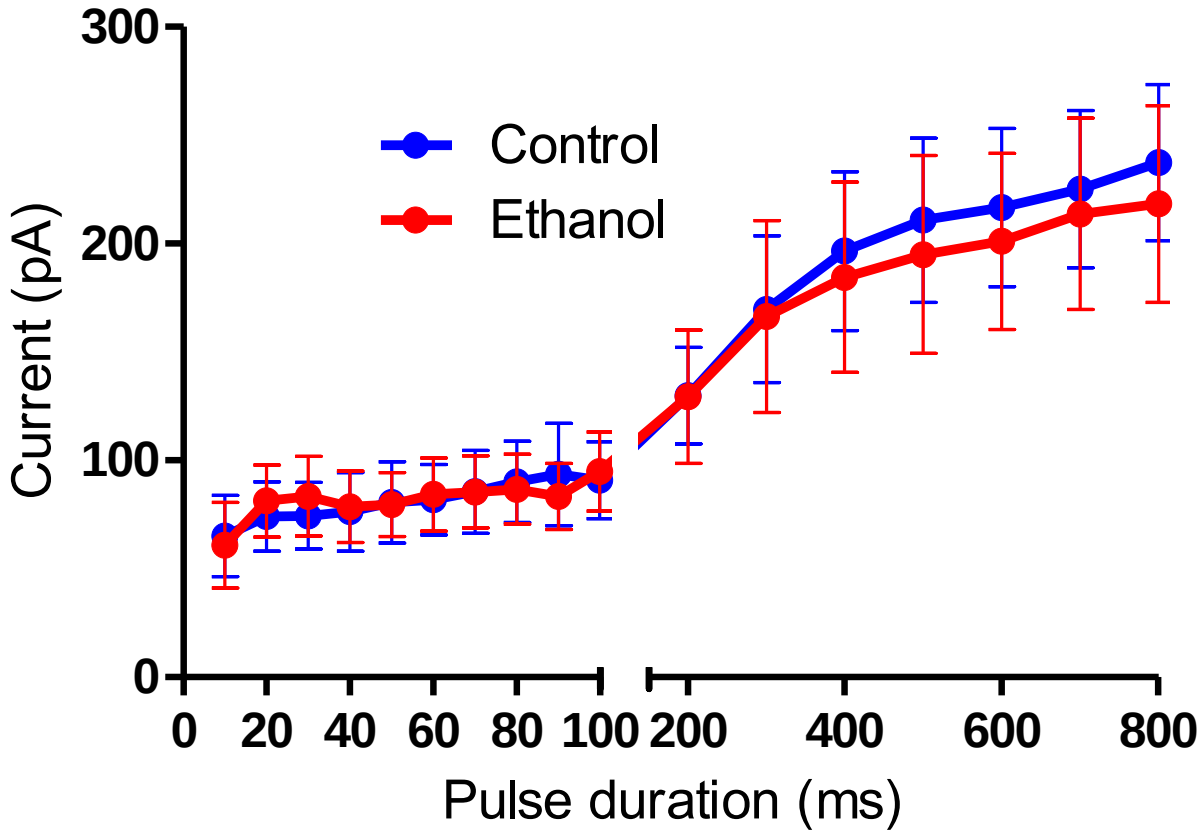


Figure 6.11 Lack of effect of ethanol vehicle on I_K measured using amphotericin-permeabilised patch

I_K was measured as the amplitude of the tail current generated after application of depolarising current pulses from -40 to + 40 mV of varying durations from 10 – 800 ms ('switched' voltage clamp, amphotericin permeabilised patch). Ethanol vehicle (0.03 %) was without significant effect on amplitude of the tail current. At 600 ms it was 93 ± 7 % of control (n = 5, $P > 0.05$; one-way ANOVA with Bonferroni post-hoc test). Representative traces from this protocol are similar to those in figure 4.22.

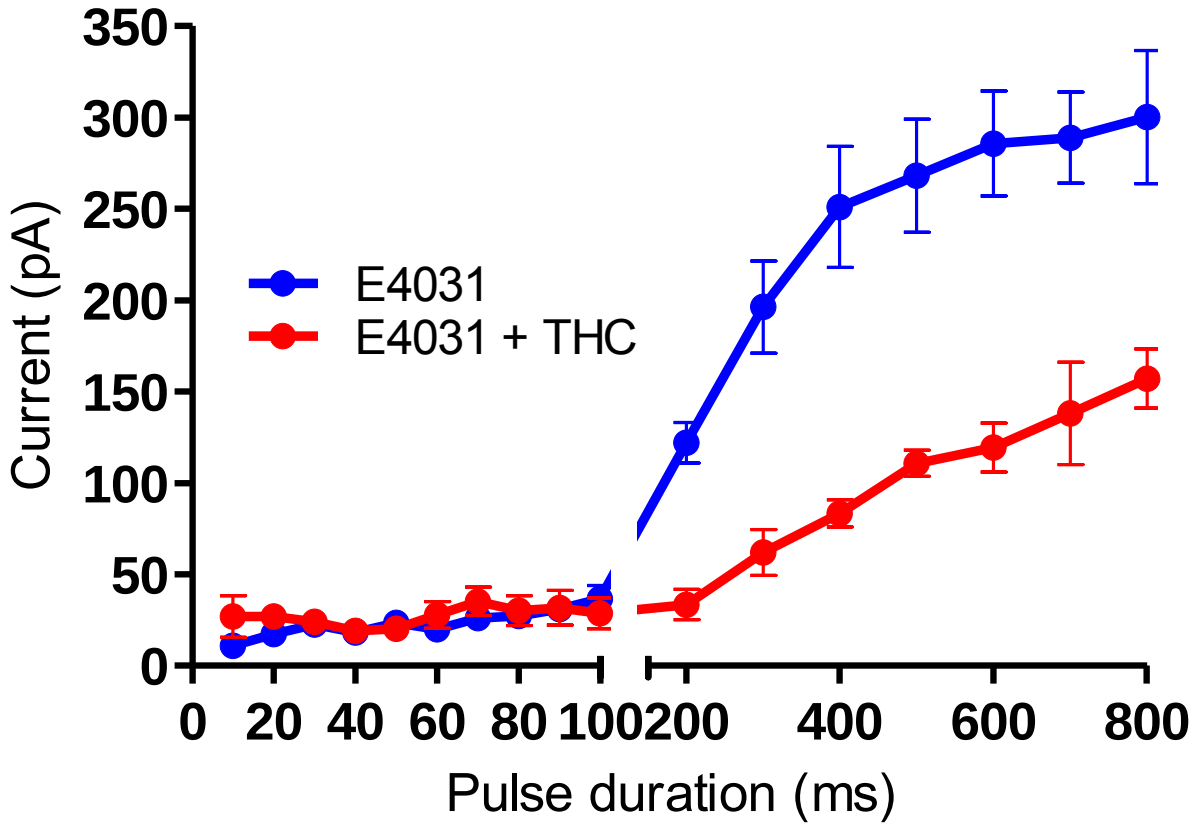


Figure 6.12 Effect of 10 µM Δ^9-THC on amplitude of I_K in the presence of 1 µM E4031

I_K was measured as the amplitude of the tail current generated after application of depolarising current pulses from -40 to + 40 mV of varying durations from 10 – 800 ms ('switched' voltage clamp, amphotericin permeabilised patch). E4031 suppressed tail currents observed after 10 – 100 ms depolarisations, indicating inhibition of I_{Kr}, and that any remaining tail currents represented I_{Ks}. At 600 ms the amplitude of the tail current was reduced by 56 ± 7 % of control (n = 4, $P < 0.01$; one-way ANOVA with Bonferroni post-hoc test).

6.3.4 Δ^9-THC reduced myocyte contractility in the presence of isoprenaline

Cells were stimulated to contract at a frequency of 1 Hz by 2 ms depolarising current pulses delivered by a patch electrode, and initially superfused with 2 nM isoprenaline until maximal contractile responses had been achieved (after approximately 2 minutes). After a further 10 minutes superfusion with 10 μM Δ^9-THC in the continued presence of 2 nM isoprenaline, the amplitude of contraction was reduced by 49 ± 3 % (n = 4, $P < 0.001$ vs peak isoprenaline-stimulated response). The magnitude of this effect was significantly reduced in comparison to that seen at the 5 minute time point in the absence of isoprenaline (Figure 6.13; reduction of 47 ± 5 % in the absence of isoprenaline vs 30 ± 2 % reduction in the presence of isoprenaline; $P < 0.05$, ANOVA with Bonferroni post-hoc test). In terms of AP configuration, superfusion with Δ^9-THC in the presence of isoprenaline resulted in a lengthening of APD. After 10 minutes APD_{90} was increased by 42 ± 11 % and APD_{20} by 65 ± 8 % (both n = 4, $P < 0.05$); this would be consistent with a potent effect of Δ^9-THC to inhibit repolarising K^+ currents, for example I_{Ks}, which is enhanced by β-adrenoceptor stimulation (Marx *et al.*, 2002). No significant effects on RMP or peak amplitude of the AP were observed in the presence of isoprenaline (n = 4, $P > 0.05$). A representative AP trace is shown in Figure 6.14A, and a representative contraction trace in Figure 6.14B.

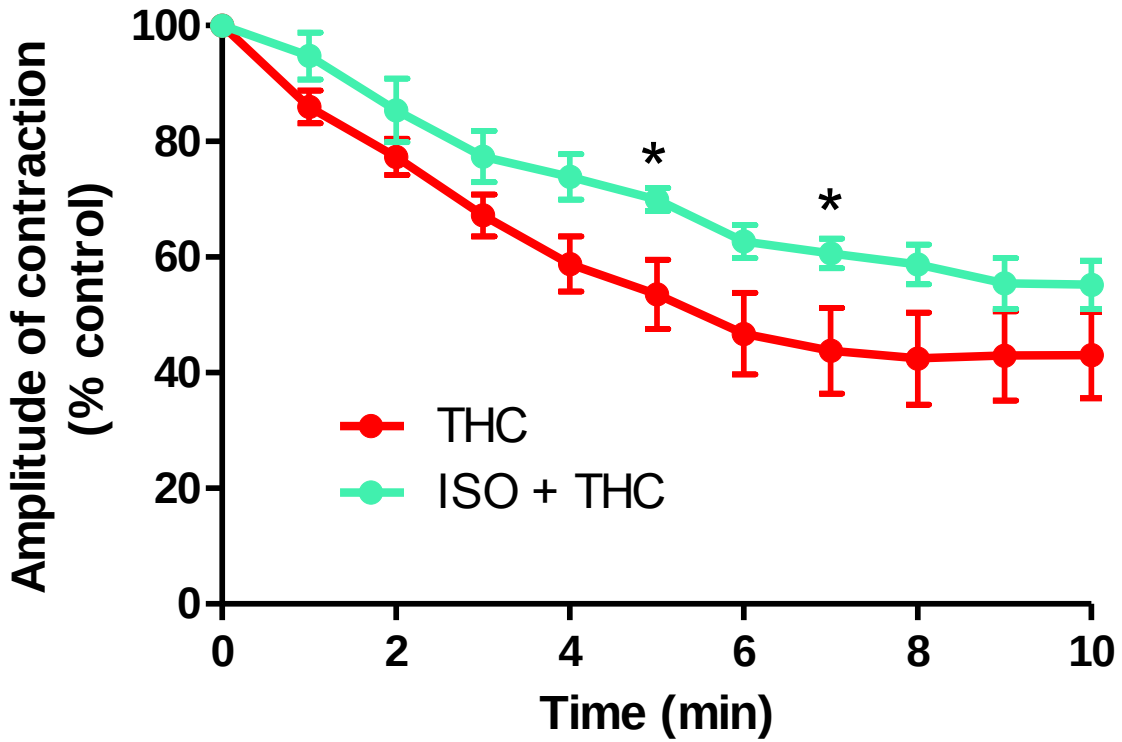


Figure 6.13 Effect of Δ^9-THC on amplitude of contraction in the presence of isoprenaline

Cells were stimulated to contract at a frequency of 1 Hz via a patch electrode; data are presented as percentage change in sarcomere shortening from control values. After 10 minutes Δ^9-THC elicited a 45 ± 4 % reduction in the amplitude of sarcomere shortening in the presence of isoprenaline (n = 4, $P < 0.01$). This reduction was significantly reduced in magnitude from the reduction seen in the absence of isoprenaline at the 5 and 7 minute time points ($P < 0.05$, one-way ANOVA with Bonferroni post-hoc test).

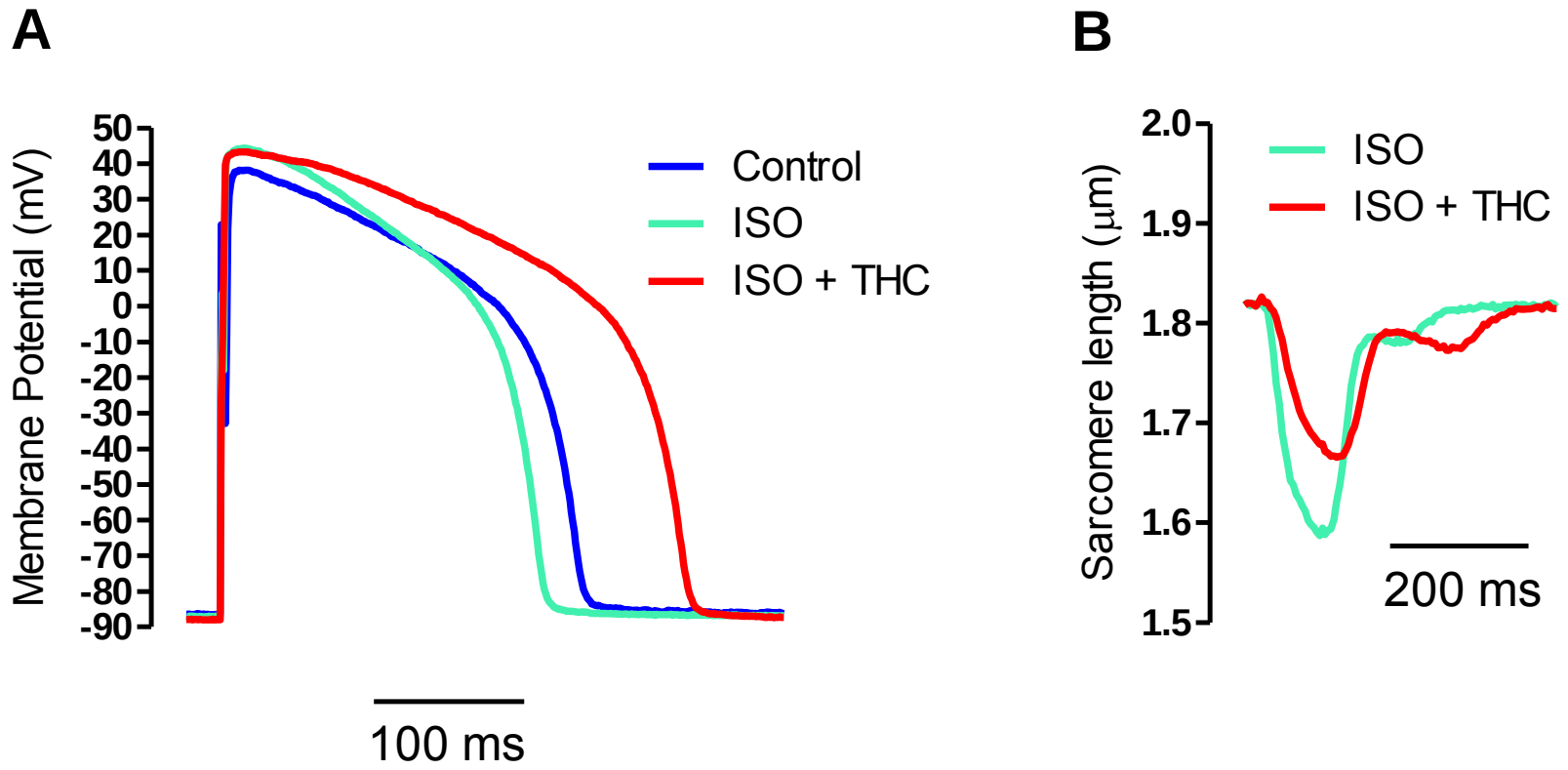


Figure 6.14 Representative trace illustrating the effects of Δ⁹-THC in the presence of isoprenaline on action potentials and contractions in guinea pig ventricular myocytes.

Cells were stimulated to fire APs and contract at 1 Hz. A: Superfusion of myocytes with isoprenaline for 3 minutes, followed by superfusion with 10 µM Δ⁹-THC in the continued presence of isoprenaline for a further 10 minutes, led to an increase in action potential duration. APD_{90} was increased by 42 ± 11 % (n = 4, $P < 0.05$). B: Contractions measured as sarcomere shortening using the IonOptix system, showing the contraction after 3 minutes superfusion with 2 nM isoprenaline, and then after 10 minutes superfusion with Δ⁹-THC in the continued presence of isoprenaline.

6.4 Discussion

The data presented here provide the first evidence concerning the electrophysiological and inotropic effects of Δ^9-THC on cardiac ventricular myocytes isolated from the guinea pig. Like anandamide, Δ^9-THC has a marked negative inotropic action (Figure 6.1), but in comparison to anandamide appears to have less pronounced effects on AP configuration (Figure 6.3 compared to Figure 4.7). It is possible that this difference between the two compounds arises as a result of a differing balance of the two compounds to inhibit the activities of I_{CaL} and I_K. In particular, data presented here show a marked effect of Δ^9-THC to inhibit I_{Ks} (Figure 6.12) which may counteract the AP shortening effect of its inhibitory effect on I_{CaL}. Nevertheless, an inhibition of I_{CaL} was still observed, both in the absence (Figure 6.6) and presence (Figure 6.8) of Cs^+. In a similar manner to anandamide, this may arise, at least in part, through an action of Δ^9-THC to accelerate the kinetics of inactivation of I_{CaL} (Figure 6.7 and Figure 6.9), although additional effects on I_{CaL} amplitude are also possible. The reduction in amplitude of contraction observed in the presence of Δ^9-THC was perhaps more marked than might be expected from the apparent lack of effect on AP configuration. The apparent lack of effect on APD might be as a consequence of compensating actions at I_K and I_{CaL}, but actions at additional targets, for example the myofilaments, to reduce their sensitivity to Ca^{2+}, cannot be ruled out.

Taken together with the observations presented in chapters 4 and 5, the observations presented here may reflect a direct interaction with, and inhibition of Ca^{2+} and K^+ channels by Δ^9-THC. In the presence of isoprenaline, the effect of Δ^9-THC to reduce the amplitude of cell contractions showed a trend towards a smaller magnitude of negative inotropic effect when compared to negative inotropic effects observed in the

absence of isoprenaline (Figure 6.13). This would be consistent with findings presented in chapter 5, and with the hypothesis that the negative inotropic effects of cannabinoid compounds under these conditions are not mediated through an effect of cannabinoid receptors to reduce the activity of adenylyl cyclases. It is possible that, in line with the ideas presented in chapter 5, the effects of Δ^9-THC to inhibit I_{CaL} are due to a direct interaction of the compound with LTCCs, which is reduced when the channel is phosphorylated under conditions of β-adrenoceptor stimulation. However, another effect of Δ^9-THC observed under conditions of β-adrenoceptor stimulation was an increase in APD. This may be mediated in part by a potent effect of Δ^9-THC to inhibit I_{Ks} as shown in Figure 6.10 and Figure 6.12, and the resultant lengthening of APD may account for the reduced contractile actions, since a prolonged AP would favour SR Ca^{2+} loading leading to enhancement of contractions (Terrar *et al.*, 1989c).

To my knowledge there are very few published studies concerning the actions of Δ^9-THC in the heart, especially in isolated cell preparations. In the vascular system, much attention has focussed on the action of endocannabinoids, while those of Δ^9-THC have largely been overlooked. However, in agreement with the suggestion that Δ^9-THC inhibits I_{CaL}, it has been demonstrated in the rat mesenteric vasculature, that micromolar concentrations of Δ^9-THC prevent the contractile response to re-introduction of Ca^{2+} to the extracellular solution, suggesting this compound prevents Ca^{2+} entry via LTCCs (O'Sullivan *et al.*, 2005). In addition, Δ^9-THC has been shown to strongly inhibit human recombinant T-type Ca^{2+} channels in the nanomolar concentration range through a direct interaction with the channel (Ross *et al.*, 2008).

Other studies of the electrophysiological and inotropic actions of Δ^9-THC in cardiac myocytes are lacking. However, Waldman and colleagues recently observed that administration of Δ^9-THC reduced infarct size after ischaemia reperfusion in mice,

which was associated with an inhibition of ERK1/2 phosphorylation, and a reduction in the release of troponin T and TNFα, 24 hours after myocardial infarction (Waldman *et al.*, 2013). Others have also demonstrated a protective action against hypoxia, involving a CB_2 receptor-mediated mechanism to increase levels of NO and stimulate mitochondrial K_{ATP} channels (Shmist *et al.*, 2006).

In summary, the data presented here provide preliminary evidence regarding the actions of Δ^9-THC in cardiac muscle and suggest that in addition to the cardioprotective actions reported in the literature, Δ^9-THC also acts to inhibit I_{CaL} and I_K in guinea pig ventricular myocytes. These actions may contribute to the putative cardioprotective effects of Δ^9-THC at high concentrations.

Chapter 7
General Discussion

7.1 Novel pathways in cardiac β-adrenoceptor signalling: NAADP

Ca^{2+} is a ubiquitous and multi-functional second messenger involved in numerous physiological processes, including cardiac excitation-contraction coupling. Modulation of cardiac Ca^{2+} handling leads to altered cardiac function both in physiological and pathophysiological conditions. Activation of cardiac muscle β-adrenoceptors, leading to amplification of CICR, is the primary mechanism by which cardiac output is increased to meet metabolic demands of the body. Recently, NAADP, the most potent Ca^{2+} mobilising signalling molecule identified (Galione *et al.*, 2009), has been implicated as a novel component of the cardiac β-adrenoceptor signalling pathway (Higashida *et al.*, 1999; Macgregor *et al.*, 2007a; Lewis *et al.*, 2012). Progress in the field of NAADP research has been made recently with the identification of TPC2 as candidate NAADP receptor (Calcraft *et al.*, 2009), and of Ned-19 as a novel antagonist of NAADP signalling (Naylor *et al.*, 2009).

The data presented in chapter 3 are the first to address the role of TPC2 proteins in modulating the contractile response to β-adrenoceptor stimulation in ventricular myocytes and Langendorff-perfused hearts, and provide support for the hypothesis that NAADP forms part of the cardiac β-adrenoceptor signalling pathway (Macgregor *et al.*, 2007a). Contractions elicited by isoprenaline (3 nM) were smaller in amplitude in myocytes and Langendorff-perfused hearts from mice lacking TPC2 proteins. Pre-treatment of guinea pig ventricular myocytes with bafilomycin A1, to inhibit endolysosomal Ca^{2+} storage, also resulted in a blunting of the contractile response to isoprenaline. Experiments performed concurrently in the Terrar laboratory have demonstrated a blunted Ca^{2+} transient response to isoprenaline in myocytes from *Tpcn2*$^{-/-}$ mice (Sam Lin Wee Khang, personal communication) which was also seen in guinea

pig ventricular myocytes treated with patch-applied bafilomycin or Ned-19 (Bayliss, DPhil Thesis, 2013). In addition, it has been shown that isoprenaline induces lysosomal alkalinisation in guinea pig ventricular myocytes, in a similar manner to NAADP-AM, consistent with an effect of isoprenaline to mobilise Ca^{2+} from intracellular stores (Elson, DPhil Thesis, 2011). One of the effects of β-adrenoceptor stimulation in the heart is an increase in the Ca^{2+} content of the SR. Conventionally, this has been attributed to PKA or CaMKII-dependent phosphorylation of phospholamban, which results in disinhibition of SERCA2. Taken together, these observations provide evidence that mobilisation of endolysosomal Ca^{2+} via TPC2 proteins may constitute an additional important component of the β-adrenoceptor signalling pathway, leading to increased SR Ca^{2+} load. Additional data from the laboratory of Dr Ming Lei has also added further weight to the argument that NAADP signalling is important under conditions of chronic β-adrenoceptor stimulation. Hearts isolated from *Tpcn2*$^{-/-}$ mice which had been treated with isoprenaline delivered by a mini-pump over a 14 day period, were found to be resistant to hypertrophy and arrhythmias associated with prolonged isoprenaline treatment (Drs Ming Lei and Yanwen Wang, personal communication). Ca^{2+} calcineurin signalling leading to altered gene transcription has been linked with the development of hypertrophy (Wilkins *et al.*, 2004), and it is possible that the reduced amplitude of the Ca^{2+} transient in *Tpcn2*$^{-/-}$ mice in response to β-adrenoceptor stimulation protects against activation of this pathway. However, it cannot be ruled out that the observations made using *Tpcn2*$^{-/-}$ have occurred as a result of changes in the expression of other proteins involved in the β-adrenoceptor signalling pathway, which are independent of NAADP signalling.

One question which arises, is to how such a small amount of Ca^{2+} released from endolysosomal stores can lead to the large enhancement in SR Ca^{2+} load observed by

Macgregor and colleagues in response to NAADP (Macgregor *et al.*, 2007a). Recent experiments in the Terrar laboratory implicate CaMKII as a downstream effector of the NAADP signalling pathway in cardiac myocytes. Exposure of cells to the CaMKII inhibitors AIP or KN93 led to an inhibition of the Ca^{2+} transient response to photorelease of a caged analogue of NAADP (Bayliss, DPhil Thesis, 2013). It is therefore possible that the localised increases in [Ca^{2+}] occurring after endolysosomal Ca^{2+} release lead to activation of CaMKII. CaMKII may then act to phosphorylate phospholamban leading to disinhibition of SERCA and increased SR Ca^{2+} load. The observation that NAADP photorelease leads to a significant acceleration of Ca^{2+} transient decay which is not seen in cells treated with AIP or KN93 (Bayliss, DPhil Thesis, 2013), is consistent with this hypothesis. However, further investigations are necessary to determine this conclusively; indeed, localised increases in [Ca^{2+}] could also act to sensitise RyR to Ca^{2+} to further increase the gain of CICR.

The activation of the NAADP signalling pathway may occur at the level of NAADP synthesising enzymes (ARCs), which are also responsible for the synthesis of cADPR (Higashida *et al.*, 1999). cADPR has also been shown to modulate cardiac excitation-contraction coupling (Macgregor *et al.*, 2007b), through a possible sensitisation of RyR to Ca^{2+} (Zhang *et al.*, 2009). Recent evidence suggests the existence of a novel ARC located to the SR (Kannt *et al.*, 2012). Furthermore, antagonists of cADPR have been shown to prevent arrhythmogenic Ca^{2+} oscillations in cardiac myocytes (Zhang *et al.*, 2009; Kannt *et al.*, 2012), and levels of both NAADP and cADPR are increased in the heart following β-adrenoceptor stimulation (Lewis *et al.*, 2012). With these data in mind, the possibility that targeting NAADP-induced mobilisation of endolysosomal Ca^{2+} may lead to antiarrhythmic actions was also considered in chapter 3. Treatment of cells with bafilomycin reduced the tendency of

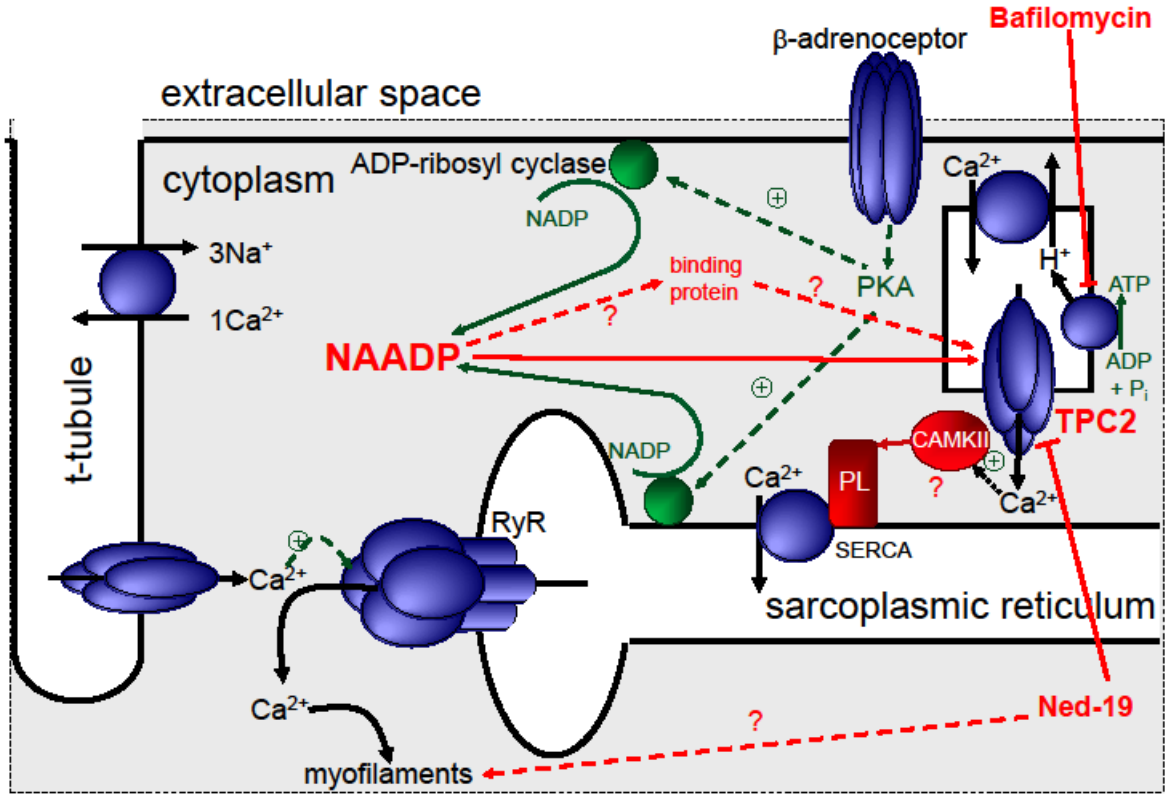


Figure 7.1 Schematic diagram illustrating the putative interaction between the β-adrenoceptor signalling pathway, NAADP and TPC2.

ADP ribosyl cyclase activity is stimulated by the cAMP/PKA pathway, leading to synthesis of NAADP. NAADP then activates TPC2 channels leading to endolysosomal Ca^{2+} release, which supplements SR Ca^{2+} load (in addition to the well-known effects of the β-adrenoceptor signalling on LTCCs and phospholamban (PLB)), leading to increased force of contraction. A possible mechanism for the increase in SR load, is an activation of CaMKII by endolysosomal Ca^{2+} release (Bayliss, DPhil Thesis) which may lead to phosphorylation of PLB and disinhibition of the sarco/endoplasmic reticulum ATPase (SERCA). Bafilomycin, acting to deplete endolysosomal stores of Ca^{2+} and Ned-19, acting to inhibit NAADP interaction with TPC2, are capable of blunting the ventricular myocyte contractile response to β-adrenoceptor stimulation. At high concentrations, it is possible that Ned-19 has additional actions, perhaps on the myofilaments as suggested in chapter 3. This diagram is modified from Prof. Derek Terrar.

guinea pig ventricular myocytes to show arrhythmias when treated with 50 nM isopenaline. This is consistent with the observations of others (Nebel *et al.*, 2013). It is therefore possible that NAADP and cADPR act together to modulate Ca^{2+} handling. An effect of cADPR to sensitise RyRs, and of NAADP to enhance and maintain SR Ca^{2+} load could together modulate and fine-tune Ca^{2+} handling during β-adrenoceptor stimulation: this requires further investigation. Modulation of this pathway may provide a protective strategy in conditions such as heart failure, where the sympathetic nervous system is known to be activated (Francis *et al.*, 1990). Furthermore, other agents currently in therapeutic use in heart failure, such as LTCC antagonists, may actually be deleterious (Goonasekera *et al.*, 2012). A schematic diagram illustrating putative components of the NAADP signalling pathway under conditions of β-adrenoceptor stimulation, is shown in Figure 7.1.

7.2 Effects of anandamide and Δ^9-THC on cardiac EC coupling

Chronic activation of the β-adrenoceptor signalling pathway is associated with various cardiac pathologies, for example heart failure and arrhythmias, which are associated with impaired cardiac Ca^{2+} handling. Recently, endogenous molecules termed 'endocannabinoids' which are ligands of specific, PTX-sensitive receptors that inhibit adenylyl cyclase activity (Howlett *et al.*, 2002), have been implicated in providing protection against such conditions (Montecucco *et al.*, 2012). In fact, modulation of these endogenous compounds, and of their receptors, has been suggested as an attractive therapeutic strategy in treating a wider array of conditions including obesity and cancer (Pacher *et al.*, 2006). Δ^9-THC, the principal psychoactive constituent of *Cannabis sativa*, is already administered to treat pain, and chemotherapy-induced nausea and vomiting (Pacher *et al.*, 2006). Since many new chemical entities fail as a

result of cardiotoxicity, an understanding of the cardiac actions of these compounds is therefore of scientific interest if cannabinoids are to be utilised therapeutically. The data presented in chapters 4, 5 and 6 concern the actions of endogenous cannabinoids and Δ^9-THC on cardiac ventricular excitation contraction coupling.

7.2.1 Evidence against a receptor-mediated negative inotropic action of cannabinoids in cardiac ventricular muscle

Given the relatively recent discoveries that cannabinoids are exert at least some of their effects through activation of specific cannabinoid receptors, many investigators have been keen to uncover molecular mechanisms of cannabinoid action, with the aim of elucidating receptor-mediated mechanisms. Data from an extremely limited number of studies has suggested that anandamide exerts negative inotropic actions in cardiac muscle via CB_1 receptors (Bonz *et al.*, 2003; Li *et al.*, 2009). The data presented in chapter 4, show for the first time in guinea pig ventricular myocytes, a reduction in the amplitude of ventricular myocyte contraction in response to anandamide, which appeared not to be mediated by its metabolites. AP duration and Ca^{2+} transient amplitude were both also reduced; effects which occurred at least in part through an inhibition of I_{CaL}. However, other mechanisms underlying the marked reduction in contractility seen with anandamide, such as direct effects on SR Ca^{2+} release, or effects to reduce myofilament Ca^{2+} sensitivity, cannot be ruled out.

The observations presented in chapter 4, showing that the effects of anandamide occurred slowly over a 10 minute time period, and were not rapidly reversible on wash is itself suggestive of a mechanism which does not depend on a G-protein coupled receptors. This has not been commented upon in previous studies concerning the

actions of anandamide in the heart. In addition, the data presented in chapter 3 show that the effects of anandamide on APD and contractions were not prevented by cannabinoid receptor antagonists (AM281 and AM630) and could therefore not be attributed to cannabinoid receptors. Furthermore, for the first time, the electrophysiological effects of selective cannabinoid receptor agonists were investigated in cardiac myocytes, with the finding that they did not mimic the actions of anandamide under the conditions of the experiments presented here.

It is unclear why Li and colleagues were able to detect a receptor-mediated mechanism in rat ventricular myocytes, while the results presented here do not support this suggestion. The possibility was considered here that additional receptor-mediated mechanisms of anandamide may be uncovered under conditions of β-adrenoceptor stimulation. In chapter 5, all experiments were performed after cells had been superfused with isoprenaline, to raise intracellular cAMP, leading to phosphorylation of various protein targets, including the LTCC, which data from chapter 4 show to be a major target of anandamide. If the suggestion of Li and colleagues is correct, then (given existing literature concerning the negative coupling of cannabinoid receptors to adenylyl cyclases (Howlett *et al.*, 2002)), it would be expected that stimulation of basal levels of adenylyl cyclase activity may lead to enhanced negative inotropic effects of anandamide, in a similar manner to other agonists such as acetylcholine and adenosine (Belardinelli *et al.*, 1995; Calloe *et al.*, 2013). Furthermore, it would be expected that inhibition of G_i proteins by PTX, would prevent the effects of anandamide. The data presented in chapter 5 show that this is not the case. The effects of anandamide to inhibit contractions and I_{CaL} were certainly not augmented in the presence of isoprenaline, and if anything, were slightly reduced. Furthermore, pre-incubation of cells with PTX did not prevent the effects of anandamide to reduce contraction and I_{CaL}

amplitude under conditions of β-adrenoceptor stimulation. In addition, the actions of selective cannabinoid receptor agonists ACEA and HU308, together with the endogenous cannabinoid 2-AG were investigated for the first time under conditions of β-adrenoceptor stimulation, with the finding that no additional effects were observed in comparison to those seen in the absence of isoprenaline in chapter 4. Previous suggestions that the negative inotropic actions of anandamide in the heart are receptor-mediated (Ford *et al.*, 2002; Bonz *et al.*, 2003; Li *et al.*, 2009), were based upon the use of cannabinoid receptor antagonists, which themselves are known to have off-target actions (Chemin *et al.*, 2001; Fong *et al.*, 2009; Andrag *et al.*, 2013). A more robust test of G_i-protein coupled receptor involvement, is by use of PTX. The present study, and recent data from Al Kury and colleagues indicate that the effects of anandamide are not sensitive to PTX pre-treatment (Al Kury *et al.*, 2014a; Al Kury *et al.*, 2014b; Kury *et al.*, 2014).

It is of note that the reported K_i values for anandamide at CB_1 and CB_2 receptors are 61 – 543 nM and 279 – 1940 nM (Pertwee, 1999; Howlett *et al.*, 2002) respectively, yet even low concentrations of anandamide (1 μM) failed to have significant negative inotropic effect under the conditions of these experiments, both in the absence and presence of β-adrenoceptor stimulation. One possibility is that the vehicle used to dissolve anandamide affects the way in which it interacts with receptor targets. Of course, it cannot be ruled out that the expression of cannabinoid receptors in guinea pig myocytes under physiological conditions is just too low to mediate a negative inotropic action. This may change in disease states, where receptor expression is reported to increase significantly (Weis *et al.*, 2010). Another possibility is that these receptors do not couple to pathways involved in regulating adenylyl cyclase activity in the heart; instead, pathways involving cell growth, proliferation and metabolism may be more

important. This suggestion is supported by other observations (Underdown *et al.*, 2005; Shmist *et al.*, 2006; Rajesh *et al.*, 2008; Montecucco *et al.*, 2009; Waldman *et al.*, 2013) and adds further weight to a possible protective role of cannabinoids under pathological conditions. It is of note, that in ischaemic canine myocardium, the concentration of the N-acylethanolamine family of phospholipids (of which anandamide is a member) was observed to be elevated to a concentration of around 500 μM (Epps *et al.*, 1979), raising the possibility that the effects of anandamide observed here have relevance in the heart under pathological conditions.

7.2.2 Possible mechanisms of action of anandamide and Δ^9-THC in ventricular muscle

At least one mechanism by which anandamide may reduce Ca^{2+} influx via LTCC under the conditions of these experiments, is through an acceleration of their inactivation, as shown in chapter 4. A similar acceleration of inactivation of LTCCs in response to anandamide has also been shown in rat ventricular myocytes (Li *et al.*, 2009). The mechanism by which anandamide has this effect is not known, but one possibility is that anandamide interacts directly with some component of the LTCC itself. For example, a C terminal binding site for the Ca^{2+} sensor calmodulin is thought to be an important determinant of Ca^{2+} dependent inactivation (Cens *et al.*, 2006). Given the lipophilic nature of anandamide and other cannabinoids, it is conceivable that these compounds could reside within the cell membrane and modulate channel function directly. Indeed, others have also observed direct interactions of anandamide and methanandamide with both LTCCs and T-type Ca^{2+} channels (Johnson *et al.*, 1993; Shimasue *et al.*, 1996; Oz *et al.*, 2000; Chemin *et al.*, 2001; Oz *et al.*, 2004; Al Kury *et al.*, 2014b). Interestingly 2-AG did not share this action to inhibit T-type Ca^{2+} channels

(Chemin *et al.*, 2001), and it is possible that differences in the structures of these two compounds influence whether or not they can interact with the channel. Chemin et al suggested the necessity of the hydroxyl group and alkyl chain of anandamide for its interaction with T-type channels (Chemin *et al.*, 2007). Interestingly, data presented in chapter 5 suggests that β-adrenoceptor stimulation may reduce the effect of nifedipine to reduce amplitude of contraction, which is in agreement with the findings of others who have demonstrated a reduced inhibition of I_{CaL} under these conditions (Legssyer *et al.*, 1997; Farkas *et al.*, 2012). It is possible that phosphorylation of LTCCs somehow reduces the effectiveness with which compounds can interact with the dihydropyridine binding site, which may explain at least in part why anandamide appears to be less potent in the presence of β-adrenoceptor stimulation.

In further support for the suggestion that anandamide and Δ^9-THC interact directly with ion channels, data presented in chapter 4 show for the first time an effect of anandamide to inhibit I_{Ks}, but not I_{Kr} in guinea pig ventricular myocytes. This action of anandamide is shared with the plant derived cannabinoid, cannabidiol (Needham *et al.*, 1998), which is inactive at cannabinoid receptors. In addition, the experiments presented in chapter 6 demonstrate actions of Δ^9-THC to inhibit I_{CaL} and I_{Ks} in a similar manner to anandamide. Although the actions of Δ^9-THC were not tested in the presence of cannabinoid receptor antagonists or PTX, when taking into account evidence from chapters 4 and 5, it is likely that Δ^9-THC has significant cannabinoid-receptor independent effects at the concentrations used here. Although the low micromolar concentrations of the cannabinoid compounds used throughout this thesis may seem high, these compounds are highly lipophilic and so the exact concentrations within cell membranes *in vivo* are unknown. Furthermore, in the *in vivo* situation it may take some time for them to equilibrate within the cell membrane, and so the micromolar

concentrations used over short time periods (10-15 minutes) in this thesis, may be the best way of replicating this *in vitro*. As an extension to the studies presented here, it may interesting to study the use and voltage-dependence of block of LTCCs by anandamide and Δ^9-THC.

The dual Ca^{2+} and K^+ channel blocking effects of anandamide and Δ^9-THC observed here would suggest that these compounds may have some anti-arrhythmic activity. Indeed, this has also been suggested by others, with positive results (Ugdyzhekova *et al.*, 2001; Krylatov *et al.*, 2002). Furthermore, Al Kury and colleagues recently observed a reduction in NCX currents after treatment with anandamide (Kury *et al.*, 2014), which may contribute to anti-arrhythmic actions. The effectiveness of potential anti-arrhythmic actions was tested in chapter 5, with anandamide possessing anti-arrhythmic activity after approximately 7 – 10 minutes. This delay in onset of action raises the possibility that anandamide would have limited utility as an antiarrhythmic agent. Furthermore, its effectiveness in reducing I_{CaL} amplitude appeared to be lessened under conditions of β-adrenoceptor stimulation (Chapter 5). Others have also recently observed disappointing results with anandamide as an anti-arrhythmic agent (Andrag *et al.*, 2013). However, these data may not completely represent the *in vivo* situation, where actions of anandamide to inhibit sympathetic outflow may predominate.

It is of interest to note that many of the actions of anandamide reported in the literature and presented in this thesis are shared with those of general anaesthetics. For example, anaesthetic agents such as halothane and isoflurane depress cell contractions and inhibit membrane currents in guinea pig ventricular myocytes (Terrar *et al.*, 1988a; Terrar *et al.*, 1988b; Terrar *et al.*, 1989a). Furthermore, some agents are also associated with prevention against reperfusion injury in the heart (Hanley *et al.*, 2004).

It is possible that anandamide, Δ^9-THC, general anaesthetics (Hanley *et al.*, 2004) and other polyunsaturated fatty acids (Voitychuk *et al.*, 2012) share common mechanisms of action in the heart. This should be borne in mind if drugs modulating endocannabinoid function are to be used therapeutically.

References

AARHUS R, GRAEFF RM, DICKEY DM, WALSETH TF, LEE HC (1995). ADP-ribosyl cyclase and CD38 catalyze the synthesis of a calcium-mobilizing metabolite from NADP. *J Biol Chem* **270**(51)**:** 30327-30333.

ABADJI V, LIN S, TAHA G, GRIFFIN G, STEVENSON LA, PERTWEE RG, *et al.* (1994). (R)-methanandamide: A chiral novel anandamide possessing higher potency and metabolic stability. *J Med Chem* **37**(12)**:** 1889-1893.

ABADJI V, LUCAS-LENARD JM, CHIN C, KENDALL DA (1999). Involvement of the carboxyl terminus of the third intracellular loop of the cannabinoid CB1 receptor in constitutive activation of Gs. *J Neurochem* **72**(5)**:** 2032-2038.

ABBOTT GW, XU X, ROEPKE TK (2007). Impact of ancillary subunits on ventricular repolarization. *J Electrocardiol* **40**(6 Suppl)**:** S42-46.

ACCILI EA, PROENZA C, BARUSCOTTI M, DIFRANCESCO D (2002). From funny current to HCN channels: 20 years of excitation. *News Physiol Sci* **17:** 32-37.

AHERN GP, JUNANKAR PR, DULHUNTY AF (1994). Single channel activity of the ryanodine receptor calcium release channel is modulated by FK-506. *FEBS Lett* **352**(3)**:** 369-374.

AL KURY LT, VOITYCHUK OI, ALI RM, GALADARI S, YANG KH, HOWARTH FC, *et al.* (2014a). Effects of endogenous cannabinoid anandamide on excitation-contraction coupling in rat ventricular myocytes. *Cell Calcium* **55**(2)**:** 104-118.

AL KURY LT, VOITYCHUK OI, YANG KH, THAYYULLATHIL FT, DOROSHENKO P, RAMEZ AM, *et al.* (2014b). Effects of endogenous cannabinoid anandamide on voltage-dependent sodium and calcium channels in rat ventricular myocytes. *Br J Pharmacol* **171** (14): 3485-3498.

ALSEIKHAN BA, DEMARIA CD, COLECRAFT HM, YUE DT (2002). Engineered calmodulins reveal the unexpected eminence of Ca^{2+} channel inactivation in controlling heart excitation. *Proc Nat Acad Sci USA* **99**(26)**:** 17185-17190.

AMORÓS I, BARANA A, CABALLERO R, GÓMEZ R, OSUNA L, LILLO MP, *et al.* (2010). Endocannabinoids and cannabinoid analogues block human cardiac Kv4.3 channels in a receptor-independent manner. *J Mol Cell Cardiol* **48**(1)**:** 201-210.

ANDRAG E, CURTIS MJ (2013). Feasibility of targeting ischaemia-related ventricular arrhythmias by mimicry of endogenous protection by endocannabinoids. *Br J Pharmacol* **169**(8)**:** 1840-1848.

ANNETTS C, TERRAR DA, WHITE E (1990). Measurement of cardiac cell length by analysis of a video image. *J Physiol* **430**.

BALSHAW DM, XU L, YAMAGUCHI N, PASEK DA, MEISSNER G (2001). Calmodulin binding and inhibition of cardiac muscle calcium release channel (ryanodine receptor). *J Biol Chem* **276**(23)**:** 20144-20153.

BARANA A, AMORÓS I, CABALLERO R, GÓMEZ R, OSUNA L, LILLO MP, *et al.* (2010). Endocannabinoids and cannabinoid analogues block cardiac hKv1.5 channels in a cannabinoid receptor-independent manner. *Cardiov Res* **85**(1)**:** 56-67.

BASSANI JW, BASSANI RA, BERS DM (1994). Relaxation in rabbit and rat cardiac cells: species-dependent differences in cellular mechanisms. *J Physiol* **476**(2)**:** 279-293.

BATKAI S, PACHER P, OSEI-HYIAMAN D, RADAEVA S, LIU J, HARVEY-WHITE J, *et al.* (2004). Endocannabinoids acting at cannabinoid-1 receptors regulate cardiovascular function in hypertension. *Circulation* **110**(14)**:** 1996-2002.

BAYLISS R Actions of NAADP and other agents in cardiac myocytes, DPhil Thesis, 2013.

BEAN BP (1989). Classes of calcium channels in vertebrate cells. *Ann Rev Physiol* **51:** 367-384.

BEAN BP, NOWYCKY MC, TSIEN RW (1984). Beta-adrenergic modulation of calcium channels in frog ventricular heart cells. *Nature* **307**(5949)**:** 371-375.

BELARDINELLI L, ISENBERG G (1983). Actions of adenosine and isoproterenol on isolated mammalian ventricular myocytes. *Circ Res* **53**(3)**:** 287-297.

BELARDINELLI L, SHRYOCK JC, SONG Y, WANG D, SRINIVAS M (1995). Ionic basis of the electrophysiological actions of adenosine on cardiomyocytes. *FASEB J* **9**(5)**:** 359-365.

BENNETT MR (2000). The concept of transmitter receptors: 100 years on. *Neuropharmacol* **39**(4)**:** 523-546.

BENOWITZ NL, JONES RT (1975). Cardiovascular effects of prolonged delta-9-tetrahydrocannabinol ingestion. *Clin Pharmacol Ther* **18**(3)**:** 287-297.

BENSAID M, GARY-BOBO M, ESCLANGON A, MAFFRAND JP, LE FUR G, OURY-DONAT F, *et al.* (2003). The cannabinoid CB1 receptor antagonist SR141716 increases Acrp30 mRNA expression in adipose tissue of obese fa/fa rats and in cultured adipocyte cells. *Mol Pharmacol* **63**(4)**:** 908-914.

BERNOFSKY C (1980). Nicotinic acid adenine dinucleotide phosphate (NAADP+). *Methods in enzymology* **66:** 105-112.

BERRIDGE MJ, DAWSON RM, DOWNES CP, HESLOP JP, IRVINE RF (1983). Changes in the levels of inositol phosphates after agonist-dependent hydrolysis of membrane phosphoinositides. *Biochem J* **212**(2)**:** 473-482.

BERRIDGE MJ, LIPP P, BOOTMAN MD (2000). The versatility and universality of calcium signalling. *Nat Rev Mol Cell Biol* **1**(1)**:** 11-21.

BERS DM (1991). Ca regulation in cardiac muscle. *Med Sci Sports Exerc* **23**(10)**:** 1157-1162.

BERS DM (2000). Calcium fluxes involved in control of cardiac myocyte contraction. *Circ Res* **87**(4)**:** 275-281.

BERS DM (2001). *Excitation-contraction coupling and cardiac contractile force*. Second edn. Kluwer Academic Publishers, Dordrecht.

BERS DM (2002). Cardiac excitation-contraction coupling. *Nature* **415**(6868)**:** 198-205.

BERS DM (2006). Altered cardiac myocyte Ca regulation in heart failure. *Physiology (Bethesda)* **21:** 380-387.

BERS DM (2008). Calcium cycling and signaling in cardiac myocytes Vol. 70, pp 23-49.

BERS DM, CHRISTENSEN DM, NGUYEN TX (1988). Can Ca entry via Na-Ca exchange directly activate cardiac muscle contraction? *J Mol Cell Cardiol* **20**(5)**:** 405-414.

BERS DM, PEREZ-REYES E (1999). Ca channels in cardiac myocytes: Structure and function in Ca influx and intracellular Ca release. *Cardiov Res* **42**(2)**:** 339-360.

BEUCKELMANN DJ, WIER WG (1988). Mechanism of release of calcium from sarcoplasmic reticulum of guinea-pig cardiac cells. *J Physiol* **405:** 233-255.

BEUCKELMANN DJ, WIER WG (1989). Sodium-calcium exchange in guinea-pig cardiac cells: Exchange current and changes in intracellular Ca^{2+}. *J Physiol* **414:** 499-520.

BIDAUT-RUSSELL M, HOWLETT AC (1991). Cannabinoid receptor-regulated cyclic AMP accumulation in the rat striatum. *J Neurochem* **57**(5)**:** 1769-1773.

BISOGNO T, HOWELL F, WILLIAMS G, MINASSI A, CASCIO MG, LIGRESTI A, *et al.* (2003). Cloning of the first sn1-DAG lipases points to the spatial and temporal regulation of endocannabinoid signaling in the brain. *J Cell Biol* **163**(3)**:** 463-468.

BISOGNO T, SEPE N, MELCK D, MAURELLI S, DE PETROCELLIS L, DI MARZO V (1997). Biosynthesis, release and degradation of the novel endogenous cannabimimetic metabolite 2-arachidonoylglycerol in mouse neuroblastoma cells. *Biochem J* **322 (Pt 2):** 671-677.

BLANKMAN JL, SIMON GM, CRAVATT BF (2007). A comprehensive profile of brain enzymes that hydrolyze the endocannabinoid 2-arachidonoylglycerol. *Chem Biol* **14**(12)**:** 1347-1356.

BOHM M, PIESKE B, UNGERER M, ERDMANN E (1989). Characterization of A1 adenosine receptors in atrial and ventricular myocardium from diseased human hearts. *Circ Res* **65**(5)**:** 1201-1211.

BOLAND LM, DRZEWIECKI MM (2008). Polyunsaturated fatty acid modulation of voltage-gated ion channels. *Cell Biochem Biophys* **52**(2)**:** 59-84.

BOLTON E, BAYLISS R, KALUNGIA CA, BLOOR-YOUNG D, DA SILVA MR, PARRINGTON J, *et al.* (2013). The Involvement of NAADP and Two-Pore Ca^{2+} Channels in the Cardiac Beta-Adrenergic Response. *Biophys J* **104**(2)**:** 614A-614A.

BOLTON EL, TERRAR DA (2011). Possible Roles of Cannabinoid Receptors in Cardiac Myocytes. *Biophys J* **100**(3, Supplement 1)**:** 575a-575a.

BOLTON EL, TERRAR DA (2012). Effects of Anandamide on Electrical Activity, Calcium Transients and Contraction in Guinea Pig Cardiac Ventricular Myocytes. *Biophys J* **102**(3)**:** 542A-542A.

BONHAUS DW, CHANG LK, KWAN J, MARTIN GR (1998). Dual activation and inhibition of adenylyl cyclase by cannabinoid receptor agonists: evidence for agonist-specific trafficking of intracellular responses. *J Pharmacol Exp Ther* **287**(3)**:** 884-888.

BONZ A, LASER M, KULLMER S, KNIESCH S, BABIN-EBELL J, POPP V, *et al.* (2003). Cannabinoids acting on CB1 receptors decrease contractile performance in human atrial muscle. *J Cardiovasc Pharmacol* **41**(4)**:** 657-664.

BOOTMAN MD, HARZHEIM D, SMYRNIAS I, CONWAY SJ, RODERICK HL (2007). Temporal changes in atrial EC-coupling during prolonged stimulation with endothelin-1. *Cell Calcium* **42**(4-5)**:** 489-501.

BOOTMAN MD, RIETDORF K, COLLINS T, WALKER S, SANDERSON M (2013). Converting fluorescence data into Ca^{2+} concentration. *Cold Spring Harbor Protocols* **8**(2)**:** 126-129.

BRAILOIU E, CHURAMANI D, CAI X, SCHRLAU MG, BRAILOIU GC, GAO X, *et al.* (2009). Essential requirement for two-pore channel 1 in NAADP-mediated calcium signaling. *J Cell Biol* **186**(2)**:** 201-209.

BRANDL CJ, GREEN NM, KORCZAK B, MACLENNAN DH (1986). Two Ca^{2+} ATPase genes: homologies and mechanistic implications of deduced amino acid sequences. *Cell* **44**(4)**:** 597-607.

BRENNAN MJ, DAVID JL, KENIMER JG, MANCLARK CR (1988). Lectin-like binding of pertussis toxin to a 165-kilodalton Chinese hamster ovary cell glycoprotein. *J Biol Chem* **263**(10)**:** 4895-4899.

BRILLANTES AB, ONDRIAS K, SCOTT A, KOBRINSKY E, ONDRIASOVA E, MOSCHELLA MC, *et al.* (1994). Stabilization of calcium release channel (ryanodine receptor) function by FK506-binding protein. *Cell* **77**(4)**:** 513-523.

BROCHET DX, XIE W, YANG D, CHENG H, LEDERER WJ (2011). Quarky calcium release in the heart. *Circ Res* **108**(2)**:** 210-218.

BROCHET DX, YANG D, DI MAIO A, LEDERER WJ, FRANZINI-ARMSTRONG C, CHENG H (2005). Ca^{2+} blinks: rapid nanoscopic store calcium signaling. *Proc Nat Acad Sci USA* **102**(8)**:** 3099-3104.

BRODDE OE, MICHEL MC (1999). Adrenergic and muscarinic receptors in the human heart. *Pharmacol Rev* **51**(4)**:** 651-690.

BROWN LA, HUMPHREY SM, HARDING SE (1990). The anti-adrenergic effect of adenosine and its blockade by pertussis toxin: a comparative study in myocytes isolated from guinea-pig, rat and failing human hearts. *Br J Pharmacol* **101**(2)**:** 484-488.

BRUM G, OSTERRIEDER W, TRAUTWEIN W (1984). Beta-adrenergic increase in the calcium conductance of cardiac myocytes studied with the patch clamp. *Pflugers Arch : Eur J Physiol* **401**(2)**:** 111-118.

BURNS DL (1988). Subunit structure and enzymic activity of pertussis toxin. *Microbiol Sci* **5**(9)**:** 285-287.

CADAS H, DI TOMASO E, PIOMELLI D (1997). Occurrence and biosynthesis of endogenous cannabinoid precursor, N-arachidonoyl phosphatidylethanolamine, in rat brain. *J Neurosci* **17**(4)**:** 1226-1242.

CADAS H, GAILLET S, BELTRAMO M, VENANCE L, PIOMELLI D (1996). Biosynthesis of an endogenous cannabinoid precursor in neurons and its control by calcium and cAMP. *J Neurosci* **16**(12)**:** 3934-3942.

CALCRAFT PJ, RUAS M, PAN Z, CHENG X, ARREDOUANI A, HAO X, *et al.* (2009). NAADP mobilizes calcium from acidic organelles through two-pore channels. *Nature* **459**(7246)**:** 596-600.

CALLOE K, GOODROW R, OLESEN SP, ANTZELEVITCH C, CORDEIRO JM (2013). Tissue-specific effects of acetylcholine in the canine heart. *Am J Physiol Heart Circ Physiol* **305**(1)**:** H66-75.

CANG C, ZHOU Y, NAVARRO B, SEO YJ, ARANDA K, SHI L, *et al.* (2013). mTOR regulates lysosomal ATP-sensitive two-pore Na(+) channels to adapt to metabolic state. *Cell* **152**(4)**:** 778-790.

CANNELL MB, BERLIN JR, LEDERER WJ (1987). Effect of membrane potential changes on the calcium transient in single rat cardiac muscle cells. *Science* **238**(4832)**:** 1419-1423.

CANNELL MB, KONG CH, IMTIAZ MS, LAVER DR (2013). Control of sarcoplasmic reticulum Ca^{2+} release by stochastic RyR gating within a 3D model of the cardiac dyad and importance of induction decay for CICR termination. *Biophys J* **104**(10)**:** 2149-2159.

CANNELL MB, KONG CHT (2012). Local control in cardiac E-C coupling. *J Mol Cell Cardiol* **52**(2)**:** 298-303.

CARONI P, CARAFOLI E (1980). An ATP-dependent Ca^{2+}-pumping system in dog heart sarcolemma. *Nature* **283**(5749)**:** 765-767.

CATTERALL WA (2000). Structure and regulation of voltage-gated Ca^{2+} channels. *Annu Rev Cell Dev Biol* **16:** 521-555.

CENS T, ROUSSET M, LEYRIS JP, FESQUET P, CHARNET P (2006). Voltage- and calcium-dependent inactivation in high voltage-gated Ca($^{2+}$) channels. *Prog Biophys Mol Biol* **90**(1-3)**:** 104-117.

CHEMIN J, MONTEIL A, PEREZ-REYES E, NARGEOT J, LORY P (2001). Direct inhibition of T-type calcium channels by the endogenous cannabinoid anandamide. *EMBO J* **20**(24)**:** 7033-7040.

CHEMIN J, NARGEOT J, LORY P (2007). Chemical determinants involved in anandamide-induced inhibition of T-type calcium channels. *J Biol Chem* **282**(4)**:** 2314-2323.

CHEN-IZU Y, MCCULLE SL, WARD CW, SOELLER C, ALLEN BM, RABANG C, *et al.* (2006). Three-dimensional distribution of ryanodine receptor clusters in cardiac myocytes. *Biophys J* **91**(1)**:** 1-13.

CHENG DKL, TUNG L, SOBIE EA (1999). Nonuniform responses of transmembrane potential during electric field stimulation of single cardiac cells. *Am J Physiol Heart Circ Physiol* **277**(1 46-1)**:** H351-H362.

CHENG H, LEDERER MR, LEDERER WJ, CANNELL MB (1996). Calcium sparks and [Ca^{2+}]i waves in cardiac myocytes. *Am J Physiol* **270**(1 Pt 1)**:** C148-159.

CHENG H, LEDERER WJ, CANNELL MB (1993). Calcium sparks: elementary events underlying excitation-contraction coupling in heart muscle. *Science* **262**(5134)**:** 740-744.

CHIESI M, WRZOSEK A, GRUENINGER S (1994). The role of the sarcoplasmic reticulum in various types of cardiomyocytes. *Mol Cell Biochem* **130**(2)**:** 159-171.

CHILDERS SR, SEXTON T, ROY MB (1994). Effects of anandamide on cannabinoid receptors in rat brain membranes. *Biochem Pharm* **47**(4)**:** 711-715.

CHING LL, WILLIAMS AJ, SITSAPESAN R (2000). Evidence for Ca($^{2+}$) activation and inactivation sites on the luminal side of the cardiac ryanodine receptor complex. *Circ Res* **87**(3)**:** 201-206.

CHINI EN, CHINI CC, KATO I, TAKASAWA S, OKAMOTO H (2002). CD38 is the major enzyme responsible for synthesis of nicotinic acid-adenine dinucleotide phosphate in mammalian tissues. *Biochem J* **362**(Pt 1)**:** 125-130.

CHINI EN, DOUSA TP (1995). Enzymatic synthesis and degradation of nicotinate adenine dinucleotide phosphate (NAADP), a Ca^{2+}-releasing agonist, in rat tissues. *Biochem Biophys Res Comm***209**(1)**:** 167-174.

CHOISY SC, HANCOX JC, ARBERRY LA, REYNOLDS AM, SHATTOCK MJ, JAMES AF (2004). Evidence for a novel K(+) channel modulated by alpha(1A)-adrenoceptors in cardiac myocytes. *Mol Pharmacol* **66**(3)**:** 735-748.

CHURCHILL GC, GALIONE A (2001a). NAADP induces Ca^{2+} oscillations via a two-pool mechanism by priming IP3- and cADPR-sensitive Ca^{2+} stores. *EMBO J* **20**(11)**:** 2666-2671.

CHURCHILL GC, GALIONE A (2001b). Prolonged inactivation of nicotinic acid adenine dinucleotide phosphate-induced Ca^{2+} release mediates a spatiotemporal Ca^{2+} memory. *J Biol Chem* **276**(14)**:** 11223-11225.

CHURCHILL GC, OKADA Y, THOMAS JM, GENAZZANI AA, PATEL S, GALIONE A (2002). NAADP mobilizes Ca($^{2+}$) from reserve granules, lysosome-related organelles, in sea urchin eggs. *Cell* **111**(5)**:** 703-708.

CLAPPER DL, WALSETH TF, DARGIE PJ, LEE HC (1987). Pyridine nucleotide metabolites stimulate calcium release from sea urchin egg microsomes desensitized to inositol trisphosphate. *J Biol Chem* **262**(20)**:** 9561-9568.

COLLINS TP, BAYLISS R, CHURCHILL GC, GALIONE A, TERRAR DA (2011). NAADP influences excitation-contraction coupling by releasing calcium from lysosomes in atrial myocytes. *Cell Calcium* **50**(5)**:** 449-458.

COLLINS TP, TERRAR DA (2012). Ca $^{2+}$-stimulated adenylyl cyclases regulate the L-type Ca $^{2+}$ current in guinea-pig atrial myocytes. *J Physiol* **590**(8)**:** 1881-1893.

COPELLO JA, QI Y, JEYAKUMAR LH, OGUNBUNMI E, FLEISCHER S (2001). Lack of effect of cADP-ribose and NAADP on the activity of skeletal muscle and heart ryanodine receptors. *Cell Calcium* **30**(4)**:** 269-284.

CRAVATT BF, DEMAREST K, PATRICELLI MP, BRACEY MH, GIANG DK, MARTIN BR, *et al.* (2001). Supersensitivity to anandamide and enhanced endogenous cannabinoid signaling in mice lacking fatty acid amide hydrolase. *Proc Nat Acad Sci USA* **98**(16)**:** 9371-9376.

CRAVATT BF, GIANG DK, MAYFIELD SP, BOGER DL, LERNER RA, GILULA NB (1996). Molecular characterization of an enzyme that degrades neuromodulatory fatty-acid amides. *Nature* **384**(6604)**:** 83-87.

CUI Y, GALIONE A, TERRAR DA (1999). Effects of photoreleased cADP-ribose on calcium transients and calcium sparks in myocytes isolated from guinea-pig and rat ventricle. *Biochem J* **342 (Pt 2):** 269-273.

CURRIE S, LOUGHREY CM, CRAIG MA, SMITH GL (2004). Calcium/calmodulin-dependent protein kinase IIdelta associates with the ryanodine receptor complex and regulates channel function in rabbit heart. *Biochem J* **377**(Pt 2)**:** 357-366.

CURRIE S, RAINBOW RD, EWART MA, KITSON S, PLIEGO EH, KANE KA, *et al.* (2008). IP3R-mediated Ca^{2+} release is modulated by anandamide in isolated cardiac nuclei. *J Mol Cell Cardiol* **45**(6)**:** 804-811.

DAVIES A, HENDRICH J, VAN MINH AT, WRATTEN J, DOUGLAS L, DOLPHIN AC (2007). Functional biology of the alpha(2)delta subunits of voltage-gated calcium channels. *Trends Pharmacol Sci* **28**(5)**:** 220-228.

DE JONGH KS, MURPHY BJ, COLVIN AA, HELL JW, TAKAHASHI M, CATTERALL WA (1996). Specific phosphorylation of a site in the full-length form of the alpha 1 subunit of the cardiac L-type calcium channel by adenosine 3',5'-cyclic monophosphate-dependent protein kinase. *Biochemistry* **35**(32)**:** 10392-10402.

DE TOMBE PP, MATEJA RD, TACHAMPA K, AIT MOU Y, FARMAN GP, IRVING TC (2010). Myofilament length dependent activation. *J Mol Cell Cardiol* **48**(5)**:** 851-858.

DEADWYLER SA, HAMPSON RE, MU J, WHYTE A, CHILDERS S (1995). Cannabinoids modulate voltage sensitive potassium A-current in hippocampal neurons via a cAMP-dependent process. *J Pharmacol Exp Ther* **273**(2)**:** 734-743.

DEUTSCH DG, GOLIGORSKY MS, SCHMID PC, KREBSBACH RJ, SCHMID HH, DAS SK, *et al.* (1997). Production and physiological actions of anandamide in the vasculature of the rat kidney. *J Clin Invest* **100**(6)**:** 1538-1546.

DEVANE WA, BREUER A, SHESKIN T, JARBE TU, EISEN MS, MECHOULAM R (1992a). A novel probe for the cannabinoid receptor. *J Med Chem* **35**(11)**:** 2065-2069.

DEVANE WA, DYSARZ FA, 3RD, JOHNSON MR, MELVIN LS, HOWLETT AC (1988). Determination and characterization of a cannabinoid receptor in rat brain. *Mol Pharmacol* **34**(5)**:** 605-613.

DEVANE WA, HANUS L, BREUER A, PERTWEE RG, STEVENSON LA, GRIFFIN G, *et al.* (1992b). Isolation and structure of a brain constituent that binds to the cannabinoid receptor. *Science* **258**(5090)**:** 1946-1949.

DHEIN S, VAN KOPPEN CJ, BRODDE OE (2001). Muscarinic receptors in the mammalian heart. *Pharmacol Res* **44**(3)**:** 161-182.

DIAZ ME, GRAHAM HK, O'NEILL S C, TRAFFORD AW, EISNER DA (2005). The control of sarcoplasmic reticulum Ca content in cardiac muscle. *Cell Calcium* **38**(3-4)**:** 391-396.

DIFRANCESCO D, TROMBA C (1988). Inhibition of the hyperpolarization-activated current (if) induced by acetylcholine in rabbit sino-atrial node myocytes. *J Physiol* **405:** 477-491.

DINH TP, CARPENTER D, LESLIE FM, FREUND TF, KATONA I, SENSI SL, *et al.* (2002). Brain monoglyceride lipase participating in endocannabinoid inactivation. *Proc Nat Acad Sci USA* **99**(16)**:** 10819-10824.

DIXON JE, SHI W, WANG HS, MCDONALD C, YU H, WYMORE RS, *et al.* (1996). Role of the Kv4.3 K+ channel in ventricular muscle. A molecular correlate for the transient outward current. *Circ Res* **79**(4)**:** 659-668.

EHARA T, NOMA A, ONO K (1988). Calcium-activated non-selective cation channel in ventricular cells isolated from adult guinea-pig hearts. *J Physiol* **403:** 117-133.

ELLIS EF, MOORE SF, WILLOUGHBY KA (1995). Anandamide and delta 9-THC dilation of cerebral arterioles is blocked by indomethacin. *Am J Physiol* **269**(6 Pt 2)**:** H1859-1864.

ELSON L Regulation of Cardiac Ca^{2+} Signalling Mechanisms and Contractile Function by Nicotinic Acid Adenine Dinucleotide Phosphate, DPhil Thesis, 2011.

ELSON L, CHURCHILL G, TERRAR DA, RAKOVIC S (2011). Actions of the NAADP Antagonist Trans-Ned19 in Cardiac Ventricular Myocytes. *Biophys J* **100**(3)**:** 81-82.

ELSON LC, OWEN WD, GAFSON AR, PARRINGTON J, GALIONE A, TERRAR DA, *et al.* (2010). Role of the Putative NAADP Receptor, Two-Pore Channel 2, in Ventricular Myocyte Responses to Isoproterenol. *Biophys J* **98**(3)**:** 100A-100A.

ENGELS W, VAN BILSEN M, DE GROOT MJ, LEMMENS PJ, WILLEMSEN PH, RENEMAN RS, *et al.* (1990). Ischemia and reperfusion induced formation of eicosanoids in isolated rat hearts. *Am J Physiol* **258**(6 Pt 2)**:** H1865-1871.

EPPS DE, SCHMID PC, NATARAJAN V, SCHMID HH (1979). N-Acylethanolamine accumulation in infarcted myocardium. *Biochem Biophys Res Comm* **90**(2)**:** 628-633.

FABIATO A (1983). Calcium-induced release of calcium from the cardiac sarcoplasmic reticulum. *Am J Physiol* **245**(1)**:** C1-14.

FABIATO A (1985a). Simulated calcium current can both cause calcium loading in and trigger calcium release from the sarcoplasmic reticulum of a skinned canine cardiac Purkinje cell. *J Gen Physiol* **85**(2)**:** 291-320.

FABIATO A (1985b). Time and calcium dependence of activation and inactivation of calcium-induced release of calcium from the sarcoplasmic reticulum of a skinned canine cardiac Purkinje cell. *J Gen Physiol* **85**(2)**:** 247-289.

FARKAS V, SZENTANDRASSY N, BARANDI L, HEGYI B, RUZSNAVSZKY F, RUZSNAVSZKY O, *et al.* (2012). Interaction between $Ca(^{2+})$ channel blockers and isoproterenol on L-type $Ca(^{2+})$ current in canine ventricular cardiomyocytes. *Acta Physiol (Oxford, England)* **206**(1)**:** 42-50.

FARMER BB, MANCINA M, WILLIAMS ES, WATANABE AM (1983). Isolation of calcium tolerant myocytes from adult rat hearts: Review of the literature and description of a method. *Life Sci* **33**(1)**:** 1-18.

FELDER CC, BRILEY EM, AXELROD J, SIMPSON JT, MACKIE K, DEVANE WA (1993). Anandamide, an endogenous cannabimimetic eicosanoid, binds to the cloned human cannabinoid receptor and stimulates receptor-mediated signal transduction. *Proc Nat Acad Sci USA* **90**(16)**:** 7656-7660.

FELDER CC, JOYCE KE, BRILEY EM, MANSOURI J, MACKIE K, BLOND O, *et al.* (1995). Comparison of the pharmacology and signal transduction of the human cannabinoid CB1 and CB2 receptors. *Mol Pharmacol* **48**(3)**:** 443-450.

FELDER CC, NIELSEN A, BRILEY EM, PALKOVITS M, PRILLER J, AXELROD J, *et al.* (1996). Isolation and measurement of the endogenous cannabinoid receptor agonist, anandamide, in brain and peripheral tissues of human and rat. *FEBS Lett* **393**(2-3)**:** 231-235.

FENG J, WIBLE B, LI GR, WANG Z, NATTEL S (1997). Antisense oligodeoxynucleotides directed against Kv1.5 mRNA specifically inhibit ultrarapid delayed rectifier K+ current in cultured adult human atrial myocytes. *Circ Res* **80**(4)**:** 572-579.

FIELDS JZ, ROESKE WR, MORKIN E, YAMAMURA HI (1978). Cardiac muscarinic cholinergic receptors. Biochemical identification and characterization. *J Biol Chem* **253**(9)**:** 3251-3258.

FILL M, COPELLO JA (2002). Ryanodine receptor calcium release channels. *Physiol Rev* **82**(4)**:** 893-922.

FONG TM, SHEARMAN LP, STRIBLING DS, SHU J, LAO J, HUANG CRR, *et al.* (2009). Pharmacological efficacy and safety profile of taranabant in preclinical species. *Drug Development Research* **70**(5)**:** 349-362.

FORD WR, HONAN SA, WHITE R, HILEY CR (2002). Evidence of a novel site mediating anandamide-induced negative inotropic and coronary vasodilatator responses in rat isolated hearts. *Br J Pharmacol* **135**(5)**:** 1191-1198.

FRANCIS GS, BENEDICT C, JOHNSTONE DE, KIRLIN PC, NICKLAS J, LIANG CS, *et al.* (1990). Comparison of neuroendocrine activation in patients with left ventricular dysfunction with and without congestive heart failure: A substudy of the Studies of Left Ventricular Dysfunction (SOLVD). *Circulation* **82**(5)**:** 1724-1729.

FRANK JS, MOTTINO G, REID D, MOLDAY RS, PHILIPSON KD (1992). Distribution of the Na(+)-Ca^{2+} exchange protein in mammalian cardiac myocytes: an immunofluorescence and immunocolloidal gold-labeling study. *J Cell Biol* **117**(2)**:** 337-345.

FUJII J, UENO A, KITANO K, TANAKA S, KADOMA M, TADA M (1987). Complete complementary DNA-derived amino acid sequence of canine cardiac phospholamban. *J Clin Invest* **79**(1)**:** 301-304.

GALFRE E, PITT SJ, VENTURI E, SITSAPESAN M, ZACCAI NR, TSANEVA-ATANASOVA K, *et al.* (2012). FKBP12 activates the cardiac ryanodine receptor Ca^{2+}-release channel and is antagonised by FKBP12.6. *PloS One* **7**(2)**:** e31956.

GALIONE A, EVANS AM, MA J, PARRINGTON J, ARREDOUANI A, CHENG X, *et al.* (2009). The acid test: the discovery of two-pore channels (TPCs) as NAADP-gated endolysosomal Ca($^{2+}$) release channels. *Eur J Physiol* **458**(5)**:** 869-876.

GAONI Y, MECHOULAM R (1964). Isolation, structure, and partial synthesis of an active constituent of hashish. *J Am Chem Soc* **86**(8)**:** 1646-1647.

GAONI Y, MECHOULAM R (1971). The isolation and structure of delta-1-tetrahydrocannabinol and other neutral cannabinoids from hashish. *J Am Chem Soc* **93**(1)**:** 217-224.

GEBREMEDHIN D, LANGE AR, CAMPBELL WB, HILLARD CJ, HARDER DR (1999). Cannabinoid CB1 receptor of cat cerebral arterial muscle functions to inhibit L-type Ca^{2+} channel current. *Am J Physiol* **276**(6 Pt 2)**:** H2085-2093.

GEE KR, BROWN KA, CHEN WNU, BISHOP-STEWART J, GRAY D, JOHNSON I (2000). Chemical and physiological characterization of fluo-4 Ca^{2+}-indicator dyes. *Cell Calcium* **27**(2)**:** 97-106.

GENAZZANI AA, GALIONE A (1996). Nicotinic acid-adenine dinucleotide phosphate mobilizes Ca^{2+} from a thapsigargin-insensitive pool. *Biochem J* **315 (Pt 3):** 721-725.

GENAZZANI AA, MEZNA M, DICKEY DM, MICHELANGELI F, WALSETH TF, GALIONE A (1997). Pharmacological properties of the Ca^{2+}-release mechanism sensitive to NAADP in the sea urchin egg. *Br J Pharmacol* **121**(7)**:** 1489-1495.

GERARD CM, MOLLEREAU C, VASSART G, PARMENTIER M (1991). Molecular cloning of a human cannabinoid receptor which is also expressed in testis. *Biochem J* **279 (Pt 1):** 129-134.

GERHARDSTEIN BL, PURI TS, CHIEN AJ, HOSEY MM (1999). Identification of the sites phosphorylated by cyclic AMP-dependent protein kinase on the beta 2 subunit of L-type voltage-dependent calcium channels. *Biochemistry* **38**(32)**:** 10361-10370.

GINSBURG KS, BERS DM (2004). Modulation of excitation-contraction coupling by isoproterenol in cardiomyocytes with controlled SR Ca^{2+} load and Ca^{2+} current trigger. *J Physiol* **556**(Pt 2)**:** 463-480.

GLASS M, FELDER CC (1997). Concurrent stimulation of cannabinoid CB1 and dopamine D2 receptors augments cAMP accumulation in striatal neurons: evidence for a Gs linkage to the CB1 receptor. *J Neurosci* **17**(14)**:** 5327-5333.

GOLDMAN DE (1943). Potential, Impedance, and Rectification in Membranes. *J Gen Physiol* **27**(1)**:** 37-60.

GONG H, SUN H, KOCH WJ, RAU T, ESCHENHAGEN T, RAVENS U, *et al.* (2002). Specific beta(2)AR blocker ICI 118,551 actively decreases contraction through a G(i)-coupled form of the beta(2)AR in myocytes from failing human heart. *Circulation* **105**(21)**:** 2497-2503.

GONSIOREK W, LUNN C, FAN X, NARULA S, LUNDELL D, HIPKIN RW (2000). Endocannabinoid 2-arachidonyl glycerol is a full agonist through human type 2 cannabinoid receptor: antagonism by anandamide. *Mol Pharmacol* **57**(5)**:** 1045-1050.

GOONASEKERA SA, HAMMER K, AUGER-MESSIER M, BODI I, CHEN X, ZHANG H, *et al.* (2012). Decreased cardiac L-type Ca(2)(+) channel activity induces hypertrophy and heart failure in mice. *J Clin Invest* **122**(1)**:** 280-290.

GRANTHAM CJ, CANNELL MB (1996). Ca^{2+} influx during the cardiac action potential in guinea pig ventricular myocytes. *Circ Res* **79**(2)**:** 194-200.

GUO T, ZHANG T, MESTRIL R, BERS DM (2006). Ca^{2+}/Calmodulin-dependent protein kinase II phosphorylation of ryanodine receptor does affect calcium sparks in mouse ventricular myocytes. *Circ Res* **99**(4)**:** 398-406.

GYORKE I, GYORKE S (1998). Regulation of the cardiac ryanodine receptor channel by luminal Ca^{2+} involves luminal Ca^{2+} sensing sites. *Biophys J* **75**(6)**:** 2801-2810.

GYORKE S, FILL M (1993). Ryanodine receptor adaptation: control mechanism of Ca^{2+}-induced Ca^{2+} release in heart. *Science* **260**(5109)**:** 807-809.

GYORKE S, GYORKE I, TERENTYEV D, VIATCHENKO-KARPINSKI S, WILLIAMS SC (2004). Modulation of sarcoplasmic reticulum calcium release by calsequestrin in cardiac myocytes. *Biol Res* **37**(4)**:** 603-607.

HAN W, WANG Z, NATTEL S (2001). Slow delayed rectifier current and repolarization in canine cardiac Purkinje cells. *Am J Physiol Heart Circ Physiol* **280**(3)**:** H1075-1080.

HANLEY PJ, TER KEURS HE, CANNELL MB (2004). Excitation-contraction coupling in the heart and the negative inotropic action of volatile anesthetics. *Anesthesiology* **101**(4)**:** 999-1014.

HANUS L, GOPHER A, ALMOG S, MECHOULAM R (1993). Two new unsaturated fatty acid ethanolamides in brain that bind to the cannabinoid receptor. *J Med Chem* **36**(20)**:** 3032-3034.

HARTZELL HC (1988). Regulation of cardiac ion channels by catecholamines, acetylcholine and second messenger systems. *Prog Biophys Mol Biol* **52**(3)**:** 165-247.

HEATH BM, TERRAR DA (1996). Separation of the components of the delayed rectifier potassium current using selective blockers of IKr and IKs in guinea-pig isolated ventricular myocytes. *Exp Physiol* **81**(4)**:** 587-603.

HEATH BM, TERRAR DA (2000). Protein kinase C enhances the rapidly activating delayed rectifier potassium current, IKr, through a reduction in C-type inactivation in guinea-pig ventricular myocytes. *J Physiol* **522 Pt 3:** 391-402.

HERKENHAM M, LYNN AB, LITTLE MD, JOHNSON MR, MELVIN LS, DE COSTE BR, *et al.* (1990). Cannabinoid receptor localization in brain. *Proc Nat Acad Sci USA* **87**(5)**:** 1932-1936.

HESS P, LANSMAN JB, TSIEN RW (1984). Different modes of Ca channel gating behaviour favoured by dihydropyridine Ca agonists and antagonists. *Nature* **311**(5986)**:** 538-544.

HIGASHIDA H, EGOROVA A, HIGASHIDA C, ZHONG ZG, YOKOYAMA S, NODA M, *et al.* (1999). Sympathetic potentiation of cyclic ADP-ribose formation in rat cardiac myocytes. *J Biol Chem* **274**(47)**:** 33348-33354.

HILEY CR, FORD WR (2004). Cannabinoid pharmacology in the cardiovascular system: potential protective mechanisms through lipid signalling. *Biol Rev Cam Phil Soc* **79**(1)**:** 187-205.

HILLARD CJ, HARRIS RA, BLOOM AS (1985). Effects of the cannabinoids on physical properties of brain membranes and phospholipid vesicles: fluorescence studies. *J Pharmacol Exp Ther* **232**(3)**:** 579-588.

HO BY, STADNICKA A, PRATHER PL, BUCKLEY AR, CURRENT LL, BOSNJAK ZJ, *et al.* (2000). Cannabinoid CB1 receptor-mediated inhibition of prolactin release and signaling mechanisms in GH4C1 cells. *Endocrinology* **141**(5)**:** 1675-1685.

HOCKERMAN GH, PETERSON BZ, JOHNSON BD, CATTERALL WA (1997). Molecular determinants of drug binding and action on L-type calcium channels. *Annu Rev Pharmacol Toxicol* **37:** 361-396.

HOHENEGGER M, SUKO J, GSCHEIDLINGER R, DROBNY H, ZIDAR A (2002). Nicotinic acid-adenine dinucleotide phosphate activates the skeletal muscle ryanodine receptor. *Biochem J* **367**(Pt 2)**:** 423-431.

HOSOHATA K, QUOCK RM, HOSOHATA Y, BURKEY TH, MAKRIYANNIS A, CONSROE P, *et al.* (1997). AM630 is a competitive cannabinoid receptor antagonist in the guinea pig brain. *Life Sci* **61**(9)**:** PL115-118.

HOWLETT AC (1984). Inhibition of neuroblastoma adenylate cyclase by cannabinoid and nantradol compounds. *Life Sci* **35**(17)**:** 1803-1810.

HOWLETT AC (1987). Cannabinoid inhibition of adenylate cyclase: Relative activity of constituents and metabolites of marihuana. *Neuropharmacol* **26**(5)**:** 507-512.

HOWLETT AC, BARTH F, BONNER TI, CABRAL G, CASELLAS P, DEVANE WA, *et al.* (2002). International Union of Pharmacology. XXVII. Classification of cannabinoid receptors. *Pharmacol Rev* **54**(2)**:** 161-202.

HOWLETT AC, FLEMING RM (1984). Cannabinoid inhibition of adenylate cyclase. Pharmacology of the response in neuroblastoma cell membranes. *Mol Pharmacol* **26**(3)**:** 532-538.

HOWLETT AC, JOHNSON MR, MELVIN LS, MILNE GM (1988). Nonclassical cannabinoid analgetics inhibit adenylate cyclase: development of a cannabinoid receptor model. *Mol Pharmacol* **33**(3)**:** 297-302.

HULME JT, LIN TW, WESTENBROEK RE, SCHEUER T, CATTERALL WA (2003). Beta-adrenergic regulation requires direct anchoring of PKA to cardiac CaV1.2 channels via a leucine zipper interaction with A kinase-anchoring protein 15. *Proc Nat Acad Sci USA* **100**(22)**:** 13093-13098.

HULME JT, WESTENBROEK RE, SCHEUER T, CATTERALL WA (2006). Phosphorylation of serine 1928 in the distal C-terminal domain of cardiac CaV1.2 channels during beta1-adrenergic regulation. *Proc Nat Acad Sci USA* **103**(44)**:** 16574-16579.

HUSSAIN AM, LEE HC, CHANG CF (1998). Functional expression of secreted mouse BST-1 in yeast. *Protein Express Purif* **12**(1)**:** 133-137.

HUXLEY AF, SIMMONS RM (1971). Proposed mechanism of force generation in striated muscle. *Nature* **233**(5321)**:** 533-538.

HUXLEY HE (1969). The mechanism of muscular contraction. *Science* **164**(3886)**:** 1356-1365.

IBRAHIM M, GORELIK J, YACOUB MH, TERRACCIANO CM (2011). The structure and function of cardiac t-tubules in health and disease. *Proc Biol Sci* **278**(1719)**:** 2714-2723.

IIJIMA T, IRISAWA H, KAMEYAMA M (1985). Membrane currents and their modification by acetylcholine in isolated single atrial cells of the guinea-pig. *J Physiol* **359:** 485-501.

IINO S, CUI Y, GALIONE A, TERRAR DA (1997). Actions of cADP-ribose and its antagonists on contraction in guinea pig isolated ventricular myocytes. Influence of temperature. *Circ Res* **81**(5)**:** 879-884.

INUI M, WANG S, SAITO A, FLEISCHER S (1988). Characterization of junctional and longitudinal sarcoplasmic reticulum from heart muscle. *J Biol Chem* **263**(22)**:** 10843-10850.

ISENBERG G, HAN S (1994). Gradation of Ca($^{2+}$)-induced Ca^{2+} release by voltage-clamp pulse duration in potentiated guinea-pig ventricular myocytes. *J Physiol* **480 (Pt 3):** 423-438.

ISHIBASHI K, SUZUKI M, IMAI M (2000). Molecular cloning of a novel form (two-repeat) protein related to voltage-gated sodium and calcium channels. *Biochem Biophys Res Comm* **270**(2)**:** 370-376.

ITO H, HOSOYA Y, INANOBE A, TOMOIKE H, ENDOH M (1995). Acetylcholine and adenosine activate the G protein-gated muscarinic K+ channel in ferret ventricular myocytes. *Naunyn-Schmiedeberg's Arch Pharmacol* **351**(6)**:** 610-617.

ITOH M, ISHIHARA K, TOMIZAWA H, TANAKA H, KOBUNE Y, ISHIKAWA J, *et al.* (1994). Molecular cloning of murine BST-1 having homology with CD38 and Aplysia ADP-ribosyl cyclase. *Biochem Biophys Res Comm* **203**(2)**:** 1309-1317.

JAMES P, INUI M, TADA M, CHIESI M, CARAFOLI E (1989). Nature and site of phospholamban regulation of the Ca^{2+} pump of sarcoplasmic reticulum. *Nature* **342**(6245)**:** 90-92.

JIN X-H, UYAMA T, WANG J, OKAMOTO Y, TONAI T, UEDA N (2009). cDNA cloning and characterization of human and mouse Ca^{2+}-independent phosphatidylethanolamine N-acyltransferases. *Biochim Biophys Acta Mol Cell Biol Lipid* **1791**(1)**:** 32-38.

JIN XH, OKAMOTO Y, MORISHITA J, TSUBOI K, TONAI T, UEDA N (2007). Discovery and characterization of a Ca^{2+}-independent phosphatidylethanolamine N-acyltransferase generating the anandamide precursor and its congeners. *J Biol Chem* **282**(6)**:** 3614-3623.

JOHNSON DE, HEALD SL, DALLY RD, JANIS RA (1993). Isolation, identification and synthesis of an endogenous arachidonic amide that inhibits calcium channel antagonist 1,4-dihydropyridine binding. *Prostaglandins Leukot Essent Fatty Acid* **48**(6)**:** 429-437.

JONES LR, SUZUKI YJ, WANG W, KOBAYASHI YM, RAMESH V, FRANZINI-ARMSTRONG C, *et al.* (1998). Regulation of Ca^{2+} signaling in transgenic mouse cardiac myocytes overexpressing calsequestrin. *J Clin Invest* **101**(7)**:** 1385-1393.

JONES RT (2002). Cardiovascular system effects of marijuana. *J Clin Pharmacol* **42**(11 Suppl)**:** 58s-63s.

JONSSON MKB, VAN DER HEYDEN MAG, VAN VEEN TAB (2012). Deciphering hERG channels: Molecular basis of the rapid component of the delayed rectifier potassium current. *J Mol Cell Cardiol* **53**(3)**:** 369-374.

JUNG KM, MANGIERI R, STAPLETON C, KIM J, FEGLEY D, WALLACE M, *et al.* (2005). Stimulation of endocannabinoid formation in brain slice cultures through activation of group I metabotropic glutamate receptors. *Mol Pharmacol* **68**(5)**:** 1196-1202.

KACZOCHA M, GLASER ST, CHAE J, BROWN DA, DEUTSCH DG (2010). Lipid droplets are novel sites of N-acylethanolamine inactivation by fatty acid amide hydrolase-2. *J Biol Chem* **285**(4)**:** 2796-2806.

KACZOCHA M, VIVIECA S, SUN J, GLASER ST, DEUTSCH DG (2012). Fatty acid-binding proteins transport N-acylethanolamines to nuclear receptors and are targets of endocannabinoid transport inhibitors. *J Biol Chem* **287**(5)**:** 3415-3424.

KAMP TJ, HELL JW (2000). Regulation of cardiac L-type calcium channels by protein kinase A and protein kinase C. *Circ Res* **87**(12)**:** 1095-1102.

KANAKIS C, JR., POUGET JM, ROSEN KM (1976). The effects of delta-9-tetrahydrocannabinol (cannabis) on cardiac performance with and without beta blockade. *Circulation* **53**(4)**:** 703-707.

KANG TM, HILGEMANN DW (2004). Multiple transport modes of the cardiac $Na+/Ca^{2+}$ exchanger. *Nature* **427**(6974)**:** 544-548.

KANNT A, SICKA K, KROLL K, KADEREIT D, GÖGELEIN H (2012). Selective inhibitors of cardiac ADPR cyclase as novel anti-arrhythmic compounds. *Naunyn-Schmiedeberg's Arch Pharmacol* **385**(7)**:** 717-727.

KANO M, OHNO-SHOSAKU T, HASHIMOTODANI Y, UCHIGASHIMA M, WATANABE M (2009). Endocannabinoid-mediated control of synaptic transmission. *Physiol Rev* **89**(1)**:** 309-380.

KARLE CA, ZITRON E, ZHANG W, KATHOFER S, SCHOELS W, KIEHN J (2002). Rapid component I(Kr) of the guinea-pig cardiac delayed rectifier K(+) current is inhibited by beta(1)-adrenoreceptor activation, via cAMP/protein kinase A-dependent pathways. *Cardiov Res* **53**(2)**:** 355-362.

KARLSSON M, CONTRERAS JA, HELLMAN U, TORNQVIST H, HOLM C (1997). cDNA cloning, tissue distribution, and identification of the catalytic triad of monoglyceride lipase. Evolutionary relationship to esterases, lysophospholipases, and haloperoxidases. *J Biol Chem* **272**(43)**:** 27218-27223.

KASLOW HR, BURNS DL (1992). Pertussis toxin and target eukaryotic cells: binding, entry, and activation. *FASEB J* **6**(9)**:** 2684-2690.

KATADA T, TAMURA M, UI M (1983). The A protomer of islet-activating protein, pertussis toxin, as an active peptide catalyzing ADP-ribosylation of a membrane protein. *Arch Biochem Biophys* **224**(1)**:** 290-298.

KOCKSKAMPER J, SEIDLMAYER L, WALTHER S, HELLENKAMP K, MAIER LS, PIESKE B (2008). Endothelin-1 enhances nuclear Ca^{2+} transients in atrial myocytes through Ins(1,4,5)P3-dependent Ca^{2+} release from perinuclear Ca^{2+} stores. *J Cell Sci* **121**(Pt 2)**:** 186-195.

KOGA D, SANTA T, FUKUSHIMA T, HOMMA H, IMAI K (1997). Liquid chromatographic-atmospheric pressure chemical ionization mass spectrometric determination of anandamide and its analogs in rat brain and peripheral tissues. *J Chromatogr B Biomed Sci Appl* **690**(1-2)**:** 7-13.

KRYLATOV AV, UZHACHENKO RV, MASLOV LN, BERNATSKAYA NA, MAKRIYANNIS A, MECHOULAM R, *et al.* (2002). Endogenous cannabinoids improve myocardial resistance toarrhythmogenic effects of coronary occlusion and reperfusion: A possible mechanism. *Bull Exp Biol Med* **133**(2)**:** 122-124.

KUMBARACI NM, NASTUK WL (1980). Effects of Δ9-tetrahydrocannabinol on excitable membranes and neuromuscular transmission. *Mol Pharmacol* **17**(3)**:** 344-349.

KURY LT, YANG KH, THAYYULLATHIL FT, RAJESH M, ALI RM, SHUBA YM, *et al.* (2014). Effects of endogenous cannabinoid anandamide on cardiac Na/Ca exchanger. *Cell Calcium* **55**(5): 231-237.

LAI FA, MISRA M, XU L, SMITH HA, MEISSNER G (1989). The ryanodine receptor-Ca^{2+} release channel complex of skeletal muscle sarcoplasmic reticulum. Evidence for a cooperatively coupled, negatively charged homotetramer. *J Biol Chem* **264**(28)**:** 16776-16785.

LAKE KD, MARTIN BR, KUNOS G, VARGA K (1997). Cardiovascular effects of anandamide in anesthetized and conscious normotensive and hypertensive rats. *Hypertension* **29**(5)**:** 1204-1210.

LAKOWICZ JR (2006). *Principles of Fluorescence Spectroscopy*. Third edn. Springer, New York, USA.

LAMONTAGNE D, LEPICIER P, LAGNEUX C, BOUCHARD JF (2006). The endogenous cardiac cannabinoid system: a new protective mechanism against myocardial ischemia. *Archives des Maladies du Coeur et des Vaisseaux* **99**(3)**:** 242-246.

LAN R, GATLEY J, LU Q, FAN P, FERNANDO SR, VOLKOW ND, *et al.* (1999). Design and synthesis of the CB1 selective cannabinoid antagonist AM281: a potential human SPECT ligand. *AAPS PharmSci* **1**(2)**:** E4.

LAVER DR, KONG CH, IMTIAZ MS, CANNELL MB (2013). Termination of calcium-induced calcium release by induction decay: an emergent property of stochastic channel gating and molecular scale architecture. *J Mol Cell Cardiol* **54:** 98-100.

LAWRENCE DK, GILL EW (1975). The effects of Δ1 tetrahydrocannabinol and other cannabinoids on spin labeled liposomes and their relationship to mechanisms of general anesthesia. *Mol Pharmacol* **11**(5)**:** 595-602.

LEBLANC N, HUME JR (1990). Sodium current-induced release of calcium from cardiac sarcoplasmic reticulum. *Science* **248**(4953)**:** 372-376.

LEDENT C, VALVERDE O, COSSU G, PETITET F, AUBERT JF, BESLOT F, *et al.* (1999). Unresponsiveness to cannabinoids and reduced addictive effects of opiates in CB1 receptor knockout mice. *Science* **283**(5400)**:** 401-404.

LEE HC (2002). Cyclic ADP-Ribose and NAADP. Structures, Metabolism and Functions. In: Lee HC (ed). *Cyclic ADP-Ribose and NAADP: A Story of Two Calcium Messengers*, edn: Kluwer Academic Publishers, Dordrecht.

LEE HC, AARHUS R (1991). ADP-ribosyl cyclase: an enzyme that cyclizes NAD+ into a calcium-mobilizing metabolite. *Cell Reg* **2**(3)**:** 203-209.

LEE HC, AARHUS R (1995). A derivative of NADP mobilizes calcium stores insensitive to inositol trisphosphate and cyclic ADP-ribose. *J Biol Chem* **270**(5)**:** 2152-2157.

LEE HC, WALSETH TF, BRATT GT, HAYES RN, CLAPPER DL (1989). Structural determination of a cyclic metabolite of NAD+ with intracellular Ca^{2+}-mobilizing activity. *J Biol Chem* **264**(3)**:** 1608-1615.

LEGSSYER AK, HOVE-MADSEN L, HOERTER J, FISCHMEISTER R (1997). Sympathetic modulation of the effect of nifedipine on myocardial contraction and Ca current in the rat. *J Mol Cell Cardiol* **29**(2)**:** 579-591.

LEVICK JR (1999). *An Introduction to Cardiovascular Physiology.* Fifth edn. Hodder Arnold, London.

LEVY MN (1971). Sympathetic-parasympathetic interactions in the heart. *Circ Res* **29**(5)**:** 437-445.

LEWIS AM, ALEY PK, ROOMI A, THOMAS JM, MASGRAU R, GARNHAM C, *et al.* (2012). ß-Adrenergic receptor signaling increases NAADP and cADPR levels in the heart. *Biochem Biophys Res Comm* **427**(2)**:** 326-329.

LEWIS ME, AL-KHALIDI AH, BONSER RS, CLUTTON-BROCK T, MORTON D, PATERSON D, *et al.* (2001). Vagus nerve stimulation decreases left ventricular contractility in vivo in the human and pig heart. *J Physiol* **534**(Pt. 2)**:** 547-552.

LI L, DESANTIAGO J, CHU G, KRANIAS EG, BERS DM (2000). Phosphorylation of phospholamban and troponin I in beta-adrenergic-induced acceleration of cardiac relaxation. *Am J Physiol Heart Circ Physiol* **278**(3)**:** H769-779.

LI Q, CUI N, DU Y, MA H, ZHANG Y (2013). Anandamide reduces intracellular Ca^{2+} concentration through suppression of $Na+/Ca^{2+}$ exchanger current in rat cardiac myocytes. *PloS One* **8**(5)**:** e63386.

LI Q, MA HJ, SONG SL, SHI M, MA HJ, LI DP, *et al.* (2012). Effects of anandamide on potassium channels in rat ventricular myocytes: a suppression of I(to) and augmentation of K(ATP) channels. *Am J Physiol Cell Physiol* **302**(6)**:** C924-930.

LI Q, MA HJ, ZHANG H, QI Z, GUAN Y, ZHANG Y (2009). Electrophysiological effects of anandamide on rat myocardium. *Br J Pharmacol* **158**(8)**:** 2022-2029.

LI Y, KRANIAS EG, MIGNERY GA, BERS DM (2002). Protein kinase A phosphorylation of the ryanodine receptor does not affect calcium sparks in mouse ventricular myocytes. *Circ Res* **90**(3)**:** 309-316.

LIPP P, LAINE M, TOVEY SC, BURRELL KM, BERRIDGE MJ, LI W, *et al.* (2000). Functional InsP3 receptors that may modulate excitation-contraction coupling in the heart. *Curr Biol* **10**(15)**:** 939-942.

LIPP P, NIGGLI E (1996). Submicroscopic calcium signals as fundamental events of excitation--contraction coupling in guinea-pig cardiac myocytes. *J Physiol* **492 (Pt 1):** 31-38.

LIU J, WANG L, HARVEY-WHITE J, OSEI-HYIAMAN D, RAZDAN R, GONG Q, *et al.* (2006). A biosynthetic pathway for anandamide. *Proc Nat Acad Sci USA* **103**(36)**:** 13345-13350.

LUKAS A (1997). Electrophysiology of myocardial cells in the epicardial, midmyocardial, and endocardial layers of the ventricle. *J Cardiovasc Pharmacol Ther* **2**(1)**:** 61-72.

LUKYANENKO V, ZIMAN A, LUKYANENKO A, SALNIKOV V, LEDERER WJ (2007). Functional groups of ryanodine receptors in rat ventricular cells. *J Physiol* **583**(Pt 1)**:** 251-269.

LUNDBY A, ANDERSEN MN, STEFFENSEN AB, HORN H, KELSTRUP CD, FRANCAVILLA C, *et al.* (2013). In vivo phosphoproteomics analysis reveals the cardiac targets of β-adrenergic receptor signaling. *Science Signaling* **6**(278).

MACGREGOR A, YAMASAKI M, RAKOVIC S, SANDERS L, PARKESH R, CHURCHILL GC, *et al.* (2007a). NAADP controls cross-talk between distinct Ca^{2+} stores in the heart. *J Biol Chem* **282**(20)**:** 15302-15311.

MACGREGOR AT, RAKOVIC S, GALIONE A, TERRAR DA (2007b). Dual effects of cyclic ADP-ribose on sarcoplasmic reticulum Ca^{2+} release and storage in cardiac myocytes isolated from guinea-pig and rat ventricle. *Cell Calcium* **41**(6)**:** 537-546.

MACKIE K, DEVANE WA, HILLE B (1993). Anandamide, an endogenous cannabinoid, inhibits calcium currents as a partial agonist in N18 neuroblastoma cells. *Mol Pharmacol* **44**(3)**:** 498-503.

MACKIE K, LAI Y, WESTENBROEK R, MITCHELL R (1995). Cannabinoids activate an inwardly rectifying potassium conductance and inhibit Q-type calcium currents in AtT20 cells transfected with rat brain cannabinoid receptor. *J Neurosci* **15**(10)**:** 6552-6561.

MACKINNON R (1991). Determination of the subunit stoichiometry of a voltage-activated potassium channel. *Nature* **350**(6315)**:** 232-235.

MAEJIMA T, OKA S, HASHIMOTODANI Y, OHNO-SHOSAKU T, AIBA A, WU D, *et al.* (2005). Synaptically driven endocannabinoid release requires Ca^{2+}-assisted metabotropic glutamate receptor subtype 1 to phospholipase Cbeta4 signaling cascade in the cerebellum. *J Neurosci* **25**(29)**:** 6826-6835.

MAIER LS, ZHANG T, CHEN L, DESANTIAGO J, BROWN JH, BERS DM (2003). Transgenic CaMKIIdeltaC overexpression uniquely alters cardiac myocyte Ca^{2+} handling: reduced SR Ca^{2+} load and activated SR Ca^{2+} release. *Circ Res* **92**(8)**:** 904-911.

MAINGRET F, PATEL AJ, LAZDUNSKI M, HONORE E (2001). The endocannabinoid anandamide is a direct and selective blocker of the background K(+) channel TASK-1. *EMBO J* **20**(1-2)**:** 47-54.

MALINOWSKA B, BARANOWSKA-KUCZKO M, SCHLICKER E (2012). Triphasic blood pressure responses to cannabinoids: do we understand the mechanism? *Br J Pharmacol* **165**(7)**:** 2073-2088.

MALINOWSKA B, KWOLEK G, GOTHERT M (2001). Anandamide and methanandamide induce both vanilloid VR1- and cannabinoid CB1 receptor-mediated changes in heart rate and blood pressure in anaesthetized rats. *Naunyn-Schmiedeberg's Arch Pharmacol* **364**(6)**:** 562-569.

MAMAS MA, TERRAR DA (2001). Actions of arachidonic acid on contractions and associated electrical activity in guinea-pig isolated ventricular myocytes. *Exp Physiol* **86**(4)**:** 437-449.

MANEUF YP, BROTCHIE JM (1997). Paradoxical action of the cannabinoid WIN 55,212-2 in stimulated and basal cyclic AMP accumulation in rat globus pallidus slices. *Br J Pharmacol* **120**(8)**:** 1397-1398.

MARKS AR (2003). Calcium and the heart: a question of life and death. *J Clin Invest* **111**(5)**:** 597-600.

MARTIN BR (1986). Cellular effects of cannabinoids. *Pharmacol Rev* **38**(1)**:** 45-74.

MARX SO, GABURJAKOVA J, GABURJAKOVA M, HENRIKSON C, ONDRIAS K, MARKS AR (2001). Coupled gating between cardiac calcium release channels (ryanodine receptors). *Circ Res* **88**(11)**:** 1151-1158.

MARX SO, KUROKAWA J, REIKEN S, MOTOIKE H, D'ARMIENTO J, MARKS AR, *et al.* (2002). Requirement of a macromolecular signaling complex for β adrenergic receptor modulation of the KCNQ1-KCNE1 potassium channel. *Science* **295**(5554)**:** 496-499.

MARX SO, ONDRIAS K, MARKS AR (1998). Coupled gating between individual skeletal muscle Ca^{2+} release channels (ryanodine receptors). *Science* **281**(5378)**:** 818-821.

MARX SO, REIKEN S, HISAMATSU Y, JAYARAMAN T, BURKHOFF D, ROSEMBLIT N, *et al.* (2000). PKA phosphorylation dissociates FKBP12.6 from the calcium release channel (ryanodine receptor): Defective regulation in failing hearts. *Cell* **101**(4)**:** 365-376.

MASGRAU R, CHURCHILL GC, MORGAN AJ, ASHCROFT SJ, GALIONE A (2003). NAADP: a new second messenger for glucose-induced Ca^{2+} responses in clonal pancreatic beta cells. *Curr Biol* **13**(3)**:** 247-251.

MATSUDA H, SAIGUSA A, IRISAWA H (1987). Ohmic conductance through the inwardly rectifying K channel and blocking by internal Mg^{2+}. *Nature* **325**(7000)**:** 156-159.

MATSUDA LA, LOLAIT SJ, BROWNSTEIN MJ, YOUNG AC, BONNER TI (1990). Structure of a cannabinoid receptor and functional expression of the cloned cDNA. *Nature* **346**(6284)**:** 561-564.

MATTICK P, PARRINGTON J, ODIA E, SIMPSON A, COLLINS T, TERRAR D (2007). Ca^{2+}-stimulated adenylyl cyclase isoform AC1 is preferentially expressed in guinea-pig sino-atrial node cells and modulates the I f pacemaker current. *J Physiol* **582**(3)**:** 1195-1203.

MCCALL E, LI L, SATOH H, SHANNON TR, BLATTER LA, BERS DM (1996). Effects of FK-506 on contraction and Ca^{2+} transients in rat cardiac myocytes. *Circ Res* **79**(6)**:** 1110-1121.

MCKINNEY MK, CRAVATT BF (2005). Structure and function of fatty acid amide hydrolase. *Annu Rev Biochem* **74:** 411-432.

MECHOULAM R, BEN-SHABAT S, HANUS L, LIGUMSKY M, KAMINSKI NE, SCHATZ AR, *et al.* (1995). Identification of an endogenous 2-monoglyceride, present in canine gut, that binds to cannabinoid receptors. *Biochem Pharm* **50**(1)**:** 83-90.

MECHOULAM R, BRAUN P, GAONI Y (1967). A stereospecific synthesis of (-)-delta 1- and (-)-delta 1(6)-tetrahydrocannabinols. *J Am Chem Soc* **89**(17)**:** 4552-4554.

MEJIA-ALVAREZ R, KETTLUN C, RIOS E, STERN M, FILL M (1999). Unitary Ca^{2+} current through cardiac ryanodine receptor channels under quasi-physiological ionic conditions. *J Gen Physiol* **113**(2)**:** 177-186.

MERY PF, ABI-GERGES N, VANDECASTEELE G, JUREVICIUS J, ESCHENHAGEN T, FISCHMEISTER R (1997). Muscarinic regulation of the L-type calcium current in isolated cardiac myocytes. *Life Sci* **60**(13-14)**:** 1113-1120.

MESZAROS V, SOCCI R, MESZAROS LG (1995). The kinetics of cyclic ADP-ribose formation in heart muscle. *Biochem Biophys Res Comm* **210**(2)**:** 452-456.

MEYER T, HANSON PI, STRYER L, SCHULMAN H (1992). Calmodulin trapping by calcium-calmodulin-dependent protein kinase. *Science* **256**(5060)**:** 1199-1202.

MIKAMI A, IMOTO K, TANABE T, NIIDOME T, MORI Y, TAKESHIMA H, *et al.* (1989). Primary structure and functional expression of the cardiac dihydropyridine-sensitive calcium channel. *Nature* **340**(6230)**:** 230-233.

MILLER LK, DEVI LA (2011). The highs and lows of cannabinoid receptor expression in disease: mechanisms and their therapeutic implications. *Pharmacol Rev* **63**(3)**:** 461-470.

MINTA A, KAO JPY, TSIEN RY (1989). Fluorescent indicators for cytosolic calcium based on rhodamine and fluorescein chromophores. *J Biol Chem* **264**(14)**:** 8171-8178.

MITCHELL MR, POWELL T, TERRAR DA, TWIST VW (1983). Characteristics of the second inward current in cells isolated from rat ventricular muscle. *Proc Royal Soc London - Biol Sci* **219**(1217)**:** 447-469.

MITCHESON JS, HANCOX JC, LEVI AJ (1998). Cultured adult cardiac myocytes: future applications, culture methods, morphological and electrophysiological properties. *Cardiov Res* **39**(2)**:** 280-300.

MITRA R, MORAD M (1986). Two types of calcium channels in guinea pig ventricular myocytes. *Proc Nat Acad Sci USA* **83**(14)**:** 5340-5344.

MONTECUCCO F, DI MARZO V (2012). At the heart of the matter: The endocannabinoid system in cardiovascular function and dysfunction. *Trends Pharmacol Sci* **33**(6)**:** 331-340.

MONTECUCCO F, LENGLET S, BRAUNERSREUTHER V, BURGER F, PELLI G, BERTOLOTTO M, *et al.* (2009). CB(2) cannabinoid receptor activation is cardioprotective in a mouse model of ischemia/reperfusion. *J Mol Cell Cardiol* **46**(5)**:** 612-620.

MORESCHI I, BRUZZONE S, MELONE L, DE FLORA A, ZOCCHI E (2006). NAADP+ synthesis from cADPRP and nicotinic acid by ADP-ribosyl cyclases. *Biochem Biophys Res Comm***345**(2)**:** 573-580.

MORGAN AJ, GALIONE A (2007). NAADP induces pH changes in the lumen of acidic Ca^{2+} stores. *Biochem J* **402**(2)**:** 301-310.

MORGAN AJ, GALIONE A (2014). Two-pore channels (TPCs): Current controversies. *BioEssays* **36**(2)**:** 173-183.

MUCCIOLI GG (2010). Endocannabinoid biosynthesis and inactivation, from simple to complex. *Drug Discov Today* **15**(11-12)**:** 474-483.

MUKHOPADHYAY S, MCINTOSH HH, HOUSTON DB, HOWLETT AC (2000). The CB(1) cannabinoid receptor juxtamembrane C-terminal peptide confers activation to specific G proteins in brain. *Mol Pharmacol* **57**(1)**:** 162-170.

MUNRO S, THOMAS KL, ABU-SHAAR M (1993). Molecular characterization of a peripheral receptor for cannabinoids. *Nature* **365**(6441)**:** 61-65.

NÄBAUER M, CALLEWAERT G, CLEEMANN L, MORAD M (1989). Regulation of calcium release is gated by calcium current, not gating charge, in cardiac myocytes. *Science* **244**(4906)**:** 800-803.

NAHAS G, TROUVE R (1985). Effects and interactions of natural cannabinoids on the isolated heart. *Proc Soc Exp Biol Med* **180**(2)**:** 312-316.

NATARAJAN V, REDDY PV, SCHMID PC, SCHMID HHO (1982). N-acylation of ethanolamine phospholipids in canine myocardium. *Biochim Biophys Acta Lipid Lipid Metab* **712**(2)**:** 342-355.

NAYLOR E, ARREDOUANI A, VASUDEVAN SR, LEWIS AM, PARKESH R, MIZOTE A, *et al.* (2009). Identification of a chemical probe for NAADP by virtual screening. *Nature Chem Biol* **5**(4)**:** 220-226.

NEBEL M, SCHWOERER AP, WARSZTA D, SIEBRANDS CC, LIMBROCK AC, SWARBRICK JM, *et al.* (2013). Nicotinic acid adenine dinucleotide phosphate (NAADP)-mediated calcium signaling and arrhythmias in the heart evoked by beta-adrenergic stimulation. *J Biol Chem* **288**(22)**:** 16017-16030.

NEEDHAM E, MAMAS MA, TERRAR DA (1998). Actions of cannabidiol on contraction of guinea-pig isolated ventricular myocytes. *Br. J. Pharmacol.* **123 (Supplement):** 322P.

NEHER E (1992). Correction for liquid junction potentials in patch clamp experiments. *Methods Enzymol* **207:** 123-131.

NETZEBAND JG, CONROY SM, PARSONS KL, GRUOL DL (1999). Cannabinoids enhance NMDA-elicited Ca^{2+} signals in cerebellar granule neurons in culture. *J Neurosci* **19**(20)**:** 8765-8777.

NIGGLI E, LEDERER WJ (1990). Voltage-independent calcium release in heart muscle. *Science* **250**(4980)**:** 565-568.

NILIUS B, HESS P, LANSMAN JB, TSIEN RW (1985). A novel type of cardiac calcium channel in ventricular cells. *Nature* **316**(6027)**:** 443-446.

NOWYCKY MC, FOX AP, TSIEN RW (1985). Three types of neuronal calcium channel with different calcium agonist sensitivity. *Nature* **316**(6027)**:** 440-443.

O'NEILL SC, EISNER DA (1990). A mechanism for the effects of caffeine on Ca^{2+} release during diastole and systole in isolated rat ventricular myocytes. *J Physiol* **430:** 519-536.

O'SULLIVAN SE, KENDALL DA, RANDALL MD (2005). The effects of Delta9-tetrahydrocannabinol in rat mesenteric vasculature, and its interactions with the endocannabinoid anandamide. *Br J Pharmacol* **145**(4)**:** 514-526.

OLSHANSKY B, SABBAH HN, HAUPTMAN PJ, COLUCCI WS (2008). Parasympathetic nervous system and heart failure: pathophysiology and potential implications for therapy. *Circulation* **118**(8)**:** 863-871.

ONO K, FOZZARD HA, HANCK DA (1993). Mechanism of cAMP-dependent modulation of cardiac sodium channel current kinetics. *Circ Res* **72**(4)**:** 807-815.

OTSU K, WILLARD HF, KHANNA VK, ZORZATO F, GREEN NM, MACLENNAN DH (1990). Molecular cloning of cDNA encoding the Ca^{2+} release channel (ryanodine receptor) of rabbit cardiac muscle sarcoplasmic reticulum. *J Biol Chem* **265**(23)**:** 13472-13483.

OZ M (2006). Receptor-independent actions of cannabinoids on cell membranes: Focus on endocannabinoids. *Pharmacol Ther* **111**(1)**:** 114-144.

OZ M, TCHUGUNOVA Y, DINC M (2004). Differential effects of endogenous and synthetic cannabinoids on voltage-dependent calcium fluxes in rabbit T-tubule membranes: comparison with fatty acids. *Eur J Pharmacol* **502**(1-2)**:** 47-58.

OZ M, TCHUGUNOVA YB, DUNN SM (2000). Endogenous cannabinoid anandamide directly inhibits voltage-dependent $Ca(^{2+})$ fluxes in rabbit T-tubule membranes. *Eur J Pharmacol* **404**(1-2)**:** 13-20.

PACHER P, BÁTKAI S, KUNOS G (2006). The endocannabinoid system as an emerging target of pharmacotherapy. *Pharmacol Rev* **58**(3)**:** 389-462.

PACHER P, BATKAI S, OSEI-HYIAMAN D, OFFERTALER L, LIU J, HARVEY-WHITE J, *et al.* (2005). Hemodynamic profile, responsiveness to anandamide, and baroreflex sensitivity of mice lacking fatty acid amide hydrolase. *Am J Physiol Heart Circ Physiol* **289**(2)**:** H533-541.

PARK KH, KIM BJ, SHAWL AI, HAN MK, LEE HC, KIM UH (2013). Autocrine/paracrine function of nicotinic acid adenine dinucleotide phosphate (NAADP) for glucose homeostasis in pancreatic beta-cells and adipocytes. *J Biol Chem* **288**(49)**:** 35548-35558.

PEREZ PJ, RAMOS-FRANCO J, FILL M, MIGNERY GA (1997). Identification and functional reconstitution of the type 2 inositol 1,4,5-trisphosphate receptor from ventricular cardiac myocytes. *J Biol Chem* **272**(38)**:** 23961-23969.

PERTWEE RG (1999). Pharmacology of cannabinoid receptor ligands. *Curr Med Chem* **6**(8)**:** 635-664.

PERTWEE RG, HOWLETT AC, ABOOD ME, ALEXANDER SPH, DI MARZO V, ELPHICK MR, *et al.* (2010). International Union of Basic and Clinical Pharmacology. LXXIX. Cannabinoid receptors and their ligands: Beyond CB 1 and CB 2. *Pharmacol Rev* **62**(4)**:** 588-631.

PETERSON BZ, DEMARIA CD, ADELMAN JP, YUE DT (1999). Calmodulin is the Ca^{2+} sensor for Ca^{2+} -dependent inactivation of L-type calcium channels. *Neuron* **22**(3)**:** 549-558.

PETIT-JACQUES J, BOIS P, BESCOND J, LENFANT J (1993). Mechanism of muscarinic control of the high-threshold calcium current in rabbit sino-atrial node myocytes. *Eur J Physiol* **423**(1-2)**:** 21-27.

PFITZER T, NIEDERHOFFER N, SZABO B (2005). Search for an endogenous cannabinoid-mediated effect in the sympathetic nervous system. *Naunyn-Schmiedeberg's Arch Pharmacol* **371**(1)**:** 9-17.

PIACENTINO V, 3RD, GAUGHAN JP, HOUSER SR (2002). L-type $Ca(^{2+})$ currents overlapping threshold Na(+) currents: could they be responsible for the "slip-mode" phenomenon in cardiac myocytes? *Circ Res* **90**(4)**:** 435-442.

PINTO JC, POTIE F, RICE KC, BORING D, JOHNSON MR, EVANS DM, *et al.* (1994). Cannabinoid receptor binding and agonist activity of amides and esters of arachidonic acid. *Mol Pharmacol* **46**(3)**:** 516-522.

PIPER HM (2000). The calcium paradox revisited: an artefact of great heuristic value. *Cardiov Res* **45**(1)**:** 123-127.

PITT SJ, FUNNELL TM, SITSAPESAN M, VENTURI E, RIETDORF K, RUAS M, *et al.* (2010). TPC2 is a novel NAADP-sensitive Ca^{2+} release channel, operating as a dual sensor of luminal pH and Ca^{2+}. *J Biol Chem* **285**(45)**:** 35039-35046.

POLING JS, ROGAWSKI MA, SALEM N, JR., VICINI S (1996). Anandamide, an endogenous cannabinoid, inhibits Shaker-related voltage-gated K+ channels. *Neuropharmacology* **35**(7)**:** 983-991.

POWELL T, TERRAR DA, TWIST VW (1980). Electrical properties of individual cells isolated from adult rat ventricular myocardium. *J Physiol* **302:** 131-153.

POWELL T, TWIST VW (1976). A rapid technique for the isolation and purification of adult cardiac muscle cells having respiratory control and a tolerance to calcium. *Biochem Biophys Res Comm* **72**(1)**:** 327-333.

PRATT PF, HILLARD CJ, EDGEMOND WS, CAMPBELL WB (1998). N-arachidonylethanolamide relaxation of bovine coronary artery is not mediated by CB1 cannabinoid receptor. *Am J Physiol* **274**(1 Pt 2)**:** H375-381.

PRESCOTT SM, MAJERUS PW (1983). Characterization of 1,2-diacylglycerol hydrolysis in human platelets. Demonstration of an arachidonoyl-monoacylglycerol intermediate. *J Biol Chem* **258**(2)**:** 764-769.

PRESTLE J, JANSSEN PM, JANSSEN AP, ZEITZ O, LEHNART SE, BRUCE L, *et al.* (2001). Overexpression of FK506-binding protein FKBP12.6 in cardiomyocytes reduces ryanodine receptor-mediated Ca^{2+} leak from the sarcoplasmic reticulum and increases contractility. *Circ Res* **88**(2)**:** 188-194.

PREVOT V, RIALAS CM, CROIX D, SALZET M, DUPOUY JP, POULAIN P, *et al.* (1998). Morphine and anandamide coupling to nitric oxide stimulates GnRH and CRF release from rat median eminence: neurovascular regulation. *Brain Res* **790**(1-2)**:** 236-244.

PRYOR PR, REIMANN F, GRIBBLE FM, LUZIO JP (2006). Mucolipin-1 is a lysosomal membrane protein required for intracellular lactosylceramide traffic. *Traffic (Copenhagen, Denmark)* **7**(10)**:** 1388-1398.

RADERMACHER M, WAGENKNECHT T, GRASSUCCI R, FRANK J, INUI M, CHADWICK C, *et al.* (1992). Cryo-EM of the native structure of the calcium release channel/ryanodine receptor from sarcoplasmic reticulum. *Biophys J* **61**(4)**:** 936-940.

RAJESH M, MUKHOPADHYAY P, HASKO G, PACHER P (2008). Cannabinoid CB1 receptor inhibition decreases vascular smooth muscle migration and proliferation. *Biochem Biophys Res Comm* **377**(4)**:** 1248-1252.

RALEVIC V, KENDALL DA, RANDALL MD, SMART D (2002). Cannabinoid modulation of sensory neurotransmission via cannabinoid and vanilloid receptors: roles in regulation of cardiovascular function. *Life Sci* **71**(22)**:** 2577-2594.

RANDALL MD, ALEXANDER SP, BENNETT T, BOYD EA, FRY JR, GARDINER SM, *et al.* (1996). An endogenous cannabinoid as an endothelium-derived vasorelaxant. *Biochem Biophys Res Comm***229**(1)**:** 114-120.

RANDALL MD, KENDALL DA (1997). Involvement of a cannabinoid in endothelium-derived hyperpolarizing factor-mediated coronary vasorelaxation. *Eur J Pharmacol* **335**(2-3)**:** 205-209.

REEVES JP, HALE CC (1984). The stoichiometry of the cardiac sodium-calcium exchange system. *J Biol Chem* **259**(12)**:** 7733-7739.

REUTER H (1967). The dependence of slow inward current in Purkinje fibres on the extracellular calcium-concentration. *J Physiol* **192**(2)**:** 479-492.

RHEE MH, BAYEWITCH M, AVIDOR-REISS T, LEVY R, VOGEL Z (1998). Cannabinoid receptor activation differentially regulates the various adenylyl cyclase isozymes. *J Neurochem* **71**(4)**:** 1525-1534.

RINGER S (1883). A further Contribution regarding the influence of the different Constituents of the Blood on the Contraction of the Heart. *J Physiol* **4**(1)**:** 29-42 23.

ROBERTS-CROWLEY ML, MITRA-GANGULI T, LIU L, RITTENHOUSE AR (2009). Regulation of voltage-gated Ca $^{2+}$ channels by lipids. *Cell Calcium* **45**(6)**:** 589-601.

ROSS HR, NAPIER I, CONNOR M (2008). Inhibition of recombinant human T-type calcium channels by Delta9-tetrahydrocannabinol and cannabidiol. *J Biol Chem* **283**(23)**:** 16124-16134.

ROSS RA, BROCKIE HC, STEVENSON LA, MURPHY VL, TEMPLETON F, MAKRIYANNIS A, *et al.* (1999). Agonist-inverse agonist characterization at CB1 and CB2 cannabinoid receptors of L759633, L759656, and AM630. *Br J Pharmacol* **126**(3)**:** 665-672.

ROUSSEAU E, MEISSNER G (1989). Single cardiac sarcoplasmic reticulum Ca^{2+}-release channel: activation by caffeine. *Am J Physiol* **256**(2 Pt 2)**:** H328-333.

ROUSSEAU E, SMITH JS, MEISSNER G (1987). Ryanodine modifies conductance and gating behavior of single Ca^{2+} release channel. *Am J Physiol* **253**(3 Pt 1)**:** C364-368.

ROUZER CA, MARNETT LJ (2008). Non-redundant functions of cyclooxygenases: oxygenation of endocannabinoids. *J Biol Chem* **283**(13)**:** 8065-8069.

RUAN Y, LIU N, PRIORI SG (2009). Sodium channel mutations and arrhythmias. *Nat Rev Cardiol* **6**(5)**:** 337-348.

RUSINKO N, LEE HC (1989). Widespread occurrence in animal tissues of an enzyme catalyzing the conversion of NAD+ into a cyclic metabolite with intracellular Ca^{2+}-mobilizing activity. *J Biol Chem* **264**(20)**:** 11725-11731.

SANCHEZ C, GALVE-ROPERH I, RUEDA D, GUZMAN M (1998). Involvement of sphingomyelin hydrolysis and the mitogen-activated protein kinase cascade in the Delta9-tetrahydrocannabinol-induced stimulation of glucose metabolism in primary astrocytes. *Mol Pharmacol* **54**(5)**:** 834-843.

SANGUINETTI MC, JIANG C, CURRAN ME, KEATING MT (1995). A mechanistic link between an inherited and an acquired cardiac arrhythmia: HERG encodes the IKr potassium channel. *Cell* **81**(2)**:** 299-307.

SANGUINETTI MC, JURKIEWICZ NK (1990). Two components of cardiac delayed rectifier K+ current. Differential sensitivity to block by class III antiarrhythmic agent. *J Gen Physiol* **96**(1)**:** 195-215.

SANGUINETTI MC, JURKIEWICZ NK, SCOTT A, SIEGL PK (1991). Isoproterenol antagonizes prolongation of refractory period by the class III antiarrhythmic agent E-4031 in guinea pig myocytes. Mechanism of action. *Circ Res* **68**(1)**:** 77-84.

SANGUINETTI MC, KASS RS (1984). Voltage-dependent block of calcium channel current in the calf cardiac Purkinje fiber by dihydropyridine calcium channel antagonists. *Circ Res* **55**(3)**:** 336-348.

SANTANA LF, GOMEZ AM, LEDERER WJ (1998). Ca^{2+} flux through promiscuous cardiac Na+ channels: slip-mode conductance. *Science* **279**(5353)**:** 1027-1033.

SCHMID PC, KREBSBACH RJ, PERRY SR, DETTMER TM, MAASSON JL, SCHMID HH (1995). Occurrence and postmortem generation of anandamide and other long-chain N-acylethanolamines in mammalian brain. *FEBS Lett* **375**(1-2)**:** 117-120.

SCRIVEN DR, DAN P, MOORE ED (2000). Distribution of proteins implicated in excitation-contraction coupling in rat ventricular myocytes. *Biophys J* **79**(5)**:** 2682-2691.

SEIDLER T, LOUGHREY CM, ZIBROVA D, KETTLEWELL S, TEUCHER N, KOGLER H, *et al.* (2007). Overexpression of FK-506 binding protein 12.0 modulates excitation contraction coupling in adult rabbit ventricular cardiomyocytes. *Circ Res* **101**(10)**:** 1020-1029.

SHACKLOCK PS, WIER WG, BALKE CW (1995). Local Ca^{2+} transients (Ca^{2+} sparks) originate at transverse tubules in rat heart cells. *J Physiol* **487 (Pt 3):** 601-608.

SHAM JS, CLEEMANN L, MORAD M (1995). Functional coupling of Ca^{2+} channels and ryanodine receptors in cardiac myocytes. *Proc Nat Acad Sci USA* **92**(1)**:** 121-125.

SHIMASUE K, URUSHIDANI T, HAGIWARA M, NAGAO T (1996). Effects of anandamide and arachidonic acid on specific binding of (+) -PN200-110, diltiazem and (-) -desmethoxyverapamil to L-type Ca^{2+} channel. *Eur J Pharmacol* **296**(3)**:** 347-350.

SHMIST YA, GONCHAROV I, EICHLER M, SHNEYVAYS V, ISAAC A, VOGEL Z, *et al.* (2006). Delta-9-tetrahydrocannabinol protects cardiac cells from hypoxia via CB2 receptor activation and nitric oxide production. *Mol Cell Biochem* **283**(1-2)**:** 75-83.

SIMMERMAN HK, COLLINS JH, THEIBERT JL, WEGENER AD, JONES LR (1986). Sequence analysis of phospholamban. Identification of phosphorylation sites and two major structural domains. *J Biol Chem* **261**(28)**:** 13333-13341.

SIMON GM, CRAVATT BF (2006). Endocannabinoid biosynthesis proceeding through glycerophospho-N-acyl ethanolamine and a role for alpha/beta-hydrolase 4 in this pathway. *J Biol Chem* **281**(36)**:** 26465-26472.

SIMON GM, CRAVATT BF (2008). Anandamide biosynthesis catalyzed by the phosphodiesterase GDE1 and detection of glycerophospho-N-acyl ethanolamine precursors in mouse brain. *J Biol Chem* **283**(14)**:** 9341-9349.

SIPIDO KR, CALLEWAERT G, CARMELIET E (1993). [Ca^{2+}](i) transients and [Ca^{2+}](i)-dependent chloride current in single Purkinje cells from rabbit heart. *J Physiol* **468:** 641-667.

SIPIDO KR, CALLEWAERT G, CARMELIET E (1995a). Inhibition and rapid recovery of Ca^{2+} current during Ca^{2+} release from sarcoplasmic reticulum in guinea pig ventricular myocytes. *Circ Res* **76**(1)**:** 102-109.

SIPIDO KR, CALLEWAERT G, PORCIATTI F, VEREECKE J, CARMELIET E (1995b). $[Ca^{2+}]$(i)-dependent membrane currents in guinea-pig ventricular cells in the absence of Na/Ca exchange. *Pflugers Arch Eur J Physiol* **430**(5)**:** 871-878.

SITSAPESAN R, WILLIAMS AJ (1994). Regulation of the gating of the sheep cardiac sarcoplasmic reticulum $Ca(^{2+})$-release channel by luminal Ca^{2+}. *J Memb Biol* **137**(3)**:** 215-226.

SLIPETZ DM, O'NEILL GP, FAVREAU L, DUFRESNE C, GALLANT M, GAREAU Y, *et al.* (1995). Activation of the human peripheral cannabinoid receptor results in inhibition of adenylyl cyclase. *Mol Pharmacol* **48**(2)**:** 352-361.

SOELLER C, CANNELL MB (1999). Examination of the transverse tubular system in living cardiac rat myocytes by 2-photon microscopy and digital image-processing techniques. *Circ Res* **84**(3)**:** 266-275.

SONG Y, BELARDINELLI L (1996). Electrophysiological and functional effects of adenosine on ventricular myocytes of various mammalian species. *Am J Physiol* **271**(4 Pt 1)**:** C1233-1243.

STATES DJ, WALSETH TF, LEE HC (1992). Similarities in amino acid sequences of Aplysia ADP-ribosyl cyclase and human lymphocyte antigen CD38. *Trends Biochem Sci* **17**(12)**:** 495.

STEIN EA, FULLER SA, EDGEMOND WS, CAMPBELL WB (1996). Physiological and behavioural effects of the endogenous cannabinoid, arachidonylethanolamide (anandamide), in the rat. *Br J Pharmacol* **119**(1)**:** 107-114.

STEIN PE, BOODHOO A, ARMSTRONG GD, COCKLE SA, KLEIN MH, READ RJ (1994). The crystal structure of pertussis toxin. *Structure* **2**(1)**:** 45-57.

STELLA N, SCHWEITZER P, PIOMELLI D (1997). A second endogenous cannabinoid that modulates long-term potentiation. *Nature* **388**(6644)**:** 773-778.

STERN MD (1992). Theory of excitation-contraction coupling in cardiac muscle. *Biophys J* **63**(2)**:** 497-517.

STERN MD, CHENG H (2004). Putting out the fire: what terminates calcium-induced calcium release in cardiac muscle? *Cell Calcium* **35**(6)**:** 591-601.

SU Z, PREUSSER L, DIAZ G, GREEN J, LIU X, POLAKOWSKI J, *et al.* (2011). Negative inotropic effect of a CB2 agonist A-955840 in isolated rabbit ventricular myocytes is independent of CB1 and CB2 receptors. *Curr Drug Safety* **6**(5)**:** 277-284.

SUGIURA T, KOBAYASHI Y, OKA S, WAKU K (2002). Biosynthesis and degradation of anandamide and 2-arachidonoylglycerol and their possible physiological significance. *Prostaglandins Leukot Essent Fatty Acids* **66**(2-3)**:** 173-192.

SUGIURA T, KODAKA T, KONDO S, TONEGAWA T, NAKANE S, KISHIMOTO S, *et al.* (1997). Inhibition by 2-arachidonoylglycerol, a novel type of possible neuromodulator, of the depolarization-induced increase in

intracellular free calcium in neuroblastoma x glioma hybrid NG108-15 cells. *Biochem Biophys Res Comm***233**(1)**:** 207-210.

SULAKHE PV, VO XT (1995). Regulation of phospholamban and troponin-I phosphorylation in the intact rat cardiomyocytes by adrenergic and cholinergic stimuli: roles of cyclic nucleotides, calcium, protein kinases and phosphatases and depolarization. *Mol Cell Biochem* **149-150:** 103-126.

SUTHERLAND EW (1972). Studies on the mechanism of hormone action. *Science* **177**(4047)**:** 401-408.

SZABO B, NORDHEIM U, NIEDERHOFFER N (2001). Effects of cannabinoids on sympathetic and parasympathetic neuroeffector transmission in the rabbit heart. *J Pharmacol Exp Ther* **297**(2)**:** 819-826.

TADA M, KIRCHBERGER MA, KATZ AM (1975). Phosphorylation of a 22,000-dalton component of the cardiac sarcoplasmic reticulum by adenosine 3':5'-monophosphate-dependent protein kinase. *J Biol Chem* **250**(7)**:** 2640-2647.

TAKAHASHI A, CAMACHO P, LECHLEITER JD, HERMAN B (1999). Measurement of intracellular calcium. *Physiol Rev* **79**(4)**:** 1089-1125.

TAMURA M, NOGIMORI K, MURAI S, YAJIMA M, ITO K, KATADA T, *et al.* (1982). Subunit structure of islet-activating protein, pertussis toxin, in conformity with the A-B model. *Biochemistry* **21**(22)**:** 5516-5522.

TANABE T, TAKESHIMA H, MIKAMI A, FLOCKERZI V, TAKAHASHI H, KANGAWA K, *et al.* (1987). Primary structure of the receptor for calcium channel blockers from skeletal muscle. *Nature* **328**(6128)**:** 313-318.

TERENTYEV D, VIATCHENKO-KARPINSKI S, GYORKE I, VOLPE P, WILLIAMS SC, GYORKE S (2003). Calsequestrin determines the functional size and stability of cardiac intracellular calcium stores: Mechanism for hereditary arrhythmia. *Proc Nat Acad Sci USA* **100**(20)**:** 11759-11764.

TERRAR DA, VICTORY JG (1988a). Effects of halothane on membrane currents associated with contraction in single myocytes isolated from guinea-pig ventricle. *Br J Pharmacol* **94**(2)**:** 500-508.

TERRAR DA, VICTORY JG (1988b). Isoflurane depresses membrane currents associated with contraction in myocytes isolated from guinea-pig ventricle. *Anesthesiology* **69**(5)**:** 742-749.

TERRAR DA, VICTORY JG (1989a). Influence of halothane on contraction at positive membrane potentials in single cells isolated from guinea-pig ventricular muscle. *J Exp Physiol* **74**(2)**:** 141-151.

TERRAR DA, WHITE E (1989b). Changes in cytosolic calcium monitored by inward currents during action potentials in guinea-pig ventricular cells. *Proc Royal Soc: Biol Sci* **238**(1291)**:** 171-188.

TERRAR DA, WHITE E (1989c). Mechanism of potentiation of contraction by depolarization during action potentials in guinea-pig ventricular muscle. *J Exp Physiol* **74**(3)**:** 355-358.

TERRENOIRE C, CLANCY CE, CORMIER JW, SAMPSON KJ, KASS RS (2005). Autonomic control of cardiac action potentials: role of potassium channel kinetics in response to sympathetic stimulation. *Circ Res* **96**(5)**:** 25-34.

TIAN X, GUO J, YAO F, YANG DP, MAKRIYANNIS A (2005). The conformation, location, and dynamic properties of the endocannabinoid ligand anandamide in a membrane bilayer. *J Biol Chem* **280**(33)**:** 29788-29795.

TIMERMAN AP, ONOUE H, XIN HB, BARG S, COPELLO J, WIEDERRECHT G, *et al.* (1996). Selective binding of FKBP12.6 by the cardiac ryanodine receptor. *J Biol Chem* **271**(34)**:** 20385-20391.

TOBIMATSU T, FUJISAWA H (1989). Tissue-specific expression of four types of rat calmodulin-dependent protein kinase II mRNAs. *J Biol Chem* **264**(30)**:** 17907-17912.

TOLLER WG, STRANZ C (2006). Levosimendan, a new inotropic and vasodilator agent. *Anesthesiology* **104**(3)**:** 556-569.

TRAFFORD AW, EISNER DA (2003). No role for a voltage sensitive release mechanism in cardiac muscle. *J Mol Cell Cardiol* **35**(2)**:** 145-151.

TSENG GN, HOFFMAN BF (1989). Two components of transient outward current in canine ventricular myocytes. *Circ Res* **64**(4)**:** 633-647.

TSIEN RW, BEAN BP, HESS P, LANSMAN JB, NILIUS B, NOWYCKY MC (1986). Mechanisms of calcium channel modulation by beta-adrenergic agents and dihydropyridine calcium agonists. *J Mol Cell Cardiol* **18**(7)**:** 691-710.

TSUBOI K, SUN YX, OKAMOTO Y, ARAKI N, TONAI T, UEDA N (2005). Molecular characterization of N-acylethanolamine-hydrolyzing acid amidase, a novel member of the choloylglycine hydrolase family with structural and functional similarity to acid ceramidase. *J Biol Chem* **280**(12)**:** 11082-11092.

TSUBOI K, ZHAO LY, OKAMOTO Y, ARAKI N, UENO M, SAKAMOTO H, *et al.* (2007). Predominant expression of lysosomal N-acylethanolamine-hydrolyzing acid amidase in macrophages revealed by immunochemical studies. *Biochim Biophys Acta* **1771**(5)**:** 623-632.

TUGBA DURLU-KANDILCI N, RUAS M, CHUANG KT, BRADING A, PARRINGTON J, GALIONE A (2010). TPC2 proteins mediate nicotinic acid adenine dinucleotide phosphate (NAADP)- and agonist-evoked contractions of smooth muscle. *J Biol Chem* **285**(32)**:** 24925-24932.

UEDA N, YAMANAKA K, TERASAWA Y, YAMAMOTO S (1999). An acid amidase hydrolyzing anandamide as an endogenous ligand for cannabinoid receptors. *FEBS Lett* **454**(3)**:** 267-270.

UGDYZHEKOVA DS, BERNATSKAYA NA, STEFANO JB, GRAIER VF, TAM SW, MEKHOULAM R (2001). Endogenous cannabinoid anandamide increases heart resistance to arrhythmogenic effects of epinephrine: Role of CB1 and CB2 receptors. *Bull Exp Biol Med* **131**(3)**:** 251-253.

UNDERDOWN NJ, HILEY CR, FORD WR (2005). Anandamide reduces infarct size in rat isolated hearts subjected to ischaemia-reperfusion by a novel cannabinoid mechanism. *Br J Pharmacol* **146**(6)**:** 809-816.

VALDIVIA HH, KAPLAN JH, ELLIS-DAVIES GC, LEDERER WJ (1995). Rapid adaptation of cardiac ryanodine receptors: modulation by Mg^{2+} and phosphorylation. *Science* **267**(5206)**:** 1997-2000.

VAN DEN BOSSCHE I, VANHEEL B (2000). Influence of cannabinoids on the delayed rectifier in freshly dissociated smooth muscle cells of the rat aorta. *Br J Pharmacol* **131**(1)**:** 85-93.

VANDECASTEELE G, ESCHENHAGEN T, FISCHMEISTER R (1998). Role of the NO-cGMP pathway in the muscarinic regulation of the L-type Ca^{2+} current in human atrial myocytes. *J Physiol* **506 (Pt 3):** 653-663.

VANDENBERG JI, YOSHIDA A, KIRK K, POWELL T (1994). Swelling-activated and isoprenaline-activated chloride currents in guinea pig cardiac myocytes have distinct electrophysiology and pharmacology. *J Gen Physiol* **104**(6)**:** 997-1017.

VARGA K, LAKE K, MARTIN BR, KUNOS G (1995). Novel antagonist implicates the CB1 cannabinoid receptor in the hypotensive action of anandamide. *Eur J Pharmacol* **278**(3)**:** 279-283.

VASUDEVAN SR, GALIONE A, CHURCHILL GC (2008). Sperm express a Ca^{2+}-regulated NAADP synthase. *Biochem J* **411**(1)**:** 63-70.

VINOGRADOVA TM, LYASHKOV AE, ZHU W, RUKNUDIN AM, SIRENKO S, YANG D, *et al.* (2006). High basal protein kinase A-dependent phosphorylation drives rhythmic internal Ca^{2+} store oscillations and spontaneous beating of cardiac pacemaker cells. *Circ Res* **98**(4)**:** 505-514.

VOGEL Z, BARG J, LEVY R, SAYA D, HELDMAN E, MECHOULAM R (1993). Anandamide, a brain endogenous compound, interacts specifically with cannabinoid receptors and inhibits adenylate cyclase. *J Neurochem* **61**(1)**:** 352-355.

VOITYCHUK OI, ASMOLKOVA VS, GULA NM, SOTKIS GV, GALADARI S, HOWARTH FC, *et al.* (2012). Modulation of excitability, membrane currents and survival of cardiac myocytes by N-acylethanolamines. *Biochim Biophys Acta Mol Cell Biol Lipid* **1821**(9)**:** 1167-1176.

WAGNER JA, ABESSER M, HARVEY-WHITE J, ERTL G (2006). 2-Arachidonylglycerol acting on CB1 cannabinoid receptors mediates delayed cardioprotection induced by nitric oxide in rat isolated hearts. *J Cardiovasc Pharmacol* **47**(5)**:** 650-655.

WALDMAN M, HOCHHAUSER E, FISHBEIN M, ARAVOT D, SHAINBERG A, SARNE Y (2013). An ultra-low dose of tetrahydrocannabinol provides cardioprotection. *Biochem Pharm* **85**(11)**:** 1626-1633.

WALKER CA, SPINALE FG (1999). The structure and function of the cardiac myocyte: A review of fundamental concepts. *J Thorac Cardiov Surg* **118**(2)**:** 375-382.

WALSH KB, KASS RS (1988). Regulation of a heart potassium channel by protein kinase A and C. *Science* **242**(4875)**:** 67-69.

WANG PF, JIANG LS, BU J, HUANG XJ, SONG W, DU YP, *et al.* (2012a). Cannabinoid-2 receptor activation protects against infarct and ischemia-reperfusion heart injury. *J Cardiovasc Pharmacol* **59**(4)**:** 301-307.

WANG X, ZHANG X, DONG XP, SAMIE M, LI X, CHENG X, *et al.* (2012b). TPC proteins are phosphoinositide-activated sodium-selective ion channels in endosomes and lysosomes. *Cell* **151**(2)**:** 372-383.

WEHRENS XH, LEHNART SE, HUANG F, VEST JA, REIKEN SR, MOHLER PJ, *et al.* (2003). FKBP12.6 deficiency and defective calcium release channel (ryanodine receptor) function linked to exercise-induced sudden cardiac death. *Cell* **113**(7)**:** 829-840.

WEI BQ, MIKKELSEN TS, MCKINNEY MK, LANDER ES, CRAVATT BF (2006). A second fatty acid amide hydrolase with variable distribution among placental mammals. *J Biol Chem* **281**(48)**:** 36569-36578.

WEIS F, BEIRAS-FERNANDEZ A, SODIAN R, KACZMAREK I, REICHART B, BEIRAS A, *et al.* (2010). Substantially altered expression pattern of cannabinoid receptor 2 and activated endocannabinoid system in patients with severe heart failure. *J Mol Cell Cardiol* **48**(6)**:** 1187-1193.

WHALLEY DW, WENDT DJ, GRANT AO (1995). Basic concepts in cellular cardiac electrophysiology: Part I: Ion channels, membrane currents, and the action potential. *Pacing Clin Electrophysiol* **18**(8)**:** 1556-1574.

WHITE R, HILEY CR (1997). A comparison of EDHF-mediated and anandamide-induced relaxations in the rat isolated mesenteric artery. *Br J Pharmacol* **122**(8)**:** 1573-1584.

WILKINS BJ, MOLKENTIN JD (2004). Calcium–calcineurin signaling in the regulation of cardiac hypertrophy. *Biochem Biophys Res Comm* **322**(4)**:** 1178-1191.

WILLIAMS GS, BOYMAN L, CHIKANDO AC, KHAIRALLAH RJ, LEDERER WJ (2013). Mitochondrial calcium uptake. *Proc Nat Acad Sci USA* **110**(26)**:** 10479-10486.

WITVLIET MH, BURNS DL, BRENNAN MJ, POOLMAN JT, MANCLARK CR (1989). Binding of pertussis toxin to eucaryotic cells and glycoproteins. *Infect Immun* **57**(11)**:** 3324-3330.

WU Y, COLBRAN RJ, ANDERSON ME (2001). Calmodulin kinase is a molecular switch for cardiac excitation-contraction coupling. *Proc Nat Acad Sci USA* **98**(5)**:** 2877-2881.

XIAO B, JIANG MT, ZHAO M, YANG D, SUTHERLAND C, LAI FA, *et al.* (2005). Characterization of a novel PKA phosphorylation site, serine-2030, reveals no PKA hyperphosphorylation of the cardiac ryanodine receptor in canine heart failure. *Circ Res* **96**(8)**:** 847-855.

XIAO B, SUTHERLAND C, WALSH MP, CHEN SR (2004). Protein kinase A phosphorylation at serine-2808 of the cardiac Ca^{2+}-release channel (ryanodine receptor) does not dissociate 12.6-kDa FK506-binding protein (FKBP12.6). *Circ Res* **94**(4)**:** 487-495.

XIAO B, ZHONG G, OBAYASHI M, YANG D, CHEN K, WALSH MP, *et al.* (2006). Ser-2030, but not Ser-2808, is the major phosphorylation site in cardiac ryanodine receptors responding to protein kinase A activation upon beta-adrenergic stimulation in normal and failing hearts. *Biochem J* **396**(1)**:** 7-16.

XIAO RP, VALDIVIA HH, BOGDANOV K, VALDIVIA C, LAKATTA EG, CHENG H (1997). The immunophilin FK506-binding protein modulates Ca^{2+} release channel closure in rat heart. *J Physiol* **500 (Pt 2):** 343-354.

XIN HB, SENBONMATSU T, CHENG DS, WANG YX, COPELLO JA, JI GJ, *et al.* (2002). Oestrogen protects FKBP12.6 null mice from cardiac hypertrophy. *Nature* **416**(6878)**:** 334-338.

YU M, IVES D, RAMESHA CS (1997). Synthesis of prostaglandin E2 ethanolamide from anandamide by cyclooxygenase-2. *J Biol Chem* **272**(34)**:** 21181-21186.

ZHANG F, LI PL (2007). Reconstitution and characterization of a nicotinic acid adenine dinucleotide phosphate (NAADP)-sensitive Ca^{2+} release channel from liver lysosomes of rats. *J Biol Chem* **282**(35)**:** 25259-25269.

ZHANG L, KELLEY J, SCHMEISSER G, KOBAYASHI YM, JONES LR (1997). Complex formation between junctin, triadin, calsequestrin, and the ryanodine receptor. Proteins of the cardiac junctional sarcoplasmic reticulum membrane. *J Biol Chem* **272**(37)**:** 23389-23397.

ZHANG X, TALLINI YN, CHEN Z, GAN L, WEI B, DORAN R, *et al.* (2009). Dissociation of FKBP12.6 from ryanodine receptor type 2 is regulated by cyclic ADP-ribose but not beta-adrenergic stimulation in mouse cardiomyocytes. *Cardiov Res* **84**(2)**:** 253-262.

ZHAO YJ, LAM CM, LEE HC (2012). The membrane-bound enzyme CD38 exists in two opposing orientations. *Science Signaling* **5**(241)**:** ra67.

ZHU MX, MA J, PARRINGTON J, CALCRAFT PJ, GALIONE A, EVANS AM (2010). Calcium signaling via two-pore channels: local or global, that is the question. *Am J Physiol Cell Physiol* **298**(3)**:** C430-441.

ZIMA AV, BARE DJ, MIGNERY GA, BLATTER LA (2007). IP3-dependent nuclear Ca^{2+} signalling in the mammalian heart. *J Physiol* **584**(Pt 2)**:** 601-611.

ZIMA AV, BLATTER LA (2004). Inositol-1,4,5-trisphosphate-dependent Ca($^{2+}$) signalling in cat atrial excitation-contraction coupling and arrhythmias. *J Physiol* **555**(Pt 3)**:** 607-615.

ZIMA AV, PICHT E, BERS DM, BLATTER LA (2008). Partial inhibition of sarcoplasmic reticulum ca release evokes long-lasting ca release events in ventricular myocytes: role of luminal ca in termination of ca release. *Biophys J* **94**(5)**:** 1867-1879.

ZIMMERMAN ANE, HÜLSMANN WC (1966). Paradoxical influence of calcium ions on the permeability of the cell membranes of the isolated rat heart. *Nature* **211**(5049)**:** 646-647.

ZYGMUNT AC, GIBBONS WR (1991). Calcium-activated chloride current in rabbit ventricular myocytes. *Circ Res* **68**(2)**:** 424-437.

ZYGMUNT PM, PETERSSON J, ANDERSSON DA, CHUANG H, SORGARD M, DI MARZO V, *et al.* (1999). Vanilloid receptors on sensory nerves mediate the vasodilator action of anandamide. *Nature* **400**(6743)**:** 452-457.